PROCESSING, MECHANICAL PROPERTIES AND TRIBOLOGICAL CHARACTERISTICS OF Al_2O_3 AND MoS_2 NANOPARTICLE REINFORCED ZA-27 ALLOY COMPOSITES

A thesis submitted in partial fulfillment of the requirements

for the award of the degree of

DOCTOR OF PHILOSOPHY

By

SHIVA KUMAR N

(ROLL NO: 701307)

Under the Guidance of

Dr. V. VASU
(Supervisor)
Department of Mechanical Engineering

Dr. N. NARASAIAH
(Co-Supervisor)
Department of Metallurgy and Materials Engineering

DEPARTMENT OF MECHANICAL ENGINEERING
NATIONAL INSTITUTE OF TECHNOLOGY
WARANGAL (T.S.) - 506 004

SEPTEMBER - 2017

THESIS APPROVAL FOR Ph.D.

This thesis entitled **"PROCESSING, MECHANICAL PROPERTIES AND TRIBOLOGICAL CHARACTERISTICS OF Al_2O_3 AND MoS_2 NANOPARTICLE REINFORCED ZA-27 ALLOY COMPOSITES"** by **Mr. Shivakumar N** is approved for the degree of Doctor of Philosophy.

Examiners

_____

_____

_____

Supervisor(s)

Dr. V. Vasu
(Supervisor)

Associate Professor, Mechanical Engineering Department, NIT Warangal

Dr. N.Narasaiah

(Co-Supervisor)

Professor, Metallurgy and Materials Engineering Department, NIT Warangal

Chairman

Prof. P.Bangaru Babu

Head, Mechanical Engineering Department, NIT Warangal

DEPARTMENT OF MECHANICAL ENGINEERING
NATIONAL INSTITUTE OF TECHNOLOGY
WARANGAL (T.S)

CERTIFICATE

This is to certify the thesis entitled **"Processing, Mechanical Properties and Tribological Characteristics of Al_2O_3 and MoS_2 Nanoparticle Reinforced ZA-27 Alloy Composites"** submitted by **Mr.ShivaKumar.N** for the award of the degree of **Doctor of Philosophy in Mechanical Engineering**, in the Faculty of Engineering of **National Institute of Technology, Warangal** is a bonafide research work carried out by him under our guidance in the **National Institute of Technology, Warangal, Telangana.**

Place: Warangal.
Date: 27/04/2018

Dr. V. VASU
Associate Professor
(Supervisor)
Department of Mechanical Engineering

Dr. N. NARASAIAH
Professor
(Co-Supervisor)
Department of Metallurgy and Materials Engineering

DEPARTMENT OF MECHANICAL ENGINEERING
NATIONAL INSTITUTE OF TECHNOLOGY
WARANGAL (T.S.)

DECLARATION

I, hereby declare that the matter embodied in this thesis titled **"Processing, Mechanical Properties and Tribological Characteristics of Al_2O_3 and MoS_2 Nanoparticle Reinforced ZA-27 Alloy Composites"** is the result of research carried out by me under the guidance of **Dr. V. Vasu** Department of Mechanical Engineering and **Prof. N. Narasaiah**, Department of Metallurgy and Materials Engineering, National Institute of Technology (Deemed University), Warangal, Telangana. This work or any part of this work has not been submitted to any other University or Institute for the award of any other degree or diploma.

Place: Warangal

Date: 27/04/2018

Shivakumar N
Research Scholar,
Department of Mechanical Engineering,
National Institute of Technology, Warangal,
Telangana.

Dedicated to My Family

And

Friends

Acknowledgements

I would like to express my special appreciation and thanks to my supervisor **Dr. V. Vasu**, Associate Professor, Dept. of Mechanical Engineering and **Dr. N. Narasaiah**, Professor, Dept. of Metallurgical and Materials Engineering, NIT, Warangal for suggesting the topic of my thesis and their ready and able guidance throughout the course of my research work, for their patience, motivation, and immense knowledge.

I wish to sincerely thank the authorities of the Institute, **Prof. N.V.RAMANA RAO, DIRECTOR**, National Institute of Technology, Warangal and other top officials who gave me an opportunity to carry out research work.

I am very much thankful to **Prof. P.Bangaru Babu**, Head, Mechanical Engineering Department for his support and also valuable suggestions. I also express my deep sense of gratitude to my doctorial scrutiny committee members, **Prof. Srinadh K V S**, Mechanical Engineering Department, **Dr. A. Kumar**, Mechanical Engineering Department and **Dr. Abdul Azeem P**, Physics Department for their constructive and encouraging suggestions during my research work. I take this opportunity to express gratitude to the entire Faculty Members of Mechanical Engineering department for their help and support.

I would like to express my sincere thanks to **Prof Subodh Kumar,** Department of Materials Engineering and **S. Seshan**, Emeritus Professor Mechanical Engineering Department, Indian Institute of Science, Bangalore for sanctioning the **UGC-NRCM** project and their encouragement and suggestion for my research work.

I am very much thankful to **Dr.M.Raja Vishwanathan,** Department of Humanities and social science, National Institute of Technology Warangal for his support and valuable suggestions during my research work.

I always remember the advices and help offered by my senior research scholar **Dr. M. Sreenivasa Rao, Dr. K.Kishore Kumar, Dr. A.Manmadha Chary** and **Dr. M.Sandeep Kumar**. I also express my sincere thanks to my friend **Dr.P.Naresh** and scholar **G. Arun Manohar** who contributed either directly or indirectly in successful completion of this research work. I would like to thank administrative and technical staff members of the institute who have been kind enough to advise and help in their respective roles.

I am very much thankful to the K.Yellaswamy workshop foreman and technician Shyam for their valuable help for the completion of my research work.

I would like to express my heartfull thanks to my dear friends D Shiva Prasad, N.Anil Kumar, M. Arun, A.Ravikumar and J.Kiran for their direct and indirect help for the completion of my research work.

Lastly, I owe a special thanks to my parents **N Bhadraiah** and **Vijaya Lakshmi**, brother **N Rajendranath** sister **Bhavani**, wife **Swathi** and my loving daughters **Srinidhi** and **Nivetha Sri** for their love and encouragement without which I never would have imagined myself to pull it this far.

Shivakumar N

ABSTRACT

The demand for composite materials is constantly growing, due to high specific strength and stiffness. This has encouraged scientific and technological communities to accomplish research and development in this direction. Currently the ceramic particles which are reinforced in the composites have attracted a great deal of attention both in the industrial sector and the academic community. The composites reinforced with ceramic particles mostly have high modulus and strength compared to matrix materials. The application of composites has been extended to their use as structural materials in defense, marine, aerospace and automotive sectors.

Zinc–aluminium (ZA) alloys have shown a considerable attention for their industrial application due to good castability and mechanical properties. ZA alloys have more advantages when compared to the aluminium-based and copper-based alloys, especially due to significantly lower casting temperature and relatively high strength. Therefore zinc - aluminium alloys are receiving extensive acceptance for bearing applications owing to their ability to replace traditional bronze bearings at low cost. Among this ZA alloys, ZA-27 alloy is the lightest alloy with better combination of wear resistance and mechanical properties.

Recently nanoparticle reinforced ceramic particulates has drawn interest of many researchers due to its versatile applications. Nanoparticles in metal matrix can improve the end use performance of the composite in many different ways. Reinforcing of inorganic particulate fillers into metal matrix has been evidenced to be an efficient way of improving the tribological and mechanical properties of the matrix material Addition of high surface area particulates to the hybrid composites definitely exhibits variation in the mechanical and tribological properties.

Therefore the present research work is focused on the fabrication of nanocomposites with the matrix material ZA-27 alloy reinforced with nanoparticles of aluminium oxide (Al_2O_3) and molybdenum disulphide (MoS_2) at different weight percentages with the help of ultrasonic assisted stir casting process. The microstructural characterization and elemental analysis of fabricated nanocomposites were examined with the aid of scanning electron microscope (SEM) and energy dispersive spectroscopy (EDS).The microhardness, tensile strength and fatigue life tests were carried out to study the mechanical properties of the ZA-27

nanocomposites. Pin on disc friction and wear testing machine were used for the tribological properties (dry sliding wear and friction coefficient) of the nanocomposites. The wear characterization of the nanocomposites were carried out according to the experimental plan by using response surface methodology (RSM) and the optimal process parameters for the tribological properties of nanocomposites were given by using analysis of variance (ANOVA). From the results it was observed that there is a homogenous distribution of the reinforcement nanoparticles in the matrix material due to the ultrasonification process. There is a minor improvement in micro hardness, tensile strength and fatigue life with addition of 0.5 wt % MoS_2 nanoparticles to ZA-27 alloy, with more addition of nanoparticles there is a decline in mechanical properties can be observed. The weight percentages of the Al_2O_3 nanoparticles increases there is an improvement in mechanical properties compare to the matrix material. The wear rate and coefficient of friction of the ZA-27 nanocomposites decreases as the reinforcement content increases in the matrix material. The most influencing factors on tribological properties of nanocomposites are reinforcement content and applied load.

In this work an attempt has also been made to prepare the hybrid nanocomposites with the combination of Al_2O_3 (1.5 wt %) and MoS_2 (0.5 wt %) nanoparticles reinforced in matrix materials by using ultrasonic assisted stir casting process. The tests were carried out to study the mechanical and tribological properties of hybrid nanocomposites. The results shows that the mechanical and wear resistance properties of hybrid nanocomposites increases compare to the ZA-27 alloy. For hybrid nanocomposites the most significant parameters influencing the wear rate are applied load and sliding distance and for coefficient of friction are applied load and sliding speed. The worn surfaces of the ZA-27 nanocomposites and hybrid nanocomposites were examined by using SEM. The ZA-27 hybrid nanocomposites are showing better mechanical and tribological properties.

Keywords: ZA-27 nanocomposites, Ultrasonic assisted stir casting, Microhardness, Tensile strength, Wear rate, Coefficient of friction.

CONTENTS

LIST OF FIGURES

LIST OF TABLES

ABBREVIATIONS

PMC	Polymer matrix composites
CMC	Ceramic matrix composites
MMC	Metal matrix composites
MMNC	Metal matrix nanocomposites
ZA	Zinc-Aluminium
ZA-27	Zinc-Aluminium 27 alloy
Al_2O_3	Aluminium oxide
MoS_2	Molybdenum disulphide
SEM	Scanning electron microscope
EDS	Energy dispersive spectroscopy
HV	Vickers's hardness
UTS	Ultimate Tensile Strength
YS	Yield Strength
DOE	Design of Experiments
RSM	Response Surface Methodology
CCD	Centered Composite Design
WR	Wear rate
COF	Coefficient of friction
ANOVA	Analysis of variance

NOMENCLATURE

ρ_{exp}	Experimental density
W_s	Weight of the specimen
W_a	Apparent immersed weight of specimen
ρ_w	Density of water
ρ_{th}	Theoretical density
W_m	Weight fraction of matrix material
W_p	Weight fraction of reinforcement particles
ρ_m	Density of matrix material
ρ_p	Density of reinforcement particles
α	Aluminium rich phase
η	Zinc rich phase
α+η	Eutectic phase (Al + Zn)
ε	Cu rich phase
Y_r	Response
X_{ir}	Value for i^{th} input process parameter of r^{th} experiment
n	Number of process parameters
b_i, b_{ii}, b_{ij}	Regression coefficients

CHAPTER 1
INTRODUCTION

1.1. Background

In recent years the improved performance of materials, as identified by various better strength, lower cost and less weight then improves their effectiveness. Materials form the essential source of all engineering applications. Scientific improvement in any field demands advancement in the field of materials. In many cases the lack of suitable material for the application has changed the course of a certain trend of development. The primary goal of any development is its suitability to the environment of application. This inherent dependence of technological development on the science of materials has resulted in the accelerated growth in several automotive applications. The greatest emphasis on material research comes from the industrial sector. Industrial development has always posed challenges to the field of material science and development. The increases in the necessity of materials and specifications that get more rigid have guided the research and development in industrial applications. The demands for evermore-superior characteristics of materials have led to the study of composites.

The development of composite as new engineering material has been one of the main innovations in the field of materials in the past couple of decades. The material which is made from the two or more essential materials with significantly different properties compared to the individual materials is known as composite material. The composites are a mixture of two different materials in which one of the materials is in the form of particulates or fibers called as reinforcing material, which is introduced in the other material called as matrix material. The presence of reinforcing particles like particulates or fibers in the composites increases the mechanical properties like hardness, strength and stiffness etc, whereas the main purpose of matrix material is to transfer the loads among the filler material to defend them from the environmental damages. The traditional materials in several high strength and light weight applications were effectively substituted in the composite materials. Mainly the composites are selected due to their high tensile strength at elevated temperatures, high strength - to - weight

ratio, high creep resistance and high toughness for the industrial applications. The reinforcement materials are hard and soft ceramic materials, whereas the matrix is generally a brittle or ductile material used in composites [1].

1.2. Metal matrix composites (MMCs)

The metal matrix composites are a new series of innovative materials used in several industrial applications where conventional materials and alloys are not suitable for use. Metal matrix composites (MMCs) are a broad family of materials aimed at achieving an enhanced combination of properties. Structurally, MMCs consist of continuous or discontinuous fibres, whiskers or particulates in an alloy matrix that solidifies in the restricting spheres among the reinforcing phases to form majority of the matrix. The relative amount and distribution of components constituting a composite are carefully monitoring and by controlling the solidification conditions, MMCs can impart a tailored set of useful engineering properties that cannot be realized with conventional monolithic material [2].

Many of the matrix materials used in the MMCs are popular alloys, selected mainly on the basis of their already established superior mechanical properties which can be further enhanced by inclusion of a suitable reinforcing material. The selection of reinforcing material is generally based on the application of the composite material being developed. If the composite material is intended for bearing applications, usually graphite and molybdenum disulphide are selected as the reinforcement since they have the well-known advantage as solid lubricants. In the same way, if service at elevated temperature is the desired property in the composite, either silicon carbide or Zircon or alumina is selected as the reinforcement. The excellent mechanical and tribological properties of MMCs composed with weight saving and the comparative low cost in fabrication makes them very attractive for a variety of engineering applications [3-4].

1.3. Nanocomposites

Nanocomposites are materials that are produced by introducing nanoparticulates into a matrix material. The nanomaterials have a trend to drastically add to the thermal and electrical conductivity as well as to the mechanical strength properties of the matrix material. In general, the nano materials used are carbon nanotubes, nanoparticles and they are distributed into

the other composite materials during processing. The percentage by weight of the nanomaterials introduced is able to remain very low due to the extremely high surface area to volume ratio of the particles. Many researchers are investigating developing more efficient combinations of materials and to impart multifunctionalities to the nanocomposites.

1.4. Metal matrix nanocomposites (MMNC)

The term "metal nanocomposite" broadly describes any number of multicomponent systems, where the primary component is the metal and the filler material has at least one dimension below 100 nm. Metal matrix nanocomposites are generally lightweight, require low filler loading, are often easy to process, and provide property enhancements extending orders of magnitude beyond those realized with traditional composites. Metal matrix nanocomposites are being considered worldwide in recent years, owing to their encouraging properties suitable for a large number of functional and structural applications [5].

1.5. Zinc- aluminium alloys

During the past twenty years, new zinc alloys have been developed for gravity casting in permanent and sand molds to compete with cast iron, bronze and aluminium. Zinc and zinc-aluminium alloy castings currently account for a significant portion of the end-use market for zinc [6]. However, the number of materials and processes that can provide feasible, cost-effective alternatives to zinc-base products is constantly expanding. Due to the excellent properties like toughness, strength, rigidity, economical cast ability and bearing performance of zinc casting alloys were used as versatile engineering materials. The small amount of copper observed in the zinc aluminium alloys acts as cost and an energy effective replacement in variety ferrous and non- ferrous alloys [7]. The ZA alloys are capable of replacing the journal bearing materials like white metal, cast iron, aluminium alloys, copper alloys and bronze alloys due to their higher mechanical properties, superior wear resistance, low weight, low melting temperature, excellent castability and low initial cost. These alloys are particularly suitable for heavy load and low speed bearing applications. The reduction in cost from 25% to 40% with aluminium alloys and 40% to 75% with brass alloys is a significant feature that makes ZA alloys attractive as matrix material for fabrication of composites. These alloys are based upon the zinc-

aluminium (ZA) systems and are designated as ZA-8, ZA-12 and ZA-27 after their nominal aluminium contents [8]. The phase diagram of ZA-alloy is shown in Figure 1.1. The ZA-alloy goes through many phases while cooling from molten melt to room temperature, as the phase diagram makes it apparent [9].

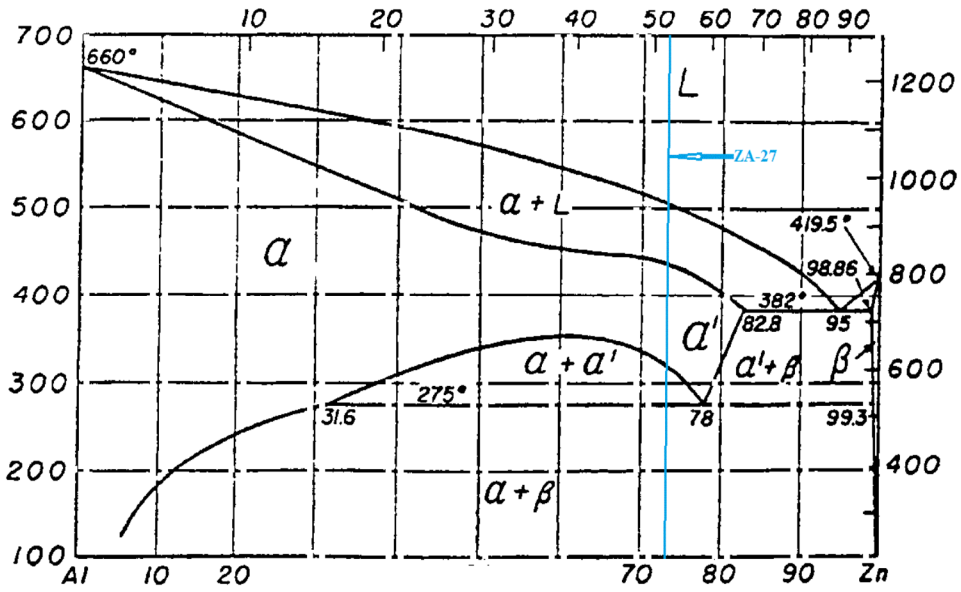

Figure .1.1 Phase diagram of Zinc-Aluminium alloy

Zinc-aluminum alloys have low melting points, require low heat inputs for melting, do not require fluxing or special protective atmospheres and are non-polluting. These alloys are also suitable for pressure die casting using cold chamber and in the case of the 27 wt. % aluminum alloy, hot chamber machines. The alloys have high fluidity and can be cast in much thinner walls than other foundry alloys, achieving tight dimensional tolerances in pressure die castings. The three ZA alloys have superior mechanical properties and are considered to be high performance alloys. They tend to be used for structural applications rather than for decorative uses. ZA alloys are used in the transportation industry for parts such as carburetors, pump bodies, wiper parts, transmission cases and other hardware. They are also used for electronic hardware and electrical fittings, as well as for parts for domestic appliances, computers and business machines. Applications of ZA alloys include many parts originally cast in iron and requiring extensive machining, aluminium cast parts receiving a hard-anodized finish and bearings compared to other alloys.

1.6. ZA-alloys used for bearing application

Materials requiring optimum strength, hardness and light weight which are have excellent wear resistance and good lubricating properties are used for the bearing application. The materials which are used for the bearing applications are bronze, brass, duralumine, white metal and ZA-27 alloy. Many researchers have studied the wear resistance properties of the different bearing materials as shown in Figure 1.2.

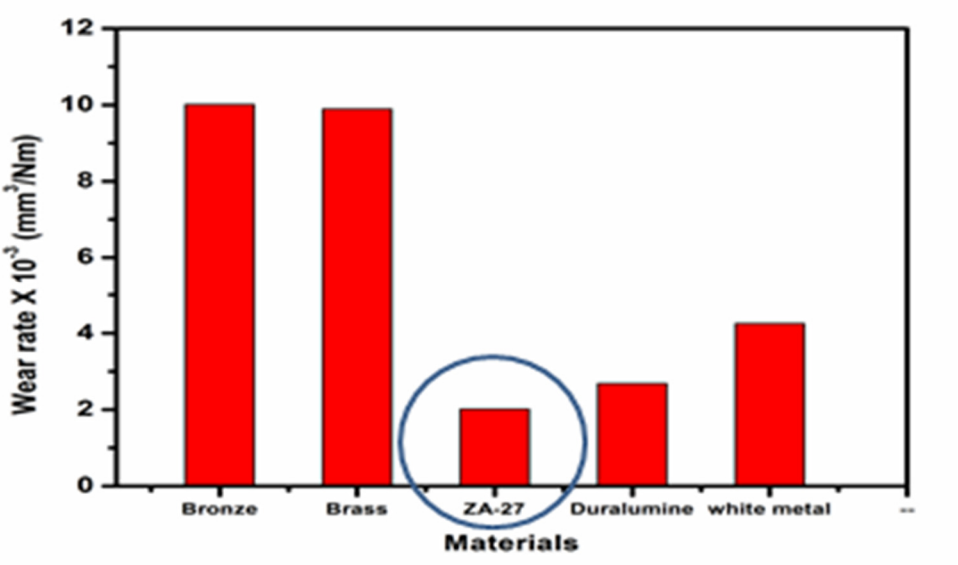

Figure .1.2 Wear rates of the different bearing materials

In recent years ZA alloys have been introduced for bearing materials due to low cost and excellent wear resistance properties as compared to other alloys like bronze. The cost of the zinc alloys on a weight basis is about one-third that of the bronze alloys. The melting-energy requirements for zinc alloys are substantially lower than those for bronze, the world supply of zinc is abundant, and the price is relatively stable compared to other materials [10]. Among the zinc alloys, ZA-27 alloy shows better wear resistance properties compared to other alloys. The failure of bearing materials is caused by the surface fatigue failure (spalling), improper assembly, insufficient lubrication, corrosion and overloading. To improve the bearing properties, reinforcement particles having good strength and excellent lubricating properties are incorporated in the matrix materials.

1.7. Zinc- aluminium 27 alloy (ZA-27)

ZA-27 alloy is the lightest alloy with a superior combination of wear resistance and mechanical strength compared to other ZA alloys. To achieve such a combination of mechanical properties and castability of the ZA-27 alloy, small amounts of magnesium and copper are added. The elemental composition of the ZA-27 alloy as shown in Table 1.1 was selected as matrix material for the fabrication of the composites [11].

Table 1.1 Chemical composition of the ZA-27 alloy as per ASTM B669-82

Material	Aluminium	Copper	Magnesium	Zinc
Weight percentage (wt %)	25-28	1-2.5	0.01-0.02	Balance

ZA-27 alloy has superior properties compared to other ZA alloys. The tensile strength is 50% higher, ductility is slightly higher and creep resistance is significantly more than the other ZA alloys. ZA-27 alloy is stronger and harder than the conventional brass and aluminium alloys. The physical and mechanical properties of ZA-27 alloy are given in the below table1.2 and table 1.3.

Table 1.2 Physical properties of the ZA-27 alloy

Physical properties	**Units**	**ZA-27 alloy**
Density	g/cm^3	5.0
Melting Range	°C	480-580
Thermal Conductivity	W/m/°K	125.5
Specific Heat	J/kg/°K	523
Pattern of Die Shrinkage	mm/m	13.0
Solidification Shrinkage	%	1.26

Table 1.3 Mechanical properties of the ZA-27 alloy

Mechanical properties	**Units**	**ZA-27 alloy**
Ultimate tensile strength	MPa	420-490

Yield strength - 0.2% offset	MPa	378
Elongation	[% in 2"]	2-8
Shear strength	MPa	290
Hardness	BHN	90-110
Fatigue strength rotary bend in $5x10^8$ cycles	MPa	103
Compressive yield strength 0.1% offset	MPa	255
Modulus of elasticity	(MPa x 10^3)	77.9
Poisson's ratio	-	0.32

In general ZA-27 alloys have the following properties:

- Lower density compared to all other bearing alloys. Hence, ZA-27 alloy bearings are lighter in weight.
- Hardness values superior to bronze and aluminium alloys when coefficient of friction are comparable. Hardness is an indicator of wear resistance.
- Higher UTS and yield strength compared to aluminium alloys, cast iron, and gunmetal and leaded bronzes.
- Higher co-efficient of thermal expansion which necessitates higher clearance between the bearing and shaft compared to other bearing alloys.
- Outstanding compression strength, comparable to that of cast iron and superior to all types of bronze alloys. This property enables ZA-27 alloys to carry very heavy loads.
- Possess higher specific heat and outstanding superior electrical and thermal conductivity compared to all other alloys.

1.7.1.Advantages of ZA-27 alloys

- They have low melting point. Therefore, they can be diecast at high productivity rates.

- Products of near-net shapes and intricate designs with close dimensional tolerances can be produced.
- Zinc-die castings can be machined, bent, swaged or coined for finishing.
- Zinc-die castings can be riveted, welded or soldered easily in assembling.
- Atmospheric corrosion resistance is very good.
- Strength is sufficient for many applications.
- Cost is competitive with aluminium and copper for many applications.

1.7.2. Disadvantages of ZA-27alloys

- ZA-27 alloys cannot be used for high temperature applications such as processes over 100°C, because of loss of strength and hardness.
- Dimensional instability at temperature above 100^{o}C
- Large co-efficient of thermal expansion
- Low damping capacity
- Hexagonal close packed crystal structure that limits plastic deformation.

To overcome the disadvantages of the ZA-27 alloy the thermally stable secondary phase reinforcement particles are added to the matric materials.

1.8. Reinforcement materials

The term reinforcement is very extensive and involves a very wide range of materials which plays a significant role for the enhancement in performance of matrix alloys and their composites. Reinforcement constituents are used to decrease the material cost, to improve the mechanical properties, wear resistance, process ability and reduces shrinkages. The matrix material and reinforcing phase of the composites are properly selected to improve the mechanical and wear resistance properties than that of the metal matrix materials. The addition of reinforcement materials into various kind of matrix material will show reasonable mechanical property considerations. A metal matrix composite system offers superior stiffness and temperature capability over the base matrix material, but decreases the ductility. The purpose of ceramic reinforcement materials is to improve the strength without compromising the several

attractive properties of the matrix materials like mechanical, wear resistance and refractoriness. Metal matrix composites with almost complete dimensional stability over an extensive range of temperature can be considered to have exceptional physical, mechanical and wear resistance properties compared to the parent matrix material which are used in industrial applications.

The composites reinforced with particulates are characterized by dispersed particles having a diameter greater than 1 μm with a weight percentage of 5 to 40 %. Fibers have one long dimension whereas particle reinforcements do not. Composites reinforced with particles show isotropy stiffness improvements with mostly minor degradation of fracture properties than whisker reinforced MMCs. In addition, particle reinforcements are cost effective since the abrasives industry provides a large established commercial production base for ceramic particles. The available particle reinforcement candidates include Sic, $A1_20_3$, Tic and Boron. Silicon carbide and aluminium oxide are currently the most widely used materials due to their favorable combination of mechanical properties, density, availability, cost and reactivity with matrix alloys [12]. In the current investigation aluminium oxide (Al_2O_3) and molybdenum disulphide (MoS_2) particles are used as reinforcement materials for the preparation of ZA-27 metal matrix composites.

1.8.1. Aluminum oxide (Al_2O_3)

Aluminium oxide (Al_2O_3), commonly referred to as alumina, is the most economical and generally used material in the family of engineering ceramics. The alumina ceramic particle has a very extensive range of applications due to its superior combination of properties such as high hardness, refractoriness, excellent dielectric properties and good thermal properties. Some typical uses of alumina are seal rings, high temperature electrical insulators, wear pads, furnace liner tubes, abrasion resistance tubes etc. The important key properties of the alumina are given in table1.4.

Table 1.4 Engineering Properties of Aluminium Oxide

Properties	**Values**	**Units**
Density	3.89	gm/cm^3

Flexural strength	379	MPa
Shear Modulus	152	GPa
Elastic Modulus	375	GPa
Bulk Modulus	228	GPa
Poisson's Ratio	0.22	----
Compressive Strength	2600	MPa
Hardness	1440	Kg/mm^3
Maximum Use Temperature	1750	^oC
Thermal Conductivity	35	W/m^oK
Coefficient of Thermal Expansion	8.4	$10^{-6}/^oC$

1.8.2. Molybdenum disulphide (MoS_2)

Molybdenum Disulfide (MoS_2) is also called as Moly Disulfide. It has been enormously popular due to its attractive price, easy availability and strength. Molybdenum disulphide (MoS_2) is a solid lubricant which has exerted a significant amount of importance in the scientific community due to its attractive layered structure. MoS_2 acts as a dry lubricant in the composites and improves the wear resistant properties. MoS_2 is widely used by NASA, by the military, aerospace and automotive industry. The key properties of MoS_2 are excellent thermal stability, oxidation resistance at high temperatures, good wear resistant and high working temperature. Table 1.5 shows the properties of molybdenum disulphide.

Table 1.5 Properties of Molybdenum disulphide

Properties	**Values**	**Units**
Density	5.06	gm/cm^3
Maximum Use Temperature	1185	^oC

Thermal Conductivity	131 (monolayer) 2.3 (bulk)	W/m^{o}K

1.9. Fabrication Techniques

A variety of processes have been developed to incorporate reinforcements into a metal matrix for the manufacture of a metal matrix composite. These may be divided into primary and secondary processes. In the primary processes, the reinforcement and matrix are combined to form a composite material. A further distinction can be made depending on whether the matrix becomes liquid at any stage. Secondary processes include consolidation and/or forming operations such as die casting, forging, rolling, extrusion and machining which are used to shape the primary composite material into a finished product.

The most commonly used primary fabrication processes as well as their applicability to the production of different types of metal matrix composites are discussed in detail. Primary liquid processing techniques involve the matrix becoming at least partially molten as it is brought into contact with the reinforcement phase. This generally promotes a strong ceramic-to-metal bond due to the intimate contact between the two phases. However, Liquid phase processing of MMCs can also lead to the formation of deleterious interfacial reaction phases. The microstructures of composites produced by liquid phase methods are sensitive to factors such as process temperature, contact time and pressure. Commonly used liquid phase processes for fabrication of metal matrix composites include:

i) Squeeze casting process
ii) Stir casting process
iii) Ultrasonic assisted stir casting process

1.9.1. Squeeze Casting

The term squeeze casting applies to various processes in which pressure is imposed on a solidifying system, usually through a hydraulically activated ram. With regard to MMCs technology, the most frequent use of squeeze casting is for primary composite fabrication. However, squeeze casting technique can be also used as a secondary process in which a

composite obtained by some other primary process is remelted and solidified under pressure to produce a near-net-shape part squeeze casting which provides fine microstructures due to the rapid cooling induced by the intimate contact between the melt and massive metal mold [13].

Figure 1.3 shows a schematic diagram of squeeze casting for primary composite fabrication. This process, also called squeeze infiltration, involves the injection of liquid metal into the interstices of an assembly of fibers or particles which is called a preform. The reinforcements in the preform are held together using a binding agent to form a strong, porous and three-dimensional array. The preform is fabricated by sedimentation of short fibers, particles or whiskers from a liquid suspension.

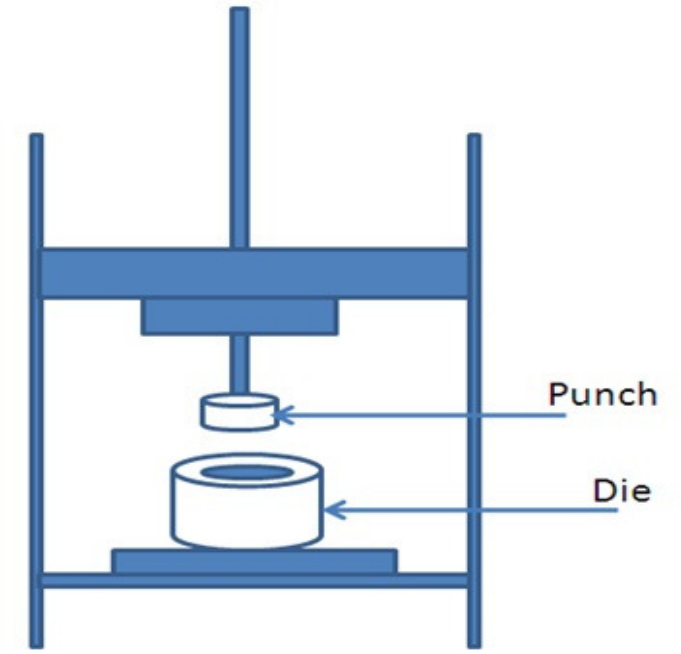

Figure 1.3 Schematic diagram of squeeze casting machine

Squeeze infiltration takes place in four consecutive steps:

- the preform is preheated and placed in a preheated die,
- the superheated melt is poured into the die,
- the ram is lowered until the desired pressure is reached and the composite is allowed to solidify under pressure,
- the casting is extracted from the mold

1.9.2. Stir Casting

Stir casting consists of mixing particle reinforcements into the liquid metal and subsequently casting and fabricating the mixture in a similar manner as the unreinforced alloys. This process, which is also called slurry casting, is the simplest and most cost effective method of MMC fabrication. The addition of particles to liquid metal causes a significant increase of the viscosity of the melt. The melt viscosity increases with an increase of the volume fraction of reinforcement and with a decrease of particle size. This effectively limits the volume fraction of particles that can be incorporated by stir casting is to about 25 vol. %. The schematic diagram of stir casting machine for the fabrication of the metal matrix composites was shown in Figure 1.4.

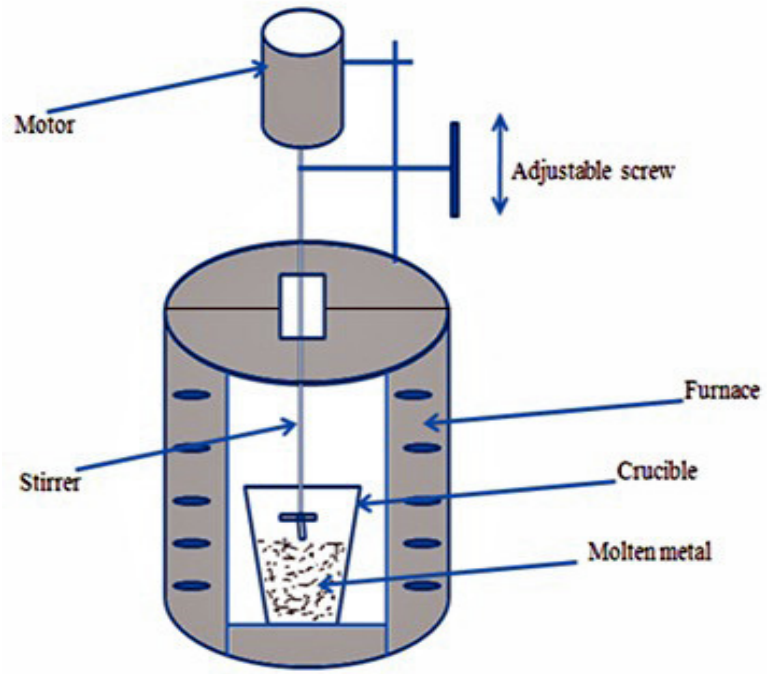

Figure 1.4 Schematic diagram of stir casting machine

The properties of metal matrix composites are influenced by their microstructure including reinforcement distribution, porosity from gas entrapment and/or inadequate feeding during solidification and interfacial reactions. The distribution of particles in the solidified composite is influenced by two factors: particle distribution during stirring and particle segregation during solidification of the composite melt [14]. The particle distribution in the melt

depends upon the efficiency of the mixing process and any sedimentation or floatation that occurs during handling of the melt prior to pouring. Even if the composite melt is well mixed with a uniform distribution of particles, segregation of the particles during solidification of the melt can result in severely non-homogeneous particle distributions. During the solidification of composite melts, the particles are rejected at the meniscus of the growing solid and are trapped in the interdendritic regions during the final stage of the solidification process. The rejection of particles to interdendritic regions means that the particle distribution in the solidified composite is governed by the solidification rate i.e. by the casting process.

1.9.3. Ultrasonic assisted stir casting

The ultrasonic assisted stir casting process is similar to stir casting method followed by the ultrasonification in the melt for the preparation of nanocomposites. The solidification process influences the reinforcement particles present in the composites in different ways such as through chemical reaction with the matrix material; settling in the melt and impingement of the solidification growth on the particles occurs as result of particle pushing. The molten metal always has the tendency to form clusters and combined together to reduce the free energy of the entire system due to the presence of small reinforcement particles in the composites. The large clusters of particles present in composites can be broken up by using mechanical stirring but the smaller cluster particles cannot be broken up due to the lesser shear stress in the melt. Thereby, some clusters still exist in the matrix metal after mechanical stirring. Furthermore, oxide inclusions are easily formed on the surface of the molten metal, and these oxide inclusions can enter into the melt during vigorous mechanical stirring. Additionally, gases are inevitably entrained in the oxide inclusions, which form the porosity in the metal after solidification. To overcome the limitations of stir casting process an ultrasonic assisted casting technique is used [15]. The schematic diagram of the ultrasonic assisted stir casting machine is shown in Figure 1.5.

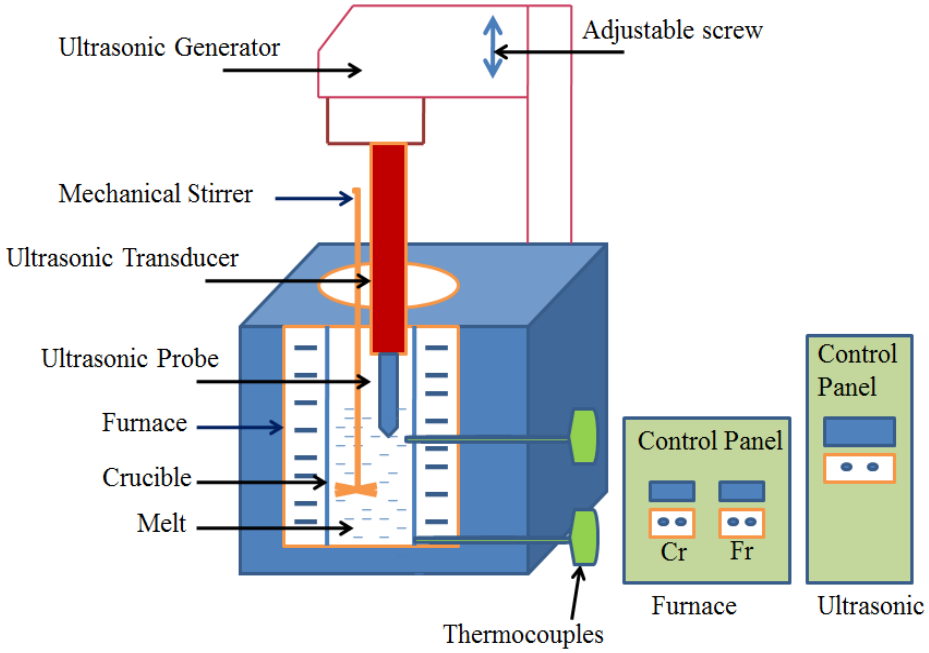

Figure 1.5 Schematic diagram of ultrasonic assisted stir casting machine

In the proposed method stir casting method is combined with ultrasonic probe processing. The process is named ultrasonic probe assisted stir casting method. The process will combine the advantages associated with ultrasonic probe as well as stir casting process. The combined process will improve the uniformity in dispersion of nano particles due to ultrasonic cavitation effect and avoid the settlement of nano particles in metal matrix due to continuous stirring with the stirrer. This will help to produce nanocomposites which enhance mechanical and tribological properties. The working principle of ultrasonic assisted stir casting process is to generate the ultrasonic waves with a frequency of 18 to 20 kHz. When these waves propagate through the molten metal, alternating compression and dilation cycles are produced. These waves are generated by mechanical vibrations of frequencies higher than 18 kHz. The high intensity ultrasonic waves at the end of alternating compression and dilation cycles make the micro bubbles develop in the liquid. When they attain a volume at which they can no longer absorb enough energy, they implode violently. This phenomenon is known as cavitation. During implosion, very high temperatures and pressures are reached inside these bubbles. At the end of the cavitation cycle; collapse of micro bubbles produce transient micro hot spots that can reach very high temperatures and pressures. Implosive impact of cavitation is strong enough to break clusters of nano particles to disperse them uniformly in the metal matrix

1.10. Characterization of metal matrix composites

Characterization of the composite materials is a vital role for the development of new materials and fabrication process. The characterization includes the physical, chemical, mechanical and tribological behavior to ensure the understanding of composite materials which are used for various industrial applications. Physical property like density of the composite materials was varied with different reinforcement content of the ceramic particles which are added in the matrix materials. The homogeneous distribution of various weight percentages of the reinforcement particles and the chemical composition of the composite materials was examined by using microstructure characterization. The mechanical properties of the composites can be subjective to the geometrical preparation of the phases, measurement of the modules and the structural process as periodicity of the component stages. Mechanical properties of the metal matrix composites are dependent on the type and mass fractions of the filler particles, defects occurring during the fabrication process and the dislocation strength of the composites [16]. The composite materials which are reinforced with the various mass fractions of the ceramic particles were tested on different machines to analyse the tensile strength, yield strength and hardness.

The metal matrix composites form a very essential class of tribo-engineering materials and regularly used in mechanical components. The loss of a solid surface, including the progressive damage to the materials due to relative motion among the surfaces and a contacting material or materials, is known as wear. There are two major terms to describe the wear modes of the composites abrasive wear and adhesive wear. The wear occurs when two contacting surfaces slide against each other and the harder particles in one cut through the other is termed as abrasive wear. This form of wear comes into play when a tangential motion causes the material removal by the simultaneous micro-ploughing and micro-cutting. The adhesive wear occurs due to confined bonding between the contacting surfaces leading to material transfer between the two surfaces or the loss from either surface. These days much attention is devoted towards the study of dry sliding wear behavior of various composites owing to the high potential use of these materials in several mechanical and structural applications.

1.11. Organization of thesis

The thesis is organized into seven chapters.

Chapter-1: Introduction

A brief background to the work has been reported in this chapter and insights into metal matrix composites and their applications are introduced. ZA-27 alloy and reinforcement particles used in this study are described here. At the end of the chapter the fabrication process is also explained briefly for the preparation of the metal matrix nanocomposites and the characterization of fabricated composites are discussed.

Chapter-2: Literature review

The literature on the topics related to metal matrix composites, ZA-27 alloys, fabrication techniques, mechanical properties, tribological behavior and optimization techniques are presented in this chapter. Based on literature survey, research gaps are identified and objectives are formulated at the end of this chapter.

Chapter-3: Experimental setup and equipments

A description on the experimental set-up and equipment with their specifications are given in this chapter. Optimization technique is used for the selection of process parameters with their ranges and levels while conducting the experiments to fulfill the wear characteristics of the present work on ZA-27 nanocomposites.

Chapter-4: Fabrication and microstructural characterization of the ZA-27 nanocomposites and hybrid nanocomposites

The fabrication procedure for the preparation of ZA-27 nanocomposites is explained in this chapter. The microstructural analysis, elemental composition and the density measurements of ZA-27 nanocomposites and hybrid nanocomposites were described in this chapter.

Chapter-5: Mechanical properties of the ZA-27 nanocomposites and hybrid nanocomposites

This chapter gives the mechanical properties such as microhardness, ultimate tensile strength, yield strength and fatigue strength of the ZA-27 nanocomposites and hybrid nanocomposites.

Chapter-6: Tribological behavior of the ZA-27 nanocomposites and hybrid nanocomposites

The tribological behavior of ZA-27 nanocomposites and hybrid nanocomposites was studied out by using pin on disc friction and wear testing machine. The optimization technique used to find the significant process parameters for the tribological properties of ZA-27 nanocomposites are explained in this chapter.

Chapter-7: Conclusions and future scope

The conclusions drawn from the results obtained by conducting experimental investigations and optimization of tribological properties of the ZA-27 nanocomposites and hybrid nanocomposites are presented in this chapter. The limitations encountered during the conduct of research and possible extensions to the present work are given in the form of scope for future research.

References

The published research work reported by earlier authors in the related area in the form of journal papers, conference papers, text books, manuals and hand books which are cited in the thesis have been listed under the heading “References”.

CHAPTER 2

LITERATURE REVIEW

2.1. Introduction

The literature survey provides the background information of the current research work in this chapter. The review of the literature reveals gaps in the previous investigations and helps to select the objectives of the present research activities. Metal matrix composites and the ZA-27 alloy MMCs have been discussed in detail, while including previous research findings. A short research history which holds several features of the metal matrix composites with a distinct reference to their fabrication techniques, mechanical properties, wear behavior and design of experiments has also been presented.

2.2. Metal matrix composites

Metal matrix composites (MMCs) are innovative materials which are used mainly for high temperature applications and presently being developed to a rapid extent. Now a days the trend is towards safe use of metal matrix composites for applications demanding metals that are have light weight, good structural rigidity, dimensional stability and good strength at high temperature [17]. The superior mechanical properties like tensile strength, yield strength, hardness, better elastic modulus, high temperature stability and wear resistance properties in comparison with the parent matrix alloy will increase the demand for stiff, strong and lightweight materials in the development of metal matrix composites reinforced with ceramic dispersoids. The popular alloys are mainly selected on the basis of their established better properties to use the matrix materials in the MMCs [18-20]. The continuous and discontinuous reinforcement materials in the form of particulates, whiskers and fibers were used in MMCs. For many engineering applications MMCs reinforced with discontinuous particulates have great potential compared to other reinforced materials. The MMCs are considered as potential engineering materials which possess excellent mechanical and tribological properties for different applications [21-23]. Some of the matrix and reinforcement materials are listed given in table 2.1.

Table 2.1 Matrix and Reinforcement materials

Matrix materials	Reinforcement materials
Aluminium and alloys	C, Be, SiO_2, B, SiC, Gr, Al_2O_3, Steel, B_4C, Mo, W, ZrO_2
Titanium and alloys	B, SiC, Mo, SiO_2, Be,ZrO_2
Zinc based alloys	SiC, Al_2O_3, B_4C, ZrO_2,Gr
Nickel and alloys	C, Be, Al_2O_3,SiC, Si_3N_4, steel, W, Mo, B
Magnesium alloys	C, B, glass, Al_2O_3
Molybdenum and alloys	B, ZrO_2
Iron and steel	B, Al_2O_3, W, SiO_2,ZrO_2
Copper and alloys	C,B, Al_2O_3, E-glass

Reinforcement materials containing metal or ceramic particulates such as SiC, Al_2O_3, graphite, aluminium diboride, cemented carbide, tungsten carbide, niobium carbide, NiAl, TiC, Si_3N_4, $MoSi_2$, Mg, TiB_2 etc. are used now a days to increase the performance of metal matrix composites to a great extent. The particulate metal matrix composites depend strongly on the particle-matrix interface adhesion, particle loading, particle content and the particle size to improve the mechanical and tribological properties. The hard and thermally stable ceramic particles reinforced in the parent matrix alloy contribute to superior elastic modulus, higher hardness, lower coefficient of thermal expansion and improves the properties of the MMCs at elevated temperatures [24-25]. Mostly particulate reinforcements are used in metal matrix for many reasons such as low cost, better processing, thermal conductivity, control of thermal expansion, density control, magnetic properties, electrical properties, improved mechanical properties and better wear resistance.

2.3. Zinc aluminium-27 MMCs

Zinc based alloys have been used for many years in various engineering and industrial applications. Among the zinc based alloys, the range of zinc-aluminum (ZA) alloys was expanded due to their improved properties. These ZA alloys are used primarily for die casting applications due to their superior properties due to the excellent castability, easy finishing,

inexpensive cost and good mechanical strength and wear resistance [26-28]. There is an extensive use of the ZA alloys in many engineering applications like aerospace and automotive industries. The major alloying element in the zinc based alloys is aluminium because it imparts fluidity to the alloys in order to achieve better engineering properties [29-31].

Many investigations were carried out to increase the properties of the zinc–aluminum based alloys and to improve their applications in the field of automobile industries. These days zinc aluminium alloys have been used for conventional journal bearing materials particularly in high load and low speed industrial applications. Materials like cast iron, white metal and bronze which have been widely used for conventional journal bearing materials were replaced with zinc aluminium based alloy because of their excellent properties. The high strength with low casting temperature of the ZA based alloys have more advantages compared to aluminium based alloys. During the recent years the major progress in zinc casting production was to introduce the new zinc alloys containing the higher aluminium, namely ZA-8, ZA-12 and ZA-27 alloys [32-35]. The numerical values indicate that the weight percentage of the aluminium content in the zinc aluminium based alloys. From these alloys ZA-27 alloy is the lightest alloy which offers excellent wear resistance and mechanical properties with significant industrial use than that of other zinc based alloys [36-39].

ZA-27 alloy exhibits high wear resistance as well as attractive physical, mechanical and technological properties such as low melting point and density, high hardness and strength at ambient temperatures, good damping behavior, easy machinability and high corrosion resistance. These superior properties of ZA-27 alloy were the reasons for the replacement of the journal bearing material instead of aluminium cast alloys, copper based alloys and bronze alloys in various engineering applications [40-42]. ZA-27 alloy was suitable for low speed and high load applications due to high hardness, strength and wear resistance. The addition of copper in ZA-27 alloy affects the structure and improves various properties like fatigue strength, creep and hardness of the alloy. The addition of magnesium in the ZA-27 alloy improves the wettability properties of the melt during the fabrication of the composites. Literature gives more evidence about the elements that contribute to increase the ZA-27 alloy properties [43-46].

2.4. Fabrication of ZA-27 composites

2.4.1. Squeeze Casting

Squeeze casting is a combination of casting and forging process, it also known as liquid metal forging. In this method the melt is poured into the preheated die and the pressure is applied with the help of punch or ram during the solidification. This method is used for the preparation of metal matrix composites. For the fabrication of the composites materials some of the researchers used squeeze casting process to obtain better mechanical and wear properties. To prepare zinc aluminium alloy ingots 99% purity of zinc, aluminium, copper and magnesium was used. The composition of the ZA-27 alloy specimen is as follows: Al-27%; Cu-2%; Mg-0.02%, and Zn-balance (weight percentages).The ZA-27 alloy were prepared with the help of squeeze casting technique to measure the different properties of the metal matrix materials [47-48].

Commercially pure zinc, aluminium, copper and magnesium were used for the preparation of ZA alloys with varying aluminium content ingots by using squeeze casting process. The process involves the melting of alloys at a temperature of 500^0C above liquidus temperature in an electric resistance furnace and pouring the melt into the preheated die. In this process, the melt is poured into the die cavity and forced with a 0.1 MN piston. ZA alloys ingots with different aluminium content are fabricated by using squeeze and gravity cast to investigate the different properties [49].

The experimental alloys were prepared by using pure zinc, pure aluminium, pure magnesium and pure copper. T4–treated aluminium alloys were fabricated with the help of gravity die casting and squeeze casting methods to study various properties of composites [50]. Aluminium oxide fibre was reinforced in ZA-12 alloy with different volume fractions for preparation of the composites by using squeeze casting process. First, the raw materials of ZA-12 alloy were melted at 500^o C temperature using an electric resistance. After melting the base alloy, the preheated reinforcement materials were added in the melt with the help of mechanical stirrer to form composites. Then the molten metal was poured into the preheated mould below the applied pressure of 100 Mpa [51].

ZA-27 alloy reinforced with SiC, ZrO_2 and C particulates with 5 volume percentage composites are prepared by using stirring route followed by squeeze casting process. The base metal was placed in the graphite crucible and heated upto 500^o C above its melting temperature. The mechanical stirrer was employed into the melt and rotated at a speed of 600 rpm to form vortex in the melt, then add the particles in the melt and stirring is continued for 1 minute. The molten melt of the composite prepared with the help of stirring process was poured into the pre heated die and the punch was lowered until it came into contact with the molten composite. The hydraulic press of 60 ton was used for the squeeze casting experiments [52].

2.4.2. Stir casting

The Stir Casting method is a commonly used method for mixing reinforcement into molten matrix material to produce composite materials. This is the simplest and most commercially used technique also known as vortex technique. The process is simple, flexible, used for large quantity production and economical. Many of the researchers have used stir casting technique for manufacture of the metal matrix composites to study the various properties [53-57]. Yu Li et al used stir casting method for the preparation of AA6061 alloy reinforced with 31 wt % (weight percentage) B_4C particles with a size of 23 μm. It was observed that AA6061/ 31% B_4C composite were prepared successfully by using a sophisticated stir casting route [58].

S.A. Sajjadi et al. concentrated on the A356 alloy as a matrix material and alumina particles of 20 μm and 50 nm were used as the filler material. Compo casting and stir casting method was used for production of composites specimens. The weight percentage of the alumina particles ranging from 1, 3, 5 and 7.5 wt % micro size and 1, 2, 3 and 4 wt % nano size particles were added into the composites. The alloy was heated at a temperature of 700^{0}C above its liquid temperature by using electric furnace and after melting the alumina particles with micro and nano size were added into the melt and stirred for 30 minutes to mix uniformly. After stirring process is completed the molten metals was poured into the preheated die to enable it to solidify [59].

The Al-Si 10Mg alloy as a base material has excellent resistance to corrosion in both normal atmospheric and marine environments collectively exhibiting high strength and hardness. Molybdenum disulphide (MoS_2), a solid lubricant with a size of 1.5 μm was used as the filler material. The melting of Al-Si10Mg alloy was carried out under argon atmosphere at 1073 K and

the MoS_2 particulates with 2 wt % and 4 wt % were incorporated into the molten metal and stirred continuously for ten minutes. The molten metal of the composite was poured into the cylindrical die to solidify. The aluminium-molybdenum-disulphide self-lubricating composites were prepared with the help of stir casting process [60].

Stir casting technique is used for the preparation of composites with pure aluminium ingot as base material and Al_2O_3 particles as reinforcement. The matrix material is placed in the graphite crucible and heated at a temperature of 700^0C by using furnace. Various weight percentages of the reinforcement materials was added into the melt and stirred for some time for proper mixing [61]. An enhanced stir casting method in an argon atmosphere was used for the preparation of Al-TiC castings with various weight percentages of reinforcement particles. To improve the wettability of the filler particles in the melt 1 % mass fraction of magnesium was added during the stirring process. The molten metal was poured into the pre-heated die located at the bottom of the furnace [62].

2.4.3. Ultrasonic assisted stir casting

The ultrasonic assisted casting process is very effective in dispersing ceramic particles with nano size in the base matrix materials. The mixing of nano-sized reinforcement particles in the base matrix materials is challenging due to the large surface to volume ratio and poor wettability of the nano-sized particles which results in agglomeration and clusters. To overcome the clusters and agglomeration in the melt and to increase the desired properties of the composites, the ultrasonic probe assisted sonication method is used for the fabrication of metal matrix nano composites [63]. The process generally requires resistance heating furnace for melting metal, nano particle feeding and an ultrasonic system. The ultrasonic processing system consists of an ultrasonic probe, a transducer and power source.

The principle of ultrasonic process is that high intensity ultrasonic waves propagating through the molten metal generate alternating dilation and compression cycles which make the micro bubbles grow in the melt. The micro bubbles no longer absorb enough energy when they attain a certain volume and the bubbles collapse violently which is called cavitation effect. The collapse of the micro bubbles produces transient micro hot spot can influence very high temperatures and pressures at the end of the cavitation cycles. The impact of the cavitation is

strong enough to break the clusters of the nano sized particles to disperse uniformly in the metal matrix [64].

Rahul Gupta et al made an attempt to fabricate aluminum matrix composites by using ultrasonic assisted stir casting process. Firstly aluminium A356 alloy was placed in the graphite crucible and melted at 750^{o} C above its liquidus temperature in the electric resistance furnace. After the alloy was melted completely, slag appeared on top of the molten metal which was removed and average particle size of 42 nm SiC was wrapped in the aluminium foil and added in the melt. Mechanical stirring was done for 15 minutes to allow the reaction between the melt and the particles for proper mixing. After stirring the ultrasonic probe made of Ti-6Al-4V titanium alloy coated with zirconia was inserted into the melt and ultrasonic stirring was done for 3 minutes for uniform distribution of the composites. The molten metal of the composites was poured into the mild steel mould to solidify [65].

R. S. Rana et al selected aluminium alloy 5083 as matrix material and silicon carbide of micron (average particle size 35 μm) and nano size (average particle size 40 nm) particles were used as reinforcement material. The raw material of the aluminium alloy 5083 was placed in the graphite crucible and heated at a temperature of 760^{o} C by using electric resistance furnace. Preheated SiC particles of micron and nano size were added into the melt with different weight percentage and the composite melt was stirred by using mechanical stirrer. Ultrasonification of the composites was done with the help of ultrasonic probe for 5 minutes after the stirring. The composites melt poured and solidified into a mild steel die. The composites have been fabricated for 3, 5, 8 and 10 wt % for micron size and 1, 2, 3 and 4 wt % of nano size through ultrasonic assisted stir casting method [66].

In the current research work the ultrasonic assisted stir casting process is used for the preparation of ZA-27 nanocomposites with different weight percentages of the reinforcement particles. The process is named ultrasonic probe assisted stir casting method because stir casting method is combined with the ultrasonic probe processing. The method will combine the benefits related with the stir casting as well as ultrasonic probe processing. The combined process will increase the homogeneity in dispersion of nano particles due to ultrasonic cavitation effect and prevent the settling of nano particles in metal matrix due to continuous stirring with the stirrer. This process increases the properties of the metal matrix nano composites.

2.5. Mechanical properties of metal matrix composites

Mechanical properties of the composites can be influenced by the geometrical arrangement of the phases, dimension of the components and the structural procedure as periodicity of the component phases. It has been seen from the literature review that the mechanical properties of the metal matrix composites can be dependent on the type and weight percentage of the filler particles, dislocation strength and the defects occurred during the fabrication process of the composites. In metal matrix composites most commonly measured mechanical properties are hardness, tensile strength, ductility, fatigue strength and fracture. The mechanical properties of the composites materials are investigated by many authors.

K. H. W. Seah et al investigated the tensile and compressive strength of the cast and heated ZA-27/graphite particulates composites. The graphite particles with average particle size of 90-150 μm are reinforced with different weight percentage ranging from 1, 3 and 5 wt %. Heat treatment of the composites was performed for 1, 2, 3 and 4 hours respectively at a temperature of 280^{o} C. It was observed from the results that as the graphite content increases in the composites, there were major increases in the ultimate tensile strength, ductility and compressive strength. The hardness of the composites drops tremendously as the graphite composition was increased. The same results were observed for the heat treated specimens of the composite [67]. Many researchers have been studied the influence of graphite and short glass fibers reinforced in ZA-27 composites on mechanical properties [68-71]

The mechanical properties and fracture mechanism were studied with the main objective of understanding the effect of the reinforcement particles on the behavior of ZA-27 alloy. The zircon particles with different weight percentages varying from 1, 3 and 5 wt % were reinforced in matrix alloy to form composites. The results revealed that an increase in the hardness, Young's modulus, ultimate tensile strength and yield strength of the composites was achieved by increasing zircon content, but ductility and impact strength decrease [72]. The presence of the hard reinforcement particles in the ZA-27 composites samples improved the fracture behavior significantly [73-75].

Silicon carbide particles with the average particle size of 100-150 μm were reinforced in ZA-27 alloy with the various weight percentages of 0 to 5% by weight for the preparation of the

composites. Heat treatment was done for the composites at 320^{o} C for 1, 2, 3 and 4 hours respectively. The mechanical properties such as ultimate tensile strength, hardness, ductility and impact strength were carried out for the composites. The results report that the adding of particles increases in the base material while the hardness and ultimate tensile strength increase but the ductility and the impact strength decrease for the composites. The heat treated composites improve the ductility and impact strength but the hardness and the ultimate tensile strength decreases when the silicon particle increases [76-77].

H. R. Ezatpour et al reported that the mechanical properties of the composites prepared with different weight percentages ranging from 3 to 7 wt % were reinforced in aluminium alloy. The ultimate tensile strength, yield strength and hardness of the aluminium matrix composite increases when alumina particle increases in the matrix alloy [78]. A356 alloy is reinforced with 10 weight percentage of silicon carbide particles of 10 μm size for preparation of the composite. The ultimate tensile strength and hardness tests were carried out for cast and T6 heat treated composite. The ultimate tensile strength and hardness of heat treated composites improves compared to the cast specimens [79].

The authors initiates that the modification effect of the zinc aluminium based master alloy will improve the tensile strength, elongation, impact toughness and hardness compared to the base alloy [80-83]. The mechanical properties of ZA-27 reinforced with 10 wt % Al_2O_3 particles with an average particle size of 0.7 μm composite were carried out and results reported that the tensile strength and hardness increases compared to the base matrix material [84]. The hard ceramic particles reinforced in the matrix materials will improves the mechanical properties of the composites was investigated by many authors [85-89]. Dong Xu-gang et al studied the mechanical and fatigue properties which effected by Cu, Fe and Ni of ZL114A alloy by using high temperature fatigue test. The results reported that Cu, Fe and Ni contents increase in the alloy the tensile strength and cyclic fatigue life improves [90].

Ting Liu, Nai-chao Si et al investigated the influence of Si addition on mechanical and fatigue behavior of zinc aluminium alloy. From the results it was observed that 0.55 wt % of Si addition in the base alloy gives the best mechanical properties and fatigue, when Si content exceeds 0.55 % Si phases become larger and agglomeration forms in the alloy which reduces the mechanical properties [91]. C.S.Ramesh et al concentrated on the fatigue analysis of Al 6061

alloy reinforced with silicon nitride particles varied from 6, 8 and 10 wt % composites. The composites and base matrix were hot forged at a temperature of 500^{o} C using a 300T hydraulic hammer. It was reported that, the fatigue strength improves significantly with increasing the reinforcement content in cast and hot forged composites than that of the matrix alloy under identical operating conditions. The hot forged alloy and its composites reveal superior fatigue strength when compare to the cast matrix alloy and its composites [92-94].

The fatigue tests for the composites with the silicon carbide particles are reinforced in the high strength spray formed series Al-alloys. The fatigue strength of the composite materials displayed an enormous increase when compare to the commercial ingot of the Al-alloys series [95-96]. Cheng-kun Zheng et al concentrated on the mechanical properties and low cycle fatigue behavior of T4- treated aluminium alloys fabricated by using gravity die casting and squeeze casting process. The mechanical properties of squeeze casting samples are considerably improved than those of gravity casting samples due to fewer cast defects. Superior fatigue properties are attained for the squeeze casting alloy compared with the gravity casting alloy [97].

2.6. Dry sliding wear behavior of metal matrix composites

Wear is defined as the process occurring at the interfaces between the two interacting surfaces of solids within the working environment which results in dimensional loss. The prominent meaning of wear as removing the material from one surface to another or movement of material within a single surface or loss of material from a surface has been familiar for last few years. The machines in which single surface rolls or slides against other surfaces either with or without the presence of an applied lubricant are used to study the wear resistance properties of the metal matrix composites [98]. In the current research work, the wear characterization of the composites were examined with the help of dry sliding wear by using pin on disc friction and wear testing machine.

Gencaga Purcek et al investigated the friction and wear behavior of zinc-based alloys and SAE 660 bronze under dry sliding conditions. From the results it was observed that the zinc-based alloys have higher wear resistance and lower coefficients of friction compared to bronze. The layered structures were formed by rubbing and surrounding the oxidized ZA alloy was hard

and measured to have contributed to their low wear rates than bronze [99]. Wear tests of lubricated journal bearings were fabricated with Si addition in ZA-27 alloy was examined. It was reported that the modified ZA-27 alloy shows significant improvement in the wear resistance compared with ZA-27 alloy [100-104].

K.H.W. Seah et al studied the dry sliding wear properties of the cast ZA-27 alloy and composites containing different weight percentages of the graphite particles were tested at various speeds and loads by using pin on disc testing apparatus. It was observed that the wear rate of composites decreases by increasing the graphite content compared to ZA-alloy. The wear rate decreased as the sliding speed increased, and increased with an increase in applied load [105]. Dry sliding friction and wear behavior were studied on the effects of the fibre mass fraction, applied load, time and the fibre orientation of the zinc aluminium alloy reinforced with alumina particles composites. It shows that the volume fraction of the alumina particles increases the wear rate and friction coefficient of the composites decreases. When the fibres were parallel to the friction surface both the wear rate and friction coefficient decreases and it depends on fibre orientation. The coefficient of friction decreased with load, and increased with time [106-108].

S. C. Sharma et al investigated the wear behavior of the composites reinforced with the short glass fibres with different weight percentages in ZA-27 alloy were carried out by using pin-on-disc apparatus. As reinforcement particles increase in the base alloy the wear rate of the composites decreases [109-111]. The unlubricated sliding wear behavior of a zinc based alloy and composites reinforced with the aluminium oxide particles were carried out by using pin on disc machine at various sliding speeds and applied pressures. The results shows that the composites attain lower wear rate at higher seizure pressures and sliding speeds compare to the matrix alloy. The presence of the dispersoids in the composites develops greater thermal stability which will reduce the wear rate than that of the zinc based alloy [112-115].

The friction characteristics of the zinc based alloy bearings were investigated by using journal bearing test machine under different operating conditions. The coefficient of friction reduced with improving bearing pressure particularly in the mixed and hydrodynamic lubrication regions [116]. The wear properties of the composites i.e Al 2024/ TiB_2 and Al 2024/ (TiB_2+h-BN), were investigated at room temperature in atmospheric environment by using pin on disc wear tester at different loads and speeds. It was reported that the reinforcement of h-BN

composites increases the wear properties particularly at low sliding speed and low load compare to the other composites [117].

Pei-peng Jin et al investigated the dry sliding wear behavior of 6061Al reinforced $Mg_2B_2O_5$ whisker coated with ZnO matrix composite by using a ball-on-disk wear-testing machine. The result shows a decrease in the wear rate of the composite as compared to the matrix alloy. The wear rate and friction coefficient of the composites decreases when increasing the sliding speed and applied load [118-120]. A. Pramanik investigated the influence of the filler material on the unlubricated sliding wear mechanism of Al 6061 alloy and 10 wt % of aluminium oxide composites was examined by considering various factors, such as sliding speed, sliding distance and sliding pressure by using pin on disc machine. The effect of the reinforcement particles increases the wear resistance of the composites when compared to the corresponding matrix alloy [121-124].

The pin on disc testing machine is used for the dry sliding wear behavior of the composites with the Al_2O_3 particles reinforced in aluminium alloy at different operating conditions. It was reported the wear loss and friction coefficient of composite increases as the load increases. When the sliding speed increases the surface temperature of the composite increases which produces the oxidation layer on the specimen due to which the wear loss and friction coefficient decreases [125]. The composites with titanium carbide particles reinforced in aluminium matrix were investigated to study the unlubricated sliding wear characteristics at different operating conditions by using pin on disc machine. The wear resistance of the composites increases by increasing the reinforcement content of titanium carbide [126].

Mehdi Rahimian et al found that the aluminium metal matrix composites with the lower size particles and higher weight percentage of the aluminum oxide reinforcement composites increases the wear resistance compared to the matrix alloy and other particle composites [127]. The dry sliding wear properties of the different particle size and weight percentages of the composites were examined by using pin on disc testing apparatus. The Zinc based and aluminium alloy matrix composites were reinforced with different ceramics particles like SiC, Si_3N_4, B_4C, Al_2O_3 and the graphite flakes without coating. The dry sliding wear characteristics of the different composites were carried out with the help of pin on disc machine at different operating conditions. The composites reinforced with various particles exhibited superior tribological

properties, with the wear becoming more uniform, the wear rate and coefficient of friction decreasing significantly and the relative seizure resistance increasing [128-132].

2.7. Mechanical and wear properties of hybrid composites

Hybrid metal matrix composites are essential class of engineering materials used in aerospace and automotive industrial applications due to their lower density, superior specific strength, better mechanical properties and higher wear resistance compared to metal matrix composites materials. The current research in the area of hybrid composites is based on different alloys strengthened with several ceramic particles. Matrix alloy composites with multiple filler particles are finding improved applications because of enhanced mechanical and tribological properties and hence are better alternatives for single reinforced composites. Many researchers have shown that hybrid composites possess higher hardness, higher tensile strength, better wear resistance and lower coefficient of friction when compared to pure alloys [133].

Mitesh Kumar et al studied the hardness and ultimate tensile strength of the hybrid composites. Aluminium oxide particles with 10 wt % and molybdenum disulphide particles with different weight percentages ranging from 3, 5, 7, and 9 wt % were reinforced in the Al 6063 alloy for preparation of hybrid composites using stir casting process. The hardness of the hybrid composites increases slightly and the ultimate tensile strength decreases due to the reinforcement of molybdenum disulphide particles varying from 3 % to 9 % by weight and with the addition of aluminium oxide particles in Al6063 matrix alloy [134]. The hybrid composites reinforced with silicon carbide particles varying from 0-9% and graphite with 3% by weight in ZA-27 alloy were used to study the mechanical properties. The results reveal that, as the percentage of silicon carbide particles was increased, ultimate tensile strength and hardness of the hybrid composites increased with reduction in ductility [135].

The mechanical and tribological properties were investigated on the copper based hybrid composites reinforced with silicon carbide particles that varied from 3wt % to 10wt % and graphite particles with 1 wt % for preparation of composites. The tensile strength and hardness of hybrid composites increases as reinforcement of silicon carbide particles increases. The presence of the graphite content in the hybrid composites reduces the wear rate and the coefficient of

friction compared to the copper alloy [136]. Mechanical and wear properties of mica and silicon carbide ceramic particle with varying weight percentages were reinforced into the Al 356 alloy hybrid composites. Better strength and hardness of the alloys are attained with Al 356 alloy reinforced with 10wt % SiC and 3 wt % mica hybrid composites. The increase in weight percentages of mica increases the wear loss of the hybrid composites [137].

Hybrid aluminum metal matrix composites reinforced with equal weight percentages of silicon carbide and graphite are extensively used to study the strength and wear resistance behavior. The result shows that the increase in reinforcement content will reduce the hardness of the composites. The coefficient of friction is influenced by the reinforcement content, applied load, sliding speed and sliding distance, the most influencing parameters being sliding speed and applied load whereas sliding distance and reinforcement content do not affect the friction coefficient [138]. The dry sliding wear and mechanical behavior of aluminum matrix hybrid composites reinforced with rice husk ash and silicon carbide particulates with equal weight percentages fabricated by stir casting method was investigated. The hybrid composites reinforced with different particles exhibit higher wear resistance than the matrix alloy [139]. The increase in the weight percentages of the reinforcement particles increases the ultimate tensile strength and yield strength, but the elongation of the hybrid composites decreases [140].

The hybrid composites reinforced with 5 wt % -10 wt % silicon carbide particles and 3 wt % - 6 wt % graphite particles in the Al2024 alloy were prepared to study the mechanical properties. From the results it was observed that the tensile strength and elongation are reduced by Gr and SiC particles added into the Al2024 matrix, while the Gr has a more negative influence on the elongation than the SiC particles in the hybrid composites [141-142]. The work was carried out to investigate mechanical properties of aluminium hybrid composites incorporated with groundnut shell ash and silicon carbide with different weight percentages. The results show that with increasing groundnut shell ash in the reinforcing phase, the hardness, tensile strength and specific strength of the composites decreased slightly compared to other hybrid composites. The fracture toughness and percentage elongation of the hybrid composites increases when increasing the reinforcement content of groundnut shell ash [143].

The mechanical properties of Al6061-SiC & Al6061-SiC/Graphite hybrid composites with different percentages were investigated with the help of stir casting process. The microstructures of the composites revealed uniform dispersion of the particles and the density of composites decreases as the reinforcement content increases in the composites. The enhancement in ultimate tensile strength of hybrid composites occurred as reinforcement content of graphite and silicon carbide particles increases in Al6061 alloy [144]. The hybrid metal matrix composite reinforced with SiC particles and Al_2O_3 whiskers was investigated for fatigue crack growth mechanism. The hybrid composite exhibits a higher threshold stress intensity factor range when compared to the composites reinforced with Al_2O_3 and Al alloy, showing superior resistance to crack growth in a lower stress intensity factor range [145].

2.8. Design of experiments for tribological behavior

Statistical techniques have been used frequently for investigation to estimate and/or for optimization for many engineering processes. In an experiment where several parameters are involved and to study the effect of each and every single condition, statistical methods were used. Tribological behavior is a difficult wear phenomenon in which a number of control parameters collectively determine the performance output i.e. the wear rate and friction coefficient for implementation of suitable statistical techniques for process optimization. The current research work addresses this feature by adopting an efficient statistical approach called response surface methodology to optimize the control factors. Many authors have reported on the tribological properties of the composites but limited work has been done on the optimization of wear processes and the influence of control factors on wear rate and friction coefficient.

S. Basavarajappa et al focused their attention on the dry sliding wear behavior of the aluminium metal matrix composites examined by using Taguchi experimental plan. The influence of the wear parameters such as sliding speed, applied load and skidding distance on the dry sliding wear of the composites was investigated with the help of orthogonal array and analysis of variance. The reinforcement particles are the most significant factor that increase the dry sliding wear resistance of the aluminium metal matrix composites [146].

Design of experiments and statistical methods were used to examine the influence of the applied load, sliding speed and solid lubricants on the tribological behavior at different operating

conditions on the copper/silica composites reinforced with graphite (Gr), boron nitride (BN) and molybdenum disulphide (MoS_2) particles. The major observations are that MoS_2 reinforced composite is the best effective lubricant in enhancing the wear resistance compare to other reinforced composites. The solid lubricant is the most influencing parameter affecting the wear resistance of the composites among the three process parameters. Among the three different types of composites MoS_2 reinforced composite shows better wear resistance properties [147].

R. Ranjith kumar et al studied the optimization of dry sliding performances on the aluminum hybrid metal matrix composites using taguchi experimental plan with an L_{27} orthogonal array. The factors selected for the dry sliding wear properties of the composites are applied load, sliding distance and sliding velocity. The composites reinforced with the molybdenum disulphide particles exhibited less wear when compare to the matrix material. It was observed that the wear rate of the composites increases with increasing sliding velocity, sliding distance and applied load [148].

Taguchi method was used to predict parameters like sliding speed, sliding distance and applied load affecting the unlubricated sliding wear behavior of the zinc based alloy composites significantly. The most significant parameters which influenced the wear volume loss of the composites are applied load followed by the sliding speed. The sliding distance exhibited a negative effect on wear indicating that increase in sliding distance reduces wear volume loss of the composites due to the presence of reinforcements [149-150].

Response surface methodology was used to plan and analyze the experiment for tribological behavior of the aluminium matrix composites reinforced with graphite particles. The process parameters used for the wear behavior of the composites is sliding speed, sliding distance, applied load and reinforcement content. It was observed that the most influencing factor for wear behavior of the composites is sliding distance while applied load has a negligible effect on the wear [151].The mechanical properties of the metal matrix composites were carried out by using the response surface methodology to optimize the process parameters [152-153].

The effect of silicon nitride particles on the dry sliding wear of aluminium alloy composites was studied by using response surface methodology with various process parameters. Result showed that sliding distance is the most influential factor and percentage reinforcement is

the factor which affects the wear least. The interaction of percentage reinforcement and load, percentage reinforcement and sliding distance, load and sliding distance, sliding speed and sliding distance also have significant effects on the wear [154-155]. K. Soorya Prakash et al investigated the dry sliding wear behavior of the aluminium matrix composites at various process parameters like reinforcement content, filler size, sliding velocities, applied load and sliding distance by using taguchi L_{27} orthogonal array. The most significant factors influencing the specific wear rate of the composites are applied load and reinforcement size followed by the sliding velocity, sliding distance and reinforcement content [156].

I. Dinaharan et al made an attempt to develop the mathematical model to predict the wear rate of the aluminium alloy reinforced ZrB_2 composites with the help of response surface methodology. The factors considered are applied load, sliding distance, sliding velocity and reinforcement content. The results show that the wear resistance increases when reinforcement content increases in the composites. The reinforcement content is the most influencing factor which affects the wear resistance of the composites compared to other process parameters [157-158].

2.9. Research gaps

From the literature survey the following research gaps were identified.

1. From the literature, ZA-27 alloys was more economic compare to the other conventional journal bearing materials such as bronze, white metal, brass and cast iron alloys. Many researchers have been investigated on ZA-27 alloy matrix material composites reinforced with various micro sizes ceramic particles (SiC, Al_2O_3, ZrO_2, Gr, and B_4C) were fabricated by using stir casting, squeeze casting and compocasting process. The above process reported no uniform dispersion in ZA-27 alloy, when reinforced particles were of nano size.
2. The mechanical properties such as ultimate tensile strength, yield strength and Micro hardness of ZA-27 alloy was enhanced mostly by reinforced with micro particles and nanoparticles of silicon carbide and aluminium oxide were reported by several researchers and very little work was carried out on the fatigue analysis of the ZA-27 alloy which is most essential property for bearing application.

3. From literature, it was observed that the reinforcement of micro sized particles like Al_2O_3, SiC will affect the subsurface hardening, micro cracking tendency, removal of reinforcement particles and damage of reinforcement particles, which leads to fatigue failure.
4. The dry sliding wear characteristics like wear rate and friction coefficient of the ZA-27 alloys incorporated with both micro and Nano silicon carbide, aluminum oxide and graphite particles were investigated by the various researchers. Less work was published using Hybrid nanoparticles.
5. Limited work has been carried out to optimize wear behavior of ZA-27 alloy by varying all the process parameters at a time i.e. reinforcement content, sliding speed, sliding distance and applied load.

2.10. Problem definition

The aim of the present work is to fabricate ZA-27 alloy reinforced with nanoparticles using novel Ultrasonic assisted stir casting process, to enhance mechanical and wear properties of ZA-27 alloy with suitable selection of reinforcement materials for the bearing applications.

2.11. Objectives of the present work

The following objectives were formulated for the present work

1. To fabricate high quality ZA-27 nanocomposites reinforced with aluminium oxide (Al_2O_3), molybdenum disulphide (MoS_2) and a combination of both (Al_2O_3 & MoS_2) by using liquid metallurgy route ultrasonic assisted stir casting technique.
2. To study morphological characteristics of ZA-27 nanocomposites by using Scanning electron microscope (SEM) and Energy dispersive spectroscopy (EDS).
3. To study the mechanical properties such as microhardness, ultimate tensile strength, yield strength and fatigue strength of ZA-27 alloy nanocomposites reinforced with different combinations of both Al_2O_3 & MoS_2 nanoparticles.

4. To study the Tribological behavior of ZA-27 nanocomposites reinforced with different combinations of both Al_2O_3 & MoS_2 nanoparticles using pin on disc apparatus under dry sliding wear conditions.
5. The response surface methodology (RSM) technique is used to optimize process parameters like reinforcement content, sliding speed, sliding distance and applied load on the tribological behavior of the ZA-27 alloy nanocomposites reinforced with different combinations of both Al_2O_3 & MoS_2 nanoparticles

2.12. Research plan

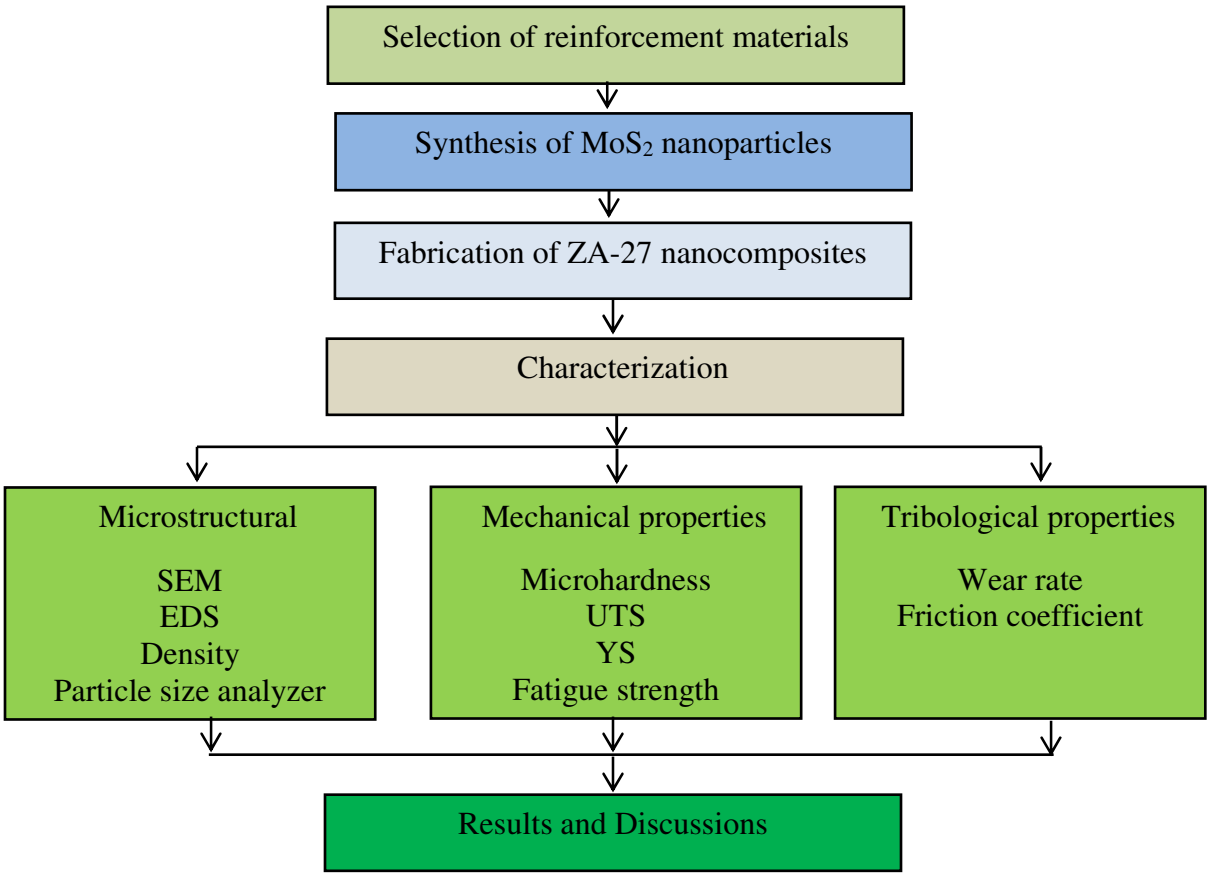

CHAPTER 3

EXPERIMENTAL SETUP AND EQUIPMENT

3.1. Introduction

This chapter discusses the experimental setup and equipments used in the present research work to conduct different set of experiments. Details of the equipments used for the synthesis and preparation of composites, microstructure characterization, microhardness and mechanical properties of the nanocomposites are supplied in the chapter. Tribological experiments to calculate the wear rate and friction coefficient of the nanocomposites is a critical part in any investigation. The trail experiments were conducted to identify the ranges and levels of the process parameters of ZA-27 nanocomposites and hybrid nanocomposites. The process parameters such as reinforcement content, sliding speed, sliding distance and applied load were used to examine the dry sliding wear behavior of the nanocomposites. The experiments were well planned and conducted to measure the wear rate and friction coefficient of the nanocomposites. The response surface methodology (RSM) is used for the experimental design and it also develops the mathematical models for wear rate and friction coefficient of different weight percentages of ZA-27 nanocomposites and hybrid nanocomposites

3.2. Experimental setup

3.2.1. Synthesis of MoS_2 nanoparticles

The planetary ball mill with tungsten balls and tungsten vial were used for the preparation of MoS_2 nanoparticles as shown in Figure 3.1. The ball mill has a single vial with a capacity of 250 ml powder that can be milled at a time. A counter weight is used on the other side to balance the weight of the vial. The MoS_2 particles with micrometer size were procured from Sisco Research Laboratories Pvt. Ltd, Hyd. The specifications of ball mill are shown in table. MoS_2 microparticles were milled for several hours in the planetary ball mill for preparing the nanoparticles. Mechanical alloying was carried out in wet medium, using toluene as process control agent. Milled particle samples were collected for various intervals to test the change in size. The specifications of the planetary ball mill are given in table 3.1.

Figure.3.1 Planetary Ball Mill

Table.3.1 Specification of Planetary Ball mill

Make	Retsch
Model	PM-100
Applications	pulverizing, mixing, homogenizing, colloidal milling, mechanical alloying
Field of application	agriculture, biology, Chemistry, construction materials, engineering / electronics, environment / recycling, geology / metallurgy, glass / ceramics, medicine / pharmaceuticals
Feed material	soft, hard, brittle, fibrous - dry or wet
Size reduction principle	impact, friction
Material feed size	< 10 mm
No. of grinding stations	1
Speed ratio	1 : 2
Sun wheel speed	100 - 650 min-1
Effective sun wheel diameter	141 mm
G-force	33.3 g
Material of grinding tools	tungsten carbide
Grinding jar sizes	250 ml
Interval time	00:00:01 to 99:59:59
Pause time	00:00:01 to 99:59:59
Measurement of input energy	Yes

possible	
Interface	RS 232 / RS 485
Drive	3-phase asynchronous motor with frequency converter
Drive power	750 W
Electrical supply data	different voltages
W x H x D closed	630 x 468 x 415 mm
Net weight	~ 86 kg
Patent / Utility patent	Counter weight (DE 20307741), FFCS (DE 20310654), Safety Slider (DE 202008008473)

3.2.2. Particle Size Analyzer

Figure 3.2.shows the Malvern nano zeta sizer is used to measure the average particle size of the MoS_2 particles which are synthesized by using planetary ball mill. The average particle size ranging from the 0.3 nm to 10 μm can be measured with the help of particle size analyzer. It works on the principal of dynamic light scattering and measures average particle size in wet medium.

Figure 3.2. Nano zeta sizer

The samples were prepared for the particle analyzer test by addition a pinch of milled MoS_2 nanoparticles in to the beaker containing deionized water and ultrasonication was done for 30 minutes. After ultrasonification the nanoparticles are uniformly distributed in the water. The

prepared nanoparticles was poured into specimen beaker and positioned into the equipment to measure the average particle size of the MoS_2 nanoparticles. Table.3.2 shows the specification of Malvern Zeta Sizer.

Table 3.2 Specification of Malvern Zeta Sizer

Measurement Range	0.3nm -10.0 microns (diameter)
Measurement Principle	Dynamic Light Scattering
Minimum sample volume	12µL
Accuracy	Better than +/-2% on NIST traceable latex standards
Sensitivity	0.1mg/mL (Lysozyme)
Precision/Repeatability	Better than +/-2% on NIST traceable latex standards

3.2.3. Ultrasonic assisted stir casting

Dispersion of nano sized reinforcement in metal matrix composite is challenging due to the nano sized particles large surface to volume ratio which results in agglomeration and clustering. These affect the resulting properties of composite materials. Poor wettability of nano particles also produces the composite with inferior mechanical properties. The ultrasonic probe assisted sonication method helps in this case to uniformly distribute the particles in metal matrix. The ultrasonic energy is widely used in the manufacturing for welding, casting and non-destructive testing. The ultrasonic cavitation effect is utilized to generate nuclei in casting. The ultrasonic cavitation based processing of nanocomposites has been successfully utilized by researchers to fabricate bulk metal matrix composite. The process is very effective in dispersing nano sized particle s in the metal matrix. The process generally requires resistance heating furnace for melting metal, nano particle feeding mechanism, inert gas envelope for protection and an ultrasonic system. The ultrasonic processing system consists of an ultrasonic probe, a transducer and power source. Figure 3.3 shows the ultrasonic assisted stir casting machine. Table 3.3 shows the specification of the machine.

Table 3.3 Specifications of Ultrasonic assisted stir casting machine

Make	Johnson Plastosonic
Ultrasonic Power	2000-4000 Watts
Output Frequency	18-20 kHz

Input Supply	230 Volts
Protection Indicators	LED indicators

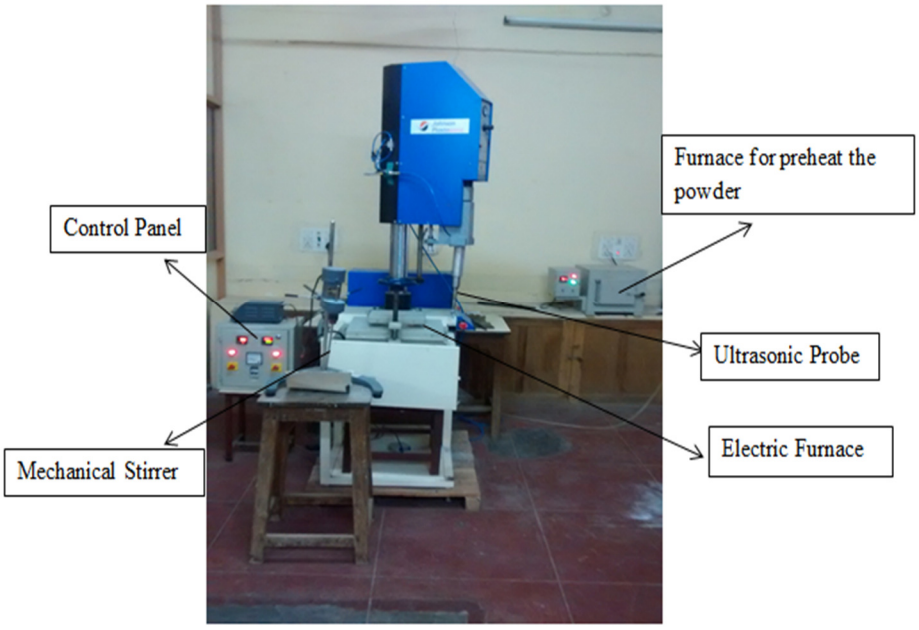

Figure 3.3 Ultrasonic assisted stir casting machine

3.2.4. Microstructural characterization

The microstructures of the composite surfaces are observed using scanning electron microscopy (SEM) as shown in Figure 3.4. SEM is a type of electron microscope that produces images of a sample by scanning it with a focused beam of electrons. The electrons interact with atoms in the sample, producing various signals that contain information about the sample's surface topography and composition. SEM is a completely computer controlled unit with conventional tungsten heated cathode intended for high and low vacuum operations. It is a sophisticated user friendly software for controlling the microscope and capturing the image using windows platform, has superior optical properties, offers good clarity of flicker-free digital image, processing and measurements, has images stored in standard formats, provides automatic

arrangement of the electron microscope and several other automated processes and these among the specific features of the equipment. The technical specifications of SEM are given in table 3.4.

Figure 3.4 Scanning electron microscope

Table 3.4 Technical specifications of SEM

Make	Tescan
Model	VEGA 3 LMU
Electron Gun	Tungsten heated cathode
Resolution	3 nm at 30 kv / 2 nm at 30 kb
Magnification	2x – 1,000,000x
Maximum field of view	24 mm at WD 30 mm
Accelerating Voltage	200 V to 30 kV
Probe current	1 pA to 2 µA
Scanning Speed	From 20 ns to 10 ms per pixel adjustable or continuously
Chamber suspension	Pneumatic
Specimen Stage	Compucentric, fully motorized

3.2.5. Energy Dispersive Spectroscopy (EDS)

The energy dispersive spectroscopy (EDS) is an analytical technique which is used for the chemical composition or elemental analysis of a material. EDS is also known as energy dispersive X-ray analysis (EDXA). It is an analytical technique used for the elemental analysis or chemical characterization of a sample. It relies on an interaction of some source of X-ray excitation and a sample. Its characterization capabilities are due in large part to the fundamental principle that each element has a unique atomic structure allowing a unique set of peaks on its electromagnetic emission spectrum. The confirmation about the elemental composition of a specimen can be overlaid on top of the magnified image of the specimen by using a process known as X-ray mapping. An EDS coupled with SEM as shown in Figure 3.5 was used in the present study.

Figure 3.5 EDS coupled with SEM

3.2.6. Measurement of micro-hardness

The term hardness refers to the ability of a material to resist permanent deformation. The larger the resistance to deformation, the harder the body appears. There are four common

methods available to measure the hardness of any material such as Brinell, Knoop, Rockwell, and Vicker's hardness tests. Vickers hardness testing method is simple as compared to others and is suited well for all metals. In this method an indenter of a straight diamond pyramid with an angle between opposite faces of 136^0, is applied under a specific load on to the surface of the material to be tested for a set time interval. According to the law of proportional resistance, the indentation surface is proportional to the force applied. For micro hardness studies, usually the range of load is taken to be 5 g to 1000 g and the dwell time is considered in the range 10 to 15 sec. In the present study a load of 200 g is applied for 10 sec as dwell time.

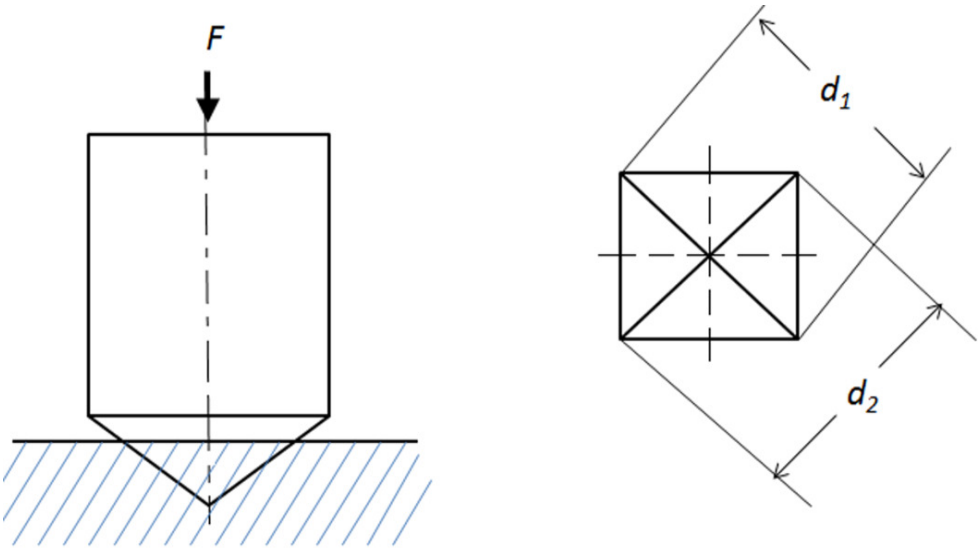

(a) Indentation (b) Measurement of indent

Figure 3.6 Hardness measurement using Vicker's hardness tester

After the test, an indentation is formed as shown in Figure 3.6. From the indentation, diagonals are measured. Micro hardness of the composite samples for Vickers method is estimated as

$$HV = \frac{0.1891F}{d^2}$$

where d is the arithmetic mean of diagonals and F is the load applied on the work material. Micro-hardness of the composite surfaces is measured using Chennai Metco make Economet VH 1 MD model as shown in figure 3.7 and the specifications are given in table 3.5.

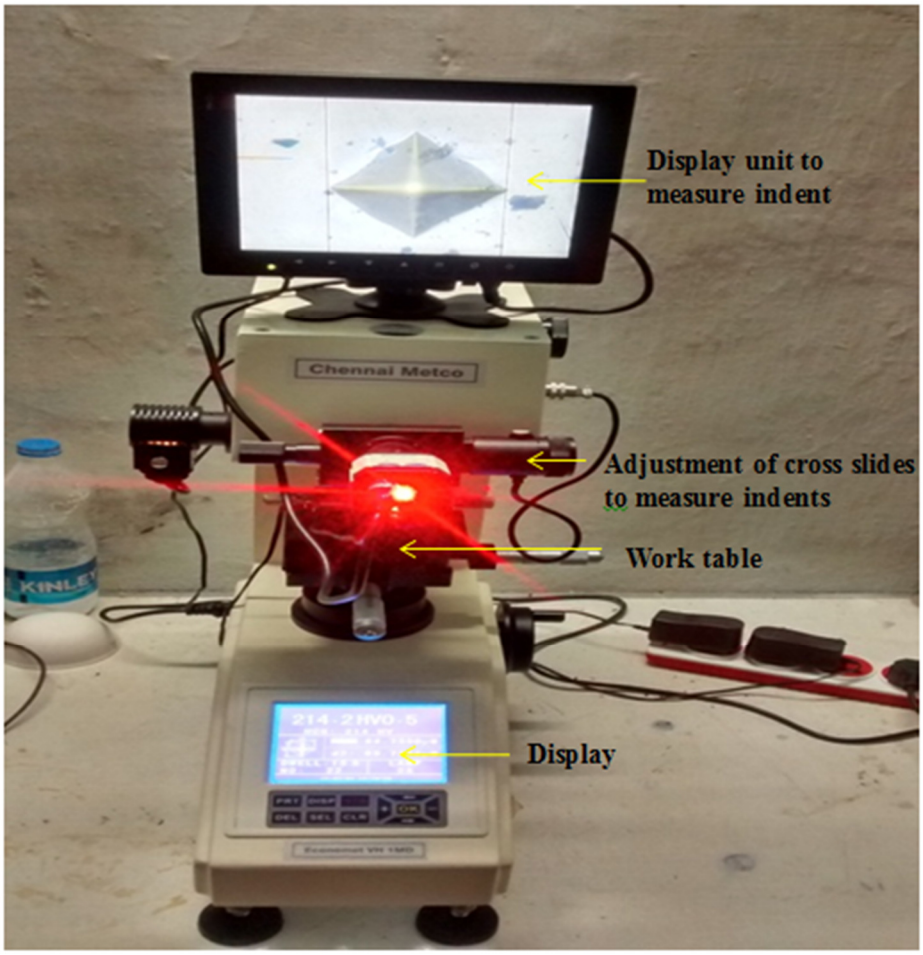

Figure 3.7 Vickers hardness tester

Table 3.5 Technical specifications of Vicker's hardness tester

Make	Chennai Metco
Model	Econome VH 1 MD Digital Automatic Turret Micro Vickers Hardness Tester with digital display
Usage Range	Heat treatment, carbide, quench hardened layer, the surface coating layer, steel, non-ferrous metal and small and thin shape parts, etc
Test Load	10gf, 25gf, 50gf, 100gf, 200gf, 300gf , 500gf & 1kgf
Method of testing force applied	Automatic (Loading, Dwell, Unloading)
Test microscope magnification	400X(Measuring), 100X (observation)
Duration time	0 to 60 s
Min measuring unit	0.031 µm

Hardness measuring range	8 to 2900 HV
Conversion Scale	HRA, HRB, HRC, HRD, HRF, HV, HK, HBW, HR15N, HR30N, HR45N, HR15T, HR30T, HR45T
Data output	LCD screen display, Inside Printer, RS-232 Max Height of Specimen: 80mm Distance of Indenter to outer wall: 95mm X-Y Testing table:
Dimension	25*25mm
Power supply	AC220V+5%

3.2.7. Tensile Test

Tensile test is one of the major types of mechanical tests to find the strength of the materials for many engineering applications. In materials the strength of importance may be measured in terms of either stress required to obtain appreciable plastic deformation or the material can withstand the maximum stress. These measures of strength are used with appropriate caution in engineering design. The various materials and processes can be compared by measuring the tensile properties of the newly developed materials and processes. Finally, tensile properties are frequently used to predict the performance of a material under forms of loading other than uniaxial tension. Tensile test were carried out on the electro mechanical tensile test machine. The test data were used to determine the ultimate tensile strength, yield strength and percentage elongation of the materials. The specification of the electro mechanical tensile test machine is given in table 3.6 and figure 3.8 shows the tensile machine.

Table 3.6 Specification of electro mechanical tensile test machine

Make	HEICO (Hydraulic and Engineering Instruments)
Model	HLC 693-30
Capacity	20KN
No of columns	2
Max Speed (mm/min)	500
Min Speed (mm/min)	0.01
Max Force at full speed (KN)	20
Max Return Speed (mm/min)	1000

Position Control (mm)	0.5
Total Crosshead travel (mm)	1130
Max Power Required (VA)	1000
Dimension (LxBxH) (mm)	760x600x2000

Figure 3.8 Electro Mechanical Tensile Test machine

3.2.8. Fatigue Test

Fatigue is the process of progressive localized permanent structural change occurring in a material subjected to conditions that produce fluctuating stresses and strains at some point or points and that may culminate in cracks or complete fracture after a sufficient number of fluctuations is termed as fatigue [159].Fatigue cracking generally results from cyclic stresses that are lower than the static yield strength of the material. The fatigue tests were carried out with different fatigue testing machines such as direct stress, plane bending, rotating bending and alternating torsion. In this present study the fatigue tests were conducted on the rotating bending

test machine because the materials used in this study is mainly for the bearing applications. Figure 3.9 shows the rotating bending test machine and table 3.7 give the specifications.

Table 3.7 Specifications of Rotating bending test machine

Make	Metsonic Engineers Private Limited
Model	FT-8
Standard dimensions (mm)	8-10
Rotating speed (rpm)	Upto 4200
Maximum bending moment (kg/cm)	400

Figure 3.9 Rotating bending test machine

3.2.9. Wear test

Wear of materials is an every-day experience and has been observed and studied for a very long time. It is a process of steady removal of a specimen from surfaces of solids subject to contact and sliding. The present work which concentrates on dry sliding wear behavior of composite materials was conducted by using pin on disc friction and wear testing machine as per ASTM G99 standards. The wear tests were examined with help of experimental plan to get the optimal output of the wear behavior. Trial experiments were carried out to identify the possible ranges for every process parameters to study the wear characteristics of the materials. After observing the results of trial experiments the ranges and levels are fixed for ZA-27 nanocomposites as presented in Table 3.8 and for hybrid nanocomposites it is presented in Table 3.9.

Table 3.8 Process parameters: Ranges and levels for ZA-27 nanocomposites

Variables	Units	Level 1	Level 2	Level 3
Reinforcement content (R)	Wt %	0.5	1	1.5
Sliding speed (S)	m/s	1	2	3
Sliding distance (D)	m	1000	2000	3000
Applied load (L)	N	30	60	90

Table 3.9 Process parameters: Ranges and levels for hybrid nanocomposites

Variables	Units	Level 1	Level 2	Level 3
Sliding speed (S)	m/s	1	2	3
Sliding distance (D)	m	1000	2000	3000
Applied load (L)	N	30	60	90

In the present study, an experimental plan is taken from the response surface methodology (RSM) technique in which a centered composite design (CCD) is used to generate experimental data. The detailed experimental plan involving number of experiments has been given in respective chapters. RSM analysis was carried out with the help of Design Expert 9.0 software. To develop adequate efficient relationships among the outputs and control factors, RSM consists of statistical and mathematical techniques are utilized. An effort has been made to investigate the

influence of control factors such as reinforcement content, sliding speed, sliding distance and applied load, on the responses such as wear rate and coefficient of friction by using response surface methodology (RSM). Figure 3.10 shows the pin on disc friction and wear testing machine and table 3.10 gives the specifications.

Figure 3.10 Pin on disc friction and wear testing machine

Table 3.10 Specifications of Pin on disc friction and wear testing machine

Make	Magnum Engineers
Model	TE-165-LE
Pin Dimension	φ3- φ12 mm, 25-30mm
Ball Diameter	10mm
Disk Material	EN31 steel
Size	φ165mm, 8mm thickness
Wear track diameter	50-100mm
Disk Rotation	200-2000 rpm
Normal load range	5-200 N
Wear measurement range	0-2000 μm
Frictional force range	0-200 N with a resolution of 1N with tare facility

CHAPTER 4

FABRICATION AND MICROSTRUCTURAL CHARACTERIZATION OF ZA-27 NANOCOMPOSITES AND HYBRID NANOCOMPOSITE

4.1. Introduction

This chapter deals with the synthesis of the molybdenum disulphide nanoparticles with the help of planetary ball mill and measures the average particle size of nanoparticles by using nano zeta sizer. ZA-27 alloy reinforced with different weight percentages of aluminium oxide (Al_2O_3), molybdenum disulphide (MoS_2) and combination of both (Al_2O_3/ MoS_2) nanoparticles for the fabrication of ZA-27 nanocomposites and hybrid nanocomposite with the help of ultrasonic assisted stir casting process. The density measurement of ZA-27 nanocomposites and hybrid nanocomposite was also studied with the help of Archimedes principle. The microstructure and chemical composition analysis of the various weight percentages of ZA-27 nanocomposites and hybrid nanocomposite is briefly explained in this chapter.

4.2. Synthesis of MoS_2 nanoparticles

In this study, Mechanical milling of the MoS_2 micro sized metal powders was carried out in Retsch Planetary Ball Mill PM-100 with Tungsten carbide vial and balls to prepare nano powders. MoS_2 micron sized powders are milled in a vial, with 50 grams of powder and 500 gram balls for 80 hours. The ball to powder weight ratio is 10:1, with a milling speed of 250 rpm in wet medium (about 50 ml of acetone) to prevent undue oxidation and agglomeration of powder. Tungsten carbide balls of 5 and 3 mm diameter were used for milling. Powder samples were collected from the vial at selected intervals of time to check the reduction in size of the particles by particle size analyzer. The description of the planetary ball mill figured in chapter 3. The specifications of the planetary ball mill for milling the MoS_2 microparticles are shown in table 4.1.

Table 4.1 Specifications for the milling system

Mill type	Retsch planetary ball mill PM 100
Milling time	80 hours
Wet milling medium	Toluene
Milling speed	250 rpm
Grinding media:	
Ball and jar material	Tungsten carbide
Ball size	5 & 3 mm dia
Ball weight/jar	500g
Ball to powder ratio	10:1
Jar dimensions:	
Length	95 mm
Diameter	75 mm

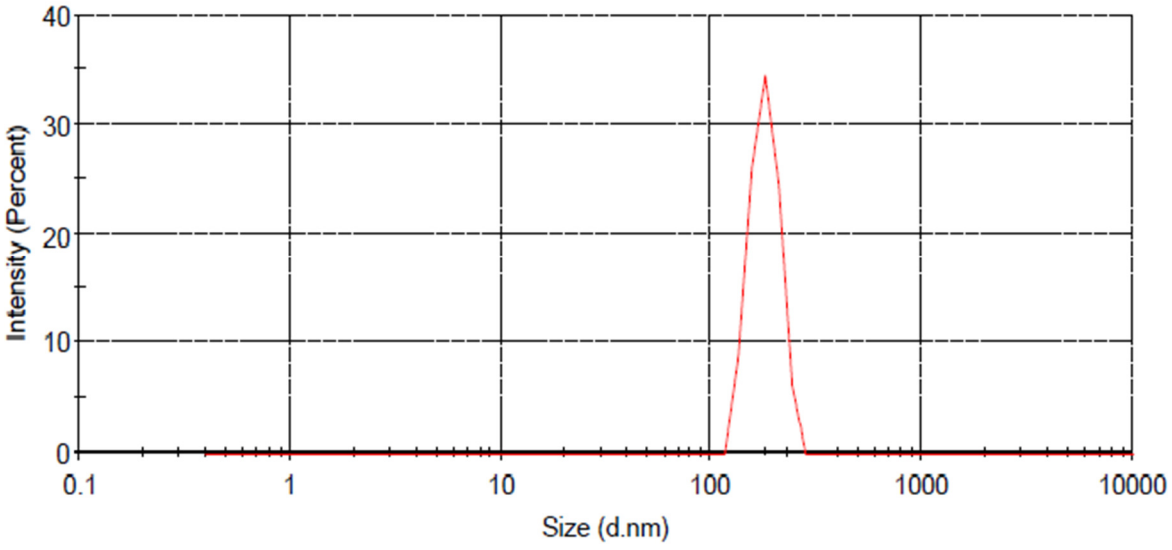

Figure 4.1 Average particle size of MoS_2 particles milled for 80 hours

The average particle size and dispersion stability of nano particles was measured by Nano zeta sizer (Model: Nano ZS, Malvern). The sample was prepared by dispersing small amounts of nano particles in deionized water with constant ultrasonication of 30 minutes each. Then the sample was kept in a sample holder with the help of syringe and analyzed. The samples were analyzed using Zeta Sizer software. It was evident from the graph that the average particle size of 80 hours milled molybdenum disulphide (MoS_2) microparticles was approximately 200 nm.

4.3. Fabrication of ZA-27 nanocomposites

Commercially available pure zinc (99.9%), aluminium (99.9%), copper (99.9%) and magnesium (99.9%) supplied by Sigma Aldrich were used to prepare the ZA-27 alloy. The elemental composition of the ZA-27 alloy mentioned in chapter 1, was selected as matrix material for the fabrication of the composites. The reinforcement materials are commonly harder, softer and more discontinuous than the matrix materials. In this present study, molybdenum disulfide (MoS_2) and Al_2O_3 and combination of both were selected as per literature to enhance both the mechanical (Al_2O_3) and Tribological properties (MoS_2) of ZA27 alloy at economical basis. The reinforcement particles of MoS_2 with the average particle size of 5 µm and aluminium oxide (Al_2O_3) with an average particle size of 50nm which was commercially sourced from Sisco Research Laboratories Pvt. Ltd, Hyderabad, India. For the fabrication of the nanocomposites ZA-27 alloy reinforced with different weight percentages ranging from 0.5, 1.0, and 1.5 wt % of the molybdenum disulphide with micro and nanoparticles and aluminium oxide nanoparticles by using ultrasonic assisted stir casting technique. The reinforcement content for the preparation of the hybrid nanocomposites were selected based on the results obtained for the individual reinforcement content of Al_2O_3 and MoS_2 nanoparticles where shown in chapter 5. The hybrid nanocomposite reinforced with the combination of both Al_2O_3 and MoS_2 micro and nanoparticles with weight percentage of 1.5 wt % of Al_2O_3 and 0.5 wt % of MoS_2 in ZA-27 alloy.

The raw materials for base alloy (ZA-27) were cut into small pieces and placed in a graphite crucible. Then the graphite crucible was placed in the electrical resistance furnace and heated above the melting temperature of 800^o C. After melting the base alloy, mechanical stirring was used to stir the molten metal for 2 min for homogenization. The reinforcement particles with different weight percentages were packed in the aluminium foils like pallets. These pallets were

pre-heated up to 500^{o} C to remove any moisture and increase the thermal stability of the molten metal. While stirring was in progress, the preheated reinforcement particles were added and stirring was continued at a speed of 500 rpm for 2–3 min so as to attain uniform distribution of reinforcement particles in the matrix material. After mechanical stirring was done in the molten metal the clusters and agglomeration were formed due to the large surface area to mass fraction and poor wettability of the nanoparticles. The ultrasonic probe was inserted into the molten metal of the nanocomposite and ultrasonification process was carried out for 3min to achieve homogenous distribution of the nanoparticles. The high intensity ultrasonic waves are produced due to the ultrasonic probe which develops the alternating compression and dilation cycles in the melt, which helps to break the clusters of nanoparticles to obtain the uniform dispersion in the matrix material. Subsequently, the melt was poured into a cylindrical die made up of mild steel. The specimens were removed from the die after solidification and standard specimens were prepared for the characterization and analysis of the composites. The ultrasonic assisted stir casting machine and its specifications was discussed in chapter 3. The cylindrical mild steel die and the cast specimens of the ZA-27 nanocomposites are shown in Figure 4.2.

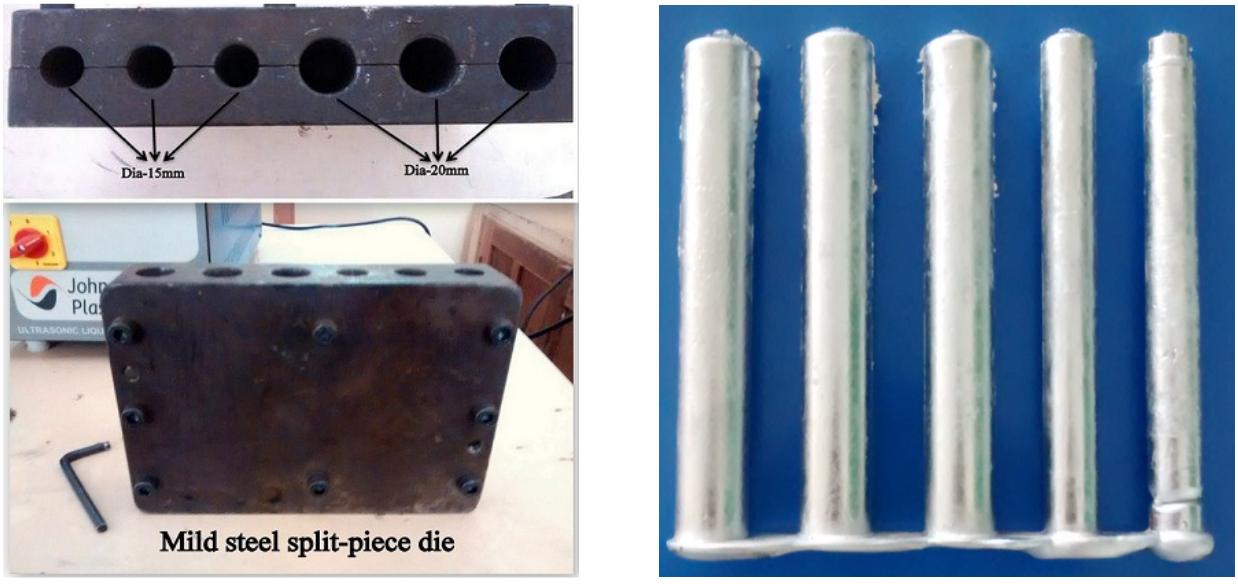

a) Cylindrical die b) Cast ZA-27 nanocomposites

Figure 4.2 Fabrication of ZA-27 nanocomposites

4.4. Density of ZA27 nanocomposites

The metal matrix nanocomposites are found to replace the conventional metals and materials mainly for their low densities in many engineering applications. Density was a material property which is of prime importance in several weight sensitive applications. It depends on the relative percentage of matrix and the reinforcing materials in the nanocomposite. There is always a difference between the experimental and the theoretical density values of a composite due to the presence of porosity. This porosity significantly affects some of the mechanical properties and even the performance of nanocomposites. In the present study the experimental densities of the cast ZA-27 alloy and ZA27 nanocomposites reinforced with the aluminium oxide (Al_2O_3) and molybdenum disulphide (MoS_2) nanoparticles were determined with the help of Archimedes principle. The measured density of ZA-27 nanocomposites and hybrid ZA27 nanocomposites in terms of weight percentages was calculated by using equation 4.1.

$$\rho_{exp} = \frac{W_s}{W_s - W_a} \times \rho_w \tag{4.1}$$

where ρ_{exp} is the experimental density, W_s and W_a represent the weight of the specimen and apparent immersed weight of specimen. ρ_w is the density of water (i.e. ρ_w =1).

The rule of mixture was used to calculate the theoretical densities of the ZA-27 nanocomposites and hybrid ZA27 nanocomposites in terms of weight percentages with the help of equation 4.2. For these calculations, the densities of ZA-27 alloy, aluminium oxide and molybdenum disulphide particles were taken to be 5.00 gm /cm^3, 3.89 gm /cm^3 and 5.06 gm /cm^3 respectively.

$$\rho_{th} = \frac{1}{\frac{W_m}{\rho_m} + \frac{W_p}{\rho_p}} \tag{4.2}$$

where ρ_{th} is the theoretical density, W and ρ represent the weight fraction and density respectively. *m* and *p* stand for the matrix material and reinforcement particles.

The porosity percentage of the different weight fraction of the ZA-27 nanocomposites and hybrid nanocomposites was calculated by using equation 4.3.

$$\text{Porosity } (\%) = \frac{\rho_{th} - \rho_{exp}}{\rho_{th}} \times 100 \quad (4.3)$$

The measured density, theoretical density and porosity of the different weight percentages of the ZA-27 nanocomposites and hybrid ZA27 nanocomposites were presented in table 4.2.

Table 4.2 Density and porosity content of ZA-27/Hybrid nanocomposites

Sl.No	Composition	Experimental Density (gm./cm^3)	Theoretical Density (gm/cm^3)	Porosity (%)
1	ZA-27 alloy	4.9436	5.0000	1.12
2	ZA-27 + 0.5% MoS_2 (µm)	4.9438	5.0003	1.12
3	ZA-27 + 1.0% MoS_2 (µm)	4.9434	5.0006	1.13
4	ZA-27 + 1.5% MoS_2 (µm)	4.9429	5.0010	1.16
5	ZA-27 + 0.5% MoS_2 (nm)	4.9435	5.0003	1.13
6	ZA-27 + 1.0% MoS_2 (nm)	4.9426	5.0006	1.15
7	ZA-27 + 1.5% MoS_2 (nm)	4.9421	5.0010	1.17
8	ZA-27 + 0.5% Al_2O_3 (nm)	4.8911	4.9930	2.07
9	ZA-27 + 1.0% Al_2O_3 (nm)	4.8482	4.9857	2.55
10	ZA-27 + 1.5% Al_2O_3 (nm)	4.8119	4.9786	2.82
11	ZA-27 + 1.5% Al_2O_3 (µm) + 0.5% MoS_2 (µm)	4.8690	4.9789	2.20
12	ZA-27 + 1.5% Al_2O_3 (nm) + 0.5% MoS_2 (nm)	4.8649	4.9789	2.28

a) Effect of MoS_2 nanoparticles

The experimental density of different weight percentages of MoS_2 nanoparticles reinforced in ZA-27 nanocomposites were shown in figure 4.3. The influence of MoS_2 nanoparticles on the measured density of the nanocomposites was negligible due to the density value of MoS_2 nanoparticles which are approximately the same as compared to ZA-27 alloy. The

0.5 wt % MoS_2 nanoparticles reinforced in ZA-27 nanocomposites are showing almost the same measured density as the matrix material. As MoS_2 nanoparticles increase in the matrix material minor change can be observed in the measured density of the ZA-27/MoS_2 nanocomposites, due to increase in porosity as shown in table 4.2.

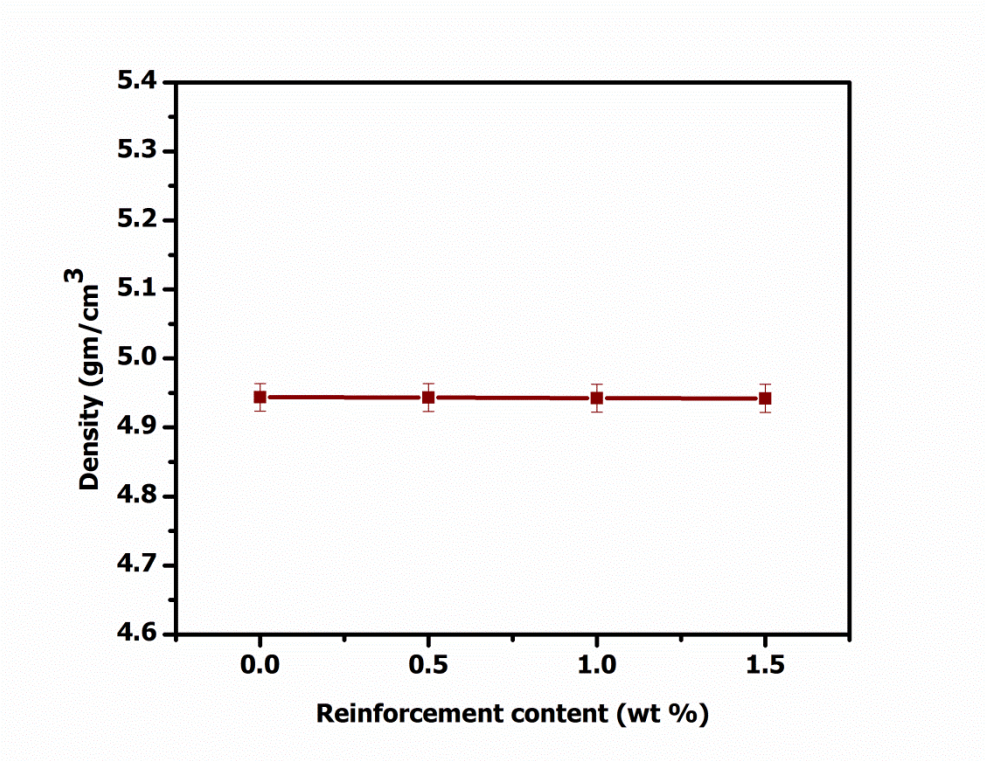

Figure 4.3 Density of ZA-27/MoS_2 nanocomposites

b) Effect of Al_2O_3 nanoparticles

The experimental density of the different weight percentages of Al_2O_3 nanoparticles reinforced in ZA-27 nanocomposites are shown in figure 4.4. It was observed from the graph that the reinforcement of Al_2O_3 nanoparticles leads to the reduction in the density of ZA-27/Al_2O_3 nanocomposites when compared to that of ZA-27 alloy because of lower density value of the nanoparticles as compared to the matrix material. As the Al_2O_3 nanoparticles increase in the matrix material, the measured density of the ZA-27/ Al_2O_3 nanocomposites decreases due to the formation of clusters in the melt. The porosity content of ZA-27 nanocomposites increases with the increasing of weight percentages of Al_2O_3 nanoparticles as shown in table 4.2. The increase

in the porosity of ZA-27 nanocomposites was due to the effect of the low wettability and agglomeration at high reinforcement content of the nanoparticles.

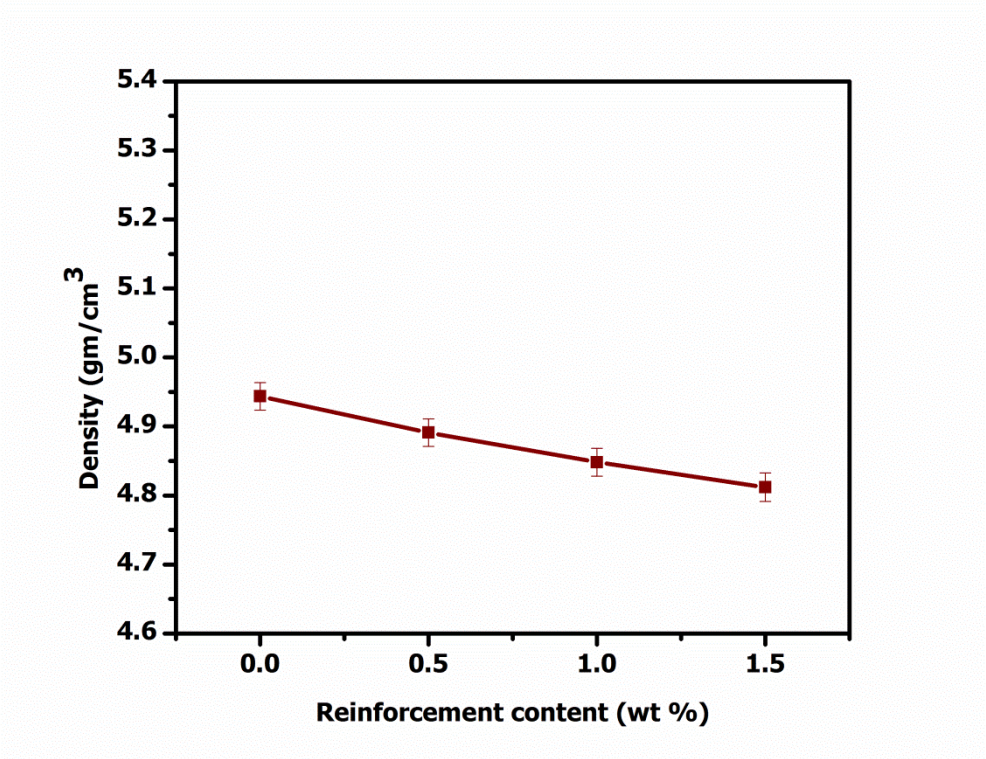

Figure 4.4 Density of ZA-27/ Al_2O_3 nanocomposites

c) Effect of hybrid Al_2O_3 and MoS_2 nanoparticles

The measured density of ZA-27 hybrid nanocomposites reinforced with 1.5wt % Al_2O_3 and 0.5 wt % MoS_2 both micro and nanoparticles are shown in Figure 4.5. It was observed from the graph that the reinforcement of 1.5 wt % Al_2O_3 micro/nanoparticles leads to the reduction in the density of the hybrid ZA27 nanocomposites when compared to that of matrix material due to the lower density value of Al_2O_3 micro/nanoparticles as compared to ZA-27 alloy. The density decreases due to the formation of porosity content in the hybrid micro/nano composite. The combination of the Al_2O_3 and MoS_2 nanoparticles will effects the density due to the low wettability property in the melt when compare to the micro particles. The porosity content of ZA-27 hybrid nanocomposite increase with the weight percentage of 1.5 wt % Al_2O_3 and 0.5 wt % of MoS_2 nanoparticles as compare to ZA-27 alloy was shown in table 4.2.

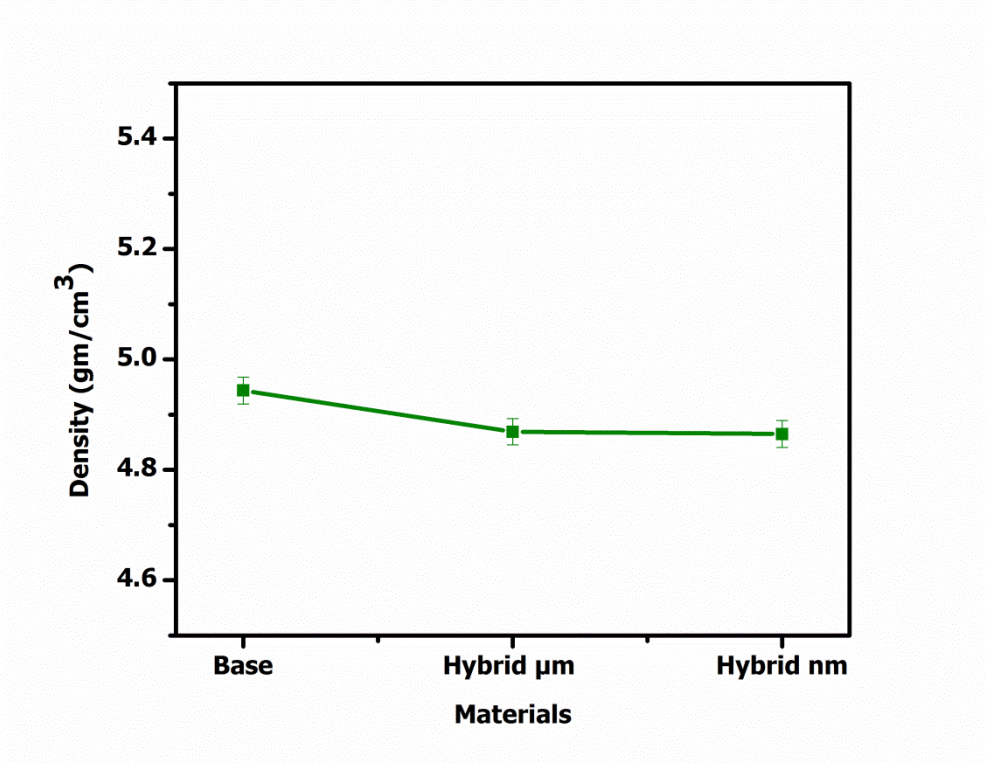

Figure 4.5 Density of ZA-27 hybrid micro/nanocomposites

4.5. Microstructure evolution of ultrasonification process

A model describing the microstructure evolution of ZA-27 nanocomposites melt during the solidification under the ultrasound field as shown in Figure 4.6. As the temperature of the nanocomposite melt falls to near the liquidus temperature, the dendrite trunks of primary α-Al begin to form in the melt, and Al_2O_3 particulates were pushed by the dendrite trunks as shown in Figure 4.6 (a). With the decreasing of temperature of the melt, the secondary and tertiary dendrite arms of primary α-Al continuously form, and more Al_2O_3 particulates were pushed into the melt by the dendrites as shown in Figure 4.6 (b). When ultrasonic vibration was injected into the melt, the dendrites were broken by the dendrite arm fracture due to the force on the arm, which would provide an artificial source of sufficient nuclei as shown in Figure 4.6 (c and d). Besides, the transient cavitations could remove the gas layer from the nanoparticle surface, improving the wettability between nanoparticles and the matrix. As a result, some Al_2O_3 nanoparticulates were captured by the growing grain as shown in Figure 4.6 (e).

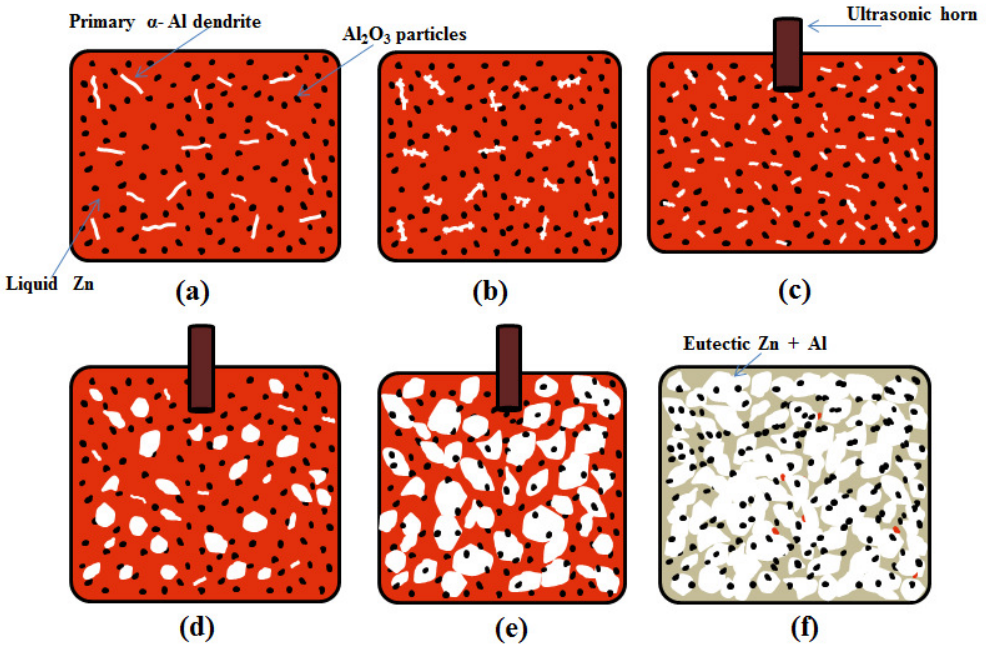

Figure 4.6 Scheme of microstructure evolution of ZA-27 nanocomposites; a) The formation of primary α-Al dendrite, b) the formation of dendrite arms, c) the breakage of the dentrites under ultrasonification process, (d and e) the growth of α-Al grains and f) the completion of the solidification.

When the temperature of the nanocomposite slurry drops to the solidus temperature, the eutectic reactions located in the inter-grains occur, and those Al_2O_3 nanoparticulates pushed by the growing grains will be surrounded by the eutectic phases as shown in Figure 4.6 (f). Therefore, the resulting nanocomposite presents fine uniform microstructure, most of the nanoparticulates were distributed in the interdentritic regions, and some nanoparticulates were located in the grain boundaries. This same microstructure evolution of ultrasonification phenomena was observed in SEM microstructures (See Figure 4.7- 4.11).

4.6. Microstructure and EDS analysis of ZA-27 nanocomposites

The microstructure analysis of ZA-27 nanocomposites and hybrid nanocomposites as ensured the uniform dispersion of the reinforcement particles of different weight percentages in ZA-27 alloy. The metallographic specimens were cut from the ZA-27 alloy and ZA27 nanocomposites for the microstructure characterization. Standard metallographic procedures were

used for the preparation of the metallographic samples. ZA-27 alloy and ZA27 nanocomposite samples were polished using different grades of silicon carbide abrasive papers, followed by disc polishing with the aid of cloth and Al_2O_3 particles. To reveal the microstructure, palmerton reagent (50 gm Cro_3, 4gm Na_2So_4, and 1000ml H_2O) used as etching agent. The microstructure and EDS analysis of ZA-27 nanocomposites and hybrid nanocomposites were obtained with the help of Scanning Electron Microscope (SEM). The description and specifications of the scanning electron microscope was discussed in chapter 3.

4.6.1. ZA-27/MoS_2 nanocomposites

The dispersion of reinforcement particles has a major effect on the properties of ZA-27/ MoS_2 composites. SEM micrographs with different weight percentage of MoS_2 micro particles reinforcement were shown in the Fig.4.7 (a) to (d). The ZA-27 alloy microstructure reveals a coarse dendritic structure of primary α phase (Al rich) dendrites surrounded by the eutectoid α+η in the interdendritic regions along with the intermetallic ε phase (Cu-rich) as shown in figure 4.7 (a). As the MoS_2 particles increase in matrix alloy the refined grain structure was obtained and the particles were invariably located at the grain boundaries of the composites as shown Figure 4.7 (c).

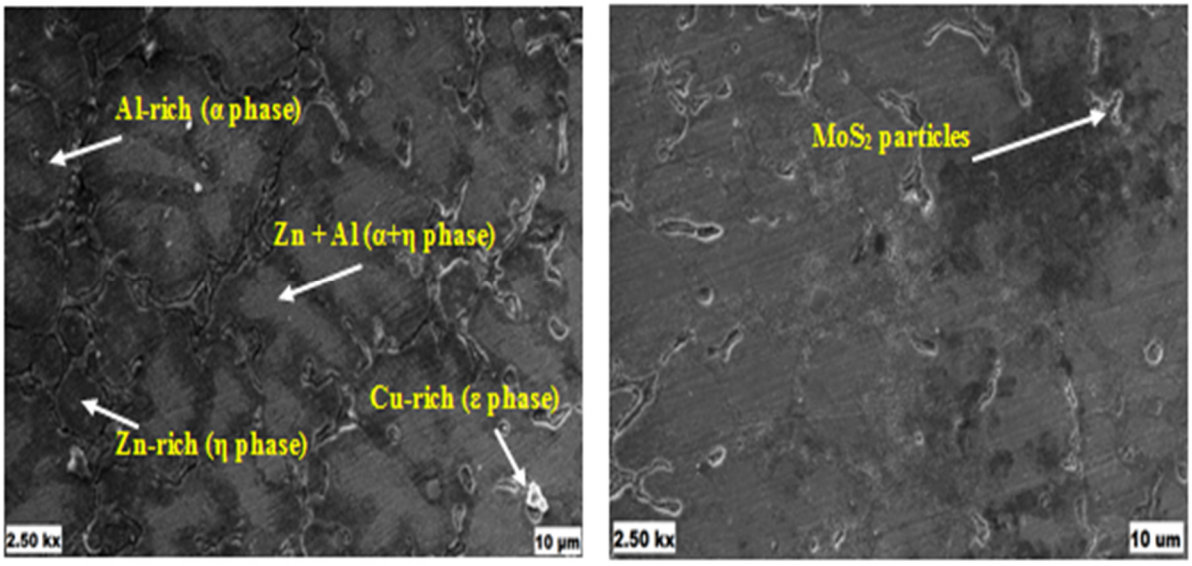

a) ZA-27 alloy b) ZA-27 + 0.5% MoS_2

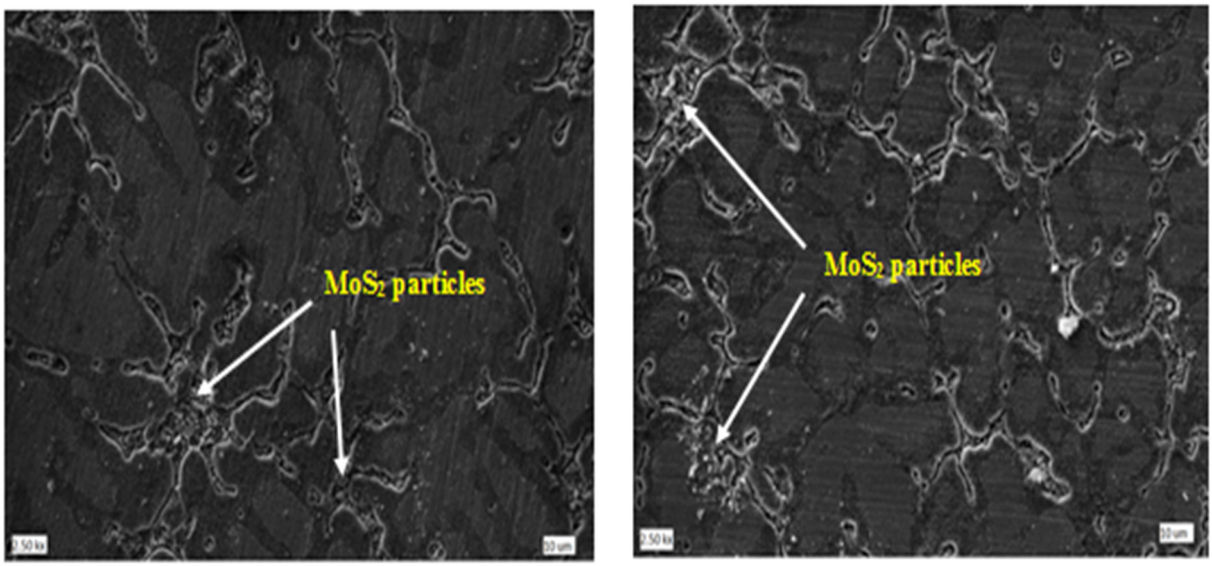

c) ZA-27 + 1% MoS_2 d) ZA-27 + 1.5 %MoS_2

Figure.4.7. Microstructures of composites as a function of MoS_2 microparticles

From the microstructures of the ZA-27/MoS_2 composites, homogenous distribution of MoS_2 particles can be seen from Fig.4.7 (d), as promoted by the ultrasonification process. Further, it may also be noticed that the MoS_2 micro particles were present at the interdendritic regions of ZA-27/MoS_2 composites.

Figure 4.8 shows the microstructures of ZA-27 nanocomposites reinforced with various weight percentages ranging from 0.5, 1.0 and 1.5 wt % of MoS_2 nanoparticles in matrix material. In case of nanocomposites the particle clustering and agglomeration are more due to the increased surface area and surface energy of nanoparticles. To overcome this particle clustering and agglomeration in the nanocomposites an ultrasonic probe is inserted in the molten metal, which breaks the clusters that are formed in the melt with the help of high intensity ultrasonic waves. It has been observed that the dispersion of the nanoparticles in the nanocomposite specimens was homogeneous and uniformity increases by increasing the weight percentage of the reinforcement particles in ZA-27 alloy as seen in Figure 4.8(c). The distribution of the reinforcement particles points to a tendency for large number of particles were located in the interdentritic regions of the nanocomposites. It was mainly due to mixing of the nanoparticles in the matrix melt at a process temperature which contains a large portion of the liquid phase and offers low resistance to the infiltration of particles in the nanocomposites.

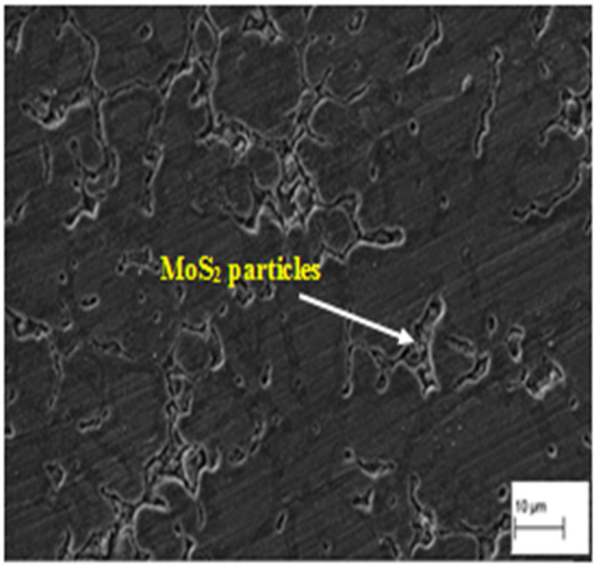

a) ZA-27 + 0.5 wt % MoS_2

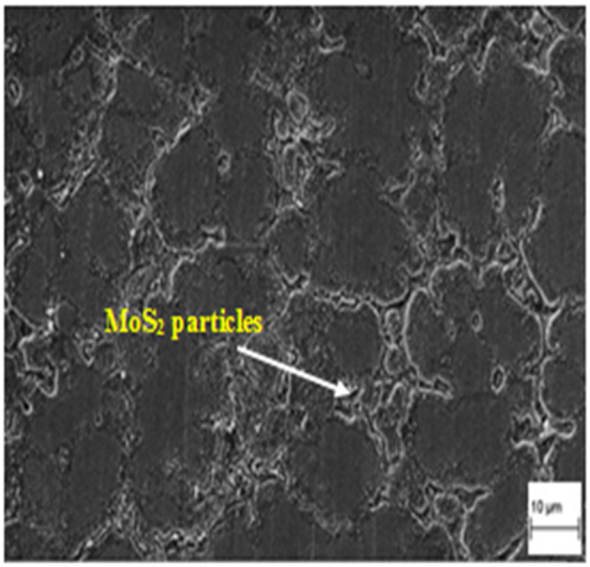

b) ZA-27 + 1.0% MoS_2

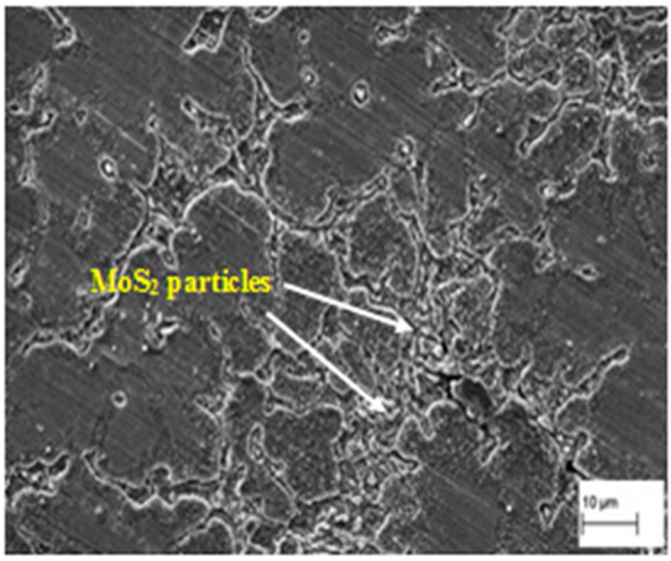

c) ZA-27 + 1.5% MoS_2

Figure 4.8 Microstructures of nanocomposites as a function of MoS_2 nanoparticles

The energy dispersive spectroscopy analysis was used for the elemental mapping for the compositional accuracy of the reinforcement particles in the ZA-27 nanocomposites. EDS analysis of ZA-27 alloy and 1.5 wt % MoS_2 nanoparticles reinforced in the base alloy is shown in figure 4.9 (a) and (b). It was evident that Zn, Al, Cu and Mg peaks are observed as per the standard of ZA-27 alloy as shown in Figure 4.9 (a). The EDS analysis confirms the Mo, S and O

peaks were observed in the elemental analysis of the nanocomposites as shown in figure 4.9 (b). Therefore, it was evident from microstructures that the MoS_2 nanoparticles were successfully incorporated in ZA-27 nanocomposites.

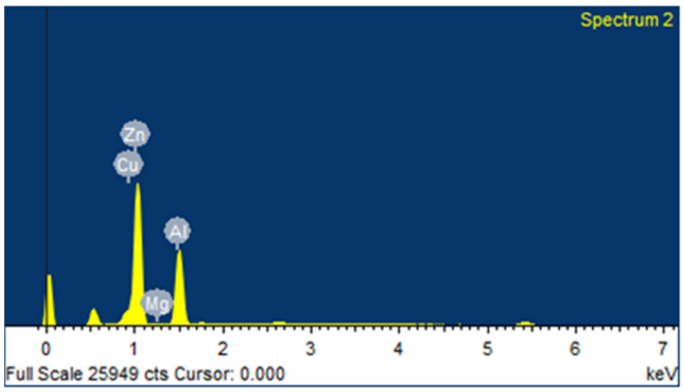

Element	Weight %
Mg	0.60
Al	33.01
Cu	1.60
Zn	64.79
Totals	100.00

a) ZA-27 alloy

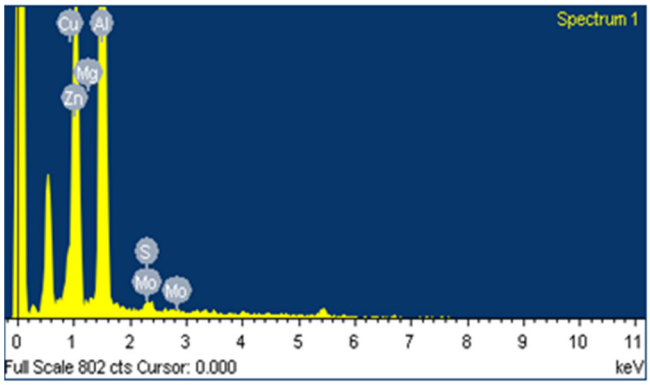

Element	Weight %
O	5.15
Mg	0.39
Al	46.74
S	1.03
Cu	1.92
Zn	44.23
Mo	0.55
Totals	100.00

b) ZA-27 + 1.5 % MoS_2 (nm)

Figure 4.9 EDS analysis of ZA-27/MoS_2 nanocomposites

4.6.2. ZA-27/Al_2O_3 nanocomposites

The microstructures of ZA-27 nanocomposites samples containing 0.5, 1.0, 1.5 weight percentages of nano-sized alumina particles fabricated by using ultrasonic assisted stir casting process was shown in Figure 4.10. The major problem encountered in preparation of the metal matrix nanocomposites was the settling of the nanoparticles in the ZA-27 alloy during casting process and this occurs due to the density differences between the reinforcement particles and the matrix alloy melt. The alumina nanoparticles were floating on the melt surfaces due to the poor wetting, while applying the mechanical stirrer improves the wettability properties and leads to addition of reinforcement particles in the melt. Heat treatment of the nanoparticles also helps to

develop the particles wettability by breaking the gas layers from the particle surface. The alumina nanoparticles were cooled down more slowly than the melt and so the temperature of the nanoparticles was slightly higher than the liquid alloy. The hotter nanoparticles may heat up their surrounding melt which will delay the solidification of surrounding liquid alloy. As a result, nucleation of α-Al phase starts in the melt at a distance away from the nanoparticles, where the temperature was lower. Therefore, the microstructures of ZA-27/Al_2O_3 nanocomposites comprise primary α-Al dendrites and eutectic α+ η phase, while alumina nanoparticles were separated at interdendritic regions and in eutectic regions. It was observed that in the ultrasonic assisted stir cast ZA-27 alloy based nanocomposites the distribution of the nanoparticles was uniform in the matrix material as shown in figure 4.10 (c). The nanoparticles were located at the interdentritic regions of ZA-27 nanocomposites, in which alumina nanoparticles were observed white in color with fine cored dentrites of aluminium rich (α) and zinc rich (η) phase.

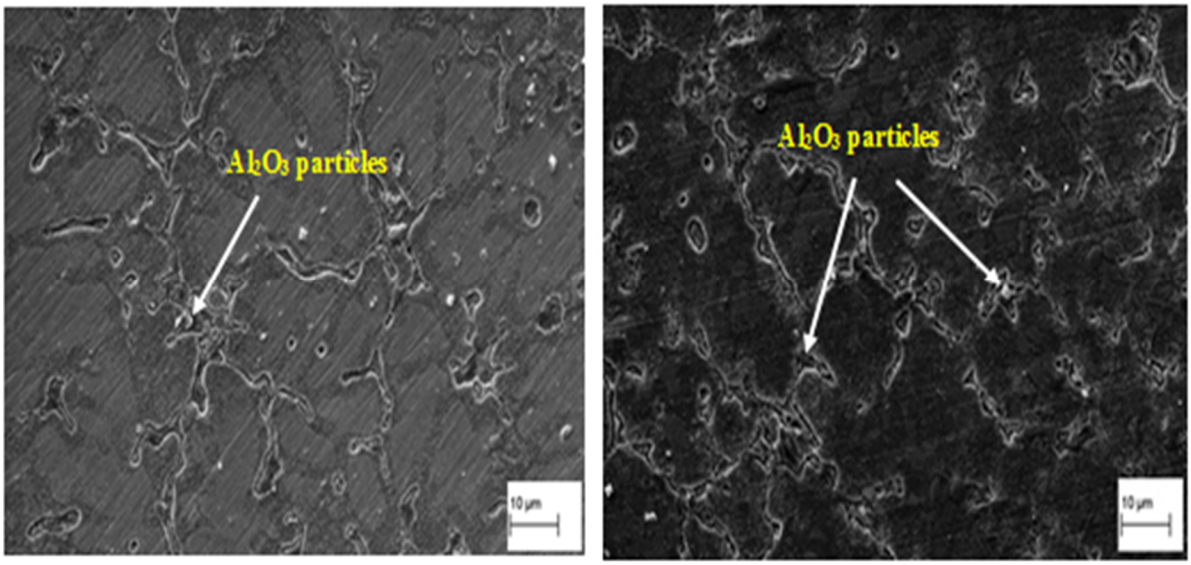

a) ZA-27 + 0.5 wt % Al2O_3 b) ZA-27+ 1.0 wt % Al2O_3

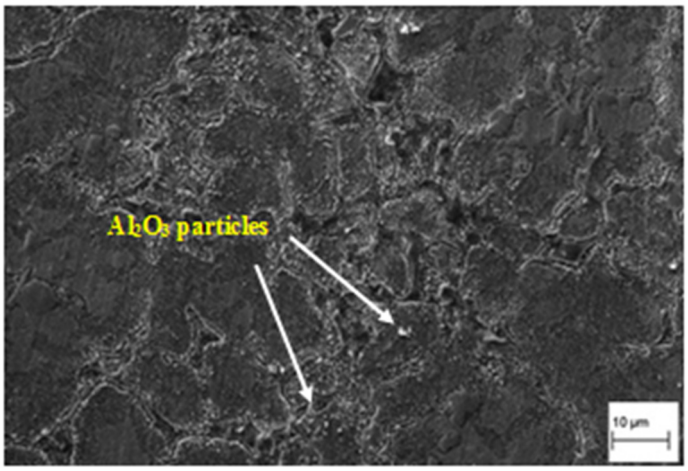

c) ZA-27 + 1.5 t %Al2O3

Figure 4.10 Microstructures of nanocomposites as a function of Al_2O_3 nanoparticles.

Energy dispersive spectroscopy analysis was used for the elemental mapping for the compositional accuracy of the reinforcement particles in ZA-27/Al_2O_3 nanocomposites. EDS analysis of 1.5 wt % Al_2O_3 nanoparticles reinforced in the base alloy was shown in figure 4.11. The EDS analysis confirms the Al and O peaks were observed in the elemental analysis, that the Al_2O_3 nanoparticles was present within ZA-27 nanocomposites

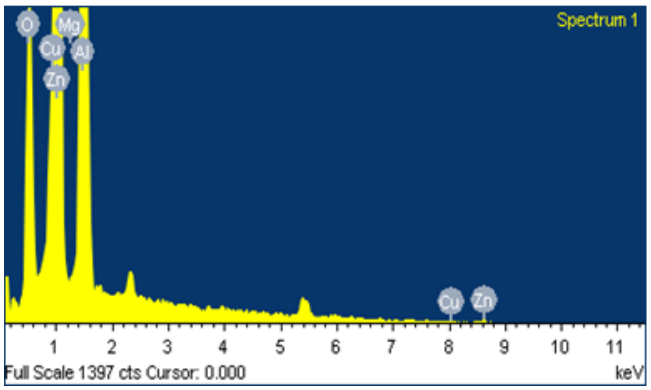

Element	Weight %
O	13.70
Mg	0.02
Al	42.07
Cu	2.02
Zn	42.19
Totals	100.00

Figure 4.11 EDS analysis of 1.5 wt % Al_2O_3

4.6.3. ZA-27 hybrid nanocomposites

The microstructure analysis plays an important role in the overall performance of ZA-27 alloy based hybrid composite. The microstructure of hybrid composite reinforced with the micro/nano sized of the Al_2O_3 and MoS_2 particles in ZA-27 alloy was shown in Figure 4.12.

From Figure 4.12 (b) clearly evident that the reinforcement particles were uniformly distributed in the ZA-27 matrix alloy which was due to the ultrasonic assisted stir casting technique.

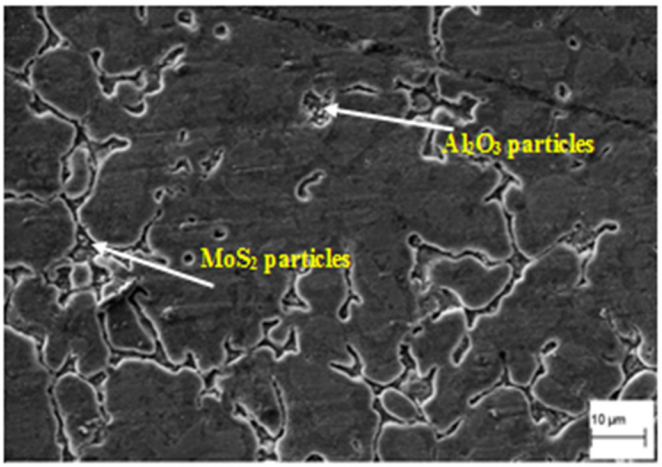

a) Hybrid composite (ZA-27+1.5wt% Al_2O_3 (µm) + 0.5 wt % MoS_2 (µm))

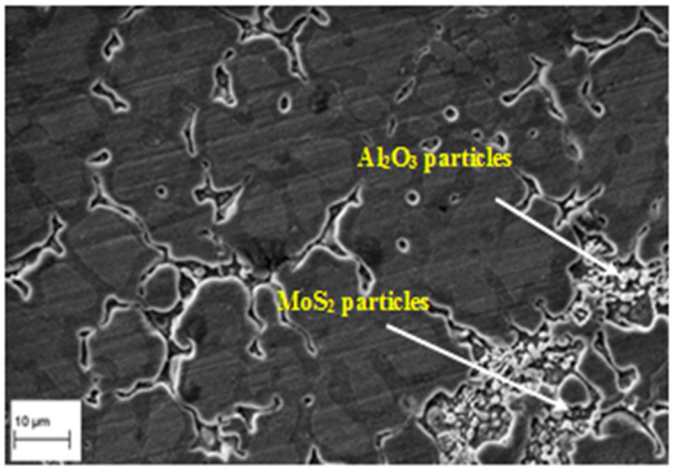

b) Hybrid nanocomposite (ZA-27+1.5wt% Al_2O_3 (nm) + 0.5 wt % MoS_2 (nm))

Figure 4.12 Microstructure of ZA-27 hybrid nanocomposites

The Al_2O_3 and MoS_2 nanoparticles were located at the interdentritic regions of the hybrid nanocomposite, in which alumina nanoparticles were observed white in color and molybdenum disulphide particles as dark black color with fine cored dendrites of aluminium phase and zinc phase. It was observed from the microstructure that the particle clustering was more in the case of hybrid nanocomposites because of increasing surface area and the surface energy nanoparticles.

The porosities were observed in the ZA-27 hybrid nanocomposites at matrix and nanoparticle interfaces, which weaken the bonding between the reinforcement particles and the ZA-27 alloy.

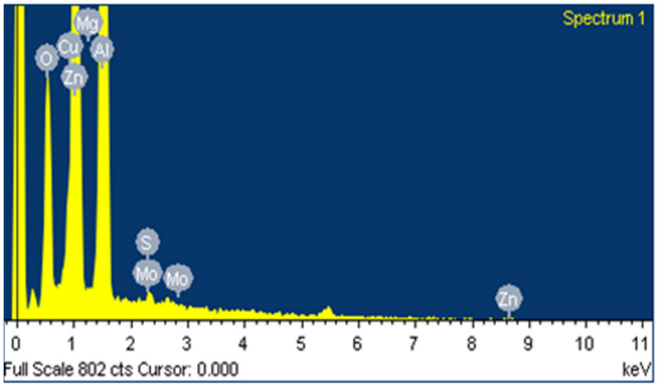

Element	Weight%
O K	13.85
Mg K	0.18
Al K	44.60
S K	1.11
Cu L	1.21
Zn L	39.05
Mo L	1.13
Totals	100.00

Figure 4.13 EDS of hybrid nanocomposite (ZA-27+1.5wt% Al_2O_3 (nm) + 0.5 wt % MoS_2 (nm))

EDS analysis of 1.5 wt % Al_2O_3 and 0.5 wt % MoS_2 nanoparticles reinforced in the base alloy is shown in figure 4.13. EDS analysis confirms that Al_2O_3 and MoS_2 nanoparticles are present within ZA-27 hybrid nanocomposites.

4.7. Summary

MoS_2 nanoparticles were prepared by using planetary ball mill and the average particle size of nanoparticles was measured with the help of particle size analyzer. The ultrasonic assisted stir casting process was used for the fabrication of different weight percentages of Al_2O_3 and MoS_2 nanoparticles in ZA-27 nanocomposites and hybrid ZA27 nanocomposite. The experimental densities of ZA-27/Al_2O_3 nanocomposites and hybrid ZA27 nanocomposite decreases compare to the ZA-27 alloy. The uniform distribution of Al_2O_3 and MoS_2 nanoparticles was observed in the microstructures of ZA-27 nanocomposites and hybrid ZA27 nanocomposites. EDS analysis showing the percentage content of all the elements present in the ZA27 nanocomposites and hybrid ZA27 nanocomposites.

CHAPTER 5

MECHANICAL PROPERTIES OF ZA-27 NANOCOMPOSITES AND HYBRID NANOCOMPOSITE

5.1. Introduction

This chapter deals with the mechanical properties of ZA-27 nanocomposites and hybrid nanocomposite reinforced with different weight percentages of the Al_2O_3 and MoS_2 reinforcement particles. Microhardness tests were carried out for different weight percentages of ZA-27 nanocomposites by using the microhardness tester. The ultimate tensile strength and yield strength of different composition of ZA-27 nanocomposites and hybrid nanocomposites were examined with the help of the electro-mechanical tensile test machine. Rotating bending test machine was used for the fatigue strength analysis of ZA-27 nanocomposites and hybrid nanocomposites. The effects of the reinforcement particles on the mechanical properties of ZA-27 nanocomposites and hybrid nanocomposites were explained in this chapter. The results acquired for ZA-27 nanocomposites and hybrid nanocomposites with different weight percentages of molybdenum disulphide and aluminium oxide particles were compared.

5.2. Mechanical tests of ZA-27 nanocomposites

The mechanical properties of the metal matrix nanocomposites are dependent on the type and weight percentage of the reinforcement particles, dislocation strength and the defects which occurred during the fabrication process of the nanocomposites. The mechanical properties such as microhardness, ultimate tensile strength (UTS) and yield strength (YS) of various weight percentages of ZA-27 nanocomposites and hybrid nanocomposite were evaluated under controlled laboratory conditions. The influence of the reinforcement particles with different weight percentages on the fatigue strength analysis of ZA-27 nanocomposites and hybrid nanocomposites were also investigated in the present study.

5.2.1. Microhardness of ZA-27/ Hybrid nanocomposites

The microhardness tests of the ZA-27 nanocomposites and hybrid nanocomposite were carried out by using (Make: Chennai Metco Pvt Ltd, Model: ECONOMET VH-1MD) microhardness tester. A diamond indenter was used for the microhardness test at an applied load of 200 g and dwell time of 10 s. Around ten measurements were taken for each ZA-27 nanocomposite and an average value of the microhardness was considered. The Vickers hardness values of ZA-27 nanocomposites and hybrid nanocomposites were shown in Table 5.1.

Table 5.1 Microhardness values of ZA-27 nanocomposites and hybrid nanocomposite

Sl.No	Composition	Hardness (HV)
1	ZA-27 alloy	118.6
2	ZA-27 + 0.5% MoS_2 (µm)	122.7
3	ZA-27 + 1.0% MoS_2 (µm)	113.3
4	ZA-27 + 1.5% MoS_2 (µm)	101.9
5	ZA-27 + 0.5% MoS_2 (nm)	124.8
6	ZA-27 + 1.0% MoS_2 (nm)	116.4
7	ZA-27 + 1.5% MoS_2 (nm)	105.6
8	ZA-27 + 0.5% Al_2O_3 (nm)	130.4
9	ZA-27 + 1.0% Al_2O_3 (nm)	135.7
10	ZA-27 + 1.5% Al_2O_3 (nm)	141.5
11	ZA-27 + 1.5% Al_2O_3 (µm) + 0.5% MoS_2 (µm)	128.4
12	ZA-27 + 1.5% Al_2O_3 (nm) + 0.5% MoS_2 (nm)	142.1

a) Effect of MoS_2 nanoparticles on microhardness

ZA-27 alloy reinforced with various weight percentages of the MoS_2 micro-sized and nano-sized particles were influenced the microhardness of ZA-27/MoS_2 nanocomposites with standard deviation as shown in Figure 5.1. It was observed that the microhardness of the nanocomposites increases slightly for 0.5 wt % MoS_2 micro and nanoparticles reinforcement content in ZA-27 alloy. This was due to reinforcement act as obstacles against the movement of

dislocations. As the weight percentages of MoS_2 micro/nanoparticles increases beyond 0.5 wt % the microhardness of the micro/nanocomposites decreases as shown in the Figure 5.1.

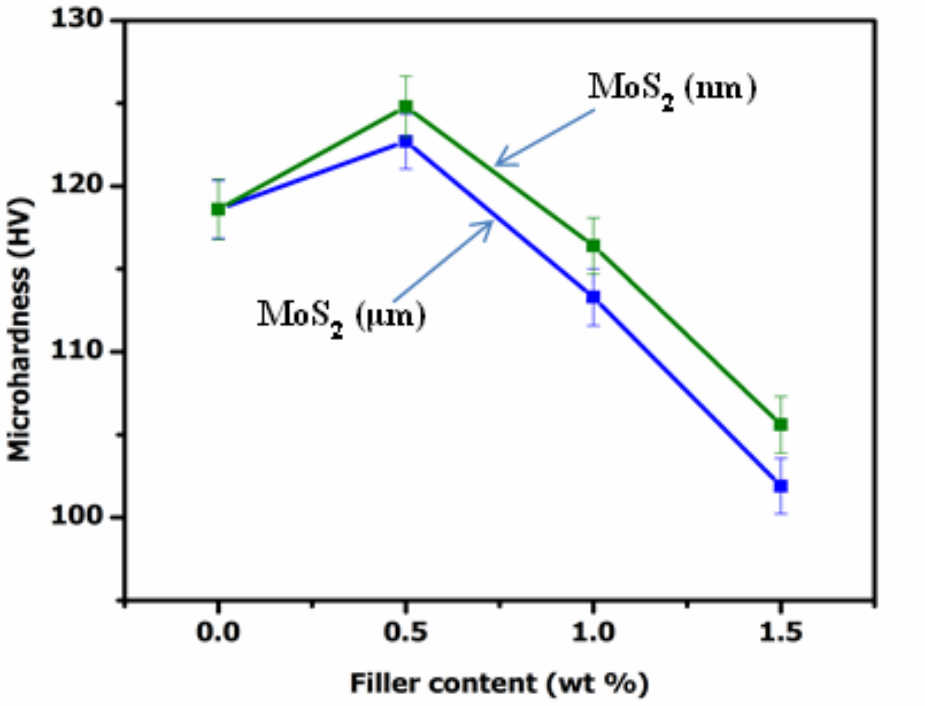

Figure 5.1 Microhardness of ZA-27/MoS_2 nanocomposites

Beyond 0.5 wt% MoS_2 micro/nanoparticles decrease in the microhardness of the micro/nanocomposites was due to the softness of MoS_2 particles. This decrease in the microhardness of micro/nanocomposites was to be estimated since MoS_2 being an effective solid lubricant, renders the material more easily deformable with respect to the indenter of the microhardness tester. The similar results were obtained by using graphite particles reinforced in the ZA-27 alloy [67-69]. The increase in MoS_2 micro/nanoparticles in ZA-27 alloy beyond 0.5 wt % will not contribute on the microhardness of the ZA-27/MoS_2 micro/nanocomposites as they can no longer act as semi-coherent barriers to the movement of dislocations due to the formation of localized microscopic clusters. The microhardness of ZA27 nanocomposites shows slight increase than that of ZA27 microcomposites. The microhardness of ZA-27/MoS_2 nanocomposites reinforced with more than 0.5 wt % of nanoparticles deceased by about 10 % when compare to the ZA-27 alloy.

b) Effect of Al_2O_3 nanoparticles on microhardness

The effect of alumina nanoparticles with different weight percentages reinforced in ZA-27 alloy on the microhardness of ZA-27/Al_2O_3 nanocomposites with standard deviation are shown in the Figure 5.2. It was evident from the figure 5.2, that the reinforcement content increases in ZA-27 alloy and the microhardness of the nanocomposites increases. The ZA-27/Al_2O_3 nanocomposite specimens show an increase in the microhardness by about 16 % as the reinforcement content of the alumina nanoparticles increased from 0 to 1.5 wt %.

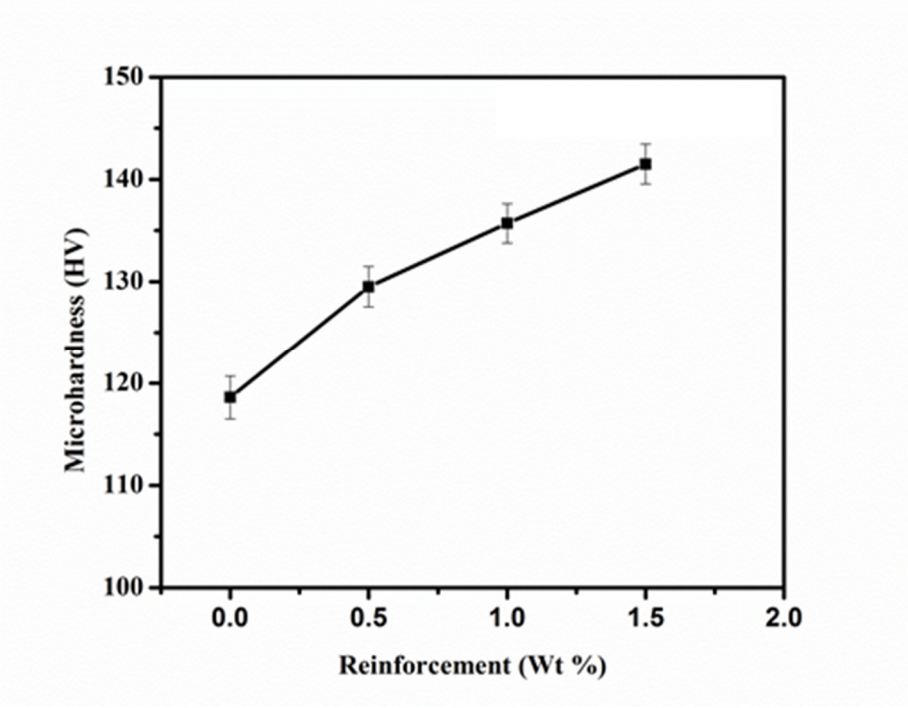

Figure 5.2 Microhardness of ZA-27/Al_2O_3 nanocomposites

The microhardness measures the resistance to indentation of the nanocomposites where there will be limited plastic deformation under identical conditions. The increase in microhardness of ZA-27/Al_2O_3 nanocomposites was due to the presence of hard ceramic particles of the alumina. The improved microhardness of nanocomposites was attributed to the alumina nanoparticles which act as obstacles to the movement of dislocations in ZA-27 alloy. The maximum microhardness value among the nanocomposites was observed for ZA-27 alloy reinforced with 1.5 wt % of Al_2O_3 nanoparticles compared to the other wt % nanocomposites. Similar results were obtained by several researchers when the hard ceramic particles reinforced with ZA-27 alloy increase the hardness of the nanocomposites [27, 76, and 82].

c) Effect of Al_2O_3 and MoS_2 nanoparticles on microhardness

From Figure 5.3, it was observed that the microhardness of ZA-27 hybrid nanocomposite reinforced with 1.5 wt % of alumina and 0.5 wt % of molybdenum disulphide nanoparticles increases as compared to the matrix material.

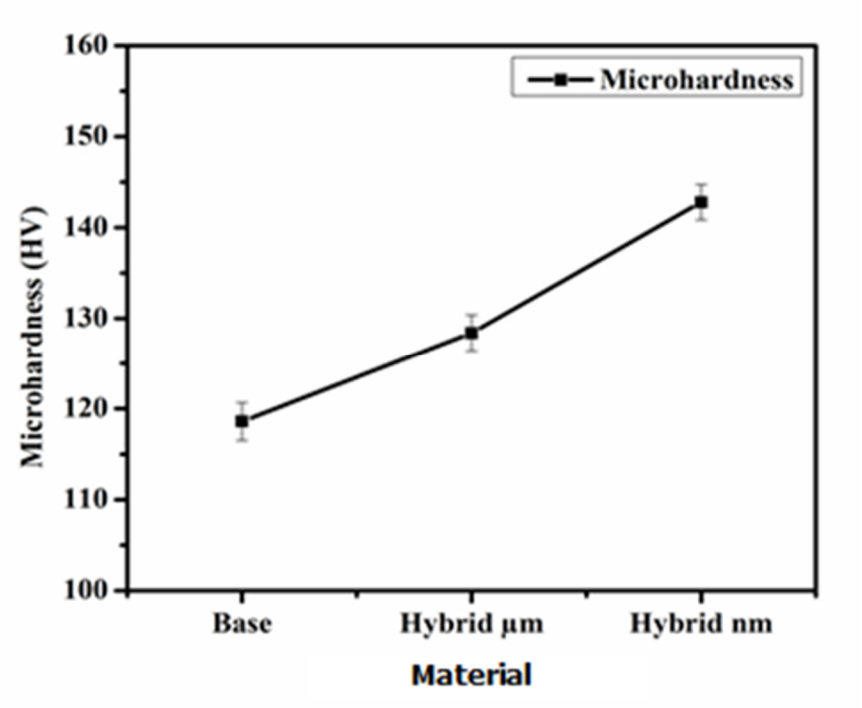

Figure 5.3 Microhardness of ZA-27 hybrid nanocomposites

The improvement in the hybrid nanocomposite was due to the major content of alumina hard ceramic nanoparticles than fewer content of MoS_2, which acts as a barrier to the movement of the dislocations in the matrix alloy. The ZA-27 hybrid nanocomposite reinforced with 1.5 wt % alumina and 0.5 wt % of MoS_2 nanoparticles shows an increase in the microhardness by about 16.5 % when compare to ZA-27 alloy.

5.2.2. Tensile strength of ZA-27 nanocomposites

The tensile test of ZA-27 nanocomposites was performed on the flat specimens. The flat tensile samples were prepared from the cast ZA-27 nanocomposites according to ASTM E8M standard having a gauge length of 25 mm, gauge width of 6 mm and the total length of the test specimen used was 100 mm as shown in figure 5.4 (b).

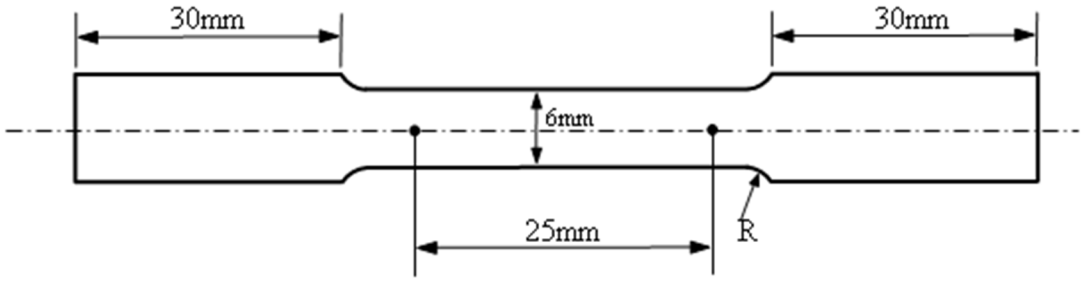

a) Tensile specimen

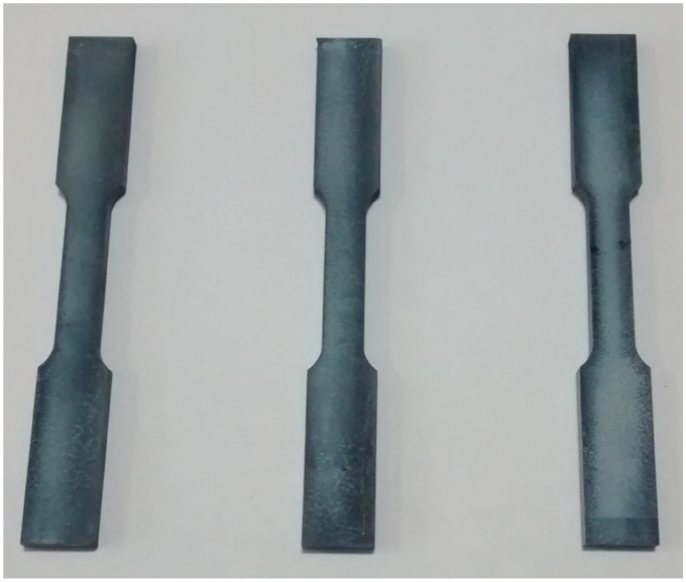

b) ZA-27 nanocomposites tensile samples

Figure 5.4 Tensile specimens of ZA-27 nanocomposites

The tensile test of ZA-27 nanocomposites and hybrid nanocomposites was carried out with the aid of electro-mechanical tensile testing machine at room temperature and at a strain rate of 0.679×10^{-4} s^{-1}. Each experiment was repeated for five times for each ZA-27 nanocomposites and hybrid nanocomposite and the average values of UTS and YS were calculated and reported in table 5.2.

Table 5.2 UTS and YS values of ZA-27 nanocomposites and hybrid nanocomposite

Sl.No	Composition	UTS(MPa)	YS(MPa)
1	ZA-27 alloy	366	256
2	ZA-27 + 0.5% MoS_2 (µm)	371	260
3	ZA-27 + 1.0% MoS_2 (µm)	362	253
4	ZA-27 + 1.5% MoS_2 (µm)	353	247
5	ZA-27 + 0.5% MoS_2 (nm)	378	269
6	ZA-27 + 1.0% MoS_2 (nm)	359	256
7	ZA-27 + 1.5% MoS_2 (nm)	345	245
8	ZA-27 + 0.5% Al_2O_3 (nm)	405	281
9	ZA-27 + 1.0% Al_2O_3 (nm)	419	293
10	ZA-27 + 1.5% Al_2O_3 (nm)	435	301
11	ZA-27 + 1.5% Al_2O_3 (µm) + 0.5% MoS_2 (µm)	392	279
12	ZA-27 + 1.5% Al_2O_3 (nm) + 0.5% MoS_2 (nm)	437	312

a) Effect of MoS_2 nanoparticles on UTS and YS

The UTS and YS of ZA-27 alloy reinforced with the various weight percentages of the MoS_2 micro/nano-sized particles were shown in Figure 5.5 (a-b). It was observed that the tensile strength and yield strength increase with addition of MoS_2 micro /nanoparticles till 0.5 wt% and then a decline was observed. The improvement in properties at 0.5 wt% MoS_2 nanocomposite was due to the small amount of MoS_2 particles reinforced in ZA-27 alloy which act as barriers to the dislocations in the microstructure. The UTS and YS of the 0.5 wt % MoS_2 nanoparticles added in nanocomposite increases upto 3.1% (UTS) and 4.2 % (YS) when compared to ZA-27 alloy. Further addition of MoS_2 nanoparticles in the ZA-27 alloy deteriorates the UTS and YS of the ZA-27/MoS_2 nanocomposites due to the formation of clusters and agglomerations. MoS_2 nanoparticles were soft and act as solid lubricant, which reduces the interfacial bonding strength of ZA-27/MoS_2 nanocomposites. The UTS and YS of the ZA-27/MoS_2 nanocomposites reinforced with 1.5 wt % of nanoparticles deceased by about 5 % (UTS) and 4.8 % (YS) when compared to ZA-27 alloy.

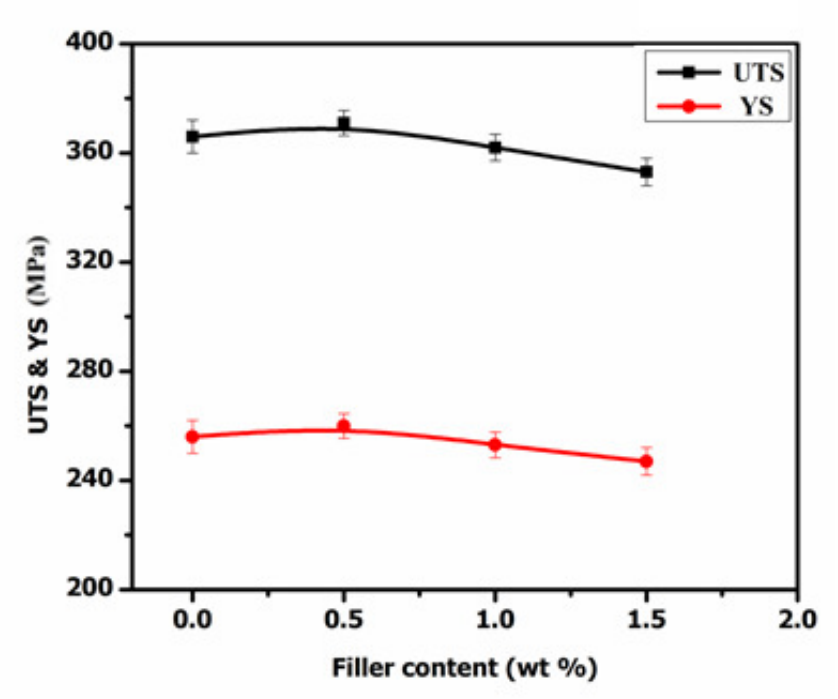

a) ZA-27/MoS_2 microcomposites

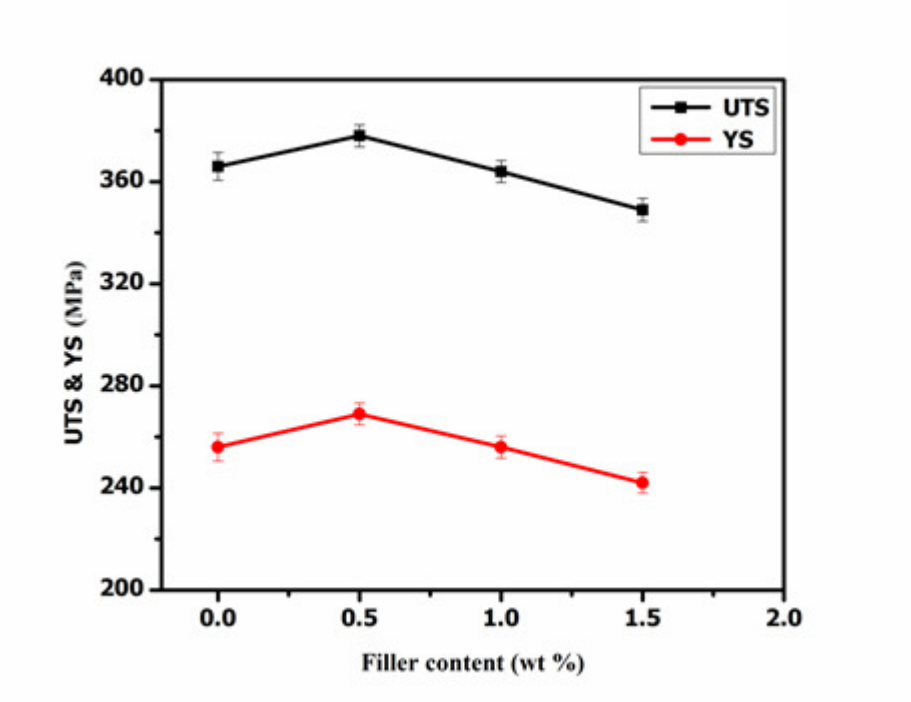

b) ZA-27/MoS_2 nanocomposites

Figure 5.5 UTS and YS of ZA-27/ MoS_2 micro and nanocomposites

b) Effect of Al_2O_3 nanoparticles on UTS and YS

From Figure 5.6 it was evident that the graphs of UTS and YS (stress required to produce a plastic srain of 0.2 %) of ZA-27 /Al_2O_3 nanocomposites samples increases as the reinforcement content of the Al_2O_3 nanoparticles increases in the ZA-27 alloy. It follows from the Figure 5.6, that ZA-27/Al_2O_3 nanocomposites show an increase in the UTS of about 15.8 % and the YS increases by about 14.6 % as the reinforcement content of alumina nanoparticles in the nanocomposites was increased from 0 to 1.5 wt %. The UTS and YS of the ZA-27/Al_2O_3 nanocomposites were affected by several factors such as the mechanical properties of the matrix material and reinforcement particles, distribution of the reinforcement particles in the matrix material and the bonding between the matrix material and the reinforcement particles [72].

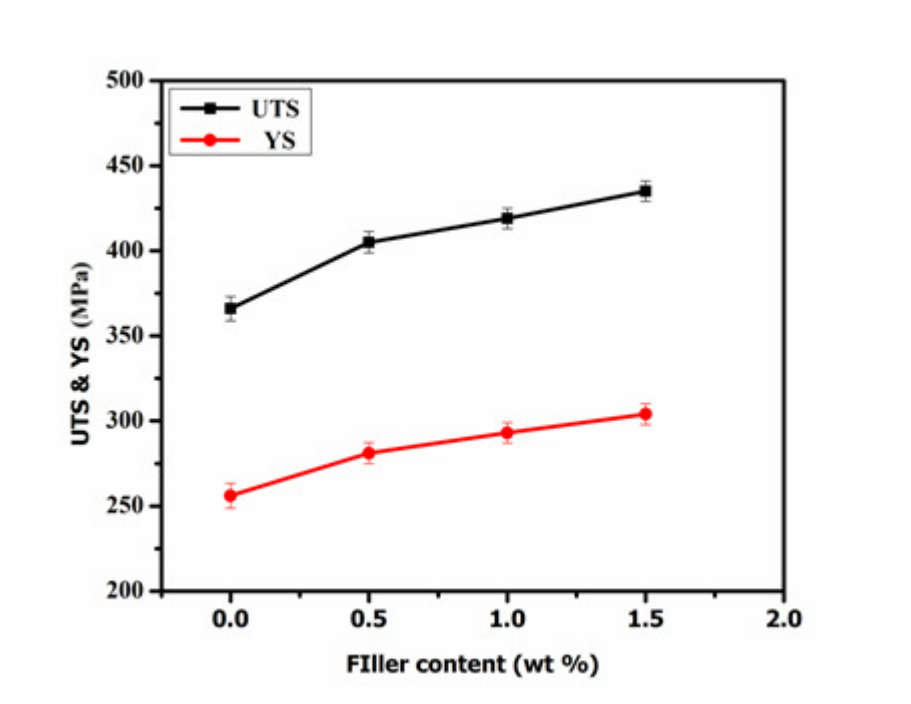

Figure 5.6 UTS and YS of ZA-27/ Al_2O_3 nanocomposites

These hard reinforcing particles will improve the strength of the matrix material and impart additional resistance to the nanocomposites against the applied tensile stresses. The maximum load was transferred to the hard and brittle ceramic reinforcement particles present in the matrix material. The uniform distribution of the alumina nanoparticles in ZA-27 alloy restricts the plastic flow and enhances the tensile strength properties in ZA-27/ Al_2O_3 nanocomposites. The increase trend in the UTS and YS was obtained by hard ceramic particle

reinforcement in several aluminum and zinc alloy matrices, depending upon the type of alloy and the amount of reinforcement were investigated by many researchers [160-161].

c) Effect of Al_2O_3 and MoS_2 nanoparticles on UTS and YS

The UTS and YS of the ZA-27 hybrid nanocomposite reinforced with 1.5 wt % of alumina and 0.5 wt % of molybdenum disulphide nanoparticles increase as compared to the ZA-27 alloy as shown in Figure 5.7.

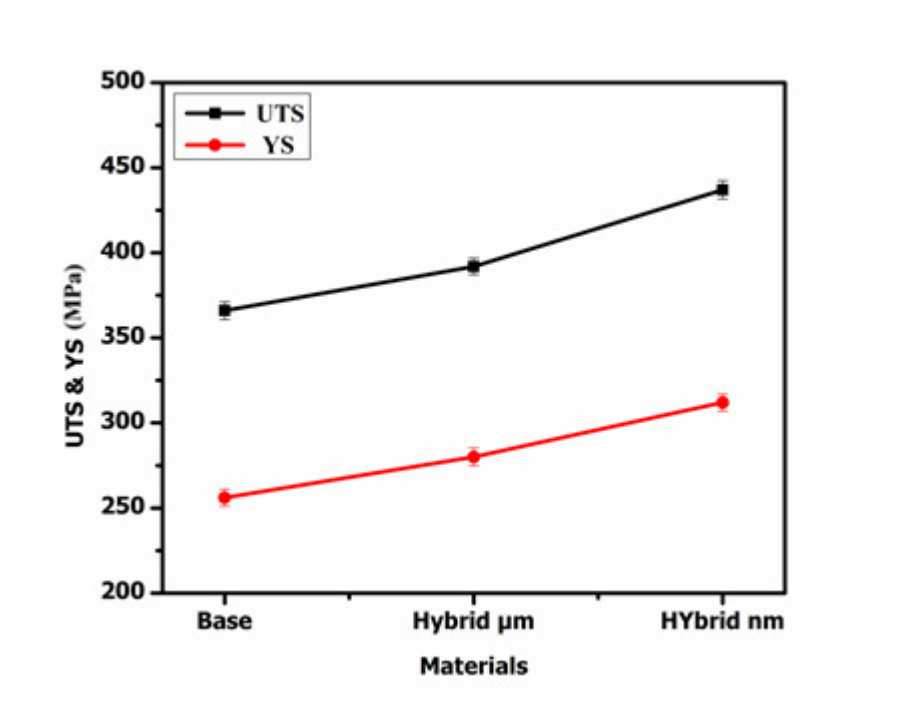

Figure 5.7 UTS and YS of ZA-27 hybrid micro and nanocomposites

The improvement in the hybrid nanocomposite was due to the major content of alumina hard ceramic nanoparticles which act as barriers to the movement of the dislocations in the matrix alloy. The dispersion-strengthening influence in the hybrid nanocomposite was estimated to be retained even at higher temperatures and for long time periods because the Al_2O_3 and MoS_2 nanoparticles were not reactive with the matrix phase. These hard reinforcing particles will improve the strength of the matrix material and impart additional resistance to the hybrid nanocomposites against the applied tensile stresses. The enhancement in the mechanical properties can be attributed to the result of several strengthening mechanism contributions such as elastic modulus (EM), coefficient of thermal expansion (CTE), Orowan strengthening and

Hall-petch strengthening effects [163-166]. The uniform distribution of the alumina and MoS_2 nanoparticles was increase the UTS and YS of ZA-27 hybrid nanocomposite about 10.5 % when compare to the hybrid micro composite.

5.2.3. Fatigue test of ZA-27 nanocomposites

The main purpose of fatigue tests was to determine the relationship between the applied load and the number of cycles to cause failure, and to obtain some estimate of the probability of failure under specified loading conditions. The fatigue test samples were prepared from the cast ZA-27 nanocomposites according to ASTM E739 standard as shown in figure 5.8(a).

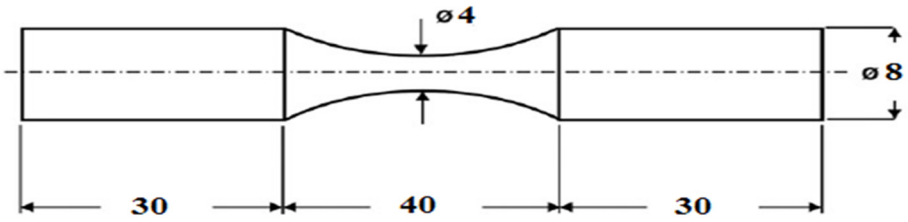

a) Fatigue specimen

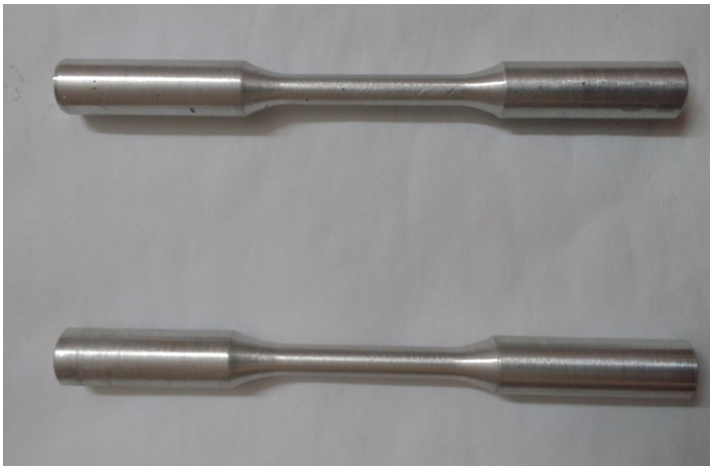

b) ZA-27 nanocomposites fatigue test specimens

Figure 5.8 Fatigue test specimens of ZA-27 nanocomposites

The fatigue strength of different weight percentages reinforced in ZA-27 nanocomposites and hybrid nanocomposite was determined by using a rotating bending fatigue test machine as

per ASTM E739 standard. Rotating bending fatigue test of ZA-27 nanocomposites were conducted in laboratory air atmosphere and stress ratio R= - 1. In each fatigue test at least two specimens were tested for one stress level and the number of cycles for fatigue failure was noted. The statistical analysis using three stress levels was done after the fatigue test results of the ZA-27 nanocomposites and hybrid nanocomposite were shown in table 5.3.

Table 5.3 Fatigue strength values of ZA-27 nanocomposites and hybrid nanocomposite

Sl.No	Composition	Stress range (MPa)	No.of cycles (10^6)
1	ZA-27 alloy	120	1.35
2	ZA-27 + 0.5% MoS_2 (µm)	123	1.59
3	ZA-27 + 1.0% MoS_2 (µm)	117	1.11
4	ZA-27 + 1.5% MoS_2 (µm)	112	1.01
5	ZA-27 + 0.5% MoS_2 (nm)	125	1.98
6	ZA-27 + 1.0% MoS_2 (nm)	120	1.65
7	ZA-27 + 1.5% MoS_2 (nm)	115	1.05
8	ZA-27 + 0.5% Al_2O_3 (nm)	130	2.17
9	ZA-27 + 1.0% Al_2O_3 (nm)	135	2.57
10	ZA-27 + 1.5% Al_2O_3 (nm)	140	3.45
11	ZA-27 + 1.5% Al_2O_3 (µm) + 0.5% MoS_2 (µm)	130	2.02
12	ZA-27 + 1.5% Al_2O_3 (nm) + 0.5% MoS_2 (nm)	140	3.55

a) Effect of MoS_2 nanoparticles on fatigue strength

The fatigue strength was affected by various weight percentages of MoS_2 micro/nano sized particles reinforced in ZA-27 nanocomposites and the curves of stress amplitude (S) versus number of cycles (N) to failure were shown in Figure 5.9 (a-b). It was observed that the 0.5 wt % of MoS_2 nanoparticles reinforced ZA-27 nanocomposite increases the fatigue strength compared to the other composition of nanocomposites and ZA-27 alloy.

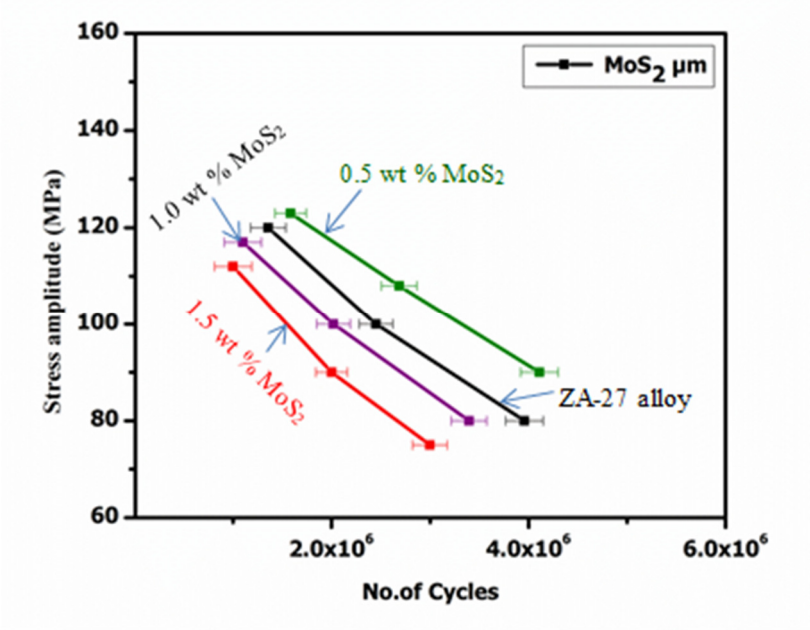

a) ZA-27/MoS_2 microcomposites

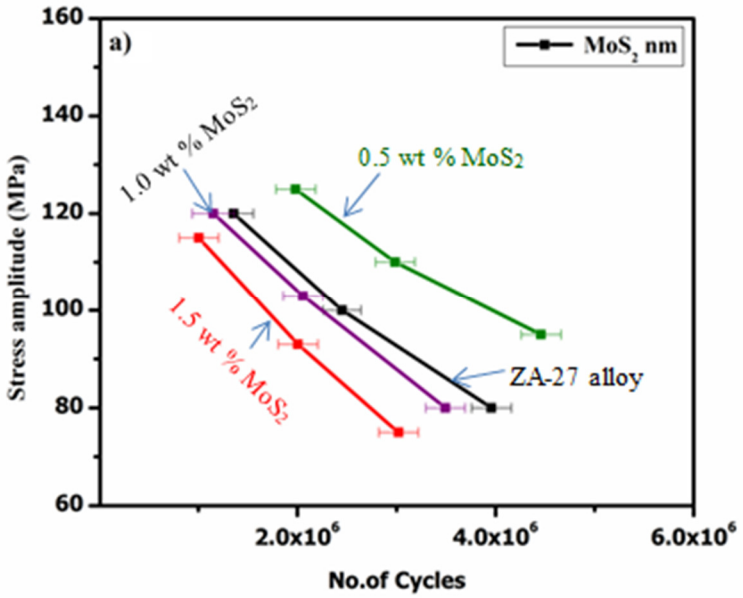

b) ZA-27/MoS_2 nanocomposites

Figure 5.9 Influence of MoS_2 particles on the fatigue strength of micro and nanocomposites

The increase in the fatigue strength of 0.5 wt % nanocomposite was due to limited amount of MoS_2 nanoparticles present in the matrix material that acts as barrier to the dislocations in the microstructure. Further increasing of MoS_2 nanoparticles beyond 0.5 wt % makes the fatigue

strength of ZA-27/MoS_2 nanocomposites decrease, since the reinforcement content increase in ZA-27 alloy will reduce the interface bonding between the nanoparticles and the matrix materials. MoS_2 particles were soft and act as a solid lubricant, which decreases the bonding strength among the base alloy and reinforcement particles of nanocomposites. As the stress amplitude decreases the fatigue strength of the ZA-27/MoS_2 nanocomposites increases because the number of cycles required for failure of the nanocomposites increases. The fatigue strength of 0.5 wt % MoS_2 nanoparticles reinforced ZA-27 nanocomposites increases by about 31.5 % compared to ZA-27 alloy.

b) Fracture surfaces of ZA-27/MoS_2 nanocomposites

The fracture surfaces of different weight percentages of MoS_2 nanoparticles reinforced ZA-27 nanocomposites were examined by using scanning electron microscope (SEM) as shown in Figure 5.10 (a) to (d). The fatigue fracture can be divided into three regions, namely crack initiation region, crack propagation region and the final rapid fracture region of the specimens were corresponding to the more or less fatigue cycles.

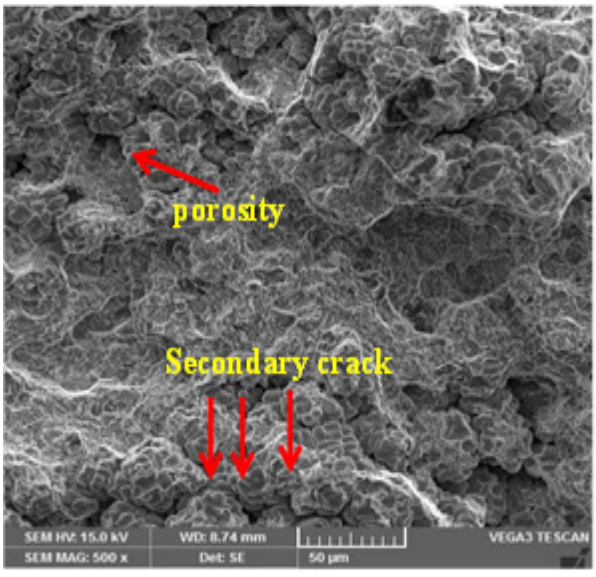

a) ZA-27 alloy

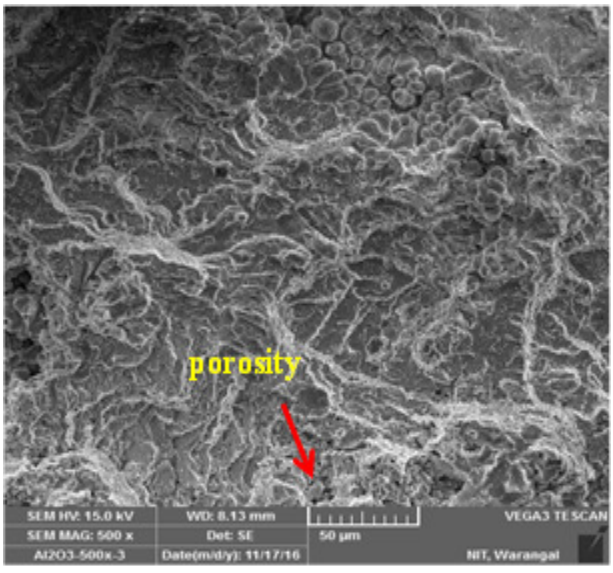

b) ZA-27 + 0.5 wt % MoS_2

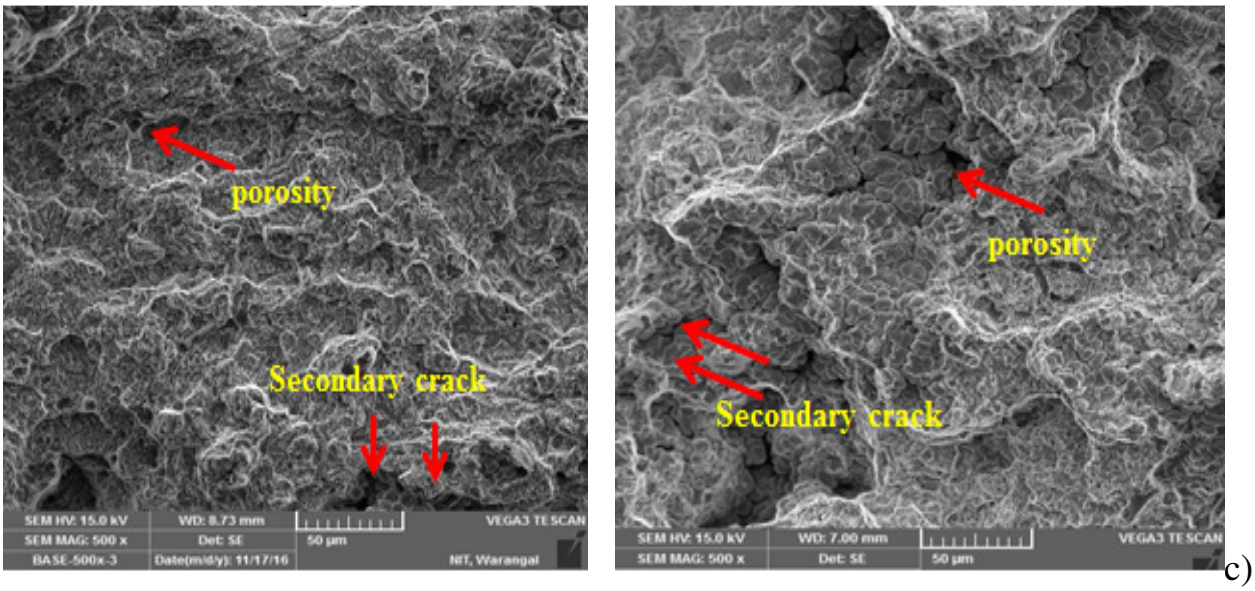

c)

ZA-27 + 1.0 wt % MoS_2 d) ZA-27 + 1.5 wt % MoS_2

Figure 5.10 Fatigue fracture surfaces of ZA-27/MoS_2 nanocomposites

The crack initiation of the fatigue was occurred at the specimen edges due to the presence of inclusions or defects caused during the fabrication process. From figure 5.10 (a) it was observed that the crack initiation of the surface starts at the edge of the specimen due to the presence of porosity. The fatigue failure that occurred in ZA-27 alloy was due to the secondary cracks, which increase the crack propagation in the fracture surface when subjected to the stress cycles. The fracture surface of 0.5 wt % MoS_2 nanocomposites is shown in figure 5.10 (b), it was observed that when the pores and secondary cracks are less compared to the ZA-27 alloy it improves the fatigue strength. As the reinforcement content of MoS_2 nanoparticles increases the porosity and secondary cracks in the base metal improves which leads to the failure of ZA-27/MoS_2 nanocomposites with fewer stress cycles as shown in figure 5.10. (c) and (d).

c) Effect of Al_2O_3 nanoparticles on fatigue strength

The fatigue strength of different weight percentages of alumina nanaparticles reinforced in ZA-27/ Al_2O_3 nanocomposites are shown in figure 5.11. It was evident that when the reinforcement content increases in nanocomposites, the fatigue strength increases when compared to ZA-27 alloy. These hard reinforcing particles improve the fatigue strength of ZA-27 alloy and impart additional resistance to the nanocomposites against the applied load. The fatigue

strength of the nanocomposites increases significantly at lower stress levels than at higher stress levels. The uniform dispersion of the reinforcement particles in ZA-27 nanocomposites enhances the plastic strain, which required causing the crack initiation in the specimen. The highest weight percentage of alumina nanoparticles reinforced in the ZA-27 alloy showed the significant improvement in the fatigue strength of ZA-27 nanocomposites.

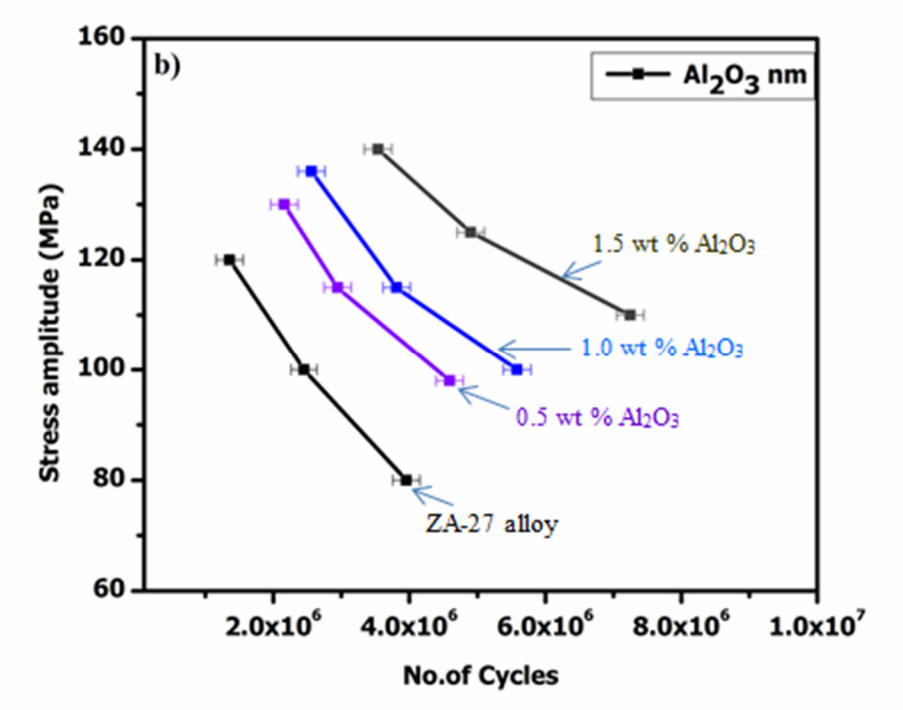

Figure 5.11 Effect of alumina nanoparticles on fatigue strength of nanocomposites

As the weight percentage of Al_2O_3 nanoparticles increases in ZA-27 alloy a significant amount of the load being transferred to the harder particulates reinforcement increases the fatigue strength of the nanocomposites. The ZA-27/Al_2O_3 nanocomposite specimens show an increase in the fatigue strength by about 60.5 % as the reinforcement content of the alumina nanoparticles increased from 0 to 1.5 wt %.

d) Fracture surfaces of ZA-27/Al_2O_3 nanocomposites

The fracture surfaces of different weight percentages of alumina nanoparticles reinforced ZA-27 nanocomposites were examined by using scanning electron microscope (SEM) as shown in Figure 5.12 (a) to (c).

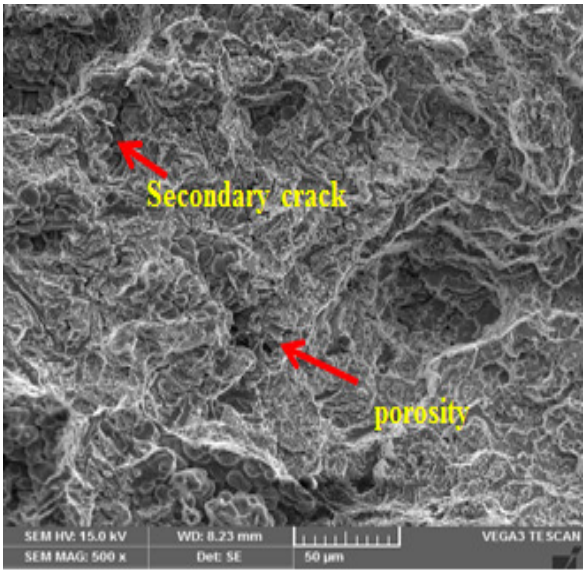

a) ZA-27 + 0.5 wt % Al_2O_3

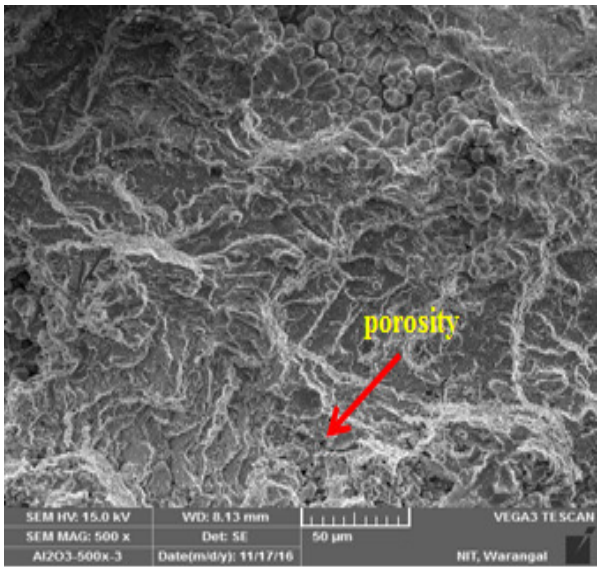

b) ZA-27 + 1.0 wt % Al_2O_3

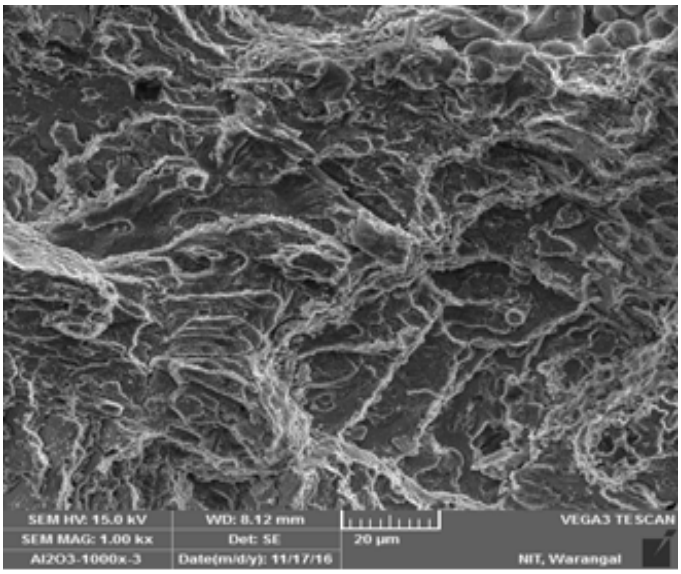

c) ZA-27 + 1.5 wt % Al_2O_3

Figure 5.12 Fatigue fracture surfaces of ZA-27/Al_2O_3 nanocomposites

It was observed from the microstructure surfaces that the fracture occurred because of the crack initiation and crack propagation in the matrix material. The formation of micro voids and the fracture of reinforcement particles in the ZA-27 alloy develop the secondary crack in the surfaces of the specimen which leads to the fatigue fracture of the nanocomposites. The presence of micro voids in ZA-27 alloy acts as a stress concentration, which helps in the crack initiation observed at edges of the surfaces in nanocomposites as shown in figure 5.12 (a-b). The fracture surface of the 1.5 wt % alumina nanopartilces reinforece ZA-27 nanocomposites was shown in figure 5.12 (c), it was observed that the pores and secondary cracks were less compare to the other composition will improves the fatigue strength of the ZA-27/Al_2O_3 nanocomposites.

e) Effect of Al_2O_3 and MoS_2 nanoparticles on fatigue strength

The influence of alumina and molybdenum disulphide nanopartilces with different weight pecentage reinforced in the ZA-27 hybrid nanocomposite on fatigue strength as shown in figure 5.13.

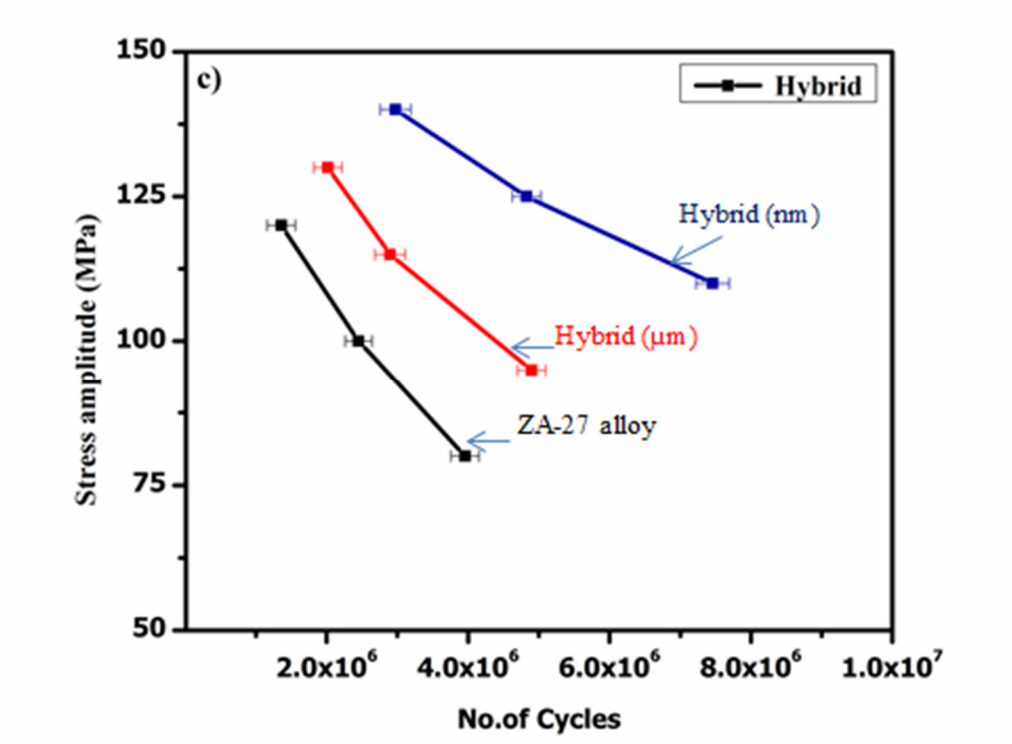

Figure 5.13 Effect of reinforcement nanoparticles on fatigue strength of hybrid nanocomposites

It was observed that the reinforcement content of 1.5 wt % Al_2O_3 and 0.5 wt % MoS_2 nanoparticles increases the fatigue strength of the hybrid nanocomposite when compared to ZA-27 alloy. The presence of hard ceramic particles of alumina nanoparticles in the matrix material will improve the fatigue strength of the hybrid nanocomposite. The addition of hard Al_2O_3 nanoparticles increases the fatigue strength of ZA-27 alloy and imparting the additional resistance to the hybrid nanocomposite against the applied load. The fatigue strength of the hybrid nanocomposites increases significantly at lower stress levels than the higher stress levels. The fatigue strength of hybrid nanocomposites increases by about 61.7 % compare to ZA-27 alloy. The hybrid nanocomposite increases the fatigue strength as compared to the individual ZA-27 nanocomposites.

f) Fracture surfaces of ZA-27 hybrid nanocomposites

The fatigue fracture surfaces of the hybrid nanocomposites reinforced with 1.5 wt % alumina and 0.5 wt % MoS_2 nanoparticles were studied by using SEM as shown in Figure 5.14.

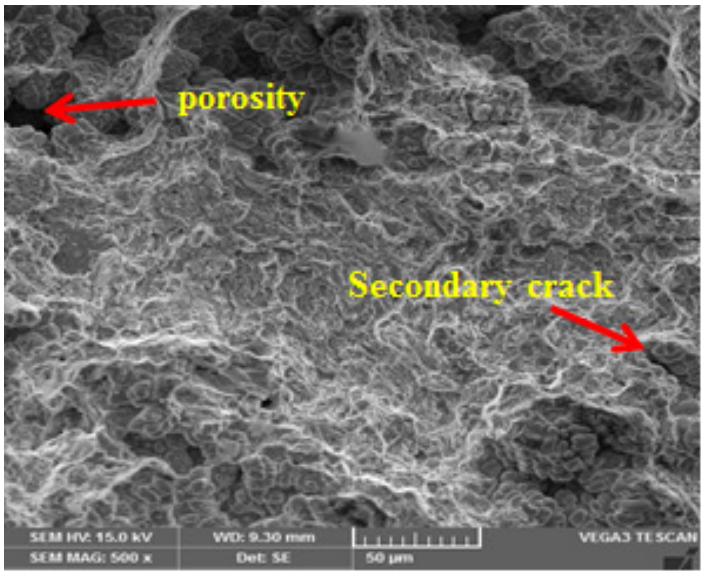

(a) Hybrid microcomposite (ZA-27 + 1.5 wt % Al_2O_3 + 0.5 wt % MoS_2)

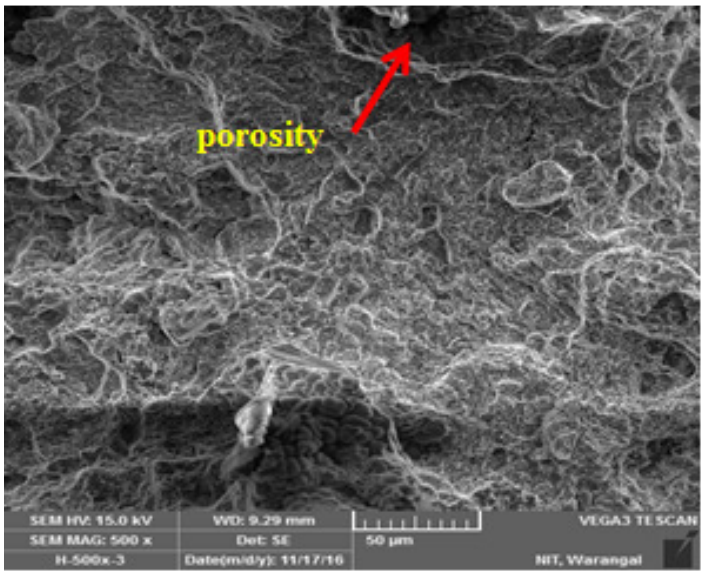

(b) Hybrid nanocomposite (ZA-27 + 1.5 wt % Al_2O_3 + 0.5 wt % MoS_2)

Figure 5.14 Fatigue fracture surfaces of ZA-2 hybrid micro and nanocomposites

It may be observed from the Figure 5.14 (b) that the few micro voids are present in fracture surface, which increases the number of cycles for the fracture of the hybrid nanocomposites compared to ZA-27 alloy. The less secondary crack were observed in the hybrid nanocomposites when compare to the hybrid micro composite which increases the fatigue strength.

5.3. Comparison of mechanical properties of ZA-27 nanocomposites

The comparison of the microhardness, UTS, YS and fatigue strength of Al_2O_3, MoS_2 and a combination of both (Al_2O_3 & MoS_2) nanoparticles reinforced in the ZA-27 nanocomposites and hybrid nanocomposite under similar test condition are shown in Figure 5.15 to 5.17. The reinforcement content of 1.5 wt % Al_2O_3 nanoparticles in ZA-27 nanocomposites and the hybrid nanocomposite reinforced with 1.5 wt % alumina and 0.5 wt % MoS_2 nanoparticles are enhancing the mechanical properties significantly compared to ZA-27 alloy.

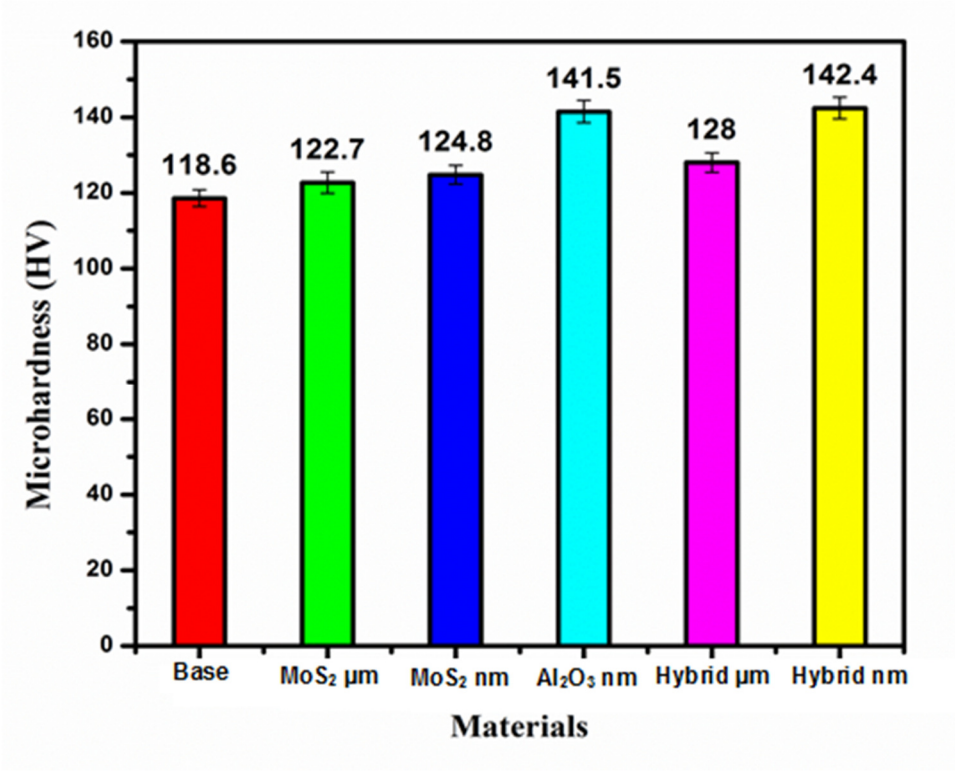

Figure 5.15 Comparison of microhardness

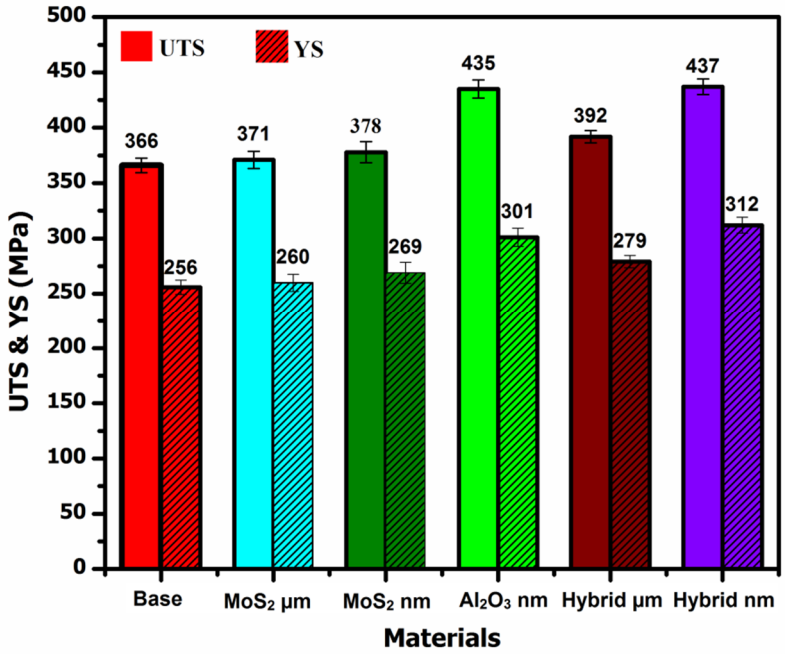

Figure 5.16 Comparisons of UTS and YS

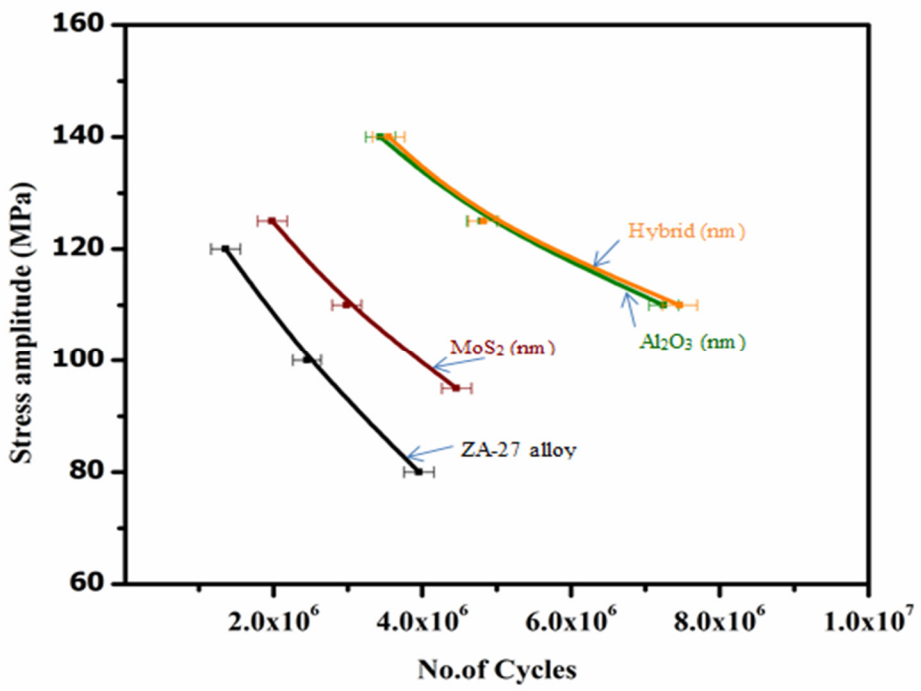

Figure 5.17 Comparison of fatigue strength

5.4. Comparative study of mechanical properties with past studies:

A comparative study was carried out to find out the enhancement in mechanical properties. Data from the previous studies was collected to compare with the present work. Figure 7.1 and 7.2 shows the microhardness and ultimate tensile strength enhancement with respect to various reinforcement particles reinforced in ZA-27 alloy which are reported in the literature and present work. The hybrid nanocomposite reinforced with 1.5 wt % Al_2O_3 and 0.5 wt % MoS_2 nanoparticles in ZA-27 alloy showing better improvement than the other reinforcement materials.

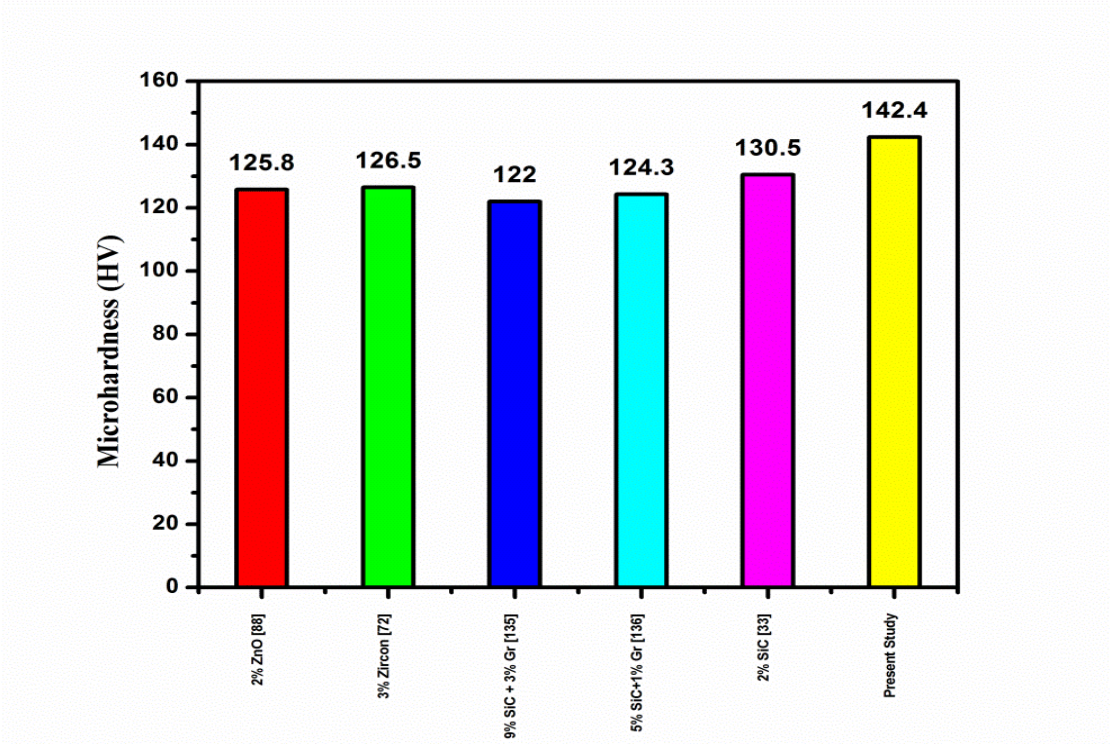

Figure 5.18.Comparative study on microhardness of past studies

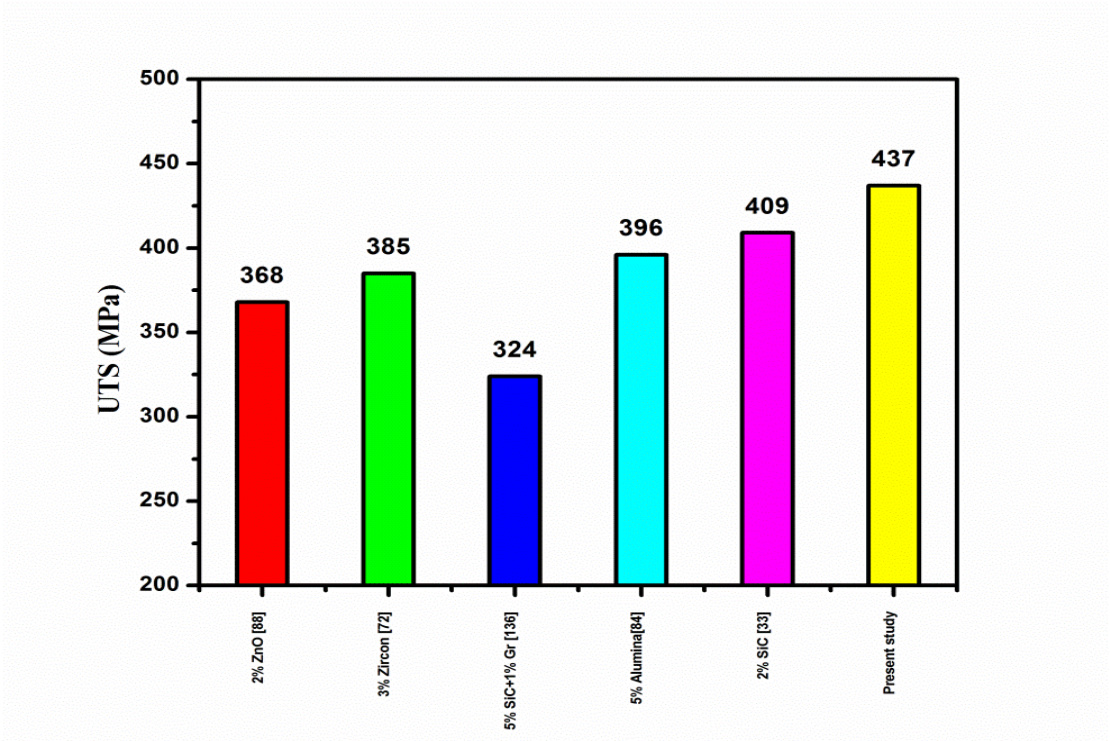

Figure 5.19.Comparative study on UTS of past studies

5.5. Summary

The analysis of mechanical properties such as microhardness, UTS, YS and fatigue strength of the various weight percentages of the alumina and MoS_2 nanoparticles reinforced in ZA-27 nanocomposites and hybrid nanocomposite was summarized in this chapter. The reinforcement content of 1.5 wt % Al_2O_3 nanoparticles in ZA-27 nanocomposites and the hybrid nanocomposite reinforced with 1.5 wt % alumina and 0.5 wt % MoS_2 nanoparticles enhance the mechanical properties significantly compared to ZA-27 alloy. The morphology of fracture surfaces of various weight percentages of the reinforcement of Al_2O_3 and MoS_2 particles reinforced in ZA-27 nanocomposites and hybrid nanocomposite was investigated with the help of SEM micrographs was also discussed in this chapter.

CHAPTER 6

TRIBOLOGICAL BEHAVIOR OF ZA-27 NANOCOMPOSITES AND HYBRID NANOCOMPOSITES

6.1. Introduction

This chapter presents the tribological behavior of different weight percentages of Al_2O_3 and MoS_2 micro/nanoparticles reinforced ZA-27 nanocomposites and hybrid nanocomposite with the help of pin on disc wear testing machine. As the tribological behavior was a difficult wear phenomenon in which a number of process parameters collectively determine the performance responses i.e. the wear rate and friction coefficient of ZA-27 nanocomposites, for implementation of suitable statistical techniques for process optimization of wear behavior. Design of experiments and statistical methods were used to examine the influence of control factors like sliding speed, sliding distance, reinforcement content and applied load on the tribological behavior at different operating conditions. In the present study the Response Surface Methodology (RSM) technique was used to investigate the dry sliding wear characteristics of the ZA-27 nanocomposites and hybrid nanocomposite. The analysis of variance (ANOVA) was performed to determine the most significant parameters which influence the tribological behavior of ZA-27 nanocomposites at various operating conditions. The morphology of worn surfaces of the various weight percentages Al_2O_3 and MoS_2 micro/nanoparticles reinforced of ZA-27 nanocomposites and hybrid nanocomposites was analyzed with the help of scanning electron microscope (SEM) as discussed in this chapter.

6.2. Design of experiments: RSM

For analyzing any system or process effectively, efficiently and economically, experiments were to be designed and conducted systematically. The aim of any experimental design was to provide an insight into the relationship between process parameters with their responses, the influence of various process parameters and also their percentage contributions. One-Variable-At-a-Time (OVAT) approach was used in manufacturing industries, where one variable was varied at a time keeping all other variables in the experiments fixed. These are often

considered as unreliable, inefficient, time consuming and may yield false optimum conditions for the process.

Factorial design of experiments was mostly used to simultaneously determine the significance of multiple independent variables and their interactions. In a full factorial design of experiments two or more factors with discrete values or levels were considered with all the possible combinations. However, it was costly to perform full factorial experiments. Instead, a fractional factorial design, which was a subset of full factorial design, was generally used which requires fewer runs. Factorial design was less preferable when more than two levels were considered. This is needed, as the number of experiments required for such designs will be considerably greater than their two level counterparts. Generally, factors in real engineering problems were continuous, but the two-level factorial design assumes that the effect was linear. In order to consider a quadratic effect, a more complicated experiment was to be selected such as central composite design. Response surface methodology (RSM) was mostly used while optimizing factors that could have quadratic effects [167].

RSM was a collection of statistical and mathematical techniques useful for the modeling and analysis of problems [168]. In RSM, the objective was to optimize the responses that are influenced by the input process parameters. Sufficient data was gathered through the designed experimental layout and a second-order regression equation was developed. A multi-variable regression analysis has been developed between the input process parameters and responses. The general second order regression equation was given by equation 6.1.

$$Y_r = b_0 + \sum_{i=1}^{n} b_i X_{ir} + \sum_{i=1}^{n} b_{ii} X_{ir}^2 + \sum_{j>i}^{n} b_{ij} X_{ir} X_{ju} \qquad 6.1$$

where, Y_r is response, X_{ir} is the value for i^{th} input process parameter of r^{th} experiment; n is the number of process parameters and b_i, b_{ii}, b_{ij} are the regression coefficients. This regression modeling was done to generate the fitness equations for the output responses.

Optimization study in RSM was carried out in three stages. The first stage is to determine the independent input parameters and their levels for experimentation. In the second stage, selection of experimental design, prediction and verification of the model equation was performed. Lastly, the response surface plots and contour plots of these response functions were used to determine the optimum points.

6.3. Wear test of the ZA-27 nanocomposites

The dry sliding wear behavior of ZA-27 nanocomposite samples was tested with the help of pin-on-disc wear testing apparatus as per ASTM G99 standard. The test specimens for wear characterization were cut from the cast samples according to the standard dimensions with 6mm diameter and 30mm height and polished metallographically. The sliding end of the pin and the disk surfaces were cleaned with acetone before testing. The sample was pressed against the rotating EN32 hardened steel disc at different operating conditions. The weight of the nanocomposite samples before and after the wear test was measured by using the electronic weighing machine which could measure up to 0.0001 g. The wear loss was measured with the difference between the initial and final weight of the specimens and wear rate (WR) was determined. The wear rate and coefficient of friction of ZA-27 nanocomposite specimens was studied and analyzed as a function of sliding speed, applied load, sliding distance and filler content with the help of response surface methodology (RSM).

Design expert 9.0 software was used for the design of experiments. The dry sliding wear experiments of ZA-27 nanocomposites were designed based on central composites design (CCD) scheme of design of experiments (DOE). In the present study to analyze the wear rate and coefficient of friction of ZA-27 nanocomposite four input process parameters and three levels and for hybrid nanocomposite three input process parameters and three levels were used. The central composite design consisting of 30 sets of coded conditions for ZA-27 nanocomposites and 20 sets of coded conditions for hybrid nanocomposites was used to investigate the tribological properties of the nanocomposites. The control process parameters and their selected levels were used for the analysis of the wear rate and coefficient of friction for ZA-27 nanocomposites and hybrid nanocomposites as shown in chapter 3. Analysis of variance (ANOVA) was performed to determine the most significant parameters which influenced the tribological behavior of ZA-27 nanocomposites at various operating conditions. Prediction models were generated for wear rate and coefficient of friction for ZA-27 nanocomposites and hybrid nanocomposite using RSM and the adequacies of these models were expressed in terms of R-square values. Figure 6.1 shows the schematic diagram of pin on disc testing machine.

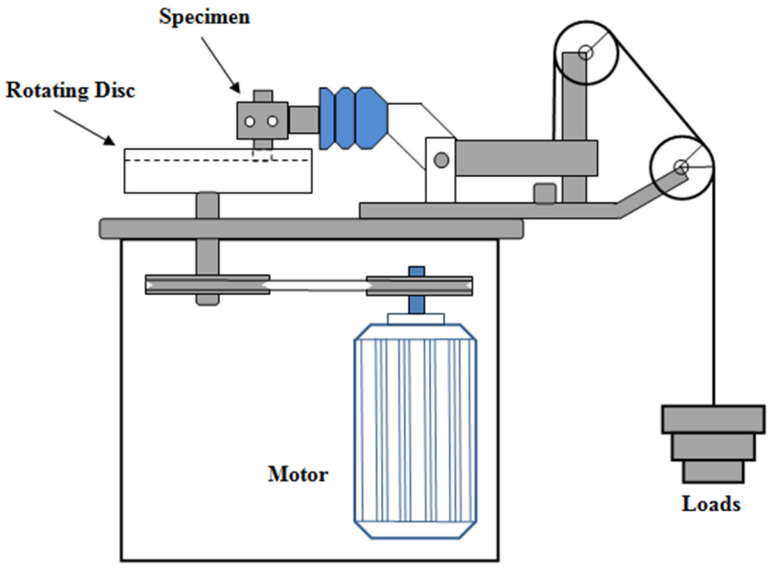

Figure 6.1 Schematic diagram of pin on disc testing machine

6.4. Results and analysis

6.4.1. ZA-27 alloy

The dry sliding wear behavior of the matrix material have been tested according to the experimental plan with sliding speed, sliding distance and applied load acting as influencing factors on the responses. The wear rate and coefficient of friction of ZA-27 alloy samples was taken from the average of three replicates in each case. Table 6.1 shows the experimental plan and results of ZA-27 alloy in the coded form.

Table 6.1 Experimental plan and results of ZA-27 alloy

Expt No	Distance (m)	Load (N)	Speed (m/s)	WR x 10^{-6} (mm^3/m)	COF
1	1000	90	3	9.122	0.38
2	1000	90	1	5.077	0.56
3	2000	60	2	6.21	0.58
4	1000	30	3	4.632	0.56
5	2000	60	3	7.12	0.46

6	3000	90	3	8.201	0.36
7	2000	60	2	5.926	0.56
8	3000	90	1	5.32	0.54
9	1000	30	1	3.823	0.75
10	2000	60	2	5.542	0.56
11	3000	60	2	5.023	0.48
12	2000	60	2	6.048	0.54
13	1000	60	2	6.493	0.56
14	3000	30	1	2.056	0.72
15	2000	60	2	5.593	0.51
16	2000	60	1	3.934	0.68
17	2000	90	2	7.332	0.41
18	2000	30	2	3.58	0.64
19	2000	60	2	6.017	0.47
20	3000	30	3	2.42	0.51

a) ANOVA analysis of wear rate

Table 6.2 shows the ANOVA analysis for the wear rate of ZA-27 alloy. The most significant parameters which affect the wear rate of the ZA-27 alloy were applied load and sliding speed. The interaction between the load and speed will also influence the wear rate of ZA-27 alloy. In the ANOVA table, column 7 shows the percentage contribution of the individual parameters and their interactions on the wear rate of the ZA-27 alloy.

Table 6.2 ANOVA results for wear rate of ZA-27 alloy

Source	Sum of Squares	DF	Mean Square	F Value	p-value Prob > F	Percentage contribution
Model	59.09713	8	7.38714	79.33748	< 0.0001	98.2
A-Distance	3.754013	1	3.75401	40.31788	< 0.0001	6.4
B-Load	34.37687	1	34.3768	369.2056	< 0.0001	57.8
C-Speed	12.73512	1	12.7351	136.7745	< 0.0001	22.1
AB	1.362075	1	1.36207	14.62861	0.0028	2.5
AC	0.32361	1	0.32361	3.475554	0.0892	0.6
BC	4.137126	1	4.13712	44.4325	< 0.0001	6.9

B^2	0.572742	1	0.57274	6.151217	0.0306	1.2
C^2	0.396634	1	0.39663	4.259822	0.0634	0.7
Residual	1.024214	11	0.09311			1.8
Cor Total	60.12134	19				100

A prediction model has been developed for wear rate of ZA-27 alloy using ANOVA and given by equation (6.2) in coded form. The R-squared, adjusted R-squared and predicted R-squared values were 98.29 %, 97.05 % and 90.45 % respectively for this model.

$$WR = +5.86 - 0.61 * A + 1.85 * B + 1.13 * C + 0.41 * A * B - 0.20 * A * C + 0.72 * B * C - 0.42 * B^2 - 0.35 * C^2. \quad (6.2)$$

Influence of process parameters on the wear rate of ZA-27 alloy are shown in figure 6.2 (a) to (e). It was observed from Figure 6.2 (a) that the wear rate of ZA-27 alloy decreases as the sliding distance increases. The asperities of pin and the disc surface which were in contact are subjected to relative motion under the influence of applied load. The asperities of the counter surface can be considered sharper and harder during initial wear stage. The initial stage of wear consists of fragmentation of asperities and removal of material due to cutting of hard asperities into the softer pin surface. Since the sliding distance increases the temperature of the contact surfaces of pin and disc increases, which leads to softening of materials and formation of tribolayer between the pin and disc. This tribolayer reduces the wear rate of ZA-27 alloy when the sliding distance increases with respect to the applied load and sliding speed. Figure 6.2 (b) shows that the wear rate of ZA-27 alloy increases with the increase in the applied load. As the applied load increases the pin and disc surfaces were not perfectly smooth and contain large number of asperities which will remove more material from the pin and induce micro ploughing. The depth of penetration of harder asperities of disc to the softer pin material increases as the applied load increases. The contact becomes intimate with increased normal load and more frictional heat was accumulated at the interface, which results in softening of the pin surface. It becomes easier for the asperities in the counter surface to penetrate into the surface of the softened pin causing increased wear rate.

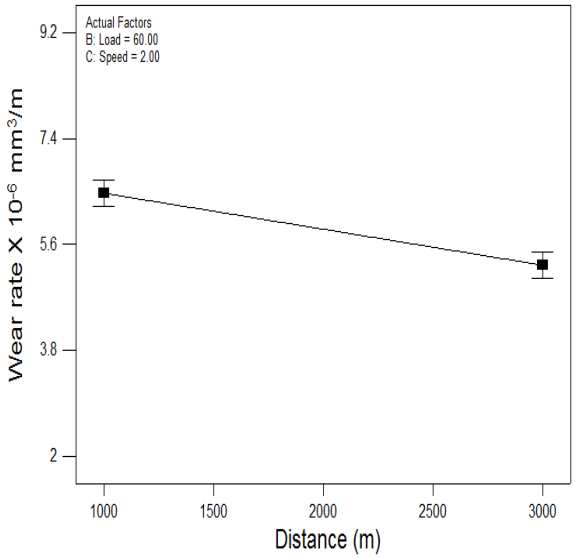

a) Distance

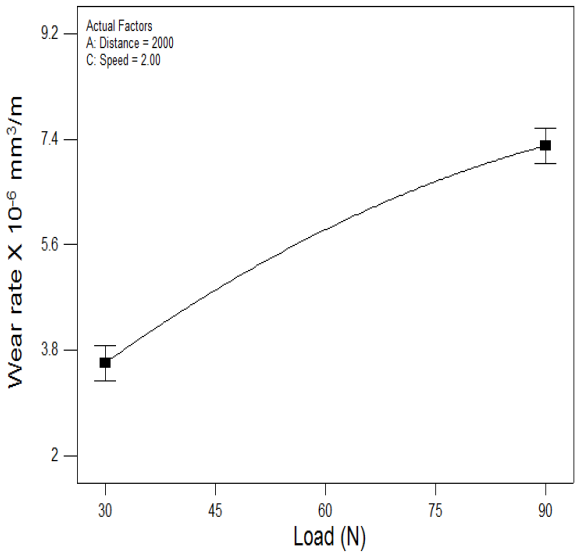

b) Load

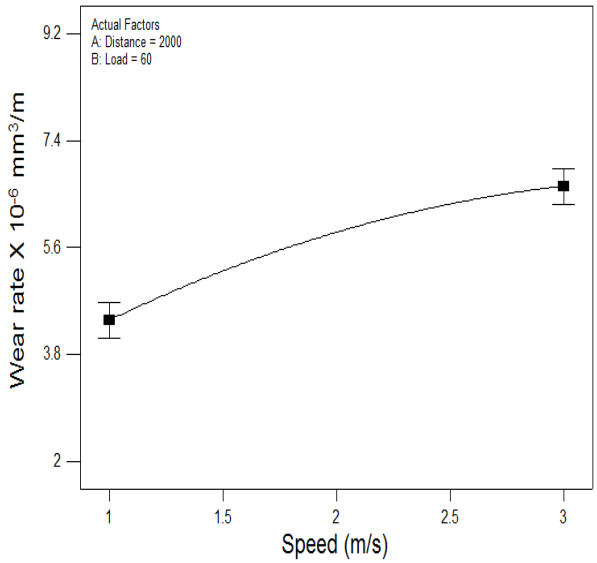

c) Speed

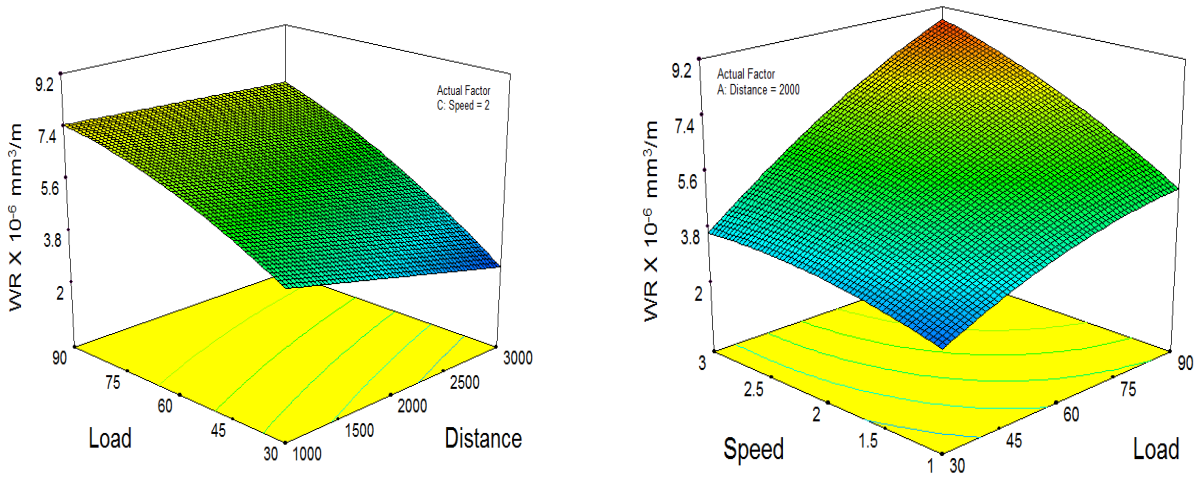

d) Load Vs Distance

e) Speed Vs Load

Figure 6.2.Effect of process parameters on wear rate of ZA-27 alloy

From Figure 6.2 (c) it was observed that the wear rate of ZA-27 alloy increases with increase in the sliding speed. Since the sliding speed increases the friction heat generated between the pin and disc surfaces will strongly influence the wear rate of the matrix material. The penetration of the hard asperities of the counter surface into the pin surface increases with the increased frictional heat. The pin was subjected to less frictional heat at low speed and the penetration of the counter surface was less, which leads to lower wear rate. As the sliding speed increases, the pin was subjected to higher frictional heat and the penetration of the counter surface becomes more, which leads to higher wear rate. The interaction effects between the load-distance and speed-load were influencing the wear rate of the ZA-27 alloy was shown in Figure 6.2 (d) and (e).

b) Model validation for wear rate

Confirmation tests have been conducted to validate the derived model for the wear rate from quadratic regression fit. The parameters and levels must lie within the ranges for which equation was derived to conduct confirmation experiments. The confirmation test parameters for wear rate of ZA-27 alloy were shown in Table 6.3. Confirmation tests have been carried out and then the comparison between experimental and predicted wear rate of ZA-27 alloy shows an error of 2.2 %.

Table 6.3 Test parameters employed for model validation for wear rate

Expt No	Speed (m/s)	Distance (m)	Load (N)	Experimental Wear rate(x 10^{-6} mm^3/m)	Predicted Wear rate (x 10^{-6} mm^3/m)	Error %
1	1	3000	30	2.056	2.010	2.2

c) ANOVA analysis of COF

Table 6.4 shows the ANOVA analysis for coefficient of friction of ZA-27 alloy. The applied load, sliding speed and sliding distance were the control factors which influences the COF of the ZA-27 alloy. The most significant parameters which affect the COF of the ZA-27 alloy were sliding speed and applied load. In the ANOVA table 6.4, column 7 shows the percentage contribution of the individual process parameters on the COF of ZA-27 alloy.

Table 6.4 ANOVA results for COF of ZA-27 alloy

Source	Sum of Squares	DF	Mean Square	F Value	p-value Prob > F	Percentage contribution
Model	0.18653	3	0.062177	67.56038	< 0.0001	93
A-Distance	0.004	1	0.004	4.34635	0.0535	2
B-Load	0.08649	1	0.08649	93.97895	< 0.0001	43
C-Speed	0.09604	1	0.09604	104.3559	< 0.0001	48
Residual	0.01472	16	0.00092			7
Cor Total	0.20125	19				100

A prediction model has been developed for COF of ZA-27 alloy using ANOVA and given by equation (6.3) in coded form. The R-squared, adjusted R-squared and predicted R-squared values are 92.68 %, 91.31 % and 90.37 % respectively for this model.

$$COF = + 0.54 - 0.020 * A - 0.093 * B - 0.098 * C. \quad (6.3)$$

The effects of individual process parameters on the coefficient of friction of ZA-27 alloy are shown in Figure 6.3 (a) to (c). It is evident from Figure 6.3 (a) that the COF decreases as the sliding distance increases. When the siding distance increases the surface temperatures of the pin and disc increase, due to which a tribolayer was formed between the pin and the disc surfaces. As the sliding distance increases between the contact surfaces of the counter disc and pin, a stable tribolayer exists which reduces the friction coefficient of ZA-27 alloy.

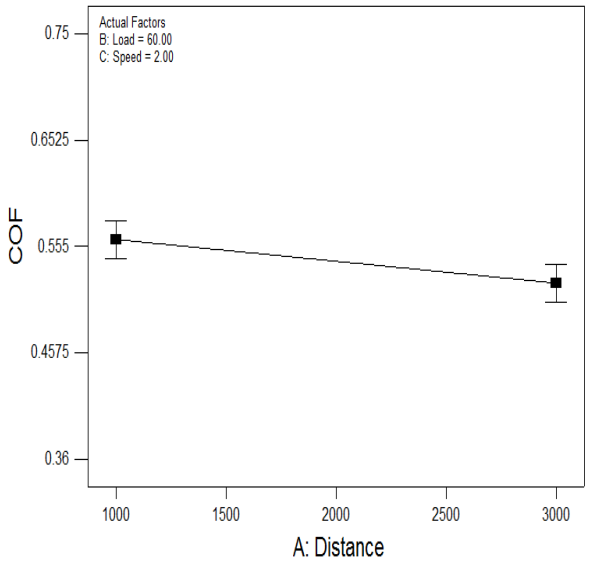

a) Distance

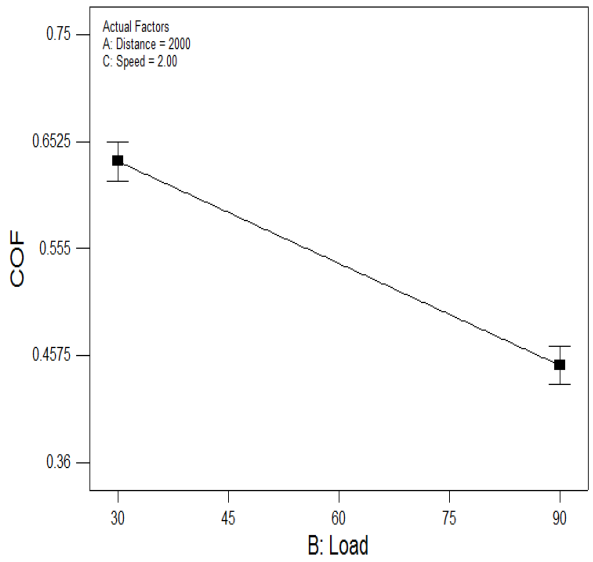

b) Load

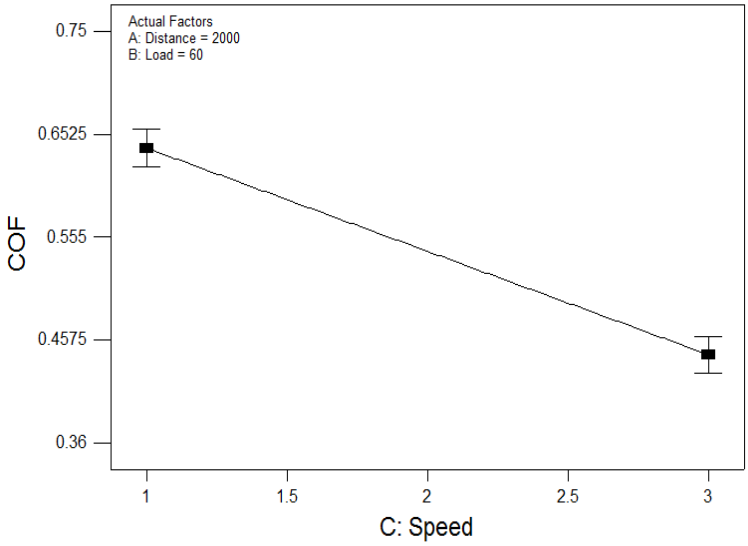

c) Speed

Figure 6.3.Effect of process parameters on coefficient of friction of ZA-27 alloy

From Figures 6.3 (b) and (c) it was observed that the coefficient of friction of the matrix material decreases as the load and speed increases. As the applied load increases the pin surface becoming softening will reduces the COF of the alloy. When the sliding speed increases less amount of contact between the pin and disc surfaces is taking place because of which coefficient of friction of ZA-27 alloy decreases.

d) Model validation for COF

Confirmation test parameters for COF of ZA-27 alloy were shown in Table 6.5, comparison between experimental and predicted coefficient of friction of ZA-27 alloy shows an error of 4.5 %.

Table 6.5 Test parameters employed for model validation for COF

Expt No	Speed (m/s)	Distance (m)	Load (N)	Experimental COF	Predicted COF	Error %
1	3	1650	90	0.375	0.358	4.5

6.4.2. ZA-27 /MoS_2 micro and nanocomposites

MoS_2 micro and nanoparticles reinforced ZA-27 composites with different combinations of parameters for dry sliding wear performance was shown in Table 6.6

Table 6.6 Experimental plan and results of ZA-27/MoS_2 micro and nanocomposites

Expt No	Speed (m/s)	Distance (m)	Load (N)	Filler (Wt %)	MoS_2 (μm)		MoS_2 (nm)	
					WR x 10^{-6} (mm^3/m)	COF	WR x 10^{-6} (mm^3/m)	COF
1	1	1000	90	0.5	3.622	0.35	2.536	0.23
2	1	1000	90	1.5	2.073	0.28	0.957	0.19
3	1	2000	60	1	1.993	0.37	1.777	0.25
4	2	2000	90	1	3.016	0.31	2.908	0.22
5	1	1000	30	0.5	2.602	0.41	2.148	0.29
6	3	2000	60	1	3.298	0.32	2.485	0.20
7	2	2000	60	1	2.671	0.36	1.956	0.24
8	3	1000	90	1.5	4.428	0.26	2.131	0.17
9	3	1000	30	1.5	3.132	0.31	1.827	0.22
10	3	3000	30	1.5	1.288	0.25	0.754	0.19
11	2	2000	60	1	3.078	0.34	2.972	0.21
12	1	3000	30	0.5	2.442	0.39	2.453	0.33
13	3	3000	90	1.5	1.677	0.23	1.218	0.14
14	2	3000	60	1	2.463	0.35	2.15	0.26
15	1	1000	30	1.5	1.641	0.36	0.478	0.28
16	2	2000	60	0.5	4.444	0.38	3.899	0.30
17	3	1000	90	0.5	5.541	0.34	4.423	0.23
18	1	3000	90	0.5	3.913	0.43	3.207	0.31
19	1	3000	30	1.5	0.828	0.31	0.536	0.22
20	3	3000	90	0.5	4.052	0.38	3.179	0.26
21	2	2000	60	1	3.141	0.35	2.845	0.23

22	2	2000	60	1.5	2.646	0.29	1.903	0.17
23	2	2000	60	1	3.162	0.34	2.94	0.22
24	2	2000	60	1	3.058	0.33	2.76	0.21
25	3	3000	30	0.5	2.088	0.39	1.782	0.31
26	3	1000	30	0.5	2.643	0.41	2.494	0.33
27	1	3000	90	1.5	1.159	0.29	0.833	0.18
28	2	2000	60	1	2.995	0.35	2.94	0.23
29	2	1000	60	1	2.985	0.34	2.985	0.22
30	2	2000	30	1	2.484	0.36	1.999	0.24

a) ANOVA analysis of Wear rate

Table 6.7 and 6.8 shows the result of ANOVA analysis for ZA-27/MoS_2 micro and nanocomposites which clearly indicates that the influence of the various parameters and interactions of the design model were about 95.2% and 94.5% confidence level. The control factors which influence the wear rate behavior of ZA-27/MoS_2 micro and nanocomposites were reinforcement content, applied load, sliding distance and sliding speed. Among all, the reinforcement content and applied load were the most significant factors to influence the wear rate of ZA-27/MoS_2 micro and nanocomposites.

Table 6.7 ANOVA results for wear rate of ZA-27/MoS_2 microcomposites

Source	Sum of Squares	DF	Mean Square	F Value	p-value Prob > F	Percentage contribution
Model	29.32655	12	2.44388	27.99431	< 0.0001	95.2
A-Speed	3.444438	1	3.444438	39.45557	< 0.0001	11.2
B-Distance	4.260281	1	4.260281	48.80095	< 0.0001	13.9
C-Load	5.931716	1	5.931716	67.94702	< 0.0001	19.2
D-Reinforcement	8.645868	1	8.645868	99.03727	< 0.0001	28.1
AB	1.589491	1	1.589491	18.2074	0.0005	5.2
AC	0.677741	1	0.677741	7.763428	0.0127	2.2
AD	0.592515	1	0.592515	6.787181	0.0185	1.9
BD	1.214955	1	1.214955	13.91715	0.0017	3.9
CD	1.503689	1	1.503689	17.22456	0.0007	4.9
A^2	0.502294	1	0.502294	5.753712	0.0282	1.6
B^2	0.332314	1	0.332314	3.80661	0.0677	1.0
D^2	0.650915	1	0.650915	7.456141	0.0142	2.1

Residual	1.484085	17	0.087299			4.8
Cor Total	30.81064	29				100

Table 6.8 ANOVA results for wear rate of ZA-27/MoS_2 nanocomposites

Source	Sum of Squares	DF	Mean Square	F Value	p-value Prob > F	Percentage contribution
Model	25.67958	12	2.139965	24.18918	< 0.0001	94.5
A-Speed	1.714952	1	1.714952	19.38503	0.0004	7.4
B-Distance	0.913501	1	0.913501	10.3258	0.0051	4.5
C-Load	2.80766	1	2.80766	31.7365	< 0.0001	11.3
D-Reinforcement	13.64509	1	13.64509	154.2378	< 0.0001	51.3
AB	1.359556	1	1.359556	15.3678	0.0011	5.9
AC	0.247009	1	0.247009	2.792076	0.113	1.5
AD	0.198025	1	0.198025	2.238384	0.153	1.2
BD	0.099225	1	0.099225	1.121594	0.3044	0.8
CD	0.467856	1	0.467856	5.288429	0.0344	2.1
A^2	1.113553	1	1.113553	12.5871	0.0025	5.6
C^2	0.262028	1	0.262028	2.96185	0.1034	1.8
D^2	0.058604	1	0.058604	0.662429	0.427	0.5
Residual	1.503954	17	0.088468			6.1
Cor Total	27.18353	29				100

A prediction model has been developed for wear rate of the ZA-27/MoS_2 micro and nanocomposites using ANOVA and given by equation (6.4) and (6.5) in coded form. The R-squared, adjusted R-squared and predicted R-squared values for microcomposites were 95.18 %, 91.78 % and 80.93 %, for nanocomposites were 94.46 %, 90.56 % and 82.55 % respectively for this model.

WR = +2.99 + 0.44 * A - 0.49 * B + 0.57 * C - 0.69 * D - 0.32 * A * B + 0.21 * A * C+0.19 * A * D - 0.28 * B * D – 0.31 * C * D - 0.42 * A^2 -0.34 * B^2 + 0.48 * D^2. (6.4)

WR = +2.71 + 0.31 * A - 0.23 * B + 0.39 * C - 0.87 * D - 0.29 * A * B + 0.12 * A * C + 0.11* A * D- 0.079 * B * D - 0.17 * C * D - 0.63 * A^2 - 0.30 * C^2 + 0.14 * D^2. (6.5)

The effects of various parameters on the wear rate of ZA-27/ MoS_2 micro/nanocomposites were shown in Figures 6.4 (a-f) and 6.5 (a-f). As the reinforcement of the particles and sliding distance increase, the wear resistance of the micro and nanocomposites increases as shown in Figures 6.4 (b & d) and 6.5 (b & d). The reinforcement particles stick to the counter surface at higher sliding distance because the temperature of the pin and disc surfaces increase as the sliding distance increases. Due to the increase in the surface temperatures the tribolayer formation was generated between the pin and disc surfaces which increase the wear resistance behavior of the micro and nanocomposites.

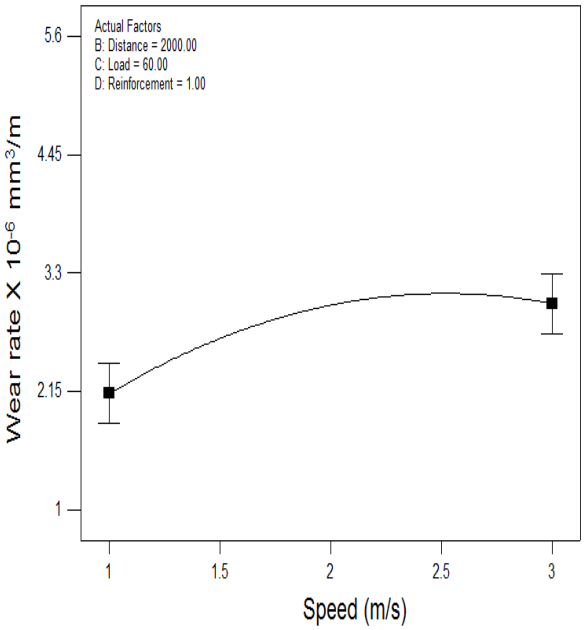

a) Speed

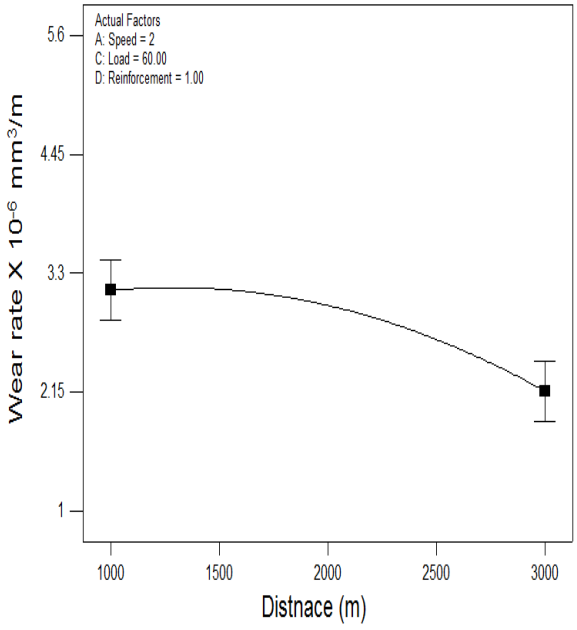

b) Distance

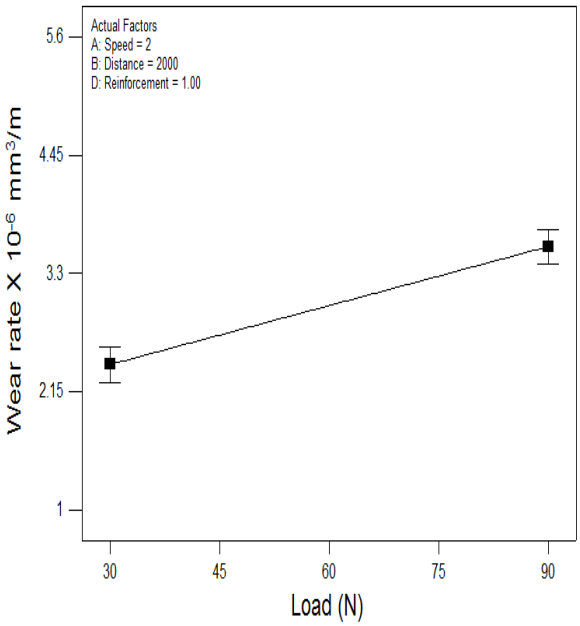

c) Load

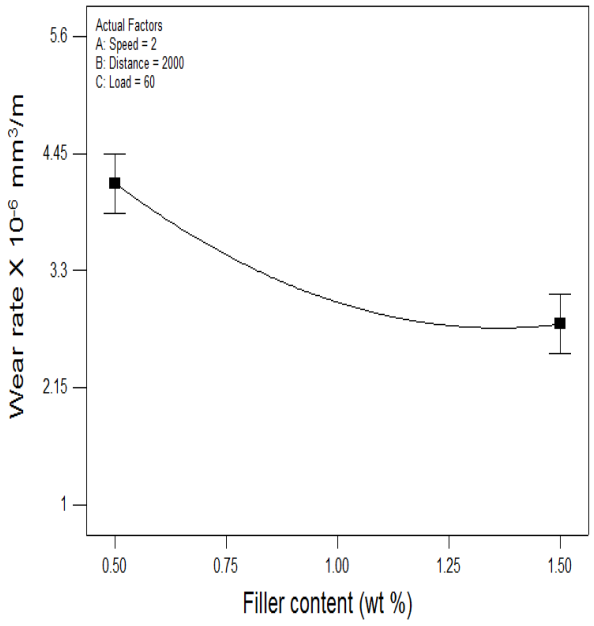

d) Filler content

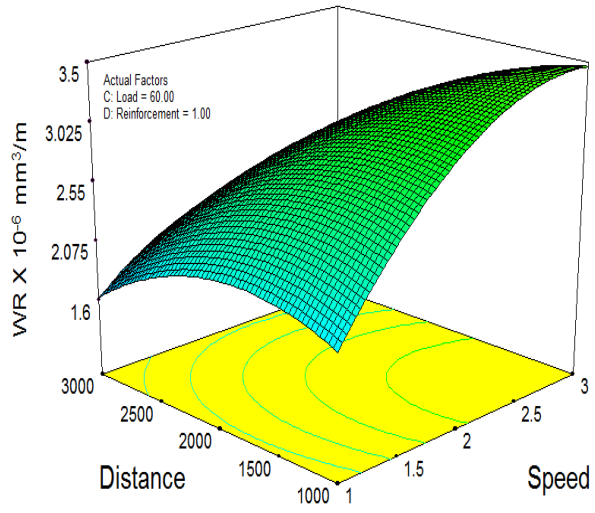

e) Distance Vs Speed

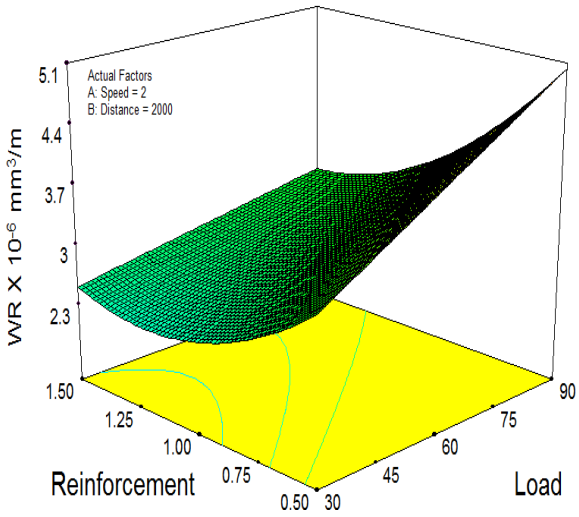

f) Reinfrocemetn Vs Load

Figure 6.4.Effect of process parameters on wear rate of ZA-27/MoS_2 microcomposites

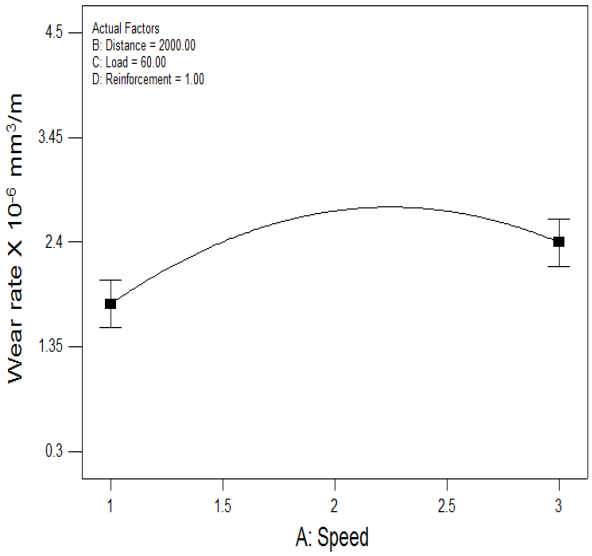

a) Speed

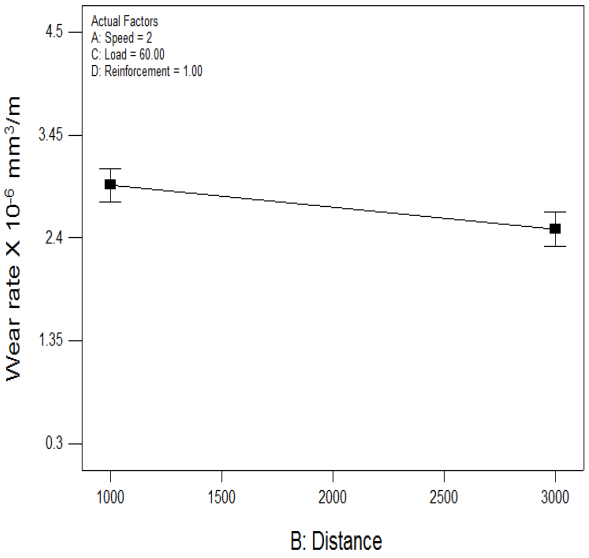

b) Distance

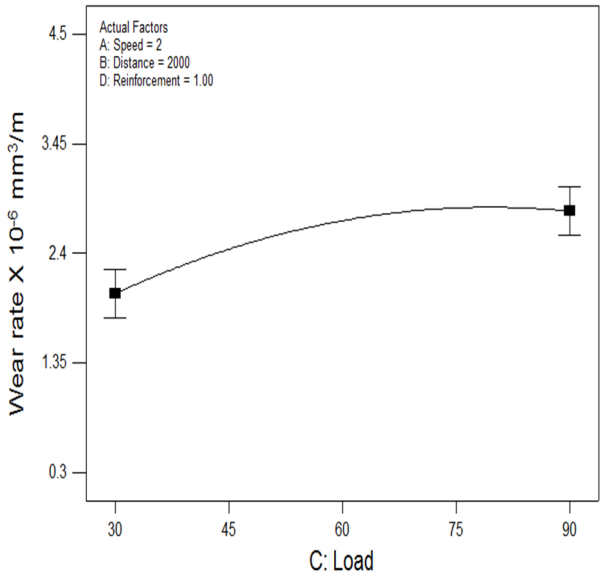

c) Load

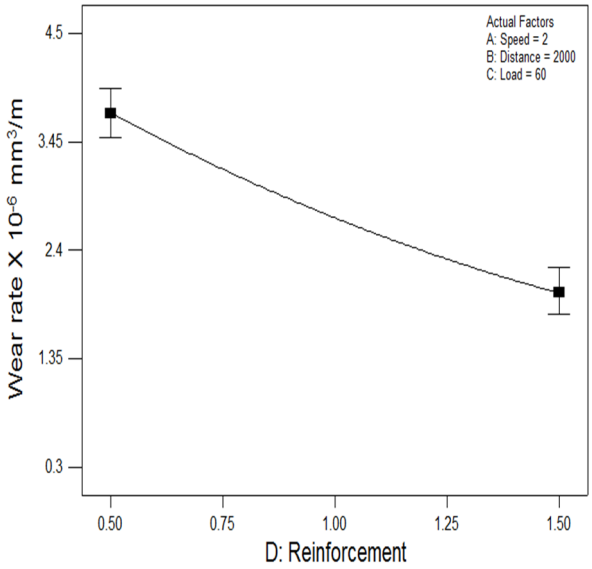

d) Reinforcement

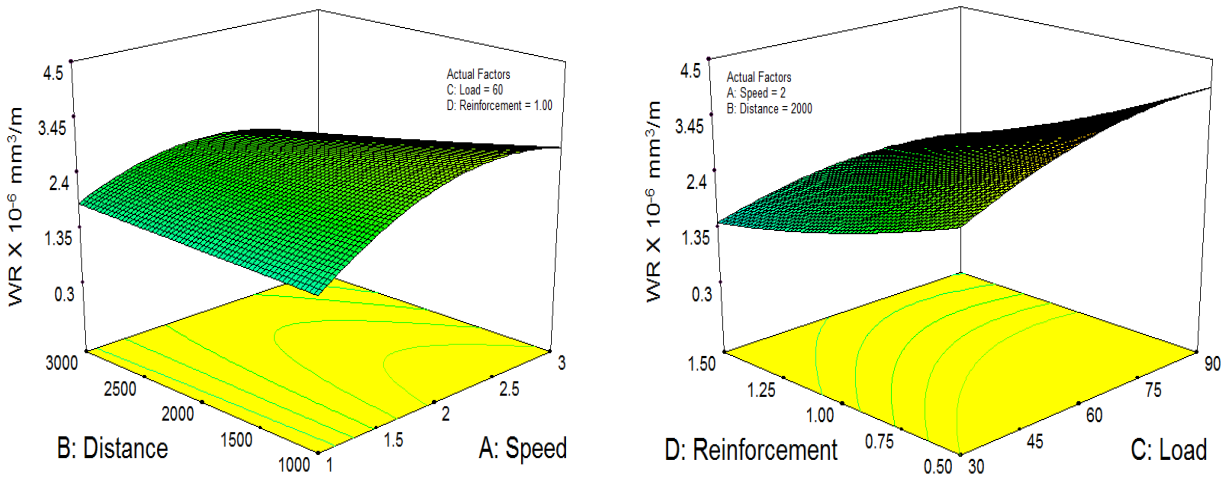

e) Distance Vs Speed f) Reinforcement Vs Load

Figure 6.5.Effect of process parameters on wear rate of ZA-27/MoS_2 nanocomposites

Figure 6.5 (a) shows that the less wear rate is observed at the lower speed because the pin is subjected to less frictional heat. The tribolayer is formed in between the pin and disc surfaces due to the increase in the sliding speed which leads to reduce the wear rate of the nanocomposites. As the applied load increases the wear rate increases because the contact between the pin and disc surfaces is close to each other and generates more friction which leads to an increase in the wear rate of ZA-27/MoS_2 nanocomposites as shown in Figure 6.5(c). The wear rate of the nanocomposites reduces more when the reinforcement content of nanoparticles increases in the ZA-27 alloy as shown in the Figure 6.5 (d). As the MoS_2 nanoparticles acts as a solid lubricant phase will enhance the wear resistance properties of the nanocomposites. The increase in the reinforcement content of the nanoparticles will produces the stable tribolayer in between the pin and disc surfaces which lead to reduces more wear rate of ZA-27/MoS_2 nanocomposites. The interaction effects between the distance-speed and reinforcement-load on the wear rate of ZA-27/MoS_2 nanocomposites are also shown in Figures 6.5 (e) and (f).

b) Model validation for wear rate

Confirmation test parameters for wear rate of ZA-27/MoS_2 micro/nanocomposites are shown in Table 6.9 and 6.10. Confirmation tests have been carried out and then the comparison between experimental and predicted wear rate of ZA-27/MoS_2 micro/nanocomposites shows an error of 1.4 % and 1.1%.

Table 6.9 Model validation for wear rate of microcomposites

Expt No	Speed (m/s)	Distance (m)	Load (N)	Filler (Wt %)	Experimental Wear rate (x 10^{-6} mm^3/m)	Predicted Wear rate (x 10^{-6} mm^3/m)	Error %
1	1	3000	30	1.5	0.882	0.870	1.4

Table 6.10 Model validation for wear rate of nanocomposites

Expt No	Speed (m/s)	Distance (m)	Load (N)	Filler (Wt %)	Experimental Wear rate (x 10^{-6} mm^3/m)	Predicted Wear rate (x 10^{-6} mm^3/m)	Error %
1	1	2800	30	1.5	0.532	0.527	1.1

c) ANOVA analysis of COF

Table 6.11 and 6.12 shows the ANOVA analysis for COF of ZA-27/MoS_2 micro and nanocomposites. The most significant parameters influencing COF of micro and nanocomposites are reinforcement content. From the ANOVA table, column 7 shows the percentage contribution of the individual parameters and their interactions.

Table 6.11 ANOVA results for COF of ZA-27/MoS_2 microcomposites

Source	Sum of Squares	DF	Mean Square	F Value	p-value Prob > F	Percentage contribution
Model	0.064365	10	0.006437	46.65238	< 0.0001	96
A-Speed	0.005	1	0.005	36.24033	< 0.0001	7.5
B-Distance	8.89E-05	1	8.89E-05	0.644273	0.4321	0.2
C-Load	0.005689	1	0.005689	41.23344	< 0.0001	8.5
D-Reinforcement	0.045	1	0.045	326.163	< 0.0001	67.1
AB	0.000506	1	0.000506	3.669333	0.0706	0.8
AC	5.63E-05	1	5.63E-05	0.407704	0.5308	0.08
AD	0.001056	1	0.001056	7.65577	0.0123	1.57
BC	0.003906	1	0.003906	28.31276	< 0.0001	5.8
BD	0.002756	1	0.002756	19.97748	0.0003	4.1
CD	0.000306	1	0.000306	2.21972	0.1527	0.45
Residual	0.002621	19	0.000138			3.9
Cor Total	0.066987	29				100

Table 6.12 ANOVA results for COF of ZA-27/MoS_2 nanocomposites

Source	Sum of Squares	DF	Mean Square	F Value	p-value Prob > F	Percentage contribution
Model	0.064159	9	0.007129	51.14566	< 0.0001	96
A-Speed	0.004356	1	0.004356	31.24907	< 0.0001	6.5
B-Distance	0.0002	1	0.0002	1.434906	0.245	0.3
C-Load	0.0098	1	0.0098	70.3104	< 0.0001	14.6
D-Reinforcement	0.043022	1	0.043022	308.6642	< 0.0001	64.3
AB	0.000756	1	0.000756	5.425739	0.0304	1.13
AD	0.000306	1	0.000306	2.1972	0.1538	0.45
BC	0.002256	1	0.002256	16.18753	0.0007	3.4
BD	0.003306	1	0.003306	23.72079	< 0.0001	4.93
CD	0.000156	1	0.000156	1.12102	0.3023	0.23
Residual	0.002788	20	0.000139			4.16
Cor Total	0.066947	29				100

A prediction model has been developed for COF of ZA-27/MoS_2 micro and nanocomposites using ANOVA and is given by equation (6.6) and (6.7) in coded form. The R-squared, adjusted R-squared and predicted R-squared values for microcomposites were 96.09 %, 94.03 % and 83.76 %, for nanocomposites were 95.83 %, 93.96 % and 84.41 % respectively for this model.

COF = +0.34-0.017 * A-2.222E-003 * B-0.018 * C-0.050 * D-5.625E-003 * A * B-1.875E-003 * A * C- 8.125E-003 * A * D+0.016 * B * C-0.013* B * D-4.375E-003 * C * D (6.6)

COF = + 0.24-0.016*A+3.333E-003*B-0.0*C-0.049*D-6.875E-003*A*B-4.375E-0.03*A*D+0.012*B*C-0.014*B*D-3.125E-003*C*D (6.7)

The effects of individual process parameters on the coefficient of friction of ZA-27/MoS_2 micro and nanocomposites are shown in Figures 6.6 (a - f) and 6.7 (a - f). It is evident from the Figure 6.6 (a) and 6.7 (a) that the COF decreases as the sliding speed increases. As the sliding speed increases between the contact surfaces of the counter disc and specimen a stable tribolayer exists which reduces the friction coefficient of ZA-27/MoS_2 micro and nanocomposites. There is a negligible influence of COF of the micro and nanocomposites as the sliding distance increases as shown in Figures 6.6 (b) and 6.7 (b). Due to the increase in the surface temperature of

specimen the particles are transferred to the disc surfaces and form a stable compacted layer which slightly affects the COF behavior of the micro and nanocomposites. It was observed that the coefficient of friction of ZA-27/MoS_2 micro and nanocomposites decreases as the applied load increases as shown in figures 6.6 (c) and 6.7 (c). The contact surfaces of the disc and pin generate more frictional heat as the applied load increases which results in softening of the pin surface. As the applied load increases the frictional heat generated is more between the pin and disc surfaces which leads to the pin surface softening and the formation of oxide layer reduces the COF of ZA-27/MoS_2 micro and nanocomposites. If the reinforcement content increases in ZA-27/MoS_2 micro and nanocomposites there exists a thick tribolayer in between the disc and pin surfaces, due to which the coefficient of friction decreases compared to the applied load and sliding speed as shown in Figure 6.7 (d).

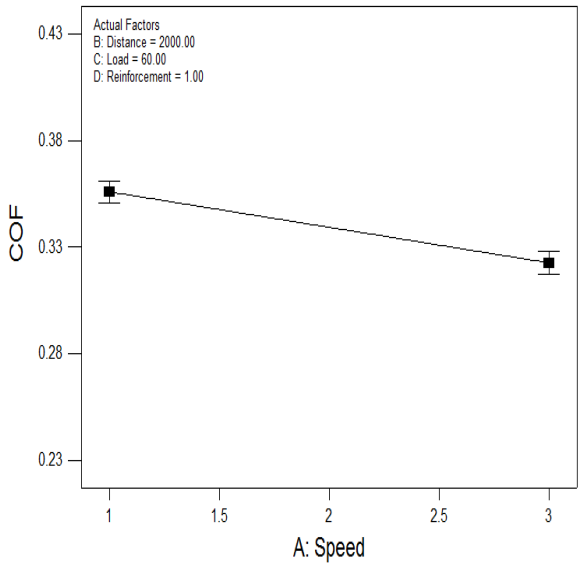

a) Speed

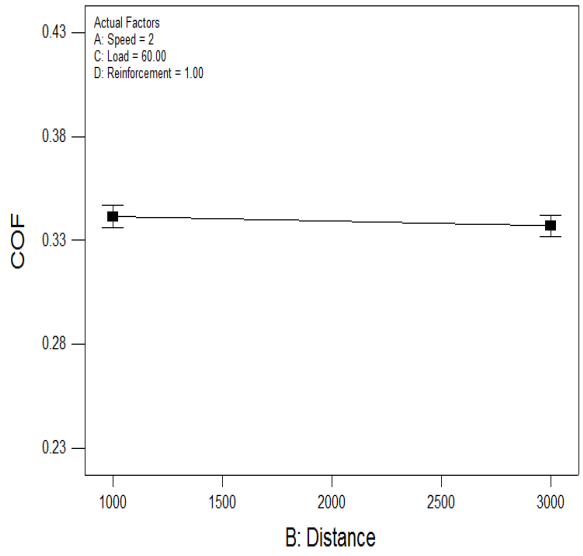

b) Distance

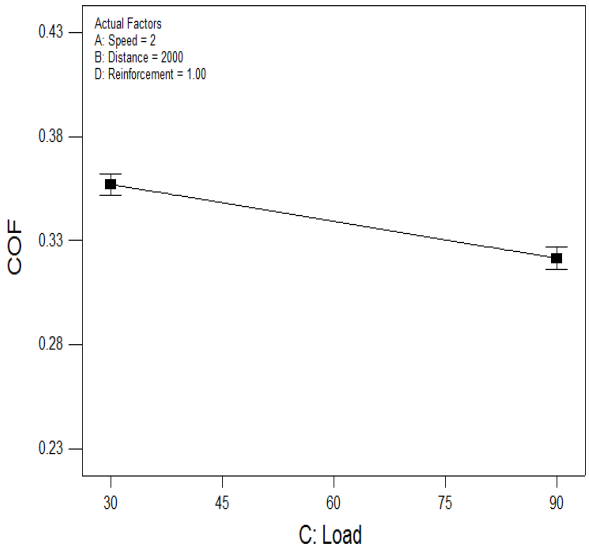

c) Load

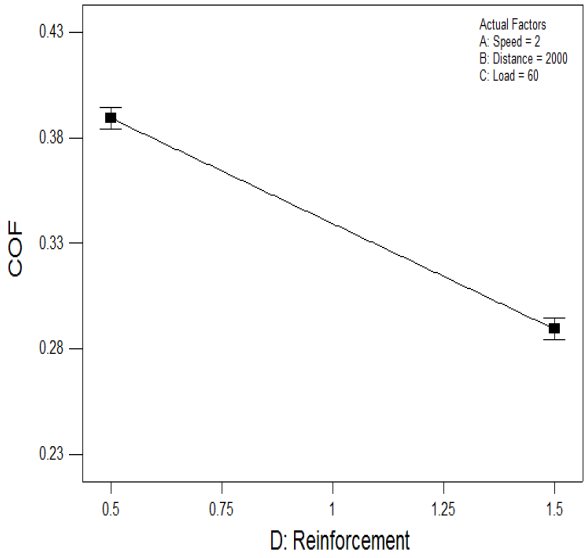

d) Reinforcement

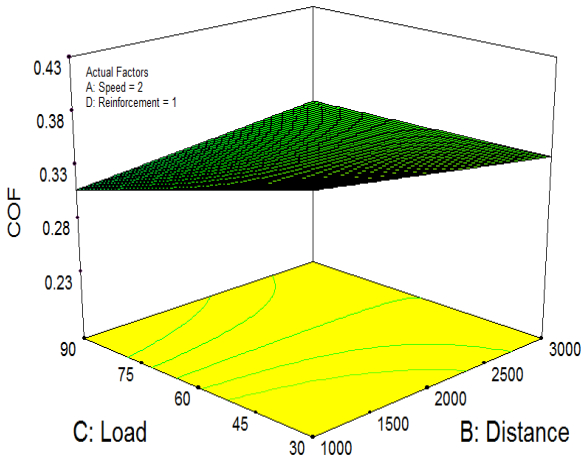

e) Load Vs Distance

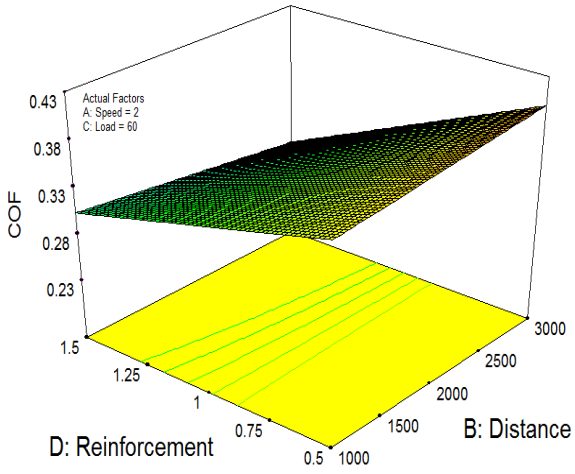

f) Reinforcement Vs Distance

Figure 6.6.Effect of process parameters on COF of ZA-27/MoS_2 microcomposites

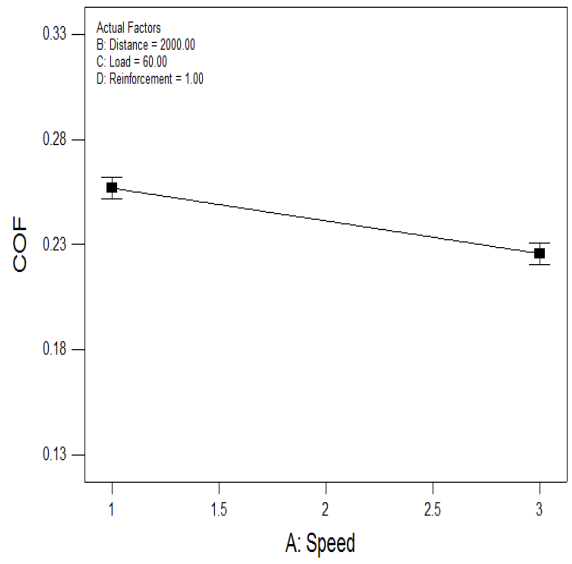

a) Speed

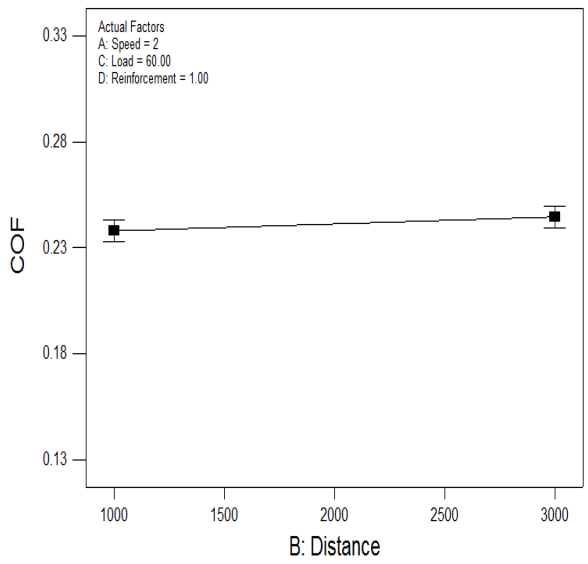

b) Distance

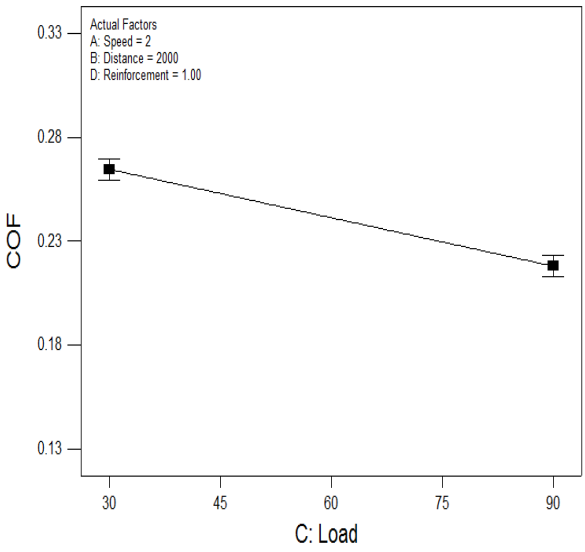

c) Load

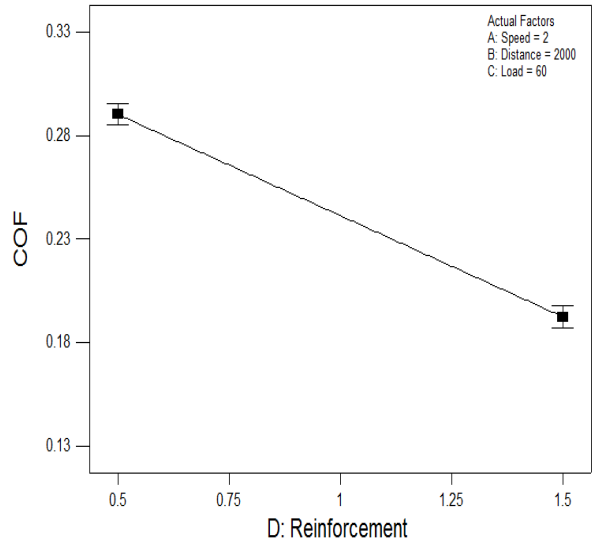

d) Reinforcement

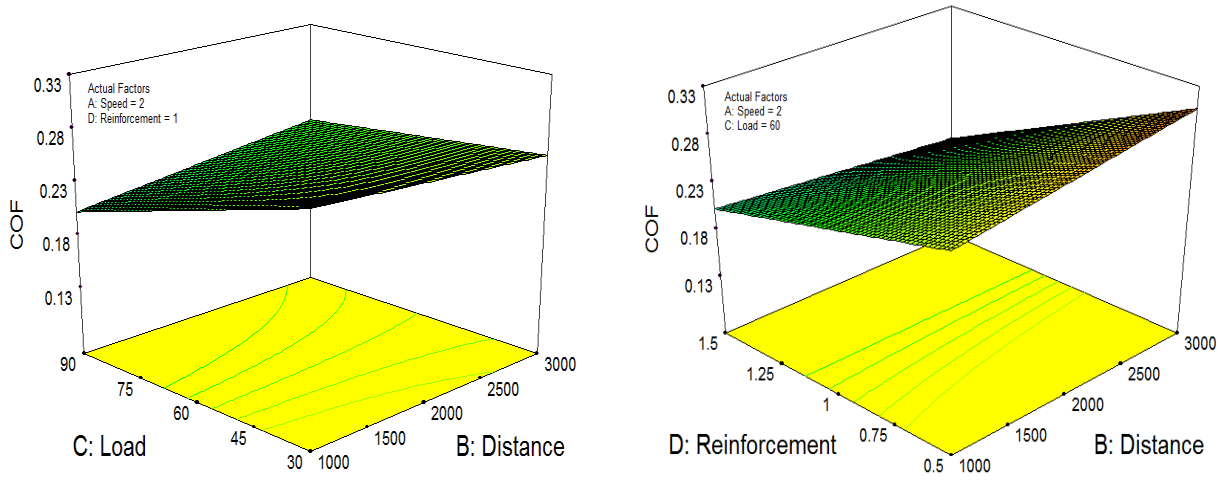

e) Load Vs Distance f) Reinforcement Vs Distance

Figure 6.7.Effect of process parameters on COF of ZA-27/MoS_2 nanocomposites

The MoS_2 nanoparticles reinforced ZA-27 nanocomposites are showing minimum friction coefficient as compared to the microcomposites. The interaction effects between the load-distance and reinforcement-distance on the COF of ZA-27/MoS_2 nanocomposites are also shown in Figure 6.7 (e) and (f).

d) Model validation for COF

Confirmation test parameters for COF of ZA-27/MoS_2 micro and nanocomposites are shown in Table 6.13 and 6.14. Confirmation tests have been carried out and then the comparison between experimental and predicted coefficient of friction of ZA-27/MoS_2 micro and nanocomposites shows an error of 1.7 % and 2.8 %.

Table 6.13 Model validation for COF of microcomposite

Expt No	Speed (m/s)	Distance (m)	Load (N)	Filler (Wt %)	Experimental COF	Predicted COF	Error %
1	3	3000	90	1.5	0.239	0.235	1.7

Table 6.14 Model validation for COF of nanocomposite

Expt No	Speed (m/s)	Distance (m)	Load (N)	Filler (Wt %)	Experimental COF	Predicted COF	Error %
1	3	3000	90	1.5	0.144	0.140	2.8

6.4.3. Worn surfaces of ZA-27/MoS_2 micro and nanocomposites

The microstructure of worn surfaces of the base alloy and ZA-27/MoS_2 micro and nanocomposites have been examined with the help of scanning electron microscope (SEM) and shown in the figures 6.8 (a-d) and 6.9 (a-d). From the microstructure of the base alloy, it is observed that deep and coarse grooves on the wear surfaces are formed due to the action of wear-hardened deposits on the pin surface as shown in Figure 6.8 (a). The reinforcement of MoS_2 micro and nanoparticles in ZA-27 alloy is expected to result in enhanced wear resistance because the MoS_2 acts as a solid lubricant phase. The SEM micrograph of 0.5 wt % MoS_2 micro and nanocomposite was shown in Figure 6.8 (b) and 6.9(b), it was observed that the grooves and ploughing marks reduce when compare to ZA-27 alloy. In accordance with this explanation, the sulphide composite materials exhibiting resistance to the formation of deep grooves and ploughing marks with increasing MoS_2 content as evident from Figure 6.8 (c) to (d) resulting in increased wear resistance of ZA-27 /MoS_2 micro and nanocomposites.

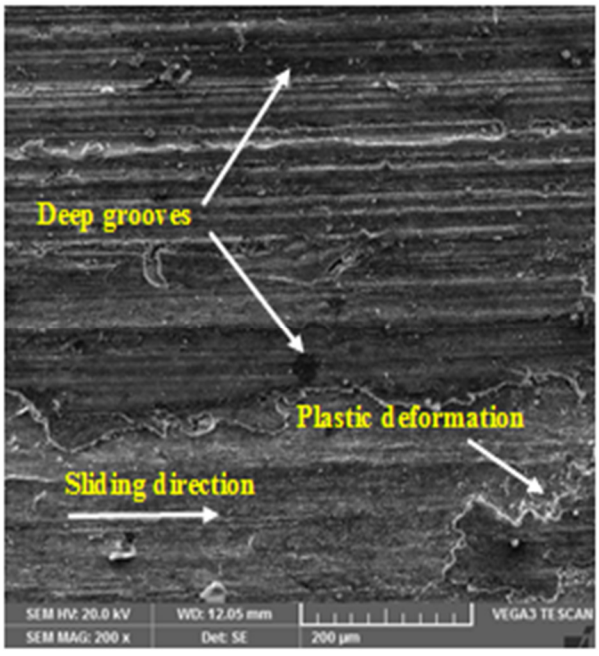

a) ZA-27 alloy

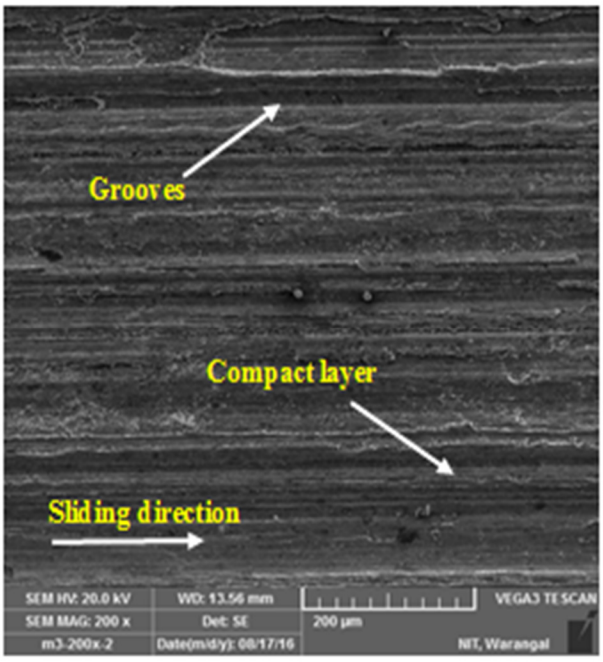

b) 0.5 wt % MoS_2

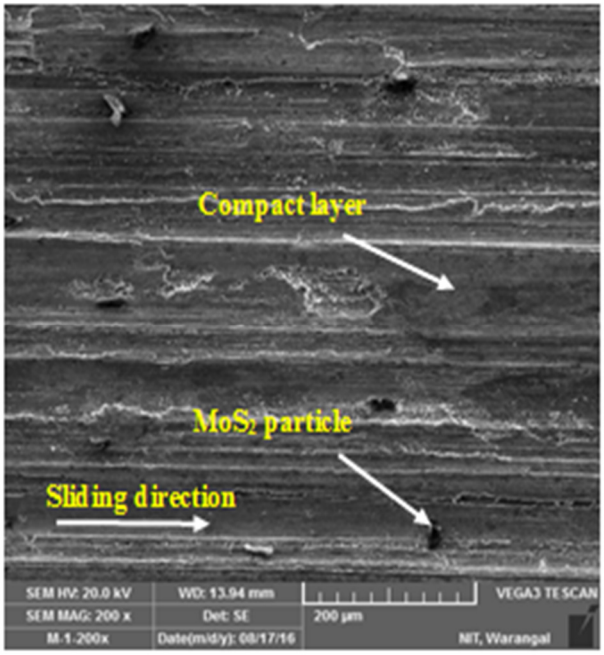

c) 1.0 wt % MoS_2

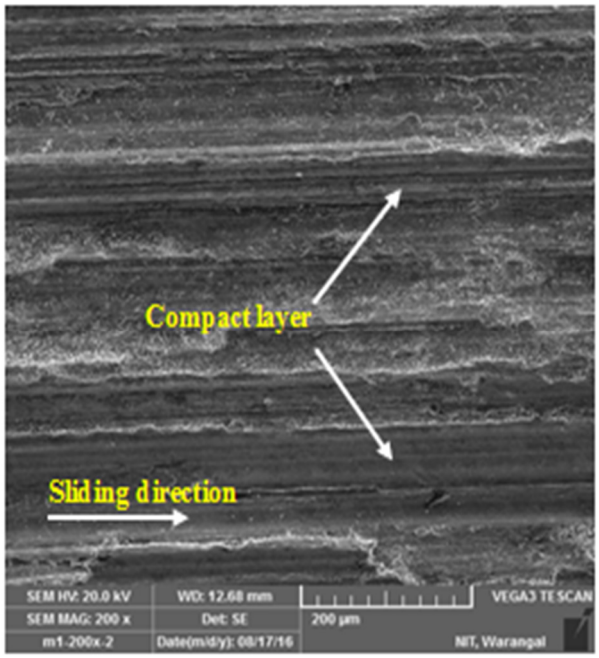

d) 1.5 wt % MoS_2

Figure 6.8.Microstructures of wear surfaces of ZA-27/MoS_2 microcomposites using SEM

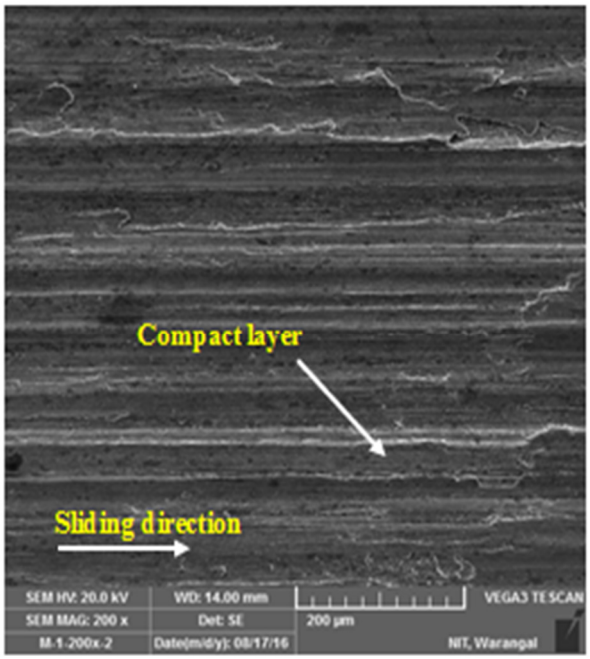

a) 0.5 wt % MoS_2

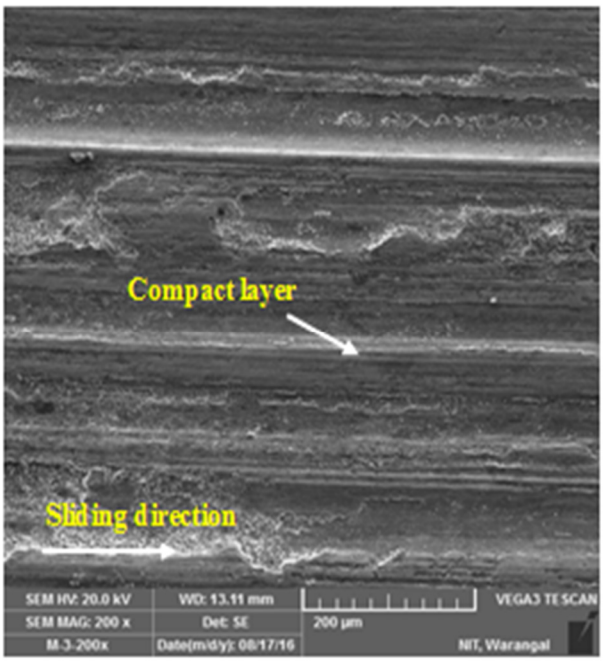

b) 1.0 wt % MoS_2

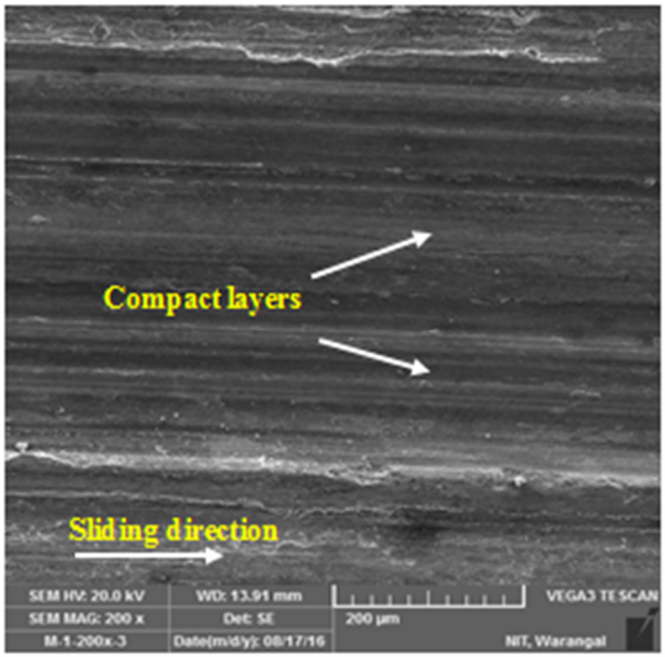

c) 1.5 wt % MoS_2

Figure 6.9.Microstructures of wear surfaces of ZA-27/MoS_2 nanocomposites using SEM

It was observed from the Figure 6.9 (b) that the reinforcement of nanoparticles were reduces the grooves and ploughing marks when compare to the micro composite. As the MoS_2 nanoparticles increasing in ZA-27 alloy the compact layers are formed in wear surfaces of the nanocomposites which increase the wear resistance. The ZA-27+1.5 wt % MoS_2 nanoparticles reinforced ZA-27 nanocomposites shows the smooth surface when compare to the other composition of ZA-27 micro and nano composites as shown in Figure 6.9 (c).

6.4.4 ZA-27/Al_2O_3 nanocomposites

The Al_2O_3 nanoparticles reinforced ZA-27 nanocomposites with different combinations of parameters for dry sliding wear performance is shown in Table 6.15

Table 6.15 Experimental plan and results of ZA-27/Al_2O_3 nanocomposites

Expt No	Speed (m/s)	Distance (m)	Load (N)	Filler (wt %)	WR x 10^{-6} (mm^3/m)	COF
1	1	1000	90	0.5	3.171	0.45
2	1	1000	90	1.5	1.834	0.35
3	1	2000	60	1	2.49	0.48

4	2	2000	90	1	3.196	0.41
5	1	1000	30	0.5	2.814	0.58
6	3	2000	60	1	3.468	0.43
7	2	2000	60	1	2.272	0.48
8	3	1000	90	1.5	2.992	0.28
9	3	1000	30	1.5	2.446	0.38
10	3	3000	30	1.5	0.895	0.41
11	2	2000	60	1	2.62	0.49
12	1	3000	30	0.5	2.618	0.56
13	3	3000	90	1.5	1.354	0.31
14	2	3000	60	1	2.145	0.46
15	1	1000	30	1.5	1.441	0.41
16	2	2000	60	0.5	4.347	0.53
17	3	1000	90	0.5	7.75	0.41
18	1	3000	90	0.5	3.948	0.43
19	1	3000	30	1.5	1.397	0.42
20	3	3000	90	0.5	4.235	0.36
21	2	2000	60	1	2.403	0.47
22	2	2000	60	1.5	2.555	0.42
23	2	2000	60	1	2.99	0.49
24	2	2000	60	1	3.055	0.48
25	3	3000	30	0.5	4.158	0.54
26	3	1000	30	0.5	7.12	0.58
27	1	3000	90	1.5	1.689	0.41
28	2	2000	60	1	2.914	0.49
29	2	1000	60	1	2.87	0.46
30	2	2000	30	1	2.229	0.47

a) ANOVA analysis of wear rate

Table 6.16 shows the ANOVA analysis for wear rate of ZA-27/Al_2O_3 nanocomposites. The reinforcement content and sliding speed are the most significant factors which influence the wear rate of ZA-27/ Al_2O_3 nanocomposites. In the ANOVA table, column 7 shows the percentage contribution of the individual parameters and their interactions.

Table 6.16 ANOVA results for wear rate of ZA-27/Al_2O_3 nanocomposites

Source	Sum of Squares	DF	Mean Square	F Value	p-value Prob > F	Percentage contribution
Model	59.47203	8	7.434004	34.94442	< 0.0001	93.5
A-Speed	9.412014	1	9.412014	44.2423	< 0.0001	14.7
B-Distance	5.554445	1	5.554445	26.10933	< 0.0001	8.7

C-Load	1.417367	1	1.417367	6.662501	0.0174	2.3
D-Reinforcement	30.83219	1	30.83219	144.9304	< 0.0001	48.3
AB	6.32271	1	6.32271	29.72065	< 0.0001	9.8
AD	5.506062	1	5.506062	25.8819	< 0.0001	8.7
BD	0.39627	1	0.39627	1.862716	0.1868	0.6
CD	0.030976	1	0.030976	0.145606	0.7066	0.5
Residual	4.467496	21	0.212738			6.8
Cor Total	63.93953	29				100

A prediction model has been developed for wear rate of ZA-27/ Al_2O_3 nanocomposites using ANOVA and is given by equation (6.8) in coded form. The R-squared, adjusted R-squared and predicted R-squared values are 93.01 %, 90.35 % and 83.43 % respectively for this model.

$$WR = +2.98 + 0.72 * A - 0.56 * B + 0.28 * C - 1.31 * D - 0.63 * A * B - 0.59 * A* D + 0.16 * B* D- 0.044 * C * D. \quad (6.8)$$

The influence of various control factors on the wear rate of ZA-27/ Al_2O_3 nanocomposites are shown in figures 6.10 (a) to (f). It was observed from figure 6.10 (a) that less wear rate is observed at lower speeds because the pin is subjected to less frictional heat and if speed is increases the frictional heat is more, which increases the wear rate of the nanocomposites. As the sliding distance increases the wear rate of the nanocomposites decreases because the temperature of the pin and disc surfaces increase. Due to the increase in the surface temperatures, the tribolayer formation is generated between the pin and disc surfaces which will reduce the wear rate behavior of the nanocomposites as shown in Figure 6.10 (b). The slight increase in the wear rate of the nanocomposites can be observed as the applied load increases as shown in figure 6.10 (c). The alumina nanoparticles are hard ceramic particles which can withstand higher loads in dry sliding wear characteristics. The wear rate of the nanocomposites is strongly influenced by the friction heat generated between the disc and pin surfaces as the applied load increases. As the applied load increases the wear rate increases because the contact between the pin and disc surfaces is close and generates a lot of friction heat which leads to increase in the wear rate of ZA-27/ Al_2O_3 nanocomposites.

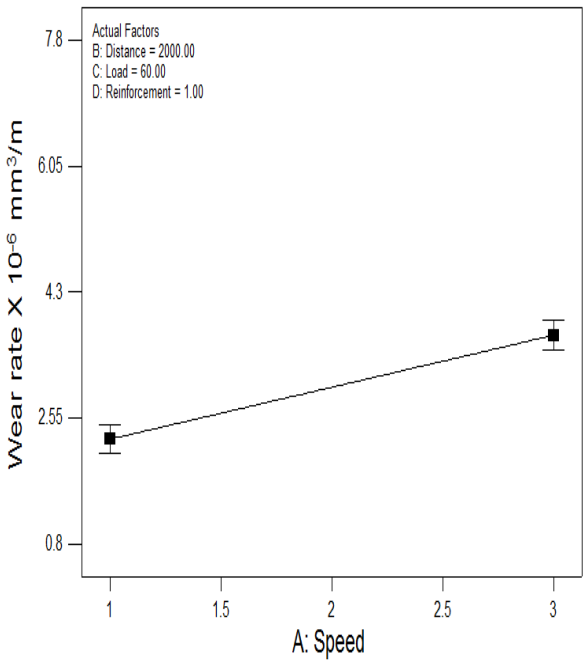

a) Speed

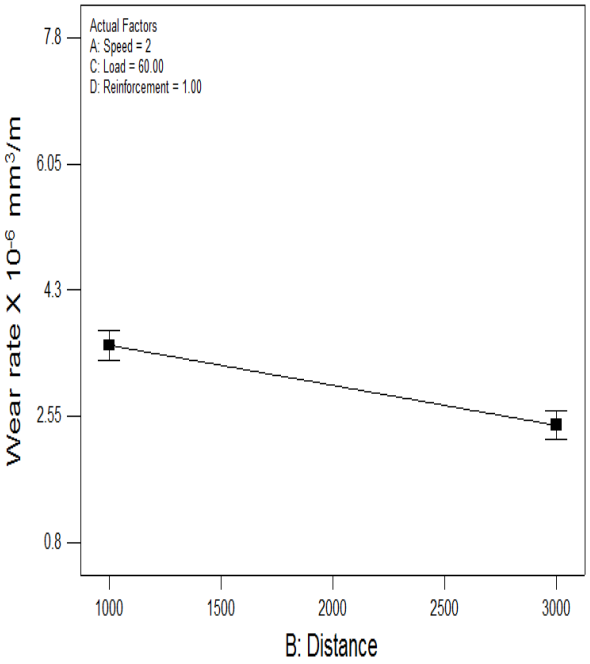

b) Distance

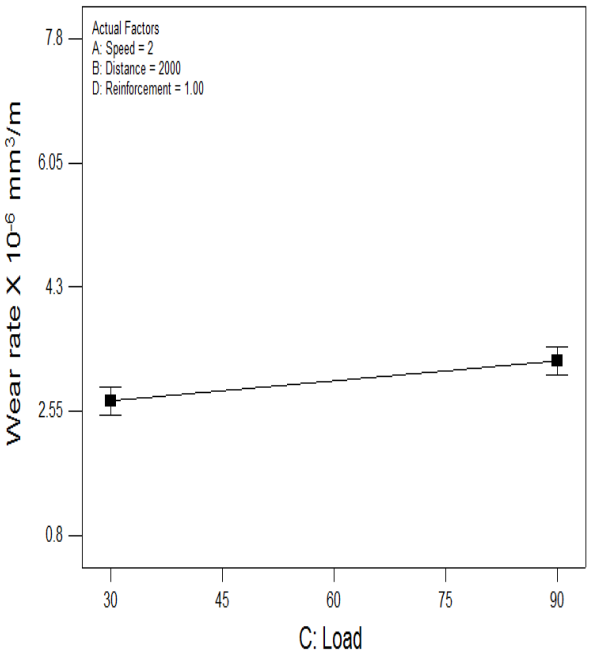

c) Load

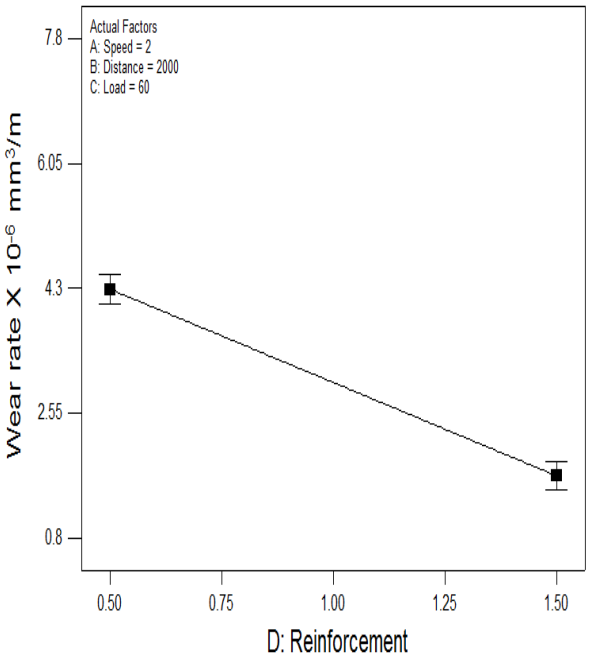

d) Reinforcement

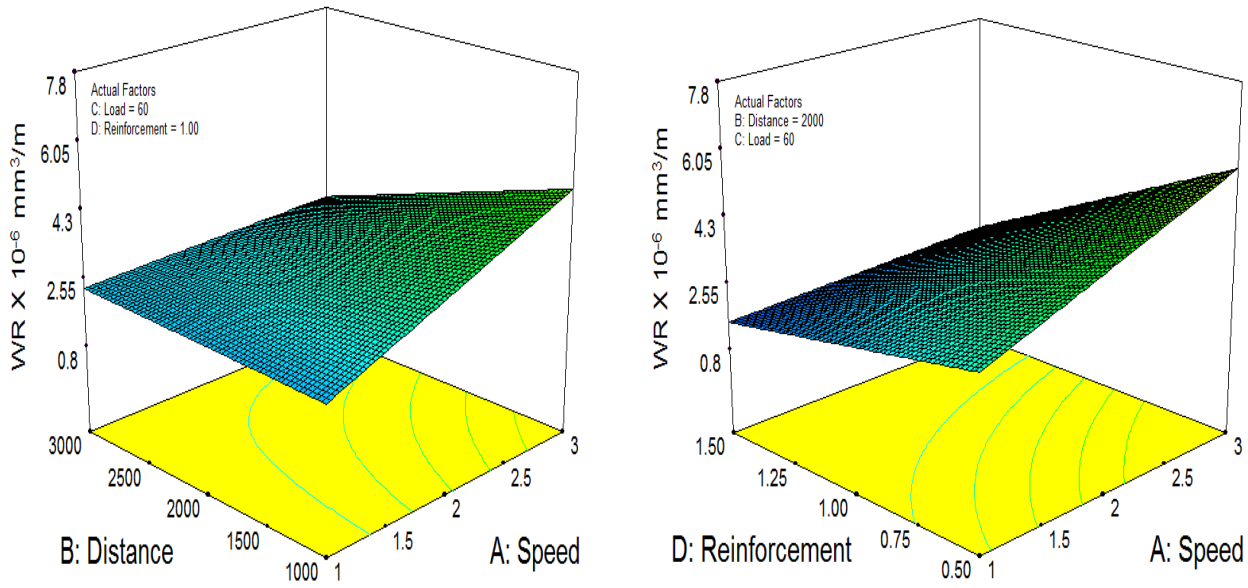

e) Distance Vs Speed

f) Reinforcement Vs Speed

Figure 6.10.Effect of process parameters on wear rate of ZA-27/Al_2O_3 nanocomposites

As the reinforcement content of nanoparticles increases from 0.5 wt % to 1.5 wt % there is extreme reduction in the wear rate of the nanocomposites, this is due to hard ceramic particles of Al_2O_3 which are used to increase the wear resistance of nanocomposites as shown in Figure 6.10 (d). The interaction effects between the distance-speed and reinforcement-speed on the wear rate of ZA-27/ Al_2O_3 nanocomposites are also shown in figures 6.10 (e) and (f).

b) Model validation for wear rate

Confirmation test parameters for wear rate of ZA-27/Al_2O_3 nanocomposites are shown in Table 6.17 Confirmation tests have been carried out and then the comparison between experimental and predicted wear rate of ZA-27/Al_2O_3 nanocomposites shows an error of 3.9 %.

Table 6.17 Test parameters employed for model validation for wear rate

Expt No	Speed (m/s)	Distance (m)	Load (N)	Filler (Wt %)	Experimental Wear rate (x 10^{-6} mm^3/m)	Predicted Wear rate (x 10^{-6} mm^3/m)	Error %
1	2.5	2900	30	1.5	0.871	0.837	3.9

c) ANOVA analysis of COF

Table 6.18 shows the ANOVA analysis for COF of ZA-27/Al_2O_3 nanocomposites. The most significant parameters which influence the COF of nanocomposites are reinforcement content and applied load. In the ANOVA table, column 7 shows the percentage contribution of the individual parameters and their interactions.

Table 6.18 ANOVA results for COF of ZA-27/Al_2O_3 nanocomposites

Source	Sum of Squares	DF	Mean Square	F Value	p-value Prob > F	Percentage contribution
Model	0.147934	14	0.010567	53.7983	< 0.0001	98
A-Speed	0.00845	1	0.00845	43.02154	< 0.0001	5.6
B-Distance	0.0001	1	0.0001	0.1254	1.00	0.01
C-Load	0.049089	1	0.049089	249.9266	< 0.0001	32.5
D-Reinforcement	0.06125	1	0.06125	311.8425	< 0.0001	40.6
AB	0.000225	1	0.000225	1.145544	0.3014	0.15
AC	0.003025	1	0.003025	15.4012	0.0014	2
AD	0.0004	1	0.0004	2.036522	0.174	0.27
BD	0.004225	1	0.004225	21.51077	0.0003	2.8
CD	0.007225	1	0.007225	36.78469	< 0.0001	4.8
A^2	0.00053	1	0.00053	2.696788	0.1213	0.35
B^2	0.000224	1	0.000224	1.140469	0.3024	0.15
C^2	0.002224	1	0.002224	11.32308	0.0043	1.48
Residual	0.002946	15	0.000196			1.95
Cor Total	0.15088	29				100

A prediction model has been developed for coefficient of friction of ZA-27/ Al_2O_3 nanocomposites using ANOVA and is given by equation (6.9) in coded form. The R-squared, adjusted R-squared and predicted R-squared values are 98.04 %, 96.22 % and 90.85 % respectively for this model.

COF = +0.48-0.022*A+0.000*B-0.052 * C-0.058 * D-3.750E-003 * A * B-0.014 * A * C-5.000E-003 * A *D+0.016 * B * D+0.021 * C * D-0.014 * A^2-9.298E-003 * B^2-0.029 * C^2. (6.9)

The effects of individual process parameters on the coefficient of friction of ZA-27/ Al_2O_3 nanocomposites are shown in figure 6.11 (a) to (f). It is observed from Figure 6.11 (a) that

the COF decreases as the sliding speed increases. When the siding speed increases, the surface temperatures of the pin and disc increases, due to this an oxide film is formed between the pin and the disc surfaces. As the sliding speed increases between the contact surfaces of the counter disc and pin, a stable oxide film will exists which decreases the friction coefficient of ZA-27/ Al_2O_3 nanocomposites.

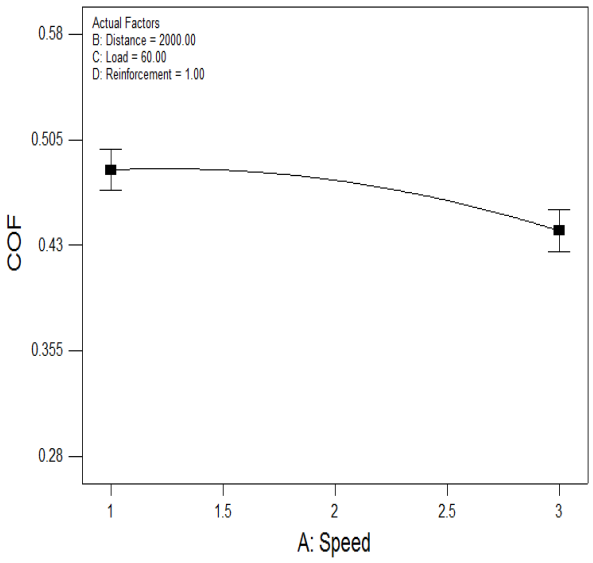

a) Speed

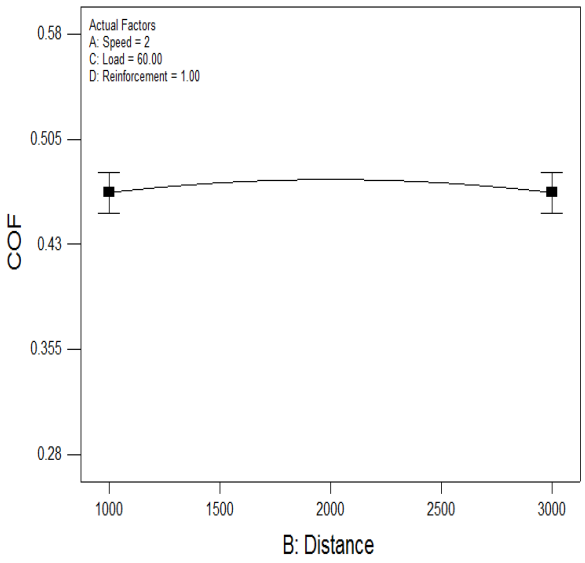

b) Distance

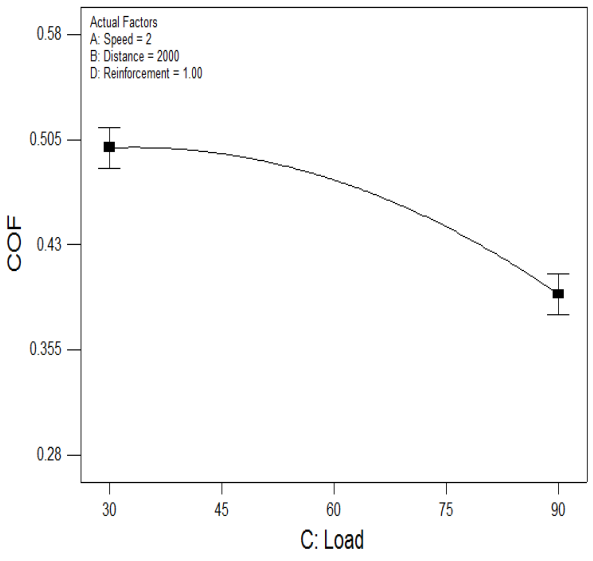

c) Load

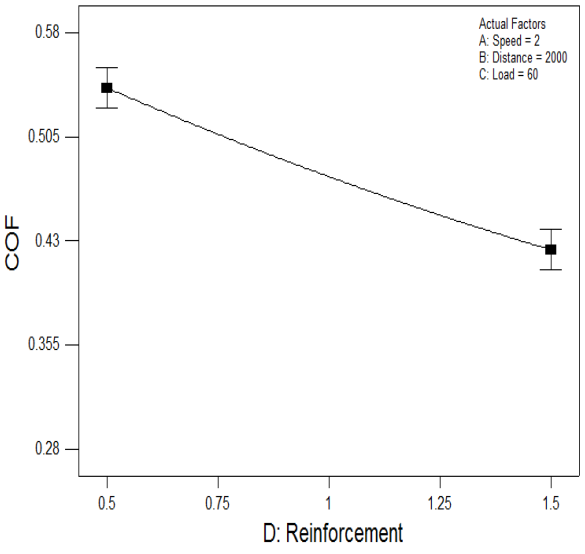

d) Reinforcement

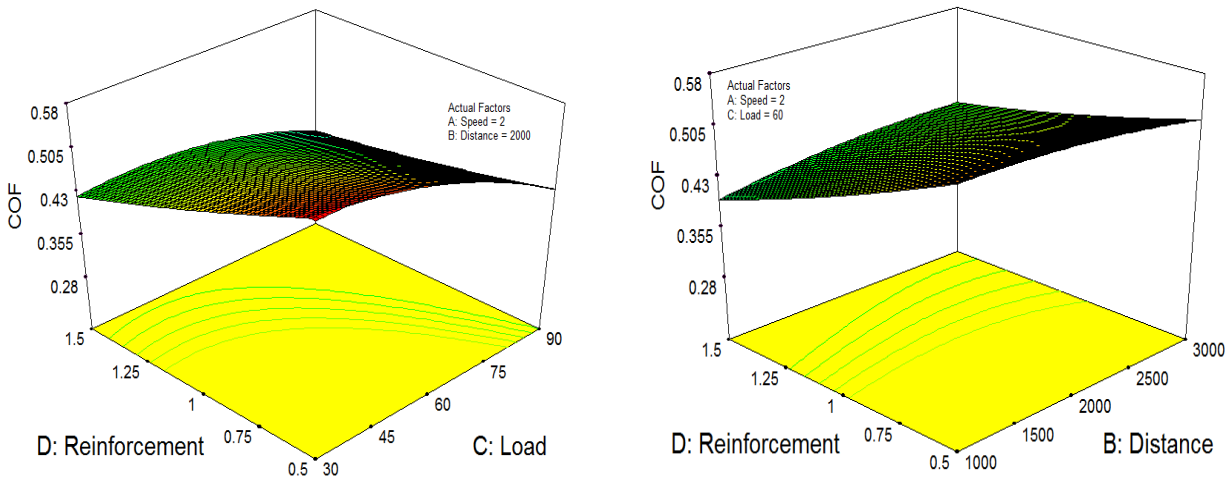

e) Reinforcement VS Load f) Reinforcement Vs Distance

Figure 6.11.Effect of process parameters on COF of ZA-27/Al_2O_3 nanocomposites

As the sliding distance increases the COF of the nanocomposites remains same because the temperature of the pin and disc surfaces increases. Due to the increase in the surface temperatures a compact layer is generated between the pin and disc surfaces which do not influence the COF behavior of the nanocomposites this is shown in figure 6.11 (b). From the Figure 6.11 (c) and (d) it was observed that the coefficient of friction of ZA-27/ Al_2O_3 nanocomposites decreases as the reinforcement content and applied load increases. The contact surfaces of the disc and pin generate more frictional heat as the applied load increases which results in the softening of the pin surface. As the applied load increases the frictional heat generated is more between the pin and disc surfaces which leads to the pin surface becoming soft and the formation of tribolayer decreases the COF of ZA-27/ Al_2O_3 nanocomposites. When the applied load increases the reinforcement particles transfer from the pin surface and penetrates the disc surface which leads to the formation of tribolayer between the disc and the pin surfaces. If the reinforcement content increases in ZA-27/ Al_2O_3 nanocomposites there exists a thick stable tribolayer between the disc and pin surfaces, due to which the coefficient of friction decreases more compare to the applied load and sliding speed. The interaction effects between the reinforcement-load and reinforcement-distance on the COF of ZA-27/ Al_2O_3 nanocomposites are also shown in figure 6.11 (e) and (f).

d) Model validation for COF

Confirmation test parameters for COF of ZA-27/Al_2O_3 nanocomposites are shown in Table 6.19 Confirmation tests have been carried out and then the comparison between experimental and predicted coefficient of friction of ZA-27/Al_2O_3 nanocomposites shows an error of 2.4 %.

Table 6.19 Test parameters employed for model validation for COF

Expt No	Speed (m/s)	Distance (m)	Load (N)	Filler (Wt %)	Experimental COF	Predicted COF	Error %
1	3	1000	90	1.5	0.292	0.285	2.4

6.4.5. Worn surfaces of ZA-27/Al_2O_3 nanocomposites

The microstructure of worn surfaces of nanocomposites have been examined with the help of scanning electron microscope (SEM) and shown in Figures 6.12 (a) to (c).

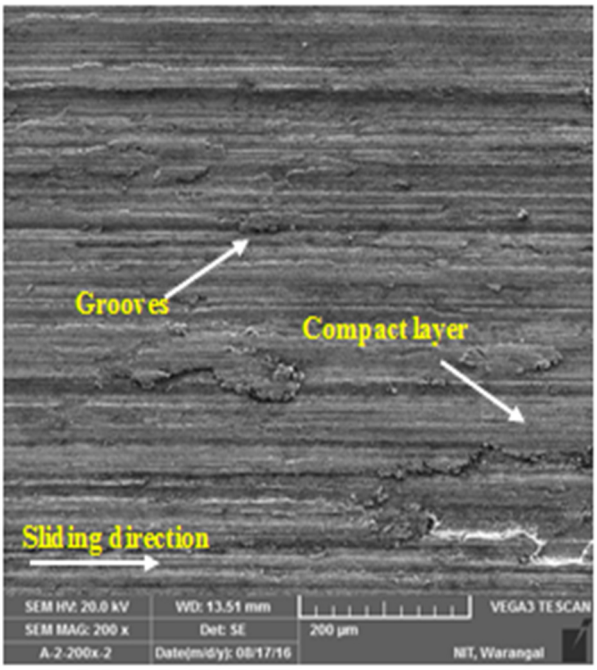

a) 0.5 wt % Al_2O_3

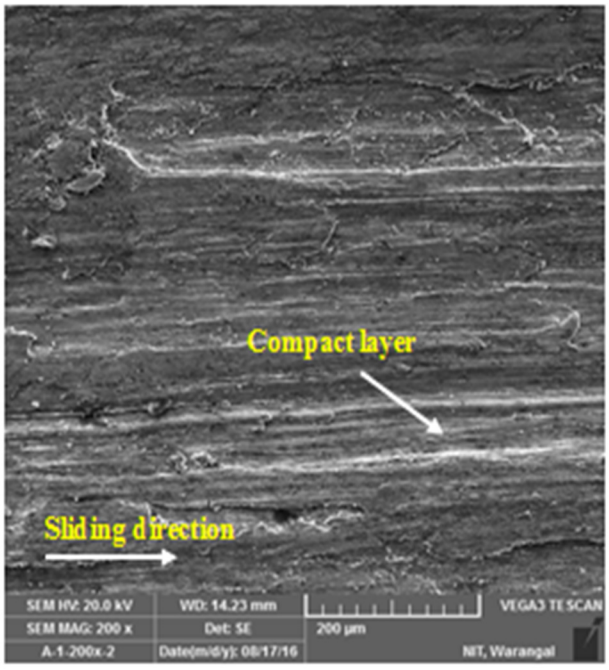

b) 1.0 wt % Al_2O_3

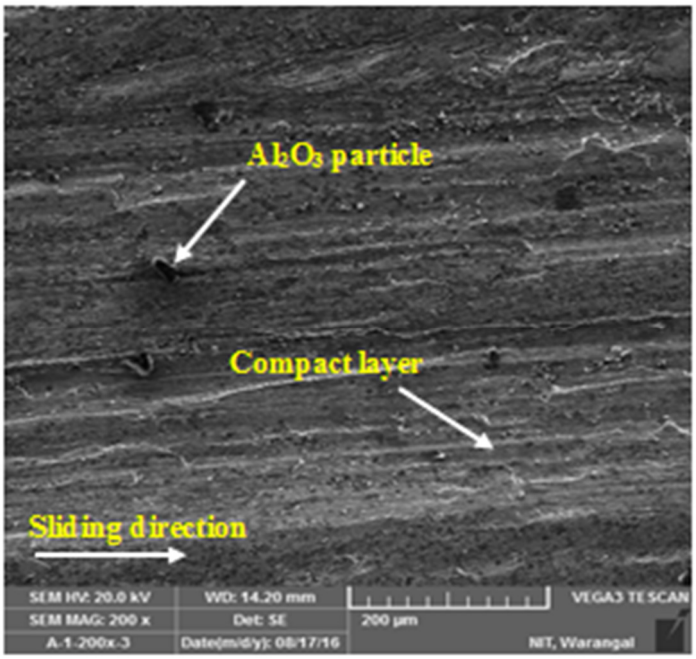

c) 1.5 wt % Al_2O_3

Figure 6.12.Microstructures of wear surfaces of ZA-27/Al_2O_3 nanocomposites using SEM

The reinforcement content of alumina nanoparticles increases from 0.5 wt % to 1.5 wt % of nanocomposites shows shallow grooves and fewer pits as shown in Figures 6.12 (b) to (c). The depth of the grooves is reduced due to the presence of Al_2O_3 nanoparticles which improve the hardness of the nanocomposites. There is lesser plastic deformation detected at the edges of the grooves, along the path of the sliding ridges and grooves are parallel and aligned. It is evident from the wear surface that when the content of Al_2O_3 nanoparticle increases, the wear rate of ZA-27 nanocomposites reduces.

6.4.6 ZA-27 hybrid micro and nanocomposite

Al_2O_3 and MoS_2 micro and nanoparticles reinforced ZA-27 hybrid micro and nanocomposites with different combinations of parameters for dry sliding wear performance is shown in Table 6.20

Table 6.20 Experimental plan and results of hybrid micro and nanocomposite

Expt No	Distance (m)	Load (N)	Speed (m/s)	Hybrid (μm)		Hybrid (nm)	
				WR x 10^{-6} (mm^3/m)	COF	WR x 10^{-6} (mm^3/m)	COF
1	1000	90	3	6.371	0.26	2.929	0.14
2	1000	90	1	3.935	0.36	1.875	0.25
3	2000	60	2	3.806	0.42	1.675	0.29
4	1000	30	3	2.693	0.49	1.496	0.34
5	2000	60	3	3.572	0.37	1.527	0.26
6	3000	90	3	4.325	0.22	1.931	0.16
7	2000	60	2	3.49	0.42	1.77	0.31
8	3000	90	1	2.74	0.47	1.229	0.35
9	1000	30	1	2.928	0.56	0.885	0.45
10	2000	60	2	3.853	0.39	1.696	0.28
11	3000	60	2	3.326	0.43	1.489	0.32
12	2000	60	2	3.583	0.42	1.959	0.31
13	1000	60	2	4.356	0.45	2.002	0.32
14	3000	30	1	1.254	0.58	0.581	0.41
15	2000	60	2	3.338	0.43	2.012	0.31
16	2000	60	1	2.354	0.51	1.064	0.39
17	2000	90	2	5.34	0.31	2.592	0.22
18	2000	30	2	2.401	0.55	1.317	0.39
19	2000	60	2	4.275	0.39	1.57	0.27
20	3000	30	3	1.678	0.47	0.765	0.15

a) ANOVA analysis of wear rate

Table 6.21 and 6.22 shows the result of ANOVA analysis for the hybrid micro and nanocomposite. The significant factors influencing the wear rate behavior of the hybrid micro and nanocomposite are applied load, Sliding distance and sliding speed. In the ANOVA table, column 7 shows the percentage contribution of the individual parameters and their interactions. Among all, the applied load and sliding distance are the most significant factors which influence the wear rate of ZA-27 hybrid micro and nanocomposite.

Table 6.21 ANOVA results for wear rate of hybrid microcomposite

Source	Sum of Squares	DF	Mean Square	F Value	p-value Prob > F	Percentage contribution
Model	26.23619	7	3.748028	36.12527	< 0.0001	95.5
A-Distance	5.12656	1	5.12656	49.41222	< 0.0001	18.7
B-Load	14.29698	1	14.29698	137.8011	< 0.0001	52.1
C-Speed	3.167438	1	3.167438	30.52928	0.0001	11.6
AB	0.015488	1	0.015488	0.149281	0.706	0.1
BC	1.648928	1	1.648928	15.89315	0.0018	6.1
B^2	0.109298	1	0.109298	1.053467	0.325	0.5
C^2	1.671287	1	1.671287	16.10866	0.0017	6.3
Residual	1.24501	12	0.103751			4.6
Cor Total	27.4812	19				100

Table 6.22 ANOVA results for wear rate of hybrid nanocomposite

Source	Sum of Squares	DF	Mean Square	F Value	p-value Prob > F	Percentage contribution
Model	6.049203	9	0.67213	35.40039	< 0.0001	97
A-Distance	1.026562	1	1.02656	54.06764	< 0.0001	16.7
B-Load	3.051458	1	3.05145	160.7162	< 0.0001	49.8
C-Speed	0.915668	1	0.91566	48.227	< 0.0001	14.7
AB	0.044551	1	0.04455	2.346449	0.1566	0.8
AC	0.073536	1	0.07353	3.87305	0.0774	1.4
BC	0.112575	1	0.11257	5.929183	0.0351	1.9
A^2	0.00182	1	0.00182	0.095868	0.7632	0.1
B^2	0.092369	1	0.09236	4.864977	0.0519	1.5
C^2	0.62237	1	0.62237	32.77942	0.0002	10
Residual	0.189866	10	0.01898			3.1
Cor Total	6.239069	19				100

A prediction model has been developed for wear rate of the ZA-27 hybrid micro and nano composite using ANOVA and is given by equation (6.10) and (6.11) in coded form. The R-squared, adjusted R-squared and predicted R-squared values for hybrid microcomposite were 95.46 %, 92.82 % and 81.57 %, for hybrid nanocomposite were 96.95 %, 94.21 % and 91.64 % , respectively for this model.

WR = +3.74 - 0.72 * A + 1.20 * B + 0.56 * C - 0.044 * A * B + 0.45 * B * C+ 0.18 * B^2- 0.72 * C^2 (6.10)

WR = +1.78 - 0.32 * A + 0.55 * B + 0.30 * C - 0.075 * A * B - 0.096 * A * C+ 0.12 * B* C- 0.026 * A^2 + 0.18 * B^2 - 0.48 * C^2. (6.11)

Influence of process parameters on the wear rate of ZA-27 hybrid micro and nano composite are shown in figures 6.13 (a - e) and 6.14 (a - e). It was observed from Figure 6.13 (a) and 6.14 (a) that the wear rate of ZA-27 hybrid micro and nanocomposite decreases as the sliding distance increases. The reinforcement particles of pin are transferred to the disc surface when sliding action taking place between both surfaces under the influence of applied load. Since the sliding distance increases the wear resistance improves for the hybrid micro and nanocomposite due to the smearing of the reinforcement particles and formation of protective layers inhibiting the wear rate. The smearing of reinforcement particles from the nanocomposites acts as ceramic mixed mechanical layer (CMML) which increases the wear resistance of hybrid nanocomposite. Figure 6.13 (b) and 6.14 (b) shows that the wear rate of ZA-27 hybrid micro and nanocomposite increases with increase in the applied load. As the applied load increases the rise in temperature was noticeable, which increases the wear rate of hybrid nanocomposites. Due to rise in temperature in the hybrid nanocomposite the reinforcement particles gradually start separating from the matrix material which resulting in the direct contact to the counter disc. The similar trend can be observed by many researches [169-171]. From the Figure 6.14 (c) it was observed that the wear rate of ZA-27 hybrid nanocomposite increases with increasing the sliding speeds. Since the sliding speed increases the friction heat generated between the pin and disc surfaces will strongly influence the wear rate of the hybrid nanocomposite. The pin was subjected to less frictional heat at low speed and the penetration of the counter surface is less, which leads to lower wear rate. If the sliding speed increases, the pin was subjected to higher frictional heat and the penetration of the counter surface becomes more, which leads to higher wear rate.

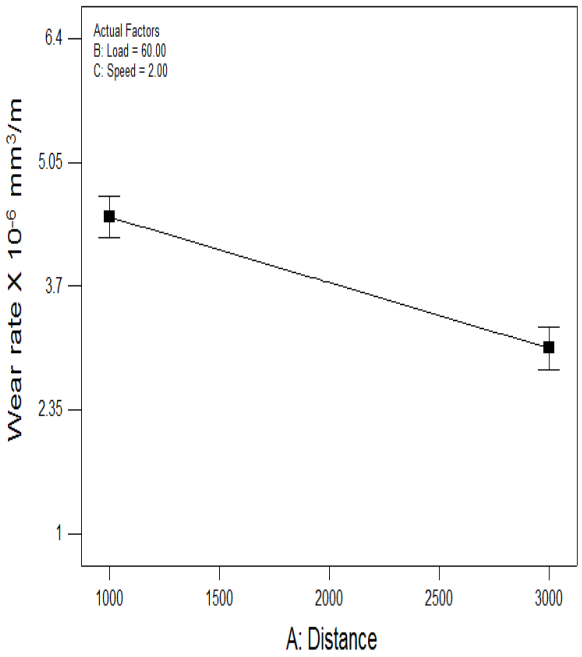

a) Distance

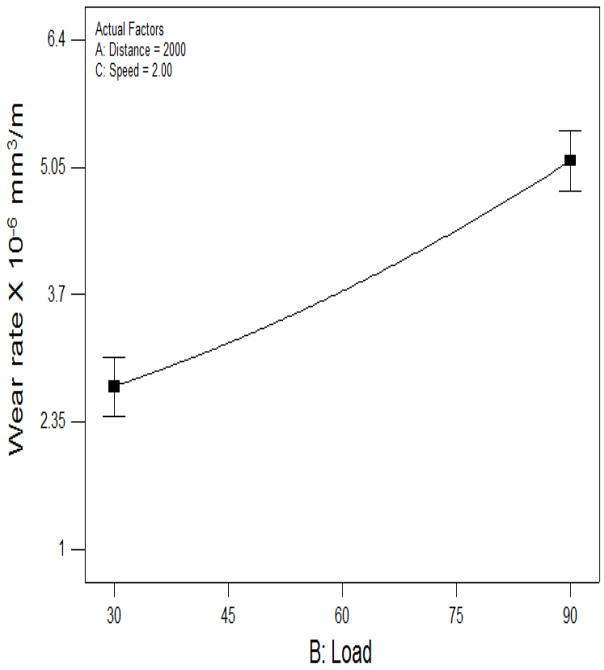

b) Load

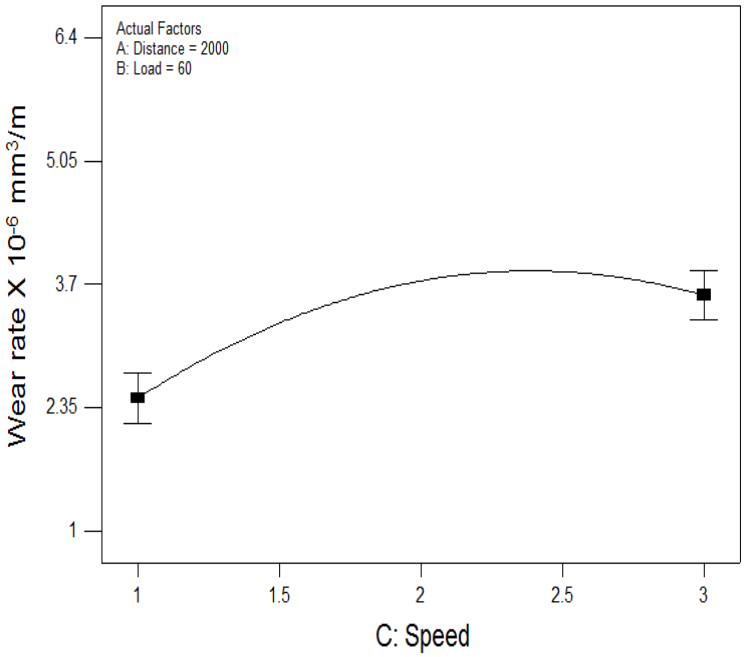

c) Speed

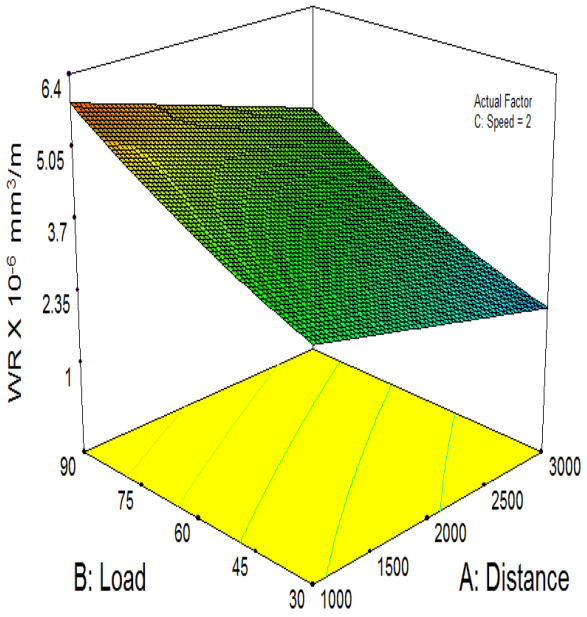

d) Load Vs Distance

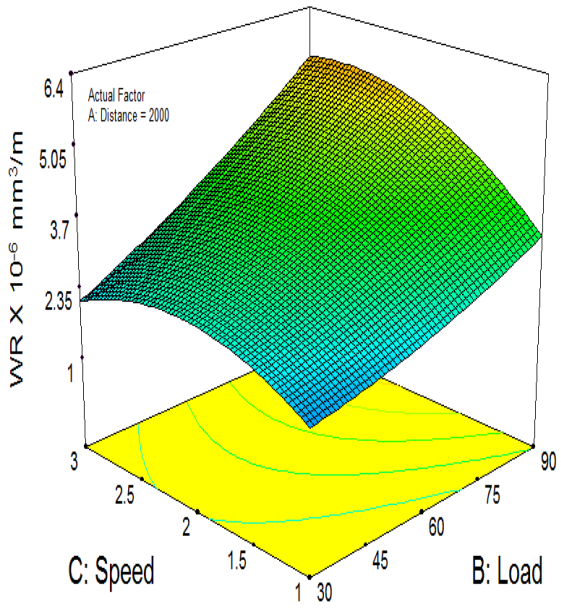

e) Speed Vs Load

Figure 6.13.Effect of process parameters on wear rate of ZA-27 hybrid composite

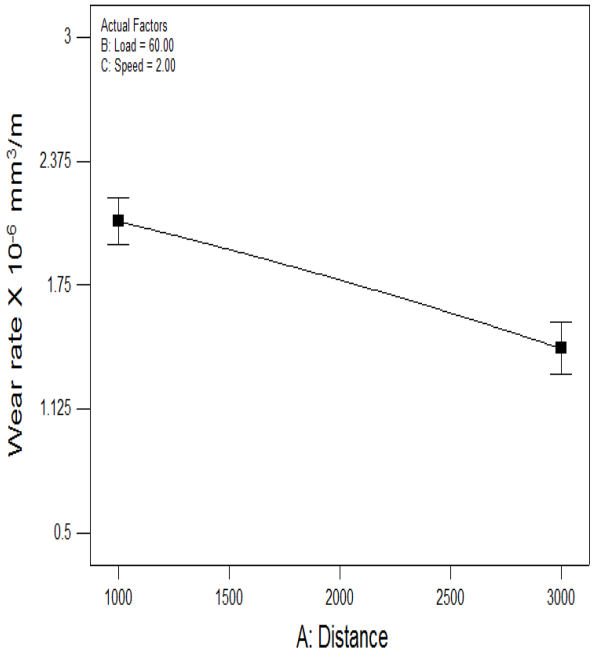

a) Distance

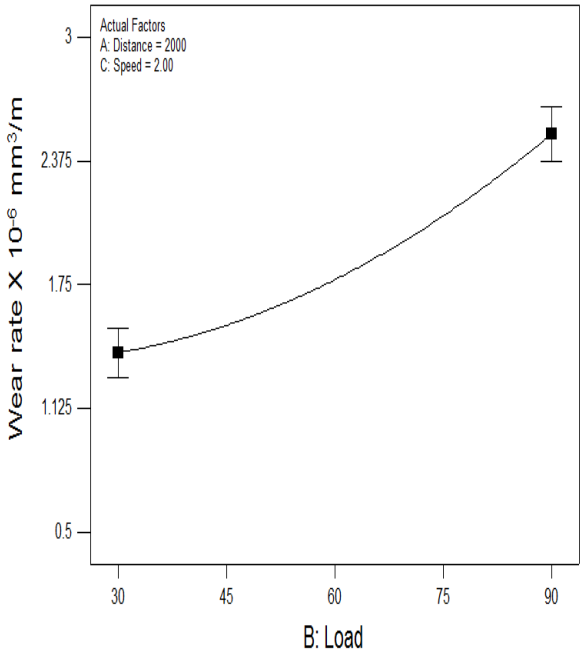

b) Load

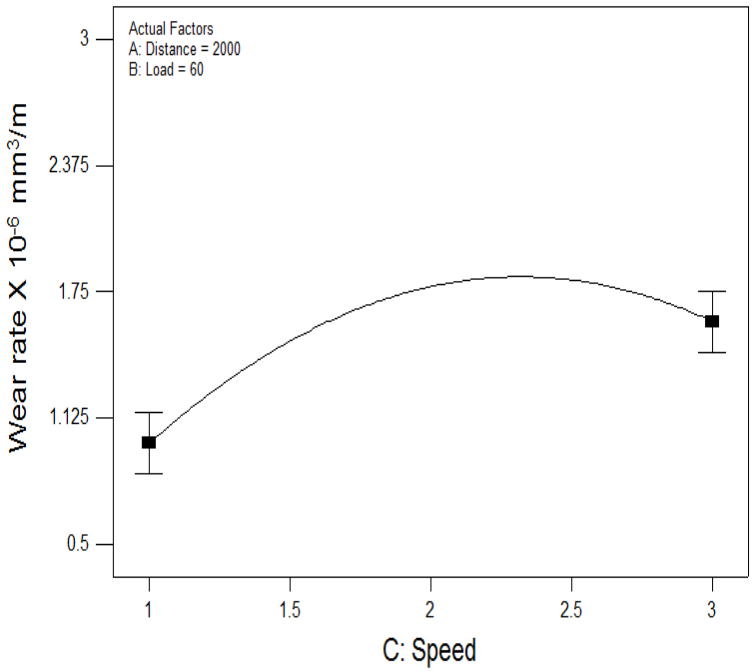

c) Speed

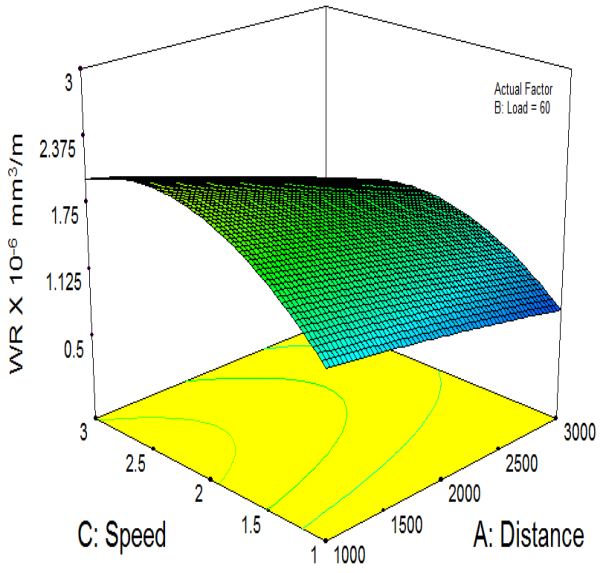

d) Speed Vs Distance

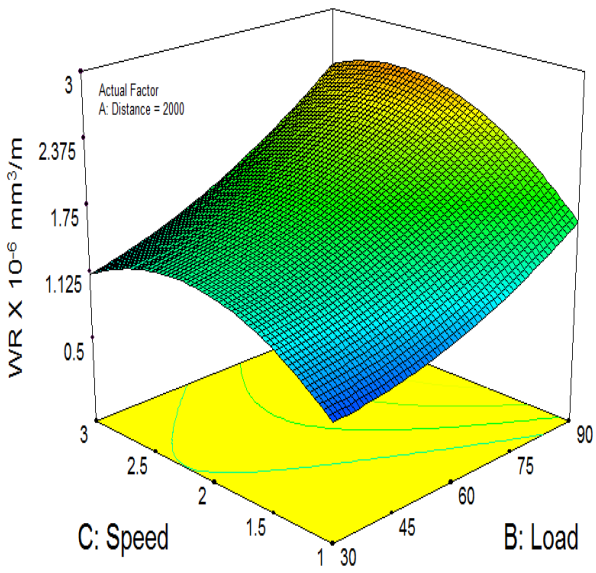

e) Speed Vs Load

Figure 6.14.Effect of process parameters on wear rate of ZA-27 hybrid nanocomposite

The metal oxides were formed because of the rise in temperature, the crushed alumina particles, the smeared MoS_2 particles along with a ZA-27 alloy crush between the pin and disc forming a ceramic mixed mechanical layer (CMML) preventing the specimen from excessive wear [172-173]. The interaction effects between the speed-distance and speed-load on the wear rate of the hybrid nanocomposite are also shown in Figure 6.14 (d) and (e).

b) Model validation for wear rate

Confirmation test parameters for wear rate of ZA-27 hybrid micro and nanocomposite are shown in Table 6.23 and 6.24 Confirmation tests have been carried out and then the comparison between experimental and predicted wear rate of ZA-27 hybrid composite shows an error of 2.5 % and 1.8 %.

Table 6.23 Model validation for wear rate of hybrid microcomposite

Expt No	Speed (m/s)	Distance (m)	Load (N)	Experimental Wear rate(x 10^{-6} mm^3/m)	Predicted Wear rate (x 10^{-6} mm^3/m)	Error %
1	1	3000	30	1.254	1.226	2.5

Table 6.24 Model validation for wear rate of hybrid nanocomposite

Expt No	Speed (m/s)	Distance (m)	Load (N)	Experimental Wear rate(x 10^{-6} mm^3/m)	Predicted Wear rate (x 10^{-6} mm^3/m)	Error %
1	1	3000	30	0.581	0.572	1.8

c) ANOVA analysis of COF

Table 6.25 and 6.26 shows the ANOVA analysis for COF of ZA-27 hybrid micro and nanocomposite. The most significant factors influencing the COF behavior of the hybrid composite are applied load and sliding speed. In the ANOVA table, column 7 shows the percentage contribution of the individual parameters and their interactions.

Table 6.25 ANOVA results for COF of hybrid microcomposite

Source	Sum of Squares	DF	Mean Square	F Value	p-value Prob > F	Percentage contribution
Model	0.16406	6	0.027343	55.23906	< 0.0001	96

A-Distance	0.00016	1	0.00016	0.323232	0.5794	0.1
B-Load	0.10816	1	0.10816	218.5051	< 0.0001	63.4
C-Speed	0.04624	1	0.04624	93.41414	< 0.0001	27.3
AB	0.00045	1	0.00045	0.909091	0.3577	0.3
AC	0.005	1	0.005	10.10101	0.0073	2.9
BC	0.00405	1	0.00405	8.181818	0.0134	2.3
Residual	0.006435	13	0.000495			3.7
Cor Total	0.170495	19				100

Table 6.26 ANOVA results for COF of hybrid nanocomposite

Source	Sum of Squares	DF	Mean Square	F Value	p-value Prob > F	Percentage contribution
Model	0.10694	5	0.021388	54.64088	< 0.0001	95
A-Distance	0.00064	1	0.00064	1.635036	0.2218	0.6
B-Load	0.06724	1	0.06724	171.781	< 0.0001	59.8
C-Speed	0.03481	1	0.03481	88.93066	< 0.0001	31
AB	0.00245	1	0.00245	6.259124	0.0254	2.2
BC	0.0018	1	0.0018	4.59854	0.0500	1.6
Residual	0.00548	14	0.000391			4.8
Cor Total	0.11242	19				100

A prediction model has been developed for COF of ZA-27 hybrid micro and nano composite using ANOVA and is given by equation (6.12) and (6.13) in coded form. The R-squared, adjusted R-squared and predicted R-squared values for hybrid microcomposite were 96.22 %, 94.48 % and 81.08 %, for hybrid nanocomposite were 95.12 %, 93.38 % and 81.74 % respectively for this model.

COF =+0.42+4.000E-003* A-0.10 * B-0.068 * C+7.500E-003*A*B-0.025*A*C
-0.022*B*C. (6.12)

COF =+0.31+8.000E-003 * A-0.082 * B-0.059 * C+0.018 * A * B-0.015 * B * C. (6.13)

The effects of individual process parameters on the coefficient of friction of ZA-27 hybrid micro and nanocomposite are shown in figures 6.15 (a - f) and 6.16 (a - f). It is evident from the Figure 6.15 (a) and 6.16 (a), that there is less influence of COF as the sliding distance increases.

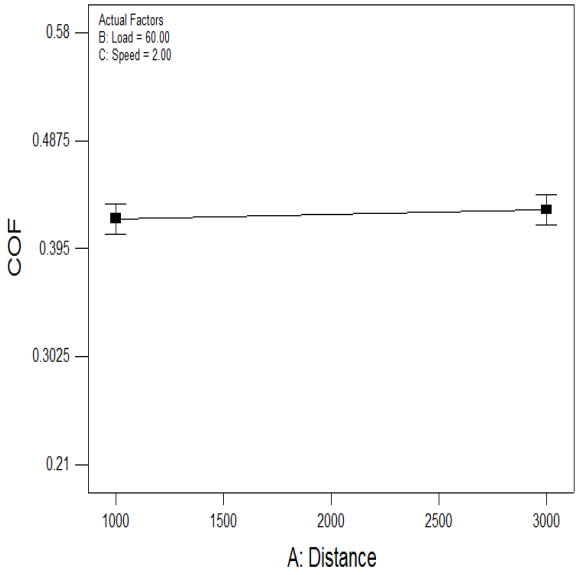

a) Distance

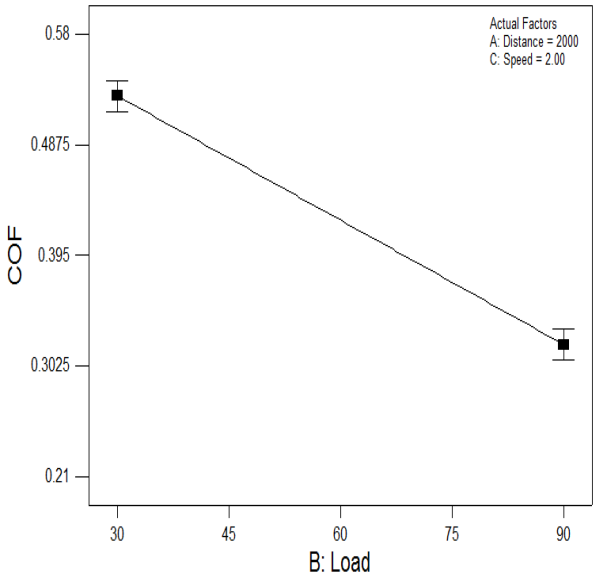

b) Load

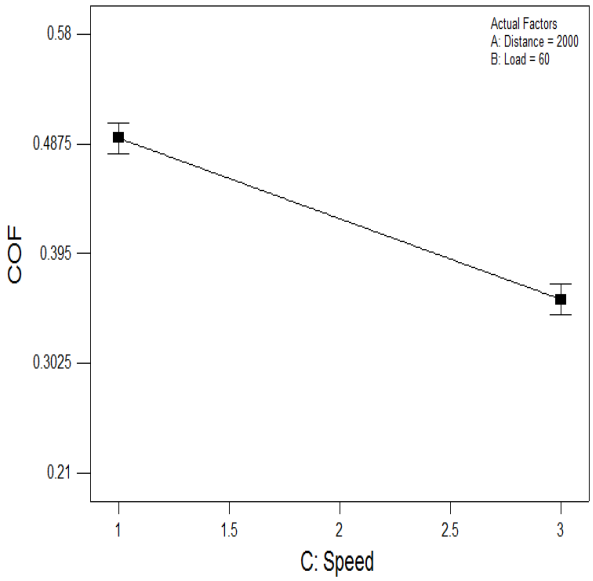

c) Speed

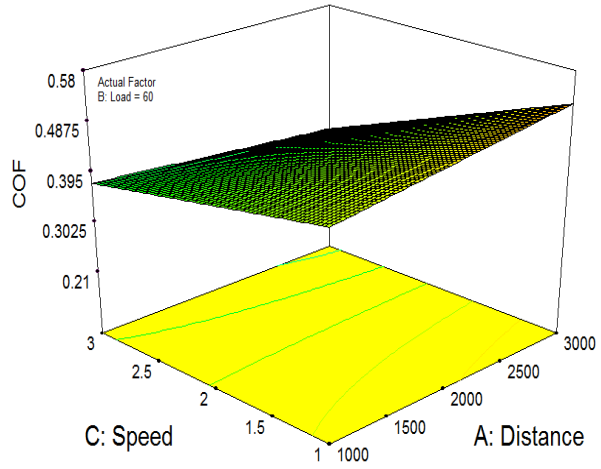

d) Speed Vs Distance

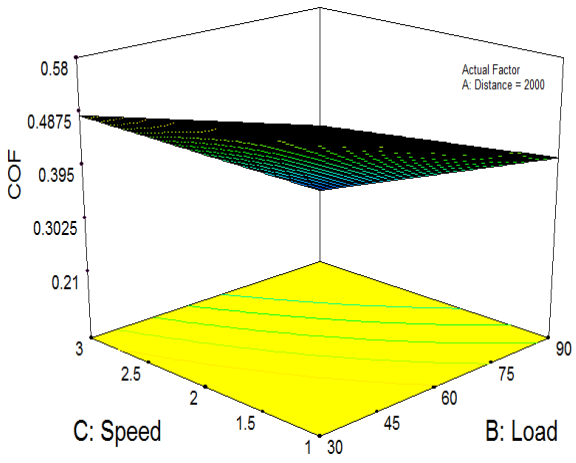

e) Speed Vs Load

Figure 6.15.Effect of process parameters on COF of ZA-27 hybrid microcomposite

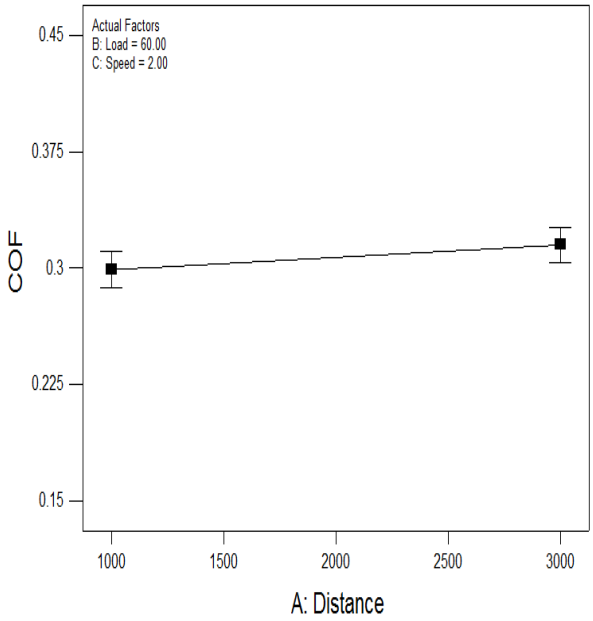

a) Distance

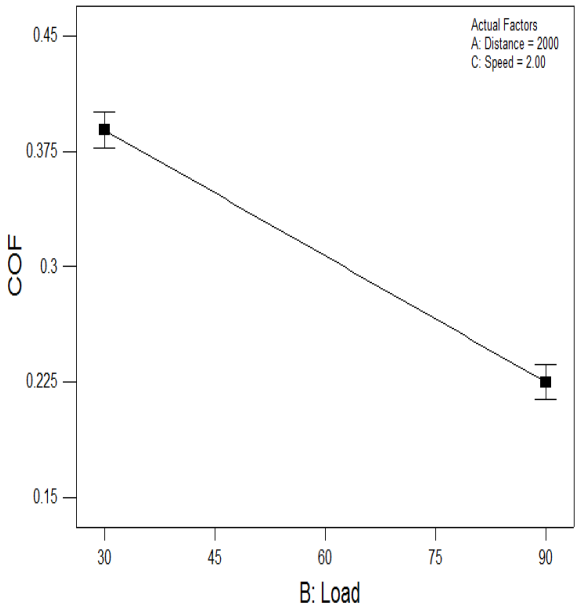

b) Load

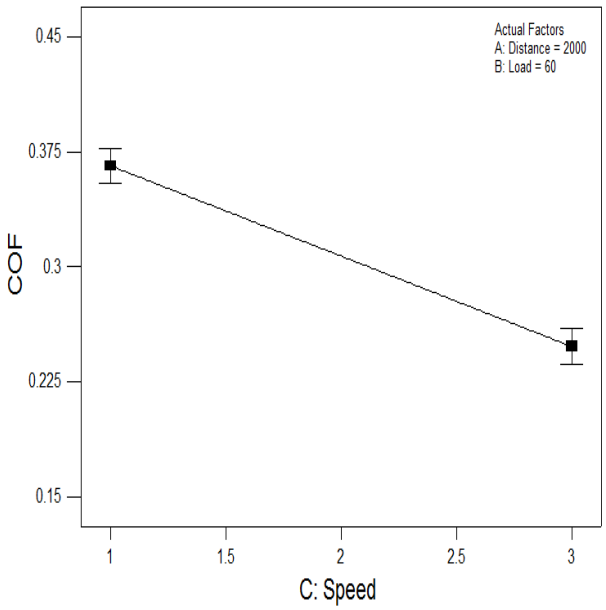

c) Speed

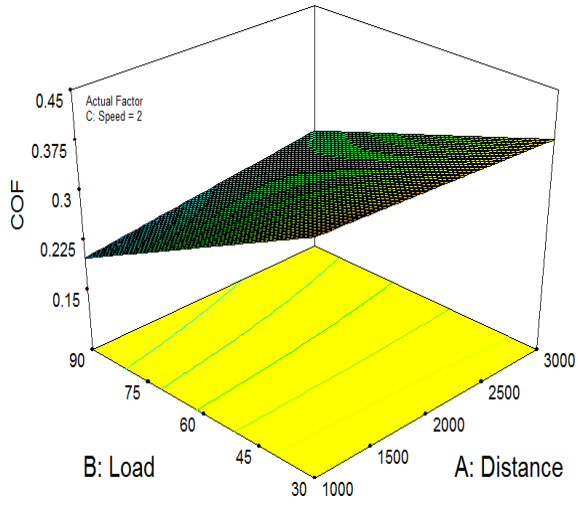

d) Load Vs Distance

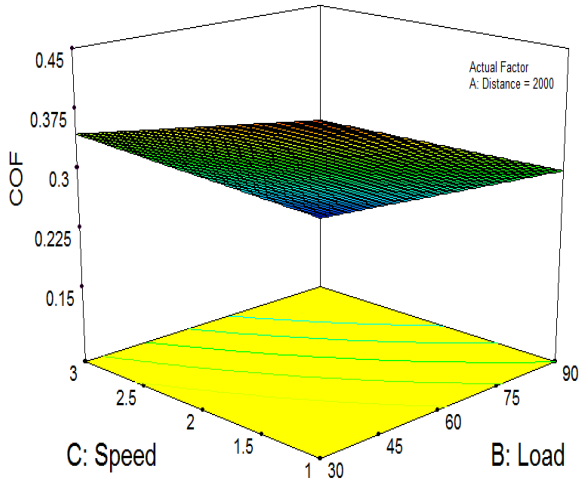

e) Speed Vs Load

Figure 6.16.Effect of process parameters on COF of ZA-27 hybrid nanocomposite

When the siding distance increases the reinforcement particles pull out from the pin and transfer to the disc surface which results in the formation of tribolayer between the pin and the disc surfaces. As the sliding distance increases between the contact surfaces of the counter disc and pin a stable tribolayer will exists which will affect the friction coefficient of ZA-27 hybrid

micro and nanocomposite. The coefficient of friction of hybrid nanocomposite is influenced by the applied load and sliding speed. From Figures 6.16 (b) and (c) it was observed that the coefficient of friction of the hybrid nanocomposite decreases as the load and speed increases. The contact surfaces of the disc and pin will generate more frictional heat as the applied load increases, which results in softening of the pin surface. Due to friction between the hybrid nanocomposite and counter disc during dry sliding wear condition, temperature rises leading the reinforcement particles that smearing out from the specimen act as a CMML which decrease the friction coefficient [174]. The interaction effects between the load-distance and speed-load on the coefficient of friction of the ZA-27 hybrid nanocomposite are also shown in Figure 6.16 (d) and (e).

d) Model validation for COF

Confirmation test parameters for COF of ZA-27 hybrid micro and nano composite are shown in Table 6.27 and 6.28. Confirmation tests have been carried out and then the comparison between experimental and predicted coefficient of friction of ZA-27 hybrid micro and nanocomposite shows an error of 2.3 % and 4.2 %.

Table 6.27 Model validation for COF of hybrid microcomposite

Expt No	Speed (m/s)	Distance (m)	Load (N)	Experimental COF	Predicted COF	Error %
1	3	3000	90	0.221	0.216	2.3

Table 6.28 Model validation for COF of hybrid nanocomposite

Expt No	Speed (m/s)	Distance (m)	Load (N)	Experimental COF	Predicted COF	Error %
1	3	1150	90	0.145	0.139	4.2

6.4.7. Worn surfaces of hybrid micro and nanocomposite

The microstructure of worn surfaces of hybrid micro and nanocomposite have been examined with the help of scanning electron microscope (SEM) and shown in the Figure 6.17 (a) to (b).

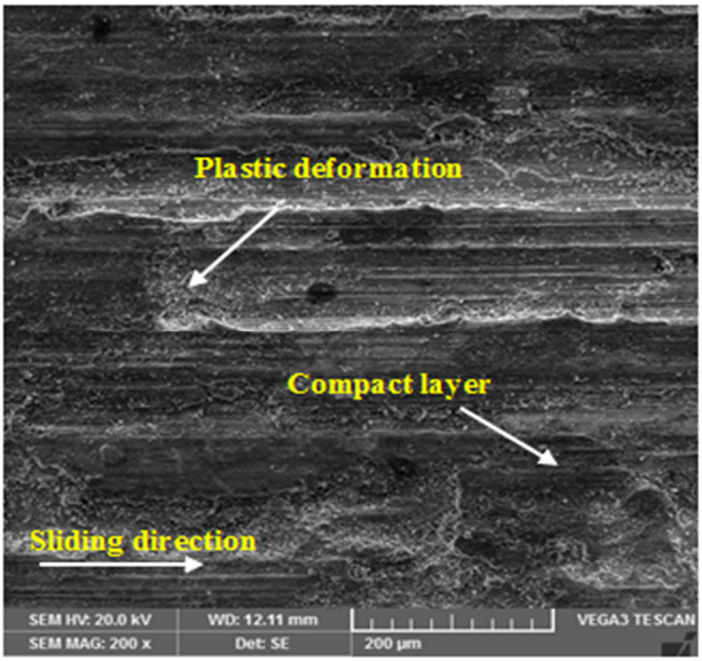

a) Hybrid microcomposite (1.5 wt % Al_2O_3 + 0.5 wt % MoS_2)

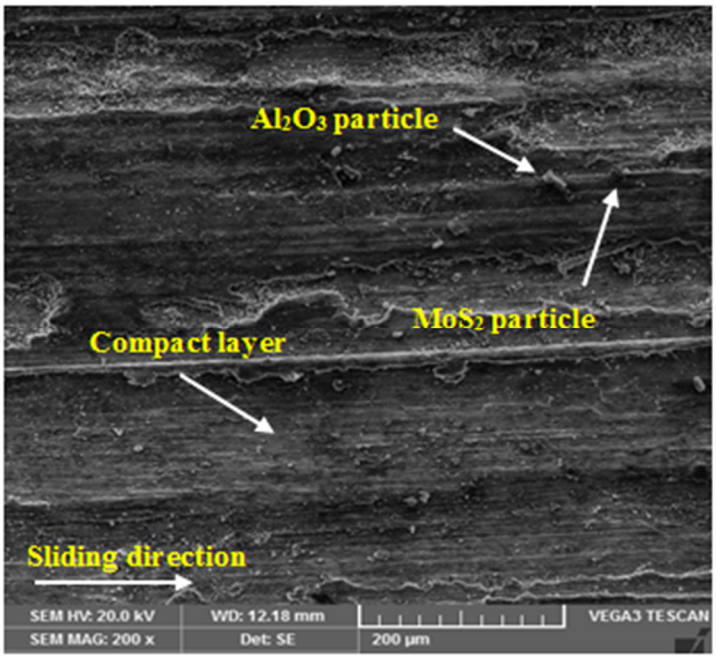

b) Hybrid nanocomposite (1.5 wt % Al_2O_3 + 0.5 wt % MoS_2)

Figure 6.17.Microstructures of wear surfaces of ZA-27 hybrid nanocomposites using SEM

The Al_2O_3 and MoS_2 nanoparticles reinforced in ZA-27 hybrid nanocomposite enhance wear resistance properties because MoS_2 particles acting as a solid lubricant and alumina particles withstand high loads in dry sliding wear characterization. The reinforcement content of alumina and MoS_2 microparticles in ZA-27 hybrid microcomposite shows shallow grooves and fewer pits as shown in Figure 6.17 (a). The depth of the grooves is reduced due to the presence of Al_2O_3 nanoparticles, which improves the hardness of the hybrid nanocomposites. MoS_2 nanoparticles reduce the wear loss of the hybrid nanocomposites because they act as a solid lubricant. Lesser plastic deformation is detected at the edges of the grooves, while along the path of sliding the ridges and grooves are parallel and aligned. It is evident from the wear surface that when Al_2O_3 and MoS_2 nanoparticles are present in the hybrid nanocomposite the wear rate decreases and smooth surface can be obtained as shown in Figure 6.17 (b).

6.5. Comparison of tribological behavior of ZA-27 nanocomposites

6.5.1. Comparison of wear rate

The comparison of the wear rates of Al_2O_3, MoS_2 and combination of both (Al_2O_3 & MoS_2) nanoparticles reinforced in ZA-27 nanocomposites and hybrid nanocomposite under similar test condition are shown in Figure 6.18. It was observed that ZA-27/MoS_2 nanocomposite operating at a condition of reinforcement content of 1.5 wt % MoS_2 nanoparticles, speed at 1 m/s, distance at 2800 m and applied load at 30 N shows better wear resistance properties compared to other operating conditions. MoS_2 nanoparticles act as a solid lubricant in ZA-27/MoS_2 nanocomposite, which enhances the wear resistance properties. ZA-27 hybrid nanocomposites also show better wear resistance properties at a speed at 1 m/s, distance of 3000 m and applied load at 30 N. The presence of alumina and MoS_2 nanoparticles improves the hardness and the wear resistance properties of the hybrid nanocomposite and reduces the wear rate. The wear rate of ZA-27 + 1.5wt% MoS_2 nanocomposite and hybrid nanocomposite are better compared to other ZA-27 nanocomposites.

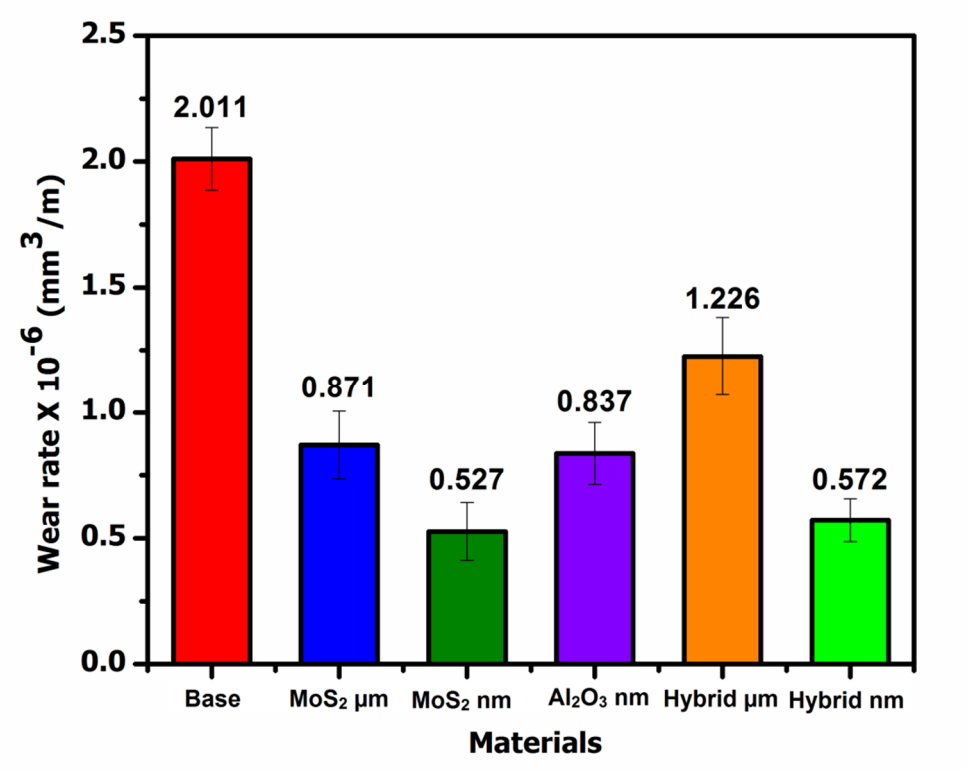

Figure 6.18.Comparison of wear rate of ZA-27 nanocomposites

6.5.2. Comparison of coefficient of friction

Figure 6.19 shows the comparison of the friction coefficient of the hybrid nanocomposite and ZA-27 nanocomposites reinforced with Al_2O_3, MoS_2 and combination of both (Al_2O_3 &MoS_2) micro and nanoparticles under identical operating conditions. It was observed that the ZA-27 hybrid nanocomposites were showing better coefficient of friction properties at a combination of speed at 3 m/s, distance at 1150 m and applied load at 90 N. The ZA-27/MoS_2 nanocomposite operating at a condition of reinforcement content of 1.5 wt % MoS_2 nanoparticles, speed at 3 m/s, distance at 3000 m and applied load at 90 N were also showing better COF properties compare to the other operating conditions. The COF of the hybrid nanocomposite and ZA27+ 1.5wt% MoS_2 nanocomposite were giving better COF results compare to the other ZA-27 nanocomposites.

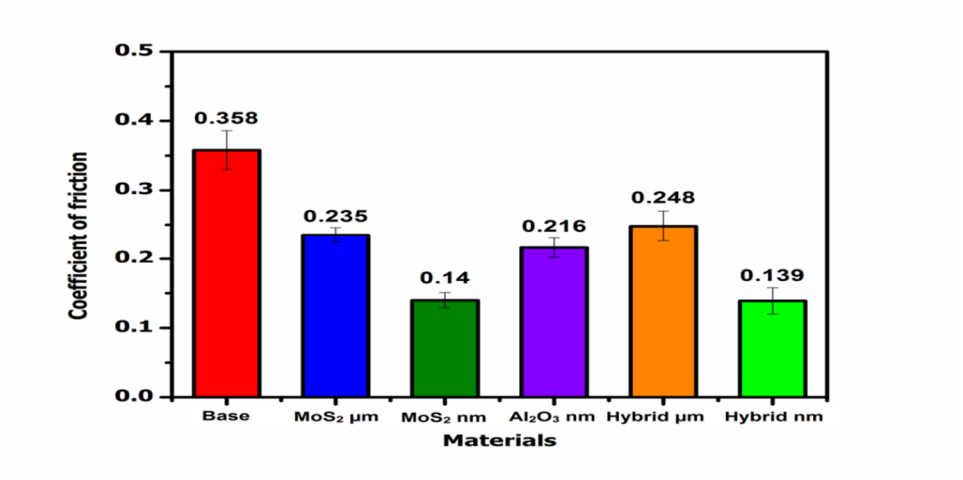

Figure 6.19.Comparison of COF of ZA-27 nanocomposites

6.6. Comparative study of wear behavior with past studies:

Figure 7.3 shows the comparative study of the wear rate behavior with respect to various reinforcement particles reinforced in ZA-27 alloy which are reported in the literature and present work. The hybrid nanocomposite reinforced with 1.5 wt % Al_2O_3 and 0.5 wt % MoS_2 nanoparticles in ZA-27 alloy exhibiting superior wear resistance than the other reinforcement materials.

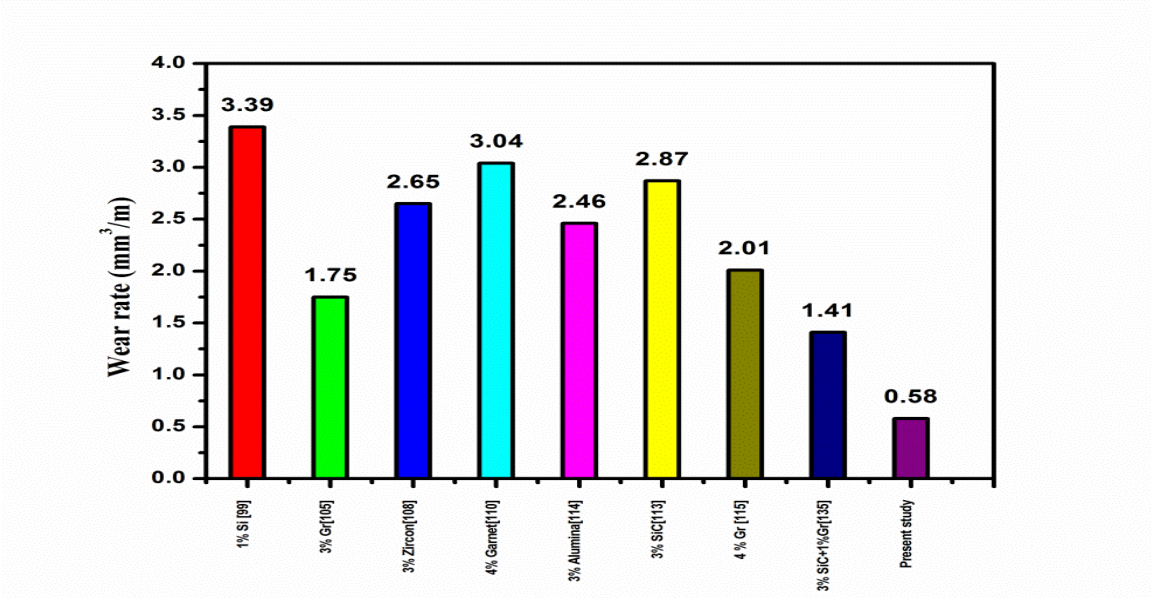

Figure 6.20.Comparative study on wear rate of past studies

6.7. Summary

The major analysis of tribological behavior of different weight percentages of alumina and molybdenum disulphide nanoparticles reinforced in ZA-27 nanocomposites and hybrid nanocomposite was examined by using response surface methodology (RSM) mentioned in this chapter. The ANOVA analysis was performed by using design expert 9.0 software to identify the most significant process parameter which influences the wear rate and coefficient of friction of hybrid nanocomposite and ZA-27 nanocomposites. The regression model was developed for wear rate and coefficient of friction of hybrid nanocomposite and ZA-27 nanocomposites by using ANOVA and the confirmation test have been conducted to validate the derived model for the responses of nanocomposites from quadratic regression fit. Among all the combinations of nanocomposites the MoS_2 nanoparticles reinforced ZA-27 nanocomposites and hybrid nanocomposites are showing superior wear resistance properties for both wear rate and coefficient of friction was discussed in this chapter. The morphology of wear surfaces of various weight percentages of the reinforcement particles reinforced in ZA-27 nanocomposites and hybrid nanocomposite was investigated with the help of scanning electron microscope (SEM) have also been discussed in this chapter.

CHAPTER 7

CONCLUSIONS AND SCOPE FOR FUTURE WORK

7.1. Conclusions

The conclusions drawn from the current research work were as follows:

Fabrication and microstructural analysis

1. ZA-27 based nanocomposites and hybrid nanocomposites reinforced with different weight percentages of Al_2O_3 and MoS_2 nanoparticles have been fabricated successfully by using Novel ultrasonic assisted stir casting process. The homogeneous distribution of the reinforcement nanoparticles in the matrix material has been observed with the help of SEM microstructures of the ZA-27 nanocomposites and hybrid nanocomposites. These uniform dispersion of the different weight percentages of nanoparticles was achieved because of the ultrasonification process done while fabricating of ZA-27 nanocomposites.
2. The density of the ZA-27/ Al_2O_3 nanocomposites decreases as the reinforcement content increases due to the lower density value of the Al_2O_3 nanoparticles as compare to the ZA-27 alloy.

Mechanical properties of ZA-27 nanocomposites

1. Mechanical properties such as microhardness, ultimate tensile strength, yield strength and fatigue strength increase with addition of 0.5 wt % MoS_2 nanoparticles and decreases with increasing beyond 0.5 wt % of MoS_2 nanoparticles in the ZA-27 alloy. The microhardness and UTS of the ZA-27/MoS_2 nanocomposites reinforced with 0.5 wt % of nanoparticles increase by about 5 % and 3.1% when compare to the ZA-27 alloy.
2. The addition of Al_2O_3 nanoparticles increases the mechanical properties of the ZA-27 nanocomposites as the reinforcement content of nanoparticles increases in the matrix material. The ZA-27/Al_2O_3 nanocomposite specimens show an increase in the microhardness and UTS by about 16 % and 15.8% as the reinforcement content of the alumina nanoparticles increased from 0 to 1.5 wt %.

3. The fatigue strength of the 0.5 wt % MoS_2 nanoparticles reinforced ZA-27 nanocomposites increases by about 31.5 % compare to the ZA-27 alloy. The ZA-27/Al_2O_3 nanocomposite specimens show an increase in the fatigue strength by about 60.5 % as the reinforcement content of the alumina nanoparticles increased from 0 to 1.5 wt %.

Tribological properties of ZA-27 nanocomposites

1. The ZA-27 + 1.5 wt% MoS_2 nanocomposites sliding against the hard counter disc under dry condition exhibited extremely minor wear rate of 0.527 x 10^{-6} mm^3/m and low coefficient of friction of 0.14. The formation of relatively soft lubricious oxides film on the surface of the counter disc significantly reduces the wear rate and coefficient of friction of the ZA-27/MoS_2 nanocomposites.
2. The ZA27 + 1.5 wt% Al_2O_3 nanocomposites sliding against hard counter disc under dry condition exhibited the minor wear rate is 0.837 x 10^{-6} mm^3/m and less coefficient of friction of 0.216. The ZA-27/MoS_2 nanocomposites are having better wear resistance properties compare to the ZA-27/Al_2O_3 nanocomposites.
3. The most significant parameters influencing the wear rate and friction coefficient of the ZA-27/MoS_2 nanocomposites are reinforcement content and applied load. The minimum wear rate was observed at a reinforcement content of 1.5 wt %, applied load of 30 N, sliding distance of 2850 m and sliding speed of 1 m/s. Low friction coefficient was observed at reinforcement content of 1.5 wt %, applied load of 90 N, sliding distance of 3000m and sliding speed of 3 m/s.
4. The most significant parameters influencing the wear rate of the ZA-27/Al_2O_3 nanocomposites are reinforcement content and sliding speed, for friction coefficient are reinforcement content and applied load. The minimum wear rate was observed at reinforcement content of 1.5 wt %, applied load of 30 N, sliding distance of 2900 m and sliding speed of 2.5 m/s. Low friction coefficient was observed at reinforcement content of 1.5 wt %, applied load of 90 N, sliding distance of 1000m and sliding speed of 3 m/s.

Mechanical and Wear behavior of Hybrid nanocomposites

1. The mechanical properties of the ZA-27 hybrid nanocomposites increase as compared to the matrix material. The ZA-27 hybrid nanocomposite reinforced with 1.5 wt % alumina and 0.5 wt % of MoS_2 nanoparticles show an increase in the microhardness and UTS by about 16.5 % and 16.2 % when compare to the ZA-27 alloy. The fatigue strength of hybrid nanocomposites increases by about 61.7 % compare to the ZA-27 alloy.
2. The tribological behavior of the ZA-27 hybrid nanocomposites increases the wear resistance as compared to the matrix material. The minimum wear rate and friction coefficient values are approximately near to the 1.5 wt % MoS_2 nanoparticles reinforced in ZA-27 nanocomposites.
3. The most significant parameters influencing the wear rate of the ZA-27 hybrid nanocomposites are applied load and sliding distance, for coefficient of friction are applied load and sliding speed. The minimum wear rate was observed is 0.581×10^{-6} mm^3/m at applied load (30 N), sliding distance (3000 m) and sliding speed (1 m/s). The low friction coefficient was observed is 0.14 at applied load (90 N), sliding distance (1150 m) and sliding speed (3 m/s).

ZA-27 hybrid nanocomposites improve the mechanical and wear resistance properties when compared to all other compositions of ZA-27 nanocomposites. Hence these hybrid nanocomposites can be used for the bearing applications in many industrial sectors.

7.2. Scope of future work

1. In the present investigation, aluminium oxide and molybdenum disulphide nanoparticles were used as reinforcement materials to prepare hybrid nanocomposites. However there exist other hard and soft ceramic particles like boron nitride and graphite etc, which can be tried and a final conclusion can be drawn.
2. From this work it was found that the addition of Al_2O_3 and MoS_2 reinforcement particles significantly improves the mechanical and tribological performance of the hybrid nanocomposite. Further ceramic or metal nanofillers with different sizes might be tried and research carried out.
3. In this work pin on disc testing machine was used to investigate the tribological properties of the nanocomposites. Other testing apparatus like erosion test can be tried as part of future research.

Visible Research Output

International Journals:

1. Shivakumar.N, V Vasu, N Narasaiah, Mechanical properties and dry sliding wear behaviour of molybdenum disulphide reinforced zinc-aluminium alloy composites, Transactions of the Indian Institute of Metals, 70(8), 2155-2163, 2017 (SCI Journal)
2. Shivakumar.N, V Vasu, N Narasaiah, Processing and dry sliding wear behavior of Al_2O_3 nanoparticles reinforced ZA-27 composites, Materials Today Proceedings, 4, 4006-4012, 2017 (Scopus Journal)
3. Shivakumar.N, V Vasu, N Narasaiah, Synthesis and Characterization of nano-sized Al_2O_3 particle reinforced ZA-27 metal matrix composites", Procedia Materials Science, 10, 159-167, 2016 (Scopus Journal)
4. Shivakumar.N, V Vasu, N Narasaiah, Tribological characteristics of Al_2O_3 nanoparticles reinforced ZA-27 alloy composites using response surface methodology, Journal of Engineering Technology. (Communicated)

International Conferences:

1. Shivakumar.N, V Vasu, N Narasaiah , Fabrication and wear behavior of ZA-27 reinfroced Molybdenum disulfide composites using stir casting process, 6th International & 27th All India Manufacturing Technology, Design and Research Conference (AIMTDR), 16 -18 December 2016, College of Engineering Pune, India .
2. Shivakumar.N, V Vasu, N Narasaiah, Processing and dry sliding wear behavior of Al_2O_3 nanoparticles reinforced ZA-27 composites, 5th International Conference of Materials Processing and Characterization (ICMPC). 12-13 March 2016, GRIET, Hyderabad, India.
3. Shivakumar.N, V Vasu, N Narasaiah, Synthesis and Characterization of nano-sized Al_2O_3 particle reinforced ZA-27 metal matrix composites, 2nd international conference on Nanomaterials and Technologies (CNT). 17-18 October 2014, Vardhaman College of Engineering, Hyderabad, India.

4. Shivakumar.N, Vasu, Narasaiah, Mechanical and wear behavior of hybrid metal matrix composite fabricated by ultrasonic assisted stir casting method, National Symposium of Mechanical Engineering Research Scholars (NSMERS). 7th October 2016 NIT Warangal, India.

REFERENCES

[1] Mathews, F.L. and Rawlings, R.D, Composite Materials; Engineering and Science, Chapman and Hall, 1994.

[2] T. W. Clyne and P. I. Withers, An Introduction to Metal Matrix Composites, Cambridge University Press, UK, 1993,1-10.

[3] Rohatgi, P. K., Metal-matrix Composites, Defence Science Journal, 1993, 43(4), 323-349.

[4] Roco, M. C. Nanoparticles and nanotechnology research. Journal of Nanoparticle Research, 1999, 1(1), 1-6.

[5] Riccardo Casati and Maurizio Vedani, Metal Matrix Composites Reinforced by Nano-Particles—A Review, Metals, 2014, 4, 65-83.

[6] E. Gervais, H. Levert and M. Bess, "The Development of a Family of Zinc-base Foundry Alloys", AFS Transactions, 1980, 88, 183-194.

[7] F. Porter, Zinc Handbook: Properties. Processing - and Use in Design, Marcel Dekker Inc., New York, 1991, 421-442.

[8] Hesham Elzanaty, Al–Addition Influence on Tribological Properties of Zn–Based Alloys, International Journal of Research in Engineering & Technology, 2014, 2(7), 63-68.

[9] F. Porter, Zinc Handbook : Properties. Processing and Use in Design, Marcel Dekker Inc., New York, 1991, 52.

[10] William Mihaichuk, Zinc-Alloy Bearings Challenge the Bronzes, Eastern Alloys Inc Maybrook, Newyork, 1981.

[11] B669-89 : Standard Specification for Zinc-Aluminum Alloys in Ingot Form for Foundry and Die Castings", Annual Book of ASTM Standards, 1993, 02.04, 521 -522.

[12] A. Ibrahim, F. A. Mohamed and E. J. Lavernia, "Particulate Reinforced Metal Matrix Composites - a Review", Journal of Materials Science, 1991, 26(5), 1137-1156.

[13] G. A. Chadwick, "Squeeze Casting of Metal Matrix Composites Using Short Fibre Preforms", Materials Science and Engineering A, 1991,135, 23-28.

[14] S.A. Sajjadi, H.R. Ezatpour, H. Beygi, Microstructure and mechanical properties of Al-Al_2O_3 micro and nano composites fabricated by stir casting, Materials Science and Engineering A, 2011, 528, 8765-8771.

[15] Xiaochun Li, Yong Yang, Xudong Cheng, Ultrasonic-assisted fabrication of metal matrix nanocomposites, Journal of Materials Science, 2004, 39, 3211-3212.

[16] R. Dalmis, H. Cuvalci, A. Canakci, O. Guler, Investigation of Graphite Nano Particle Addition on the Physical and Mechanical Properties of ZA-27 Composites, Advanced Composites Letters, 2016, 25(2), 37-42.

[17] Satish Kumar T, Subramanian R, Shalini S, Synthesis, microstructural and mechanical properties of ex situ zircon particles (ZrSiO4) reinforced Metal Matrix Composites (MMCs): a review, Journal of Materials Research and Technology, 2015, 4(3), 333-347.

[18] MeijuanLi, Kaka Ma, Lin Jiang, HanryYang, Enrique J.Lavernia, Lianmeng Zhang, Julie M.Schoenung, Synthesis and mechanical behavior of nanostructured Al 5083 / n-TiB_2 metal matrix composites, Materials Science & Engineering A, 2016, 656, 241-248.

[19] Brandon A. McWilliams, K.T. Ramesh, Chian-Fong Yen, Probabilistic response of heterogeneous particle reinforced metal matrix composites with particle size dependent strengthening, Computational Materials Science, 2013, 79, 15-24.

[20] Xin Gao, Hongyan Yue, Erjun Guo, Hong Zhang, Xuanyu Lin, Longhui Yao, Bao Wang, Preparation and tensile properties of homogeneously dispersed graphene reinforced aluminum matrix composites, Materials and Design, 2016, 94, 54-60.

[21] Mehdi Rahimiana, Nader Parvin, Naser Ehsani, Investigation of particle size and amount of alumina on microstructure and mechanical properties of Al matrix composite made by powder metallurgy, Materials Science and Engineering A, 2010, 527, 1030-1038.

[22] Shaolin Li, Lehua Q, Ting Zhang, Jiming Zhou, Hejun Li, Interfacial microstructure and tensile properties of carbon fiber reinforced Mg-Al-RE matrix composites, Journal of Alloys and Compounds, 2016, 663, 686-692.

[23] A. Thionnet, J. Renard, Experimental and numerical study of a fibre/matrix interface of SiC/titanium composites, Aerospace Science and Technology, 1998, 6, 369-379.

[24] S Jerry Andrews Fabian, B. Selvam, Densification behaviour of Aluminium reinforced with Tungsten Carbide particulate Metal Matrix Composite processed by P/M, IOSR Journal of Mechanical and Civil Engineering, 2010, 24-29.

[25] GENG Lin, XU Hong-yu, YU Kuai, WANG Hong-lin, Aging behavior of A1203 short fiber reinforced A1-Cu alloy composites, Transactions of Nonferrous Metals Society of China, 2007, 17, 1018-1021.

[26] Hamdullah Cuvalcı, Hasan Bas, Investigation of the tribological properties of silicon containing zinc–aluminum based journal bearings, Tribology International, 2004, 37, 433-440.

[27] Srimant Kumar Mishra, Sandhyarani Biswas, Alok Satapathy, A study on processing, characterization and erosion wear behavior of silicon carbide particle filled ZA-27 metal matrix composites, Materials and Design, 2014, 55, 958-965.

[28] B.M. Girish, K.R. Prakash, B.M. Satish, P.K. Jain, Phani Prabhaka, An investigation into the effects of graphite particles on the damping behavior of ZA-27 alloy composite material, Materials and Design, 2011, 32, 1050-1056.

[29] K. H. W. Seah, S. C. Sharma, B. M. Girish, Corrosion Characteristics of ZA-27 graphite Particulate Composites, Corrosion Science, 1997, 39(1), 1-7.

[30] S.C. Sharma, K.H.W. Seah, B.M. Satish, B.M. Girish, Corrosion Characteristics of ZA-27/ Glass-Fibre Composites, Corrosion Science, 1997, 39(12), 2143-2150.

[31] Yang LIU, Hong-ying LI, Hao-fan JIANG, Xiao-chao LU, Effects of heat treatment on microstructure and mechanical properties of ZA27 alloy, Trans. Nonferrous Met. Soc. China, 2013, 23, 642-649.

[32] Ahmet Turk, Can Kurnaz, Huseyin Sevik, Comparison of the wear properties of modified ZA-8 alloys and conventional bearing bronze, Materials and Design, 2007, 28, 1889-1897.

[33] Shanta Sastry, M. Krishna, Jayagopal Uchil, A study on damping behaviour of aluminite particulate reinforced ZA-27 alloy metal matrix composites, Journal of Alloys and Compounds, 2001, 314, 268-274.

[34] H. Aashuri, A. Razavimanesh, A. Kolahi, M. Mohiedin, Impact and tensile behaviour of fractional melting processed ZA-27 alloy, Materials Science and Engineering A, 2002, 333, 115-122.

[35] Biljana Bobic, Jelena Bajat, Zagorka Acimovic-Pavlovic, Ilija Bobic, Bore Jegdic, Corrosion behaviour of thixoformed and heat-treated ZA27 alloys in NaCl solution, Trans. Nonferrous Met. Soc. China, 2013, 23, 931-941.

[36] S.C. Sharma, B.M.Girish, Rathnakar Kamath, B.M. Satish, Graphite particles reinforced ZA-27 alloy composite materials for journal bearing applications, Wear, 1998, 219, 162-168.

[37] Marco Zurko, Carlos Enrique Schvezov, Alicia Esther Ares, Investigation on Al2O3-Reinforced Zinc-Aluminum Matrix Composites, Procedia Materials Science, 2015, 8, 424-433.

[38] S.C.Sharma, D.R.Somashekar, B.M.Satish, A note on the corrosion characterization of ZA-27/zircon particulate composites in acidic medium, Journal of Materials Processing Technology, 2001, 118, 62-64.

[39] Fei Yan, Guozhen Wang, Chunming Wang, Xiyuan Hu, Yajun Wang, Yun Tan, Zhichun Chen, Shuo Li, Microstructures and properties of laser welding joint of super-eutectic ZA alloy, Materials and Design, 2013, 43, 25-30.

[40] Amar Patnaik, T.G. Mamatha, Sandhyarani Biswas, Predeep Kumar, Damage assessment of titania filled zinc–aluminum alloy metal matrix composites in erosive environment: A comparative study, Materials and Design, 2012, 36, 511-521.

[41] B.K. Prasad, O.P. Modi, Slurry wear characteristics of zinc-based alloys: Effects of sand content of slurry, silicon addition to alloy system and traversal distance, Trans. Nonferrous Met. Soc. China, 2009, 19, 277-286.

[42] S. Muthukumarasamy and S. Seshan, Structure and properties of fibre reinforced Zn-27% Al alloy based cast MMCs, Composites, 1995, 26, 387-393.

[43] Biljana Bobic, Jelena Bajat, Zagorka Acimovic-Pavlovic, Marko Rakin, Ilija Bobic, The effect of T4 heat treatment on the microstructure and corrosion behaviour of Zn27Al1.5Cu0.02Mg alloy, Corrosion Science, 2011, 53, 409-417.

[44] LI Zi-quan, Zhou Heng-Zhi, Luo Xin-Yi, Wang Tao, Shen Kai, Aging microstructural characteristics of ZA-27 alloy and SiC/ZA-27 composite, Trans. Nonferrous Met. Soc. China, 2006, 16, 98-104.

[45] S.C.Sharma, D.R.Somashekar, B.M.Satish, A note on the corrosion characterization of ZA-27/zircon particulate composites in acidic medium, Journal of Materials Processing Technology, 2001, 118, 62-64.

[46] Wislei Riuper Osorio, Celia Marina Freire, Amauri Garcia, The effect of the dendritic microstructure on the corrosion resistance of Zn–Al alloys, Journal of Alloys and Compounds, 2005, 397, 179-191.

[47] LI Run-xia, LI Rong-de, BAI Yan-hua, QU Ying-dong, YUAN Xiao-guang, Effect of specific pressure on microstructure and mechanical properties of squeeze casting ZA27 alloy, Trans. Nonferrous Met. Soc. China, 2010, 20, 59-63.

[48] S. Muthukumarasamy, A. Guruprasad, A. Sudhakar, and S. Seshan, The Performance of Zinc Alloy Based Metal Matrix Composites Produced Through Squeeze Casting, Materials and Manufacturing Processes, 1996, 11(3), 351-366.

[49] H.X. Zhu and S.K. Liu, Mechanical properties of squeeze cast zinc alloy matrix composites containing α-alumina fibres, Composites, 1993, 24(5), 437-442.

[50] Cheng-Kun Zheng, Wei-Wen Zhang, Da-Tong Zhang, Yuan-Yuan Li, Low cycle fatigue behavior of T4-treated Al–Zn–Mg–Cu alloys prepared by squeeze casting and gravity die casting, Trans. Nonferrous Met. Soc. China, 2015, 25, 3505-3514.

[51] Fatih Cay, S. Can Kurnaz, Hot tensile and fatigue behaviour of zinc–aluminum alloys produced by gravity and squeeze casting, Materials and Design, 2005, 26, 479-485.

[52] M.T. Abou El-khaira, A. Lotfya, A. Daouda, A.M. El-Sheikh, Microstructure, thermal behavior and mechanical properties of squeeze cast SiC, ZrO_2 or C reinforced ZA27 composites, Materials Science and Engineering A, 2011, 528, 2353-2362.

[53] N. Mathan Kumar, S. Senthil Kumaran, L.A. Kumaraswamidhas, Aerospace application on Al 2618 with reinforced – Si_3N_4, AlN and Zrb_2 in-situ composites, Journal of Alloys and Compounds, 2016.

[54] Amir Hussain Idrisi, Vikas Dev Singh, Vipul Saxena, Development and testing of Al 5083 alloy reinforced by SiC particles, International Journal of Scientific Research Engineering & Technology, 2014, 2(11), 697-704.

[55] Dipti Kanta Das, Purna Chandra Mishra, Saranjit Singh and Swati Pattanaik, Fabrication and heat treatment of ceramic reinforced aluminium matrix composites – a review, International Journal of Mechanical and Materials Engineering, 2014, 1(6), 1-15.

[56] J. Hashim, L. Looney, M.S.J. Hashmi, Metal matrix composites: production by the stir casting method, Journal of Materials Processing Technology, 1999, 92(93), 1-7.

[57] S.A. Sajjadi, H.R. Ezatpour, H. Beygi, Microstructure and mechanical properties of Al–Al_2O_3 micro and nano composites fabricated by stir casting, Materials Science and Engineering A, 2011,528, 8765-8771.

[58] Yu Li, Qiu-Lin Li, Dong Li, Wei Liu, Guo-Gang Shu, Fabrication and characterization of stir casting AA 6061−31% B_4C composite, Trans. Nonferrous Met. Soc. China, 2016, 26, 2304-2312.

[59] S.A. Sajjadi, H.R. Ezatpour, M. Torabi Parizi, Comparison of microstructure and mechanical properties of A356 aluminum alloy/Al2O3 composites fabricated by stir and compo-casting processes, Materials and Design, 2012, 34, 106-111.

[60] Kannappan S V, Ramanathan S, Somasundaram D, Balu A, Mechanical and Tribological Characteristics of Stir-Cast Al-Si10mg and Self-Lubricating Al-Si10Mg/MoS_2 Composites, Materials and technology, 2012, 46(5), 497-501.

[61] H. R. Ezatpour, M. Torabi-Parizi, S. A. Sajjadi, Microstructure and mechanical properties of extruded Al/Al_2O_3 composites fabricated by stir-casting process, Trans. Nonferrous Met. Soc. China, 2013, 23, 1262-1268.

[62] S. Gopalakrishnan, N. Murugan, Production and wear characterisation of AA 6061 matrix titanium carbide particulate reinforced composite by enhanced stir casting method, Composites: Part B, 2012, 43, 302-308.

[63] Xiaochun Li, Yong Yang, Xudong Cheng, Ultrasonic-assisted fabrication of metal matrix nanocomposites, Journal of Materials Science, 2004, 39, 3211-3212.

[64] Aniruddha V. Muley, Ultrasonic Probe Assisted Stir Casting Method For Metal Matrix Nano-Composite Manufacturing : An Innovative Method, Proceedings of 10th SARC-IRF International Conference, 2015,24-26.

[65] Rahul Gupta, B.S.S.Daniel, G.P.Chaudhari, Ultrasonic Assisted Casting of Aluminum Matrix Composite, International Journal of Applied Research in Mechanical Engineering, 2013, 3(1), 26-30.

[66] R. S. Rana, Rajesh Purohit and S. Das, Fabrication and Testing of Ultrasonically Assisted Stir Cast AA 5083-Sicp Composites, Int. Journal of Engineering Research and Applications, 2013, 3(5), 386-393.

[67] K. H. W. Seah, S. C. Sharma and B. M. Girish, Mechanical properties of as-cast and heat-treated ZA-27/graphite particulate composites, Composites Part A, 1997, 28, 251-256.

[68] K. H. W. Seah, S. C. Sharma and B. M. Girish, Mechanical properties of cast ZA-27/graphite particulate composites, Materials & Design, 1995, 16(5), 271-275.

[69] K. H. W. Seah, S. C. Sharma and B. M. Girish, Effect of artificial ageing on the hardness of cast ZA-27/graphite particulate composites, Materials & Design, 1995, 16(6), 337-341.

[70] S. C. Sharmaa, K. H. W. Seah, B.M. Satisha, B. M. Girish, Effect of short glass fibers on the mechanical properties of cast ZA-27 alloy composites, Materials & Design, 1996, 17(5/6), 245-250.

[71] S. C. Sharma, B. M. Girish, R. Kamath, B. M. Satish, K. H. W. Seah, Hardness of aged ZA-27/short glass fibre reinforced composites, Materials & Design, 1997, 18(3), 155-159.

[72] S.C. Sharma, B.M. Girish, D.R. Somashekar, Rathnakar Kamath, B.M. Satish, Mechanical properties and fractography of zircon-particle-reinforced ZA-27 alloy composite materials, Composites Science and Technology, 1999, 59, 1805-1812.

[73] Ali Safinajafabadi, Rasoul Sarraf-Mamoory, Zahra Karimi, Effect of organic dispersants on structural and mechanical properties of Al_2O_3/ZrO_2 composites, Materials Research Bulletin, 2012, 47, 4210-4215.

[74] S.C. Sharma, Shanta Sastry, M. Krishna, E ffect of aging parameters on the micro structure and properties of ZA-27/ aluminite metal matrix composites, Journal of Alloys and Compounds, 2002, 346, 292-301.

[75] Yang Liu, Hong-Ying Li, Hao-Fan Jiang, Xiao-Chao Lu, Effects of heat treatment on microstructure and mechanical properties of ZA27 alloy, Trans. Nonferrous Met. Soc. China, 2013, 23, 642-649.

[76] K. H. W. Seah, S. C. Sharma, P.R.Rao and B. M. Girish, Mechanical properties of as-cast and heat-treated ZA-27/silicon carbide particulate composites, Materials & Design, 1995, 16(5), 277-281.

[77] Z. Mei, Y.H. Zhu, W.B. Lee, T.M. Yue, G.K.H. Pang, Microstructure investigation of a SiC whisker reinforced eutectoid zinc alloy matrix composite, Composites: Part A, 2006, 37, 1345-1350.

[78] H. R. Ezatpour, M. Torabi-Parizi, S. A. Sajjadi, Microstructure and mechanical properties of extruded Al/Al2O3 composites fabricated by stir-casting process, Trans. Nonferrous Met. Soc. China, 2013, 23, 1262-1268.

[79] Pu-Yun Dong, Hai-Dong Zhao, Fei-Fan Chen, Jun-Wen Li, Microstructures and properties of A356−10%SiC particle composite castings at different solidification pressures, Trans. Nonferrous Met. Soc. China, 2013, 23, 2222-2228.

[80] Huang Jianfeng, Wang Jianhua, Su Xuping, Jiang Lingling, Wu Changjun, Li Jielin, Modification effect of Al–30Zn–5Zr–1B on ZnAl4Y alloy, Materials Characterization, 2012, 71, 41-48.

[81] T. Savaskan, M.S. Turhal, Relationships between cooling rate, copper content and mechanical properties of monotectoid based Zn–Al–Cu alloys, Materials Characterization, 2003, 51, 259-270.

[82] Aleksandar Vencl, Ilija Bobic, Filip Vucetic, Biljana Bobic, Jovana Ruzic, Structural, mechanical and tribological characterization of Zn25Al alloys with Si and Sr addition, Materials and Design, 2014, 64, 381-392.

[83] Eleani M. da Costa, Cesar Edil da Costa, Felipe Dalla Vecchia, Cristiane Rick, Study of the influence of copper and magnesium additions on the microstructure formation of Zn–Al hypoeutectic alloys, Journal of Alloys and Compounds, 2009, 488, 89-99.

[84] D. Bozic, J. Stasic V. Rajkovic, Microstructures and Mechanical Properties of ZA27-Al_2O_3 Composites Obtained by Powder Metallurgy Process, Science of Sintering, 2011, 43, 63-70.

[85] I. Bobic, M.T. Jovanovic, N. Ilic, Microstructure and strength of ZA-27-based composites reinforced with Al_2O_3 particles, Materials Letters, 2003, 57, 1683-1688.

[86] Hai Su, Wenli Gao, Zhaohui Feng, Zheng Lu, Processing, microstructure and tensile properties of nano-sized Al2O3 particle reinforced aluminum matrix composites, Materials and Design, 2012, 36, 590-596.

[87] T.G. Mamatha, Amar P, Sandhyarani B, B.K. Satapathy, Amit Kumar R, Thermo-mechanical and crack position on stress intensity factor in particle-reinforced Zinc–aluminium alloy composites, Computational Materials Science, 2012, 55, 100-112.

[88] B.O. Fatile, B.O. Adewuyi, H.T. Owoyemi, Synthesis and characterization of ZA-27 alloy matrix composites reinforced with zinc oxide nanoparticles, Engineering Science and Technology, an International Journal, 2017.

[89] Afsaneh D M, Emad O, Pradeep L. M, Pradeep K. R, Mechanical and tribological properties of self-lubricating metal matrix nanocomposites reinforced by carbon nanotubes (CNTs) and grapheme- A review, Composites Part B, 2015, 77, 402-420.

[90] Dong Xu-Gang, Zhou Jie, Jia Yao-Jun, Liu Bin, Effect of alloying on high temperature fatigue performance of ZL114A (Al–7Si) alloy, Trans. Nonferrous Met. Soc. China, 2012, 22, 661-667.

[91] Ting Liu, Nai-Chao Si, Guang-Lei Liu, Rui Zhang, Chang-Yang Qi, Effects of Si addition on microstructure, mechanical and thermal fatigue properties of Zn–38Al–2.5Cu alloys, Trans. Nonferrous Met. Soc. China, 2016, 26, 1775-1782.

[92] C.S.Ramesh, R.Keshavamurthy, J.Madhusudhan, Fatigue behavior of Ni-P coated Si_3N_4 reinforced Al6061 composites, Procedia Materials Science, 2014, 6, 1444-1454.

[93] M.M. Sharma, C.W. Ziemian, T.J. Eden, Fatigue behavior of SiC particulate reinforced spray-formed 7XXX series Al-alloys, Materials and Design, 2011,32, 4304-4309.

[94] Zhen Li, Xiang-Jun Tian, Hai-Bo Tang, Hua-Ming Wang, Low cycle fatigue behavior of laser melting deposited TC18 titanium alloy, Trans. Nonferrous Met. Soc. China, 2013, 23, 2591-2597.

[95] Cevdet Kaynak, Suha Boylu, Effects of SiC particulates on the fatigue behaviour of an Al-alloy matrix composite, Materials and Design, 2006, 27, 776-782.

[96] Murat Aydrn, Temel Savas¸kan, Fatigue properties of zinc–aluminium alloys in 3.5% NaCl and 1% HCl solutions, International Journal of Fatigue, 2004, 26, 103-110.

[97] Cheng-Kun Zheng, Wei-Wen Zhang, Da-Tong Zhang, Yuan-Yuan Li, Low cycle fatigue behavior of T4-treated Al–Zn–Mg–Cu alloys prepared by squeeze casting and gravity die casting, Trans. Nonferrous Met. Soc. China, 2015, 25, 3505-3514.

[98] Alfred Zmitrowicz, Wear Patterns and Laws of Wear-A Review, Journal of Theoretical and Applied Mechanics, 2006, 44(2), 219-253.

[99] Gencaga Purcek, Temel Savaskan, Tevfik Kucukomeroglu, Samuel Murphy, Dry sliding friction and wear properties of zinc-based alloys, wear, 2002, 252, 894-901.

[100] Marjorie H, Emanuel L, Jacques M, Si-modified ZA alloy for journal bearing applications, wear, 1996, 192, 128-133.

[101] Temel Savas¸kan, Zeki Azakl, An investigation of lubricated friction and wear properties of Zn–40Al–2Cu–2Si alloy in comparison with SAE 65 bearing bronze, wear, 2008, 264, 920-928.

[102] T. Savaskan, G. Purcek, S. Murphy, Sliding wear of cast zinc-based alloy bearings under static and dynamic loading conditions, wear, 2002, 252, 693-703.

[103] Miroslav Babic, Slobodan Mitrovic, Branislav Jeremic, The influence of heat treatment on the sliding wear behavior of a ZA-27alloy, Tribology International, 2010, 43, 16-21.

[104] Reza M, Hamid R S, Relationship between cooling rate, microstructure features and wear behavior in end-chill cast Zn–27%Al alloys containing more than 2% Cu, Wear, 2011, 271, 2899-2908.

[105] K.H.W. Seah, S.C. Sharma, B.M. Girish, S.C. Lim, Wear characteristics of as-cast ZA-27/graphite particulate composites, Materials & Design, 1996, 17(2), 63-67.

[106] Sirong Yu, Zhenming He, Kai Chen, Dry sliding friction and wear behaviour of short fibre reinforced zinc-based alloy composites, Wear, 1996, 198, 108-114.

[107] Ahmet Turk, Can Kurnaz, Huseyin S, Comparison of the wear properties of modified ZA-8 alloys and conventional bearing bronze, Materials and Design, 2007, 28, 1889-1897.

[108] S.C. Sharma, B.M. Girish, D.R. Somashekar, B.M. Satish, Sliding wear behaviour of zircon particles reinforced ZA-27 alloy composite materials, Wear, 1999, 224, 89-94.

[109] S.C.Sharma, B.M. Satish, B.M. Girish, Rathnakar K, Dry sliding wear of short glass fibre reinforced zinc–aluminium composites, Tribology International, 1998, 31(4), 183-188.

[110] G. Ranganath, S.C. Sharma, M. Krishna, Dry sliding wear of garnet reinforced zinc/aluminium metal matrix composites, Wear, 2001, 251, 1408-1413.

[111] Mukundadas P K, Kanakuppi S, Gundenahalli P P, Satyappa B, Dry Sliding Wear Behaviour of Garnet Particles Reinforced Zinc-Aluminium Alloy Metal Matrix Composites, Materials Science, 2006, 12(3), 209-213.

[112] O.P. Modia, S. Rathoda, B.K. Prasada, A.K. Jhaa, G. Dixitb, The influence of alumina particle dispersion and test parameters on dry sliding wear behaviour of zinc-based alloy, Tribology International, 2007, 40, 1137-1146.

[113] S.C.Sharma, B.M. Girish, Rathnakar K, Effect of SiC particle reinforcement on the unlubricated sliding wear behaviour of ZA-27 alloy composites, Wear, 1997, 213, 33-40.

[114] Miroslav B, Slobodan M, Fatima Z, Effects of Al_2O_3 particle reinforcement on the lubricated sliding wear behavior of ZA-27 alloy composites, Journal of Material Science, 2011, 46, 6964-6974.

[115] Miroslav B, Mitrovic S, Dragan D, Branislav J, Tribological Behavior of Composites Based on ZA-27 Alloy Reinforced with Graphite Particles, Tribol Lett, 2010, 37, 401-410.

[116] Seenappa, K.V.Sharma, Tribological behavior of Zn-Al-Cu journal bearing with high load and low speed, Int Journal of Science and Advanced Technology, 2011,1(9), 263-271.

[117] Haitao Chi, Longtao J, Guoqin C, Pengchao K, Xiu Lin, Dry sliding friction and wear behavior of (TiB2+h-BN)/2024Al composites, Materials and Design, 2015,87, 960-968.

[118] Pei-Peng Jin, Geng Chen, Li Han, Jin-Hui Wang, Dry sliding friction and wear behaviors of $Mg_2B_2O_5$ whisker reinforced 6061Al matrix composites, Trans. Nonferrous Met. Soc. China, 2014, 24, 49-57.

[119] K. Soorya Prakash, A. Kanagaraj, P. M. Gopal, Dry sliding wear characterization of Al 6061/rock dust composite, Trans. Nonferrous Met. Soc. China, 2015,25, 3893-3903.

[120] I. Dinaharan, N. Murugan, Dry sliding wear behavior of AA6061/ZrB_2 in-situ composite, Trans. Nonferrous Met. Soc. China, 2012, 22, 810-818.

[121] A. Pramanik, Effects of reinforcement on wear resistance of aluminum matrix composites, Trans. Nonferrous Met. Soc. China, 2016, 26, 348-358.

[122] Linlin Yuan, Jingtao Han, Jing Liu, Zhengyi Jiang, Mechanical properties and tribological behavior of aluminum matrix composites reinforced with in-situ AlB_2 particles, Tribiology International, 2016.

[123] Afsaneh D M, Emad O, Pradeep L. M, Pradeep K. R, Mechanical and tribological properties of self-lubricating metal matrix nanocomposites reinforced by carbon nanotubes (CNTs) and grapheme- A review, Composites Part B, 2015, 77, 402-420.

[124] Prasanta Sahoo, Shouvik Ghosh, Tribological Behaviour of Aluminium Metal Matrix Composites– A Review, Journal of Tribology Research, 2011, 2(1), 1-14.

[125] Xiao-song J, Nai-juan W, De-gui Z, Friction and wear properties of in-situ synthesized Al_2O_3 reinforced aluminum composites, Trans. Nonferrous Met. Soc. China, 2014, 24, 2352-2358.

[126] S. Gopalakrishnan, N. Murugan, Production and wear characterisation of AA 6061 matrix titanium carbide particulate reinforced composite by enhanced stir casting method, Composites Part B, 2012, 43, 302-308.

[127] Mehdi Rahimian, Nader Parvin, Naser Ehsani, The effect of production parameters on microstructure and wear resistance of powder metallurgy Al–Al_2O_3 composite, Materials and Design, 2011, 32, 1031-1038.

[128] Sui Xiandong, Luo Chengping, Luo Zhuoxuan, Ouyang Liuzhang, The Fabrication and Properties of Particle Reinforced Cast Metal Matrix Composites, Journal ofMaterials Processing Technology, 1997, 63, 426-431.

[129] O. Zgalat-Lozynskyy, V.Varchenko, N.Tischenko, A.Ragulya, Tribological behaviour of Si_3N_4- based nanocomposites, Tribology International, 2015, 91, 85-93.

[130] M. Dhanabalakrishnan, P. Sangaravadivel, N. Babu, R. Shenbagaraj, Development of Particulate Reinforced MMC to Improve Tribological Properties for Bush Bearing, International Journal of Scientific & Engineering Research, 2013, 4(1), 1-8.

[131] S. Dhanasekaran, R. Gnanamoorthy, Dry sliding friction and wear characteristics of Fe–C–Cu alloy containing molybdenum di sulphide, Materials and Design, 2007, 28, 1135-1141.

[132] K.H. Hu, J. Wang, S. Schraube, Y.F. Xu, X.G. Hu, R. Stengler, Tribological properties of MoS2 nano-balls as filler in polyoxymethylene-based composite layer of three-layer self-lubrication bearing materials, Wear, 2009, 266, 1198-1207.

[133] Slobodan M, Miroslav B, Blaza S, Nenad M, Tribological Potencial of Hybrid Composites Based on Zinc and Aluminium Alloys Reinforced with Sic and Graphite Particles, 12th Int Conference on Tribology, Serbian Tribology Society, 2011, 138-145.

[134] Mitesh Kumar, A K Mishra, Mechanical behavior of Al 6063/ MoS_2/Al_2O_3 hybrid metal matrix composites, Int Journal of Scientific and Research Publications, 2014, 4(12), 1-4.

[135] Kiran, T. S, M. Prasanna Kumar, Basavarajappa, Mechanical Properties of As-Cast ZA-27/Gr/Sicp Hybrid Composite for the Application of Journal Bearing, Journal of Engineering Science and Technology, 2013, 8(5), 557-565.

[136] C.S. Ramesh, R. Noor Ahmed, M.A. Mujeebu, Development and performance analysis of novel cast copper–SiC–Gr hybrid composites, Materials and Design, 2009, 30,1957-1965.

[137] T. Rajmohan, K. Palanikumar, S. Ranganathan, Evaluation of mechanical and wear properties of hybrid aluminium matrix composites, Trans. Nonferrous Met. Soc. China, 2013, 23, 2509-2517.

[138] S. Suresha, B.K. Sridhara, Friction characteristics of aluminium silicon carbide graphite hybrid composites, Materials and Design, 2012, 34, 576-583.

[139] D Siva Prasad, Chintada Shoba, Hybrid composites – a better choice for high wear resistant materials, Journal of Mat Research and Tech, 2014, 3(2), 172-178.

[140] D. Siva Prasada, C. Shobab, N. Ramanaiah, Investigations on mechanical properties of aluminum hybrid composites, Journal of Mat Research and Tech, 2014, 3(1), 79-85.

[141] Cheng-Jin Hu, Hong-Ge Yan, Ji-Hua Chen, Bin Su, Microstructures and mechanical properties of 2024Al/Gr/SiC hybrid composites fabricated by vacuum hot pressing, Trans. Nonferrous Met. Soc. China, 2016, 26, 1259-1268.

[142] T.S. Kiran, M. Prasanna Kumar, S. Basavarajappa, B.M. Viswanatha, Dry sliding wear behavior of heat treated hybrid metal matrix composite using Taguchi techniques, Materials and Design, 2014, 63, 294-304.

[143] K K Alaneme, M O Bodunrin, A A Awe, Microstructure, mechanical and fracture properties of groundnut shell ash and silicon carbide dispersion strengthened aluminium matrix composites, Journal of King Saud University – Engineering Sciences, 2016.

[144] M.Vamsi Krishna, Anthony.M.Xavior, An Investigation on the Mechanical Properties of Hybrid Metal Matrix Composites, Procedia Engineering, 2014, 97, 918-924.

[145] A Asif Iqbal, Yoshio Arai, Wakako Araki, Fatigue crack growth mechanism in cast hybrid metal matrix composite reinforced with SiC particles and Al_2O_3 whiskers, Trans. Nonferrous Met. Soc. China, 2014, 24, 1-13.

[146] S. Basavarajappa, G. Chandramohan, J. Paulo Davim, Application of Taguchi techniques to study dry sliding wear behaviour of metal matrix composites, Materials and Design, 2007, 28, 1393-1398.

[147] T. Ram Prabhu, Effects of solid lubricants, load, and sliding speed on the tribological behavior of silica reinforced composites using design of experiments, Materials and Design, 2015, 77, 149-160.

[148] R. Ranjith kumar, C. Velmurugan, Optimization of tribological properties in molybdenum di sulphide and titanium carbide reinforced Aluminium composites, IOSR Journal of Mechanical and Civil Engineering,47-54.

[149] T.S. Kiran, M. Prasanna Kumar, S. Basavarajappa, B.M. Viswanatha, Dry sliding wear behavior of heat treated hybrid metal matrix composite using Taguchi techniques, Materials and Design, 2014, 63, 294-304.

[150] B.M. Girish, K.R. Prakash, B.M. Satish, P.K. Jain, Kameshwary Devi, Need for optimization of graphite particle reinforcement in ZA-27 alloy composites for tribological applications, Materials Science and Engineering A, 2011, 530, 382-388.

[151] Pardeep Sharma, Dinesh Khanduja, Satpal Sharma, Dry sliding wear investigation of Al6082/Gr metal matrix composites by response surface methodology, Journal of Mat Research and Tech, 2016, 5(1), 29-36.

[152] K. Niranjan, P. R. Lakshminarayanan, Optimization of process parameters for in situ casting of Al/TiB_2 composites through response surface methodology, Trans. Nonferrous Met. Soc. China, 2013, 23, 1269-1274.

[153] V. Vembu, G. Ganesan, Heat treatment optimization for tensile properties of 8011 Al/15% SiCp metal matrix composite using response surface methodology, Defence Technology, 2015, 11, 390-395.

[154] Pardeep Sharma, Dinesh Khanduja, Satpal Sharma, Parametric Study of Dry Sliding Wear of Aluminium Metal Matrix Composites by Response Surface Methodology, Materials Today: Proceedings, 2015, 2, 2687-2697.

[155] Blaza S Sandra V Aleksandar V, Miroslav B, Optimization and Prediction of Aluminium Composite Wear Using Taguchi Design and Artificial Neural Network, Tribological Journal Bultrib, 2016, 6, 38-45.

[156] K. Soorya Prakash, A. Kanagaraj, P. M. Gopal, Dry sliding wear characterization of Al 6061/rock dust composite, Trans. Nonferrous Met. Soc. China, 2015, 25, 3893-3903.

[157] I. Dinaharan, N. Murugan, Dry sliding wear behavior of AA6061/ZrB2 in-situ composite, Trans. Nonferrous Met. Soc. China, 2012, 22, 810-818.

[158] P. Suresh, K. Marimuthu, S. Ranganathan, Optimization of machining parameters in turning of Al−SiC−Gr hybrid metal matrix composites using grey-fuzzy algorithm, Trans. Nonferrous Met. Soc. China, 2014, 24, 2805-2814.

[159] F.C.Campbell, Fatigue and Fracture (Understanding the basic), The materials information society, ASM International, 2012.

[160] Nardone VC, Prewo KM. On the strength of discontinuous silicon carbide reinforced aluminium composites. Scripta Metall 1987, 21, 1313-1319.

[161] Srivatsan TS. Microstructure, tensile properties and fracture behaviour of Al_2O_3 particulate reinforced aluminium alloy metal matrix composites. J Mater Sci 1996,31, 1375-1388.

[162] McDanels DL. Analysis of stress-strain, fracture, and ductility behaviour of aluminium matrix composites containing discontinuous silicon carbide reinforcement. Metall Trans 1985, 16A, 1105-1514.

[163] A. Sanaty-Zadeh, Comparison between current models for the strength of particulate-reinforced metal matrix nanocomposites with emphasis on consideration of Hall-Petch effect, Mat. Sci. Eng, 2012, 531, 112–118.

[164] P. Luo, D.T. McDonald, W. Xu, S. Palanisamy, M.S. Dargusch, K. Xia, A modified Hall-Petch relationship in ultrafine-grained titanium recycled from chips by equal channel angular pressing, Scripta Mater, 2012, 66, 785–788.

[165]] D. Dzunic, S. Mitrovic , M. Babic, I. Bobic , M. Pantic, D. Adamovic B. Nedeljkovic, Nano indentation of ZA-27 alloy based nanocomposites reinforced with Al2O3 particles, in: 14th Int. Conf. on Tribology, 2015, 1–8.

[166] Z. Zhang, D.L. Chen, Contribution of Orowan strengthening effect in particulate-reinforced metal matrix nanocomposites, Mat. Sci. Eng. A, 2008, 148–152.

[167] Rao R V, Advanced Modeling and Optimization of Manufacturing Processes, International Research and Development, Springer-Verlag, London, 2011.

[168] Montgomery D C, Design and Analysis of Experiments. 6th edition, John Wiley & Sons, Inc., USA, 2005.

[169] Wilson S, Alpas AT. Wear mechanism maps for metal matrix composites. Wear 1997, 212, 1, 41–49.

[170] Ravindran P, Manisekar K, Narayanasamy R, Narayanasamy P. Tribological behaviour of powder metallurgy-processed aluminium hybrid composites with the addition of graphite solid lubricant. Ceram Int 2013, 39 (2), 1169–1182.

[171] Venkatraman B, Sundararajan G. Correlation between the characteristics of the mechanically mixed layer and wear behavior of aluminium, Al-7075 alloy and Al-MMCs. Wear, 2000, 245, 22–38.

[172] Basavarajappa S, Chandramohan G, Arjun M, Thanagavelu M, Subramanian R, Gopalkrishnan P. Influence of sliding speed on the dry sliding wear behaviour and the subsurface deformation on hybrid metal matrix composite. Wear ,2007,262, 1007–1012.

[173] Suresha S, Sridhara BK. Wear characteristics of hybrid aluminium matrix composites reinforced with graphite and silicon carbide particulates. Compos Sci Technol, 2010, 70 (11), 1652–1659.

[174] Suresha S, Sridhara BK. Effect of silicon carbide particulates on wear resistance of graphitic aluminium matrix composites. Mater Des, 2010. 31(9), 4470–4477.